Effects of floating photovoltaic systems on reservoir hydrodynamics and water quality

Zur Erlangung des akademischen Grades einer

DOKTORIN DER INGENIEURWISSENSCHAFTEN (Dr.-Ing.)

von der KIT Fakultät für
Bauingenieur-, Geo- und Umweltwissenschaften des
Karlsruher Instituts für Technologie (KIT)
genehmigte

DISSERTATION

von
Camila Bergmann Goulart,
aus Porto Alegre, Brazil

Tag der mündlichen Prüfung: 22.05.2025

Referent: Dr.-Ing. Stephan Fuchs (KIT)
Referent: Dr.-Ing. Tobias Bleninger (UFPR)

Curitiba (Brazil) / Karlsruhe (Germany)
2025

UNIVERSIDADE FEDERAL DO PARANÁ

CAMILA BERGMANN GOULART

EFFECTS OF FLOATING PHOTOVOLTAIC SYSTEMS ON RESERVOIR HYDRODYNAMICS AND WATER QUALITY

Curitiba (Brasil) / Karlsruhe (Alemanha)

2025

CAMILA BERGMANN GOULART

EFFECTS OF FLOATING PHOTOVOLTAIC SYSTEMS ON RESERVOIR HYDRODYNAMICS AND WATER QUALITY

Tese apresentada como requisito à obtenção do título de Doutora, do Programa de Pós-Graduação em Engenharia de Recursos Hídricos e Ambiental, Setor de Tecnologia da Universidade Federal do Paraná em regime de cotutela entre a UFPR e o KIT (Instituto de Tecnologia de Karlsruhe), na Alemanha.

Orientador: Dr.-Ing. Tobias Bleninger (UFPR)

Coorientador: Dr.-Ing. Stephan Fuchs (KIT)

Curitiba (Brasil) / Karlsruhe (Alemanha)

2025

Catalogação na Fonte: Sistema de Bibliotecas, UFPR
Biblioteca de Ciência e Tecnologia

Goulart, Camila Bergmann
Effects of floating photovoltaic systems on reservoir hydrodynamics and water quality. / Camila Bergmann Goulart. – Curitiba, 2025.
1 recurso on-line : PDF.

Tese (Doutorado) - Universidade Federal do Paraná. Programa de Pós-Graduação em Engenharia de Recursos Hídricos e Ambiental, em parceria com Instituto de Tecnologia de Karlsruhe (Alemanha).

Orientador: Dr.-Ing. Tobias Bleninger (UFPR)
Coorientador: Dr.-Ing. Stephan Fuchs (KIT)

1. Sistemas de energia fotovoltaica. 2.Hidrodinâmica de reservatórios. 3. Modelagem. 4. Lagos. I. Universidade Federal do Paraná. II. Programa de Pós-Graduação em Engenharia de Recursos Hídricos e Ambiental. III. Instituto de Tecnologia de Karlsruhe. IV. Bleninger, Tobias. V. Fuchs, Stephan. VI. Título.

Bibliotecária: Roseny Rivelini Morciani CRB-9/1585

ATA Nº89

MINUTES OF PUBLIC DEFENSE SESSION OF DISSERTATION TO OBTAIN THE DEGREE OF PHILOSOPHY DOCTOR IN ENGENHARIA DE RECURSOS HÍDRICOS E AMBIENTAL

On 22/05/2025 at 09:30, in Auditório do CEHPAR & Híbrido via teams. , Centro Politécnico, UFPR, Curitiba - PR. of the Federal University of Paraná, the activities pertaining to the rite of defense of work entitled: **Effects of floating photovoltaic systems on reservoir hydrodynamics and water quality** by CAMILA BERGMANN GOULART, under the supervision of Dr. TOBIAS BERNWARD BLENINGER, were undertaken. The Examining Board, designated by the Faculty of the Graduate Program of the Federal University of Paraná in ENGENHARIA DE RECURSOS HÍDRICOS E AMBIENTAL was composed of the following Members: TOBIAS BERNWARD BLENINGER (UNIVERSIDADE FEDERAL DO PARANÁ), MARIO JORGE RODRIGUES PEREIRA DA FRANCA (KARLSRUHE INSTITUTE OF TECHNOLOGY), STEPHAN FUCHS (KARLSRUHE INSTITUTE OF TECHNOLOGY), CRISTOVÃO VICENTE SCAPULATEMPO FERNANDES (UNIVERSIDADE FEDERAL DO PARANÁ). The Board Chair initiated the rites as defined by the Faculty of the Program and, after the remarks of the members of the examining commitee and the respective responses were addressed, the final evaluation of the examining board was read, wich was decided by APPROVAL. This result should be made official by the Faculty of the Program, through the fulfillment of all recommendation and corrections requested by the examining board within the procedural deadlines defined by the program. The granting of the title of philosophy doctor is contigent upon the fulfillment of all the requirements and terms determined int the regulations of the Graduate Program. There being no further business to transact, the Chair adjourned the session, of which, I, TOBIAS BERNWARD BLENINGER, drew up these minutes, which are signed by me and the other members of the Examining Board.

Comments: Defense following the cotutelle agreement with the Karlsruhe Institute of Technology, Faculty of Civil- and Environmental Engineering and Geosciences. Process: 23075.045849/2024. Obtained grade: very good - 1,0.

CURITIBA, May 22th, 2025.

Eletronic Signature
24/05/2025 18:16:58.0
TOBIAS BERNWARD BLENINGER
President of the Examining Board

Eletronic Signature
27/05/2025 09:55:57.0
MARIO JORGE RODRIGUES PEREIRA DA FRANCA
External Member (KARLSRUHE INSTITUTE OF TECHNOLOGY)

Eletronic Signature
24/05/2025 12:39:38.0
STEPHAN FUCHS
Co-Advisor

Eletronic Signature
27/05/2025 22:35:20.0
CRISTOVÃO VICENTE SCAPULATEMPO FERNANDES
Internal Member(UNIVERSIDADE FEDERAL DO PARANÁ)

AKNOWLEDGMENTS

I would like to thank a series of people who have played a fundamental role throughout this doctorate, supporting me, helping me, or just hanging in there through my ups and downs.

To my parents, for all their hard work that got me this far. Without you, nothing would have been possible. To my sister, who was always open to talking and giving advice.

To my supervisor, Tobias Bleninger, for all the support and opportunities throughout my doctorate. Thank you for all the discussions, motivation, enthusiasm, guidance when needed and partnership.

To my co-supervisor, Dr. Ing Stephan Fuchs, for welcoming me to KIT and for the discussions to improve my work.

To Prof. Cristóvão, for all his sensitivity, concern, and motivation, always noticing when something was wrong. Thank you for believing, even when I didn't.

To my friends, Thamarys and Eduarda, who have been there for me practically throughout my PhD. For all the Friday night pizzas, meetings to relax and philosophize about life. You were a great gift.

To my colleagues and friends at PPGERHA and PPGEA, especially Diego Casas, for all the friendship, support, help and many Python scripts that always gave me a headache. For all the beers in America to relax and, at the same time, come up with new ideas. Diego, I really appreciate you being part of this journey, even though you judge me when I accidentally spill water on things.

To the entire team of the FotoÁgua project and the Paranapanema project for the work and discussions that were essential for developing this work and all the others derived from the project.

To Hilgert and Klajdi, for all their efforts in the field campaigns in Germany so that we would have data to work with. To Fritzi and Victoria, for their company and friendship specially during the 12 months in Germany and KIT, which thanks to them were not lonely. To Ursel for her friendship and for welcoming me so well into her home and life, and to Iara for her friendship and instant connection. My time in Germany would never have been the same without all of you.

Finally, to Adolfo, for all his support, patience, and understanding over the last few months. Also to my colleagues at HIDROBR, who have been with me over the last year, always giving me strength and a push to finish this thesis, especially the SOS+Take group.

To SANEPAR and the FotoÁgua Project for financing the field campaigns and sharing the data.

To ANA and the Paranapanema Project for providing data and funding at the start of my doctorate.

Part of this study was financed in part by the Coordenação de Aperfeiçoamento de Pessoal de Nível Superior - Brasil (CAPES) - Finance Code 001, and I was supported by a sandwich doctorate scholarship by the Coordination for the Improvement of Higher Education Personnel (CAPES) during my time in Germany - Capes PrInt, Call No. 01/2022 CAPES-PRINT-UFPR - SANDUICH DOCTORATE.

Look deep into nature, and then
you will understand everything better.

Albert Einstein

ABSTRACT

Investigations into the impacts of floating photovoltaic panels (FPV) have shown that these are dependent on the area of coverage, as well as the characteristics of the water body in which they are located. Two case studies were monitored, a gravel pit lake located in the south of Germany, with 8% covered area, and a subtropical reservoir in the south of Brazil, with 0.01% covered area. The former was monitored from September 2023 to July 2024, while the latter was monitored from October 2022 to April 2023, both with fixed temperature and oxygen sensors, and punctual measurements with multi-parameter sensors. For both sites, it was found that the temperature variation showed no statistically significant differences between the covered and uncovered points. On the other hand, the dissolved oxygen results showed reductions in concentration due to the presence of panels. Cover expansion scenarios were also simulated in order to assess their impact on advective transport and on the reaeration process. The models were calibrated for temperature and dissolved oxygen, showing satisfactory results. Five scenarios were simulated for the lake (base, current, and three expansions) and two for the reservoir (current and expansion). Both showed a reduction in surface temperature, thermocline depth and Schmidt stability. Regarding dissolved oxygen, which was modeled considering only the reaeration process, there was an increase in concentrations. Both models showed a reduction in evaporation, which was higher in the reservoir than in the lake, considering similar coverage percentages. In terms of velocities, the models differed between the environments, with an increase in velocity in the lake compared to the base scenario, and a reduction in the reservoir. In general, the impacts of FPV are not linear and depend on the system's configurations, as well as the environment in which they are inserted, and can increase the spatial heterogeneity of environments. The computer modeling approach used is considered promising and could be complemented to consider more water quality processes in the future.

Keywords: lake modeling; floating photovoltaic system; reservoir hydrodynamics

RESUMO

As investigações sobre os impactos dos painéis fotovoltaicos flutuantes (FPV) mostraram que estas são dependentes da área de cobertura, bem como das características do corpo hídrico em que se encontram. Foram monitorados dois estudos de caso, um lago de pedreira localizado no sul da Alemanha, com 8% de área coberta, e um reservatório subtropical no sul do Brasil, com 0.01% de área coberta. O primeiro foi monitorado de setembro de 2023 a julho de 2024, enquanto o segundo foi monitorado de outubro de 2022 a abril de 2023, ambos com sensores fixo de temperatura e oxigênio, e medições pontuais com sensores multiparâmetro. Para ambos os locais, constatou-se que a variação de temperatura não apresentou diferenças estatisticamente significativas entre os pontos coberto e não coberto. Já os resultados de oxigênio dissolvido apresentaram reduções de concentração devido à presença de painéis. Ainda, foram simulados cenários de expansão de cobertura a fim de avaliar seus possíveis impactos no transporte advectivo e no processo de reaeração. Os modelos foram calibrados para temperatura e oxigênio dissolvido, apresentando resultados satisfatórios. Foram simulados 5 cenários para o lago (base, atual, 3 de expansão) e 2 para o reservatório (atual e expansão). Ambos apresentaram redução da temperatura superficial, da profundidade da termoclina e da estabilidade de schmidt. Com relação ao oxigênio dissolvido, que foi modelado considerando apenas o processo de reaeração, houve um aumento de concentrações. Em ambos os modelos houve redução da evaporação, que apresentou maiores proporções no reservatório que no lago, considerando porcentagens de cobertura semelhantes. Em termos de velocidades, os modelos divergiram entre os ambientes, obtendo-se um aumento de velocidade no lago em relação ao cenário base, e uma redução no reservatório. De maneira geral, observa-se que os impactos do FPV não são lineares e dependem das configurações do sistema, bem como do ambiente em que estão inseridos, e podem aumentar a heterogeneidade espacial do ambiente. Considera-se a abordagem da modelagem computacional utilizada promissora, podendo ser complementada para considerar mais processos de qualidade da água no futuro.

Palavras-chave: modelagem de lagos; sistema fotovoltaico flutuante; hidrodinâmica de reservatórios

ZUSAMMENFASSUNG

Untersuchungen zu Auswirkungen schwimmender Photovoltaikanlagen (FPV) haben gezeigt, dass die bedeckten Fläche sowie die Eigenschaften des Gewässers, auf dem sich die Anlagen befinden, entscheidenden Einfluss haben. Im Rahmen der Arbeit wurden zwei Fallstudien durchgeführt: eine in einem Kiesgrubensee in Süddeutschland mit 8% bedeckter Fläche und eine weitere in einem subtropischen Stausee im Süden Brasiliens mit 0,01% bedeckter Fläche. Der Kiesgrubensee wurde von September 2023 bis Juli 2024 überwacht, der Stausee von Oktober 2022 bis April 2023. In beiden Gewässern wurden kontinuierliche Temperatur- und Sauerstoffaufzeichnungen ergänzt durch punktuellen Messungen mit Multiparameter-Sensoren. Für beide Standorte wurde gezeigt, dass bei den festgestellten Temperaturschwankungen keine statistisch signifikanten Unterschiede zwischen den bedeckten und den unbedeckten Messpunkten aufweisen. Andererseits zeigten die Ergebnisse für den gelösten Sauerstoff eine Verringerung der Konzentration unterhalb der Photovoltaikanlagen. In Modellbetrachtungen wurden Szenarien für die Erweiterung der Abdeckung simuliert, um Auswirkungen auf den advektiven Transport und den Wiederbelüftungsprozess zu bewerten. Die Modelle wurden für Temperatur und gelösten Sauerstoff kalibriert und zeigten zufriedenstellende Ergebnisse. Es wurden fünf Szenarien für den Kiesgrubensee (Basis, aktueller Zustand und drei Erweiterungen) und zwei für den Stausee (aktueller Zustand und Erweiterung) simuliert. Beide zeigten eine Verringerung der Oberflächentemperatur, der Sprungschichttiefe und der Schmidt-Stabilität. Beim gelösten Sauerstoff, der nur unter Berücksichtigung der physikalischen Wiederbelüftung modelliert wurde, kam es zu einem Anstieg der Konzentrationen. Beide Modelle zeigten eine Verringerung der Verdunstung, die im Stausee höher war als im Kiesgrubensee, wenn man von ähnlichen Bedeckungsgraden ausgeht. Hinsichtlich der Geschwindigkeiten unterschieden sich die Modelle zwischen den Umgebungen, wobei die Geschwindigkeit im See im Vergleich zum Basisszenario anstieg und im Stausee sank. Im Allgemeinen sind die Auswirkungen von FPV nicht linear und hängen von den Systemkonfigurationen sowie der Umgebung ab, in der sie eingesetzt werden, und können die räumliche Heterogenität der Umgebungen erhöhen. Der verwendete Computermodellierungsansatz wird als vielversprechend angesehen und könnte ergänzt werden, um in Zukunft weitere Wasserqualitätsprozesse zu berücksichtigen.

Schlüsselwörter: Seemodellierung; schwimmender Photovoltaikanlagen; Hydrodynamik von Stauseen.

CONTENTS

1 INTRODUCTION

Artificial reservoirs play an important role in environmental sanitation. Among the largest and most important are reservoirs for public water supply. However, its construction interrupts the natural river flow, potentially resulting in problems with siltation, eutrophication, and increased evaporation (Hogeboom et al., 2018). These problems can result in both the loss of the desired quality and its use to meet water demand if not properly monitored and controlled.

The use of floating photovoltaic systems (FPV) can create a mutual benefit for reservoirs, since they generate energy and can reduce evaporation by up to 90% if the entire surface area is covered by modules, according to mesocosm experiments (Taboada et al., 2017). According to Scavo et al. (2020), coverage of 50% of the water surface reduced evaporation by 30 to 73%, depending on the type of system array. The reduction in insulation can also result in a reduction in algae growth (World Bank Group, 2019), in addition to electricity production. Another advantage is that the installation on reservoirs that produce hydroelectricity, or reservoirs that capture water, reduces the cost of installing the system, since the existing electrical infrastructure for transmitting energy can be used. Using the water surface reduces the cost of acquiring land, which also makes installation difficult due to topographical restrictions. In addition, installation above a water surface benefits photovoltaic modules due to their greater cooling and thermal control (Bahaidarah et al. (2013); Choi et al. (2020)). Due to the worldwide growth in photovoltaic module applications, their costs have reduced significantly, encouraging the construction of several of these floating photovoltaic plants (IRENA, 2018).

Initial floating photovoltaic plant projects (from 2007) were summarized in Trapani & Redón Santafé (2015), with installations starting at 175kWp in California, Europe, and South Asia, mainly. In 2020 there was already a total installed capacity of 2.6 GWp, with the majority in China (73%), and large capacities in Japan, South Korea, and Europe (World Bank Group (2019); IRENA (2018); Haugwitz (2020)). Many systems have been implemented in hydroelectric plant reservoirs, but there are also applications in lakes and closed mining areas. The expected growth rate in installed power is 20% (Haugwitz, 2020), but mostly on a small scale (less than 3 MWp). According to Lee et al. (2020), the greatest growth is expected in Asian countries and countries with a greater number of hydroelectric plants and public supply reservoirs. Gonzalez Sanchez et al. (2021) showed that the potential for Africa could double existing hydroelectric production with coverage of 1% of the area of reservoirs currently built. It is noteworthy that, in addition to photovoltaic electricity production, an important benefit has been the reduction of evaporation that threatens reservoirs during recent severe droughts. Equivalent results are reported by Ravichandran et al. (2021) for India. For Brazil, Silvério et al. (2018) evaluated that, for the São Francisco River basin, there could be an energy gain of up to 73% with the exploitation of 2% of the reservoirs' surface area, on average, in relation to current production by hydroelectricity. Santos et al. (2019) predicted significant gains with coverages of 10% for the Sobradinho, Tucuruí, Balbina and Itaipu reservoirs. Lopes et al. (2020) estimated the reduction in evaporation for reservoirs

in the semi-arid region and, in a recent article, Lopes et al. (2022) estimated that a coverage of 1% of Brazilian reservoirs could generate energy equivalent to 12.5% of current national demand. In addition, Lee et al. (2020) evaluate Brazil as having the second largest potential in the world, with 739 GWp.

Many analyses of FPV systems, installed in various locations around the world, have been based on technical (i.e. anchoring) and sizing considerations, as well as estimates of growth potential and economic analyses, with a focus on small plants (less than 3MWp). Studies on environmental benefits focus on evaporation processes, but with few in-situ studies. Haas et al. (2020) point out that a major scientific challenge of large installations is related to ecosystem effects, on which they focus on the hypothetical analysis (without field measurements) of the effect of reduced light penetration, reducing the photosynthesis potential of organisms. They argue, as qualitatively cited in other studies (World Bank Group, 2019), of the favorable effect, inhibiting potentially toxic algal blooms and eutrophication events, but point out that large installations can reduce basic primary production, affecting the food chain. Abdelal (2021) argues along the same lines but does not present measurement results or quantitative approaches. Some recent studies include measurements of water temperature and water quality parameters (Ji et al., 2022; Yang et al., 2022a; Ilgen et al., 2023; Nobre et al., 2025). These studies show that there is no linearity between impacts and coverages (Ji et al., 2022; Ilgen et al., 2023; Nobre et al., 2025). Furthermore, some studies show a reduction in water temperature, while others show an increase (Yang et al., 2022a). Some modeling studies showed the dependency on the array/design of the FPV system (Exley et al., 2021).

In this research, two study sites were chosen. The first, Passaúna Reservoir, located in a tropical region and influenced by surface water. Second, a gravel pit lake located in a temperate climate, with no tributaries and only groundwater flow. After a year of field measurements (for both water bodies), where parameters like water temperature, pH, dissolved oxygen (DO), total phosphorus, chlorophyll-a, phytoplankton, nitrate, COD, and photosynthetic active radiation were analyzed, a modeling approach is proposed to calibrate a 3D hydrodynamic model and to assess the impact of potential extensions in coverage of the FPV system on the lakes. After calibrating the model, there is a discussion about different expansion scenarios, aiming to find an optimized case between coverage area and impact on the water body. Figure 1-1 presents the flowchart of the stages developed during this doctoral research.

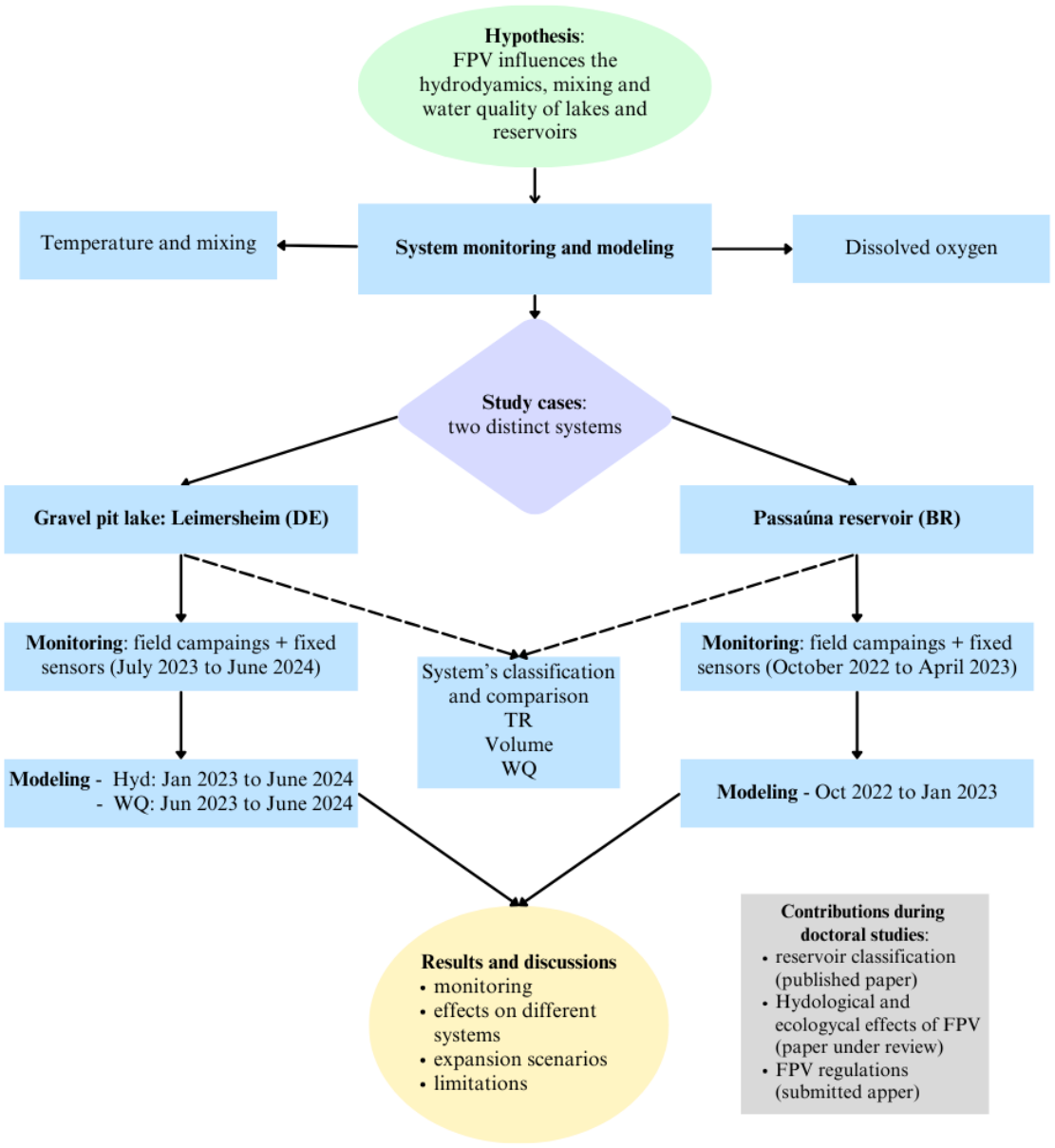

Figure 1-1. Flowchart of the stages developed during the research.

1.1 RESEARCH QUESTIONS AND HYPOTHESIS

The main open research question that guided the development of this thesis is: *do floating photovoltaic systems impact the transfer processes at the air-water interface and generate changes on water quality*?

Based on this, the following questions were defined, and the following hypotheses were described.

QUESTION 1: How is advective transport and mixing affected by the presence of these structures?
The hypothesis is that FPVs can have an impact on advective transport and mixing by reducing water velocity and turbulence, due to the reduction of wind shear on the water surface. This impact can extend to thermal stratification (variations in the depth of the thermocline), depending on the covered area. This would be the primary effect of coverage by FPV, which can influence the behavior of transport and mixing of other substances.

QUESTION 2: How does the presence of these structures affect the physical processes of dissolved oxygen?
The hypothesis is that the presence of these systems might reduce dissolved oxygen concentrations, since there is a reduction in the effect of the wind induced velocity and mixing, thus renewal efficiency, and the reduced area of the air-water interface.

This thesis aims to investigate the environmental impacts of FPV systems on aquatic ecosystems, specifically focusing on how these structures influence the transfer processes at the air-water interface and subsequently alter water quality.

1.2 THESIS OUTLINE

The introduction is followed by chapter 2, that presents the theoretical background, with basic concepts of hydrodynamics and water quality in reservoirs, and reservoir modeling. Chapter 3 presents the state of the art of studies related to floating photovoltaic systems. Chapter 4 presents the materials and methos, including the software and the two case studies of this thesis. Chapter 5 contains the results and discussions of the thesis, divided into case studies and a general comparison at the end. The conclusions are summarized in chapter 6, while chapter 7 lists the technical-scientific contributions developed during the PhD period.

2 THEORETICAL BACKGROUND

2.1 HYDRODYNAMICS AND WATER QUALITY

Reservoirs are usually different to lakes, as they are considered man-made artificial structures. Reservoirs can behave both as lentic and lotic environments. The latter, like run-of-the-river reservoirs, have hydrodynamic characteristics similar to rivers, dominated mainly by the water inflow, presenting shorter residence times. These structures tend to suffer less from thermal or chemical stratification processes since they present higher velocities. On the other hand, lentic environments, such as accumulation reservoirs or lakes, are the ones that present lower velocities, having their processes strongly influenced mainly by meteorological forcing (wind, radiation). They are more susceptible to stratification processes, which influence water quality.

Reservoirs with large depths tend to stratification, which occurs due to changes in fluid density, that can be caused by temperature differences and suspended solids. Temperature stratification, a result of solar heating at the surface, is characterized by the following structure (Figure 2-1):

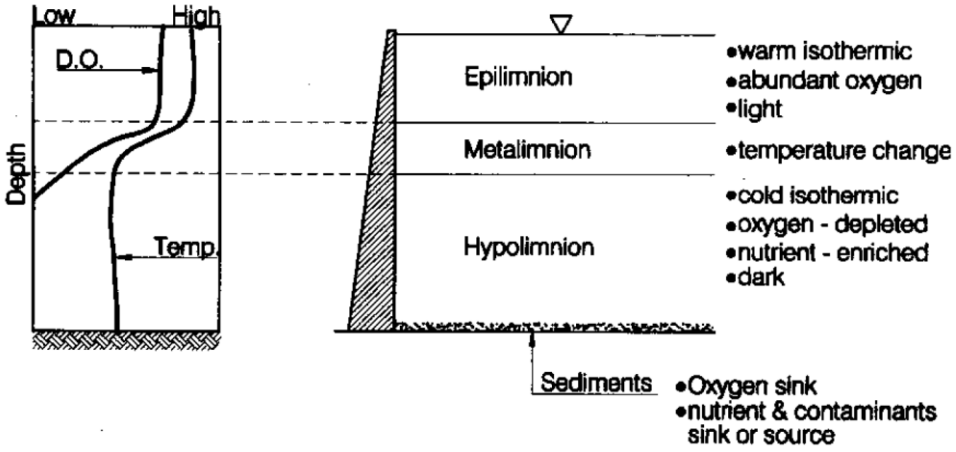

Figure 2-1. Reservoir vertical stratification (Morris & Fan, 1998)**.**

- *epilimnion*: a vertically mixed layer of warmer, well-oxygenated surface water;
- *metalimnion*: zone of rapid change in temperature and density; it encompasses the thermocline;
- *hypolimnion*: deep, colder, and darker zone, lacking oxygen.

The thermocline is the zone where the temperature gradient is greatest, relatively narrow, and encompassed by the metalimnion, with the adjacent transition layer between the shallow and deep zones of the reservoir.

The wind is the main factor causing horizontal and vertical circulation, and mixing in reservoirs, where wind velocities of high magnitude can cause deeper circulation patterns. Winds of sufficient strength and duration can erode temperature-induced stratification, causing full mixing of the

water column. However, small reservoirs are also susceptible to changes due to high inflows, which can mix the layers, as well as being able to renew the stored water. This, however, is generally a very local effect, limited to the inflow region.

In the mass balance equation (2-1), in reservoirs, here represented in the 1D longitudinal representation for simplicity, the dispersion term often has an equal or greater magnitude than the advection term.

$$\frac{\partial C}{\partial t} = -U\frac{\partial C}{\partial x} + \frac{\partial}{\partial x}\left(D\frac{\partial C}{\partial x}\right) + S + R \qquad (2\text{-}1)$$

C being the concentration, t the time, x the longitudinal distance from inflow to the dam, U the advection velocity in x-direction, D the dispersion coefficient (combination of advection by mean velocity profile and mixing by eddy diffusivity/turbulence), S sources and sinks, such as intakes, outflows (spillway or groundwater outlet) or alike, R the chemical and/or biological reactions, including deposition and resuspension processes.

Reservoirs exhibit characteristics of both rivers and lakes. Generally, they are river-like in the upstream region, where the main tributaries enter, and lake-like in the regions closest to the dam. In addition to vertical stratification, these water bodies can present significant longitudinal variations in terms of hydrodynamic and water quality characteristics (Ji, 2008). Longitudinally, the reservoir can be divided into three main zones (Figure 2-2):

- *riverine*: usually narrower and still dominated by the inflow of the river, this zone presents characteristics of higher speeds and complete mixing, generally with significant transport of suspended solids and characterized by higher turbidity. In the transport equation (2-1), the advection term is dominant.
- *transition*: between the riverine and lacustrine zones, is where velocities begin to decrease, and suspended solids begin to settle.
- *lacustrine*: a zone that presents lake-like characteristics, with greater depth and lower velocities. Usually with low concentrations of suspended solids, with greater penetration of solar radiation, more susceptible to the process of temperature stratification.

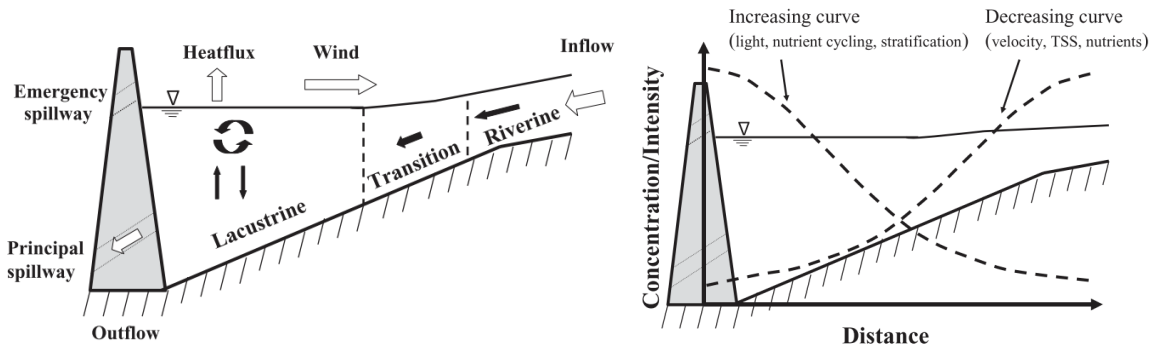

Figure 2-2. Main longitudinal zones of a reservoir (left) and longitudinal distribution of hydro-dynamic and water quality variables (Ji, 2008).

Primary producers (autotrophs) create organic matter from inorganic matter, using solar radiation as an energy source. In most reservoirs, phosphorus and nitrogen are the main nutrients limiting productivity. These nutrients are rapidly removed assimilated from the water phase by attaching to sediments in much higher concentrations than those present in the water (Morris & Fan, 1998).

A large part of the organic matter and nutrients present in the reservoir are particulates, undergoing the same sedimentation process as suspended sediments. Suspended organic matter is subjected to physical processes and settles, usually forming a gradient, from upstream towards the dam. In some tropical reservoirs, nutrients are incorporated into the algae biomass, contributing to the sedimentation of organic matter, as these organisms die and settle to the bottom of the reservoir.

Reservoirs are closely linked to their contributing basins. Thus, the characteristics of this basin, such as land use, climate, and size, among others, directly or indirectly affect the water quality of these water bodies. A high drainage area to surface area ratio, DA/SA, usually indicates the potential for high nutrient and/or sediment loads reaching the reservoir (Sotiri et al., 2022).

Several factors determine the hydrodynamic conditions of reservoirs, including their morphometry (length, depth, volume, surface area), water inflows and outflows, their hydraulic residence time, and the occurrence of stratification. Water Residence time (RT), despite presenting different concepts in the literature, is commonly known as the average time that the water resides inside the reservoir (Bernardo, 2018), and is calculated as

$$RT = \frac{V}{Q} \tag{2-2}$$

where V is the reservoir volume, in m³, and Q is the average reservoir inflow, in m³/s. This is one of the main parameters for understanding reservoir processes. If the residence time is high, it is expected that processes such as internal mixing, stratification and nutrient flows will directly affect the water quality. In reservoirs with lower residence times, such as run-of-the-river reservoirs, it is expected that the processes are influenced more significantly by the inflow and advection.

2.2 LAKE AND RESERVOIR MODELING

Modeling lakes and reservoirs can be accomplished by zero, one-, two-, and three-dimensional models. The definition of which model to use should be based on the processes prevailing and the objectives of the model. Becker et al. (2023) compared a 0D and a 3D model for a reservoir in Brazil. Their results show that simplified numerical schemes can be potential tools for initial analysis of water dynamics. An overview of these models and their considerations is presented in Table 2-1.

Zero-dimensional models are the result of averaging over the entire volume of the system. For transport models, it is the basis for input-output water quality models (Martin & Mccutcheon, 1999). The Bathtub model is an example of a zero-dimensional, steady-state model that simulates water quality problems related to eutrophication in lakes and reservoirs (total phosphorus, total nitrogen, chlorophyll-a, water transparency, and oxygen depletion) using empirical relationships (Nadim et al., 2007). In Brazil,

Becker et al. (2023) developed a zero-dimensional water quality model for the Paranapanema reservoirs that showed goods results in comparison with more complex models.

One-dimensional models (averaged over the longitudinal and transversal directions) have been widely used to simulate thermal structures in reservoirs, identification of mixing periods, and coupled with water quality models (Martin & Mccutcheon (1999); Weinberger & Vetter (2012)). The MTCR-1 model (Polli & Bleninger, 2019) is a one-dimensional (vertical) heat transport model that assumes homogeneity in the horizontal direction. The GLM (General Lake Model) is a hydrodynamic model that simulates vertical stratification (Hipsey et al., 2019) and is suitable for simulations in water bodies with little horizontal variability. The GLM model can be coupled with ecological models to perform modeling of water quality and ecological processes. The GLM model can be coupled with the FABM model (Framework for Aquatic Biogeochemical Models), in which turbidity, dissolved oxygen, nutrients, phytoplankton, zooplankton, pathogens, and chemical variables can be simulated (Hipsey et al., 2019).

Two-dimensional models averaged over the cross-section simulate water quality changes in the longitudinal and vertical directions (Martin & Mccutcheon, 1999). These models are applicable in reservoirs that exhibit thermal stratification and whose lateral variations can be neglected (Martin & Mccutcheon, 1999). The CE-QUAL-W2 model is a hydrodynamic and water quality model for rivers, lakes, reservoirs, and estuaries. The model assumes lateral homogeneity and is therefore suitable for narrow and long water bodies that have longitudinal and vertical gradients (Cole & Wells, 2013). It simulates basic eutrophication-related processes such as temperature (Zouabi-Aloui & Gueddari (2014); Bonalumi et al. (2012)), nutrients, algae, dissolved oxygen, organic matter, and sediment relationships (Cole & Wells, 2013).

However, all above models assume none or small horizontal changes over the entire reservoir, thus have strong limitations whenever horizontal variations exist. This is the case for non-uniform wind forcing, heterogeneous distributions of point-sources (Goulart et al., 2024) but especially considering partial coverage as it is the case for FPVs. In those cases, three-dimensional models are necessary to represent all processes adequately. Three-dimensional models solve the continuity, quantity of motion, and transport equations in all three dimensions. Delft3D is a three-dimensional model widely used in solving problems related to reservoirs and thermal stratification (Soulignac et al. (2017); Wahl & Peeters (2014); Smits et al. (2009)) and water quality (Smits et al., 2009). The Delft3D-FLOW hydrodynamic module simulates two-dimensional (vertically averaged) and three-dimensional unsteady flow and transport due to meteorological forcing and includes density effects (due to temperature and salinity). The FLOW module also includes suspended sediment transport. The water quality (WAQ) module allows the simulation of various substances, such as nutrients, dissolved oxygen, and micropollutants (Deltares, 2025b). The PART module simulates transport and simple water quality processes by the particle tracking method (Deltares, 2025a).

Table 2-1. Models for simulating water quality in reservoirs.

Model	zero-dimensional	one-dimensional	two-dimensional	three-dimensional
Equation	empirical relationships	Transport	RANS+ transport	RANS+ transport
Simplifications	Average in volume	Horizontal homogeneity	Lateral homogeneity; Hydrostatic and Boussinesq approaches	Hydrostatic and Boussinesq approaches
Discretization	-	Finite differences or finite volumes	Finite differences	Finite differences
Grid	Allows segmentation of the water body	Staggered	Staggered	Staggered
Coordinates	Cartesian	Cartesian	Cartesian	Cartesian/Spherical
Turbulence model	-	In general, a function of Richardson number; some models adopt the k-ε model	Nickuradase formulations; Parabolic, W2, W2 with Nickuradase mixing length, RNG, k-ε	Constant coefficient; Algebraic equation; k-L turbulence model; k-ε model.
Heat flux model	-	Parameterized or calculated term by term; solar radiation absorbed at the depth of the water column	Parameterized or calculated term by term; solar radiation absorbed at the depth of the water column	Calculated term by term; solar radiation absorbed at the depth of the water column
Light Extinction/ Secchi depth	Constant	Constant	Constant	Constant
Heat transfer in the sediment	-	Not considered	Considered	Not considered
Water Quality	Total phosphorus, total nitrogen, chlorophyll-a, water transparency, and oxygen depletion	Turbidity, dissolved oxygen, nutrients, phytoplankton, zooplankton, pathogens, and chemical variables	Temperature, nutrients, algae, dissolved oxygen, organic matter, and sediment relationships	Temperature, nutrients, dissolved oxygen, and micropollutants

3 FLOATING PHOTOVOLTAIC SYSTEMS

Floating photovoltaic systems gained ground on the world market mainly after 2010, although a few small systems appeared from 2007 onwards. The first FPV was built in 2007 in Aichi, Japan, followed by several other countries, including France, Italy, Korea, Spain and the United States. All tested small-scale systems for research and demonstration purposes. The first commercial installation (175 kWp) appeared in California in 2008, and floats on a reservoir of approximately 0.4 ha, in conjunction with solar panels arranged on land (Trapani & Redón Santafé, 2015). The initial aim was not only to generate energy, but also to avoid land occupation. Medium to large systems (larger than 1 MWp) began to emerge in 2013 and, after an initial wave of deployment concentrated in Japan, Korea and the United States, the FPV market has spread to China (now the leader), Germany, Australia, Brazil, among others. Nobre et al. (2024) spotted 643 FPV power plants across the globe, in 28 countries, mainly concentrated in Asia.

Floating systems have been used in Brazil but on a much smaller scale. One of the factors justifying the lack of use of FPV in Brazil is the high availability of land and its low cost, close to the places where the energy generated is consumed, especially in regions with the highest solar irradiation (Empresa de pesquisa energética - EPE, 2021). According to EPE (2021), this type of technology will begin to be more widely used in this country when costs decrease compared to land-based systems.

As exemplified above, FPV have emerged as an alternative way of eliminating the need to use large areas of land. According to YSG Solar (2022), the five largest plants in the world today are:

1. Dezhou Dingzhuang Floating Solar Farm (320 MW), China (Figure 3-1);
2. Three Gorges New Energy Floating Solar System (150 MW), China (Figure 3-2);
3. CECEP Floating Solar farm (70 MW), China (Figure 3-3);
4. Sembcorp Floating Solar Farm (60 MW), Singapore (Figure 3-4);
5. Sirindhorn Dam Floating Solar farm (45 MW), Thailand (Figure 3-5).

Figure 3-1. Dezhou Dingzhuang Floating Solar Farm, China (YSG Solar, 2022).

Figure 3-2. Three Gorges New Energy Floating Solar Farm, China (YSG Solar, 2022).

Figure 3-3. CECEP Floating Solar Farm, China (YSG Solar, 2022).

Figure 3-4. Sembcorp Floating Solar Farm, Singapore (YSG Solar, 2022).

Figure 3-5. Sirindhorn Dam Floating Solar Farm, Thailand (YSG Solar, 2022).

In Brazil, despite the great potential in terms of available area, there are still only small systems and few of them. According to EPE (2020), Brazil has 36,271 km² of available area, in 299 water bodies. Using 1%, 5% and 10% of this area, it would have 36, 181 and 363 GWp of power, and the energy delivered would be 58, 290 and 581 TWh/year, respectively. The forecast is that Brazil could reach 4.5 TWh/year, according to the National Energy Plan (PNE) 2050. This potential would supply almost 1% of the country's consumption for an entire year, using the 474.2 TWh consumed in 2020 as a reference, according to data from the Energy Research Company (EPE).

In the state of Paraná (Brazil), there are currently two FPV in operation. One of them is the pilot plant in the Passaúna Reservoir, located in the western portion of the city of Curitiba, that opened in 2019 with 396 modules and a maximum capacity of 130 kWp, covering an area of approximately 1,200 m² (SANEPAR, 2021). The forecast is for expansion of up to 5 MWp in this or other of Sanepar's reservoirs in the short term. Recently, another FPV plant was inaugurated in the reservoir of the Santa Clara Hydroelectric Plant[1], between the cities of Candói and Pinhão, consisting of 276 photovoltaic modules, with an installed power of 100 kWp, occupying an area of 1,100 m².

The floating photovoltaic plant in the Passaúna reservoir is still a small experimental system. However, as the reservoir is used for public supply, if there is an expansion of the photovoltaic plant area, the Collection Station's pumping system will be able to take advantage of the energy generated, thus adding environmental and sanitation management benefits.

According to EPE (2021), the main FPVs in Brazil are to be found:

- at the Sobradinho hydropower reservoir, in the state of Bahia, on the São Francisco River, with 11,000 m², 3,792 modules, and a capacity at the end of the project (2020) of 2.5 MWp;

[1] https://mestrado.lactec.com.br/dissertacoes/395-sistema-de-monitoramento-para-a-integracao-de-diferentes-dispositivos-eletronicos-de-uma-planta-solar-fotovoltaica-flutuante-instalada-na-uhe-santa-clara-pr/

- at the Passaúna reservoir, in the state of Paraná, with 1,200 m², 396 photovoltaic modules and a capacity of 130 kWp, with plans to expand it to 5 MWp;
- at the Santa Clara hydroelectric plant reservoir, with 1,100 m², 276 photovoltaic modules and a capacity of 100.7 KWp.
- by 2024, the FPV Araucária was installed at Billings reservoir, in the state of São Paulo, with 10,500 modules and 5MW 50,000 m² of coverage area. This is the largest FPV system in Brazil (CETESB, 2024; SEMIL (2024)).

Figure 3-6 – FPV power plant on the Billings reservoir, São Paulo/Brazil.

As of early 2024, Germany had an operational FPV capacity of around 21 megawatts (MW), with another 62 MW either approved or under development. In October 2024, the country launched its largest floating PV system on Philippsee Lake in southern Germany. This facility, covering 8 ha, consists of 27,160 solar modules and has a total capacity of 15 MW. It is anticipated to produce around 16 million kilowatts of electricity each year. The location is Bad Schönborn, Baden-Württemberg (Roider, 2024).

Figure 3-7 – FPV system on Philippsee, Bad Schönborn, state of Baden-Württemberg – Germany (Roider, 2024).

3.1 ENVIRONMENTAL IMPACTS OF FPVS

FPVs can impact on the aquatic system during the assembly and installation phases and, above all, during the system's useful life. Among the main impacts are the blocking or limitation of sunlight, changes in ecosystems, reduction in photosynthesis, changes in currents and wind patterns, reduction in evaporation, leaching of substances/heavy metals and, consequently, changes in water quality (Mathijssen et al., 2020). The environmental impacts depend on the dimensions, design, and proportions of the system in relation to the size of the lake/reservoir, as well as the characteristics of the aquatic system (currents, mixing, temperature profile) and climatic conditions.

There are currently few studies quantifying these impacts on the aquatic environment. This is because this technology has only recently begun to be used on the market. However, there are studies that have already addressed some of these impacts for other types of floating structures, for example, floating houses (Lenz, 2018), docks (Alexander & Robinson, 2006) and other structures (de Lima et al. (2021)).

Blocking or decreasing solar radiation and reducing wind shear at the water surface can cause changes in water quality, in terms of dissolved oxygen, nutrients and algae, and physical changes, such as reduced evaporation, temperature, luminosity and changes in circulation patterns and stratification conditions. As a result, behavioral changes can occur in the local fauna with the creation of new niches. For example, low concentrations of dissolved oxygen cause an unbalanced ecosystem, with fish mortality, odors and other aesthetic nuisances. When oxygen concentrations are reduced, aquatic animals are forced to alter their breathing patterns or decrease their level of activity (COX, 2003). pH is also an important parameter, as it influences various naturally occurring chemical balances, contributing to the precipitation of toxic chemical elements, such as heavy metals, and can have an effect on nutrient solubility. The criteria for protecting aquatic life set the pH between 6 and 9 (Stumm & Morgan, 1996).

Water temperature is one of the parameters with the greatest influence on aquatic life and systems (Cathcart & Wheaton, 1987). It can influence physical, chemical and biological processes, such as circulation patterns, oxygen concentrations and fish growth and mortality. In addition, various biological conditions are linked to the river thermal regime (Benyahya et al., 2007). Nitrogen can occur in the forms of organic nitrogen, ammonia, nitrite and nitrate in water bodies (ANA, 2022) and contributes to the phenomenon of eutrophication (excessive algae growth) along with other nutrients such as phosphorus. This phenomenon can harm public supply, recreation and the preservation of aquatic life.

Changes in the circulation pattern and mixing within a reservoir can lead to changes in suspended solids concentrations. Suspended solids are ubiquitous pollutants in water and cause significant environmental damage as well as economic costs (Clark et al., 1985). The most ecologically significant and visual impact of suspended sediment is optical: the reduced transmission of light through water/light attenuation. The attenuation of light by suspended matter has two main types of biotic effects:

reduced penetration of light into the water for photosynthesis and reduced visual range of sighted organisms (Vogel & Beauchamp, 1999).

Several review studies have been conducted about the environmental impacts resulting from the installation and use of FPVs, which brought together the main research and results to date on the subject (Gonçalves et al., 2025, Rocha et al., 2024). According to them, studies on the environmental impacts of FPVs have only emerged since 2013, with high growth in recent years. Currently, most of the research on environmental impacts related to FPVs is concentrated in temperate regions with a low coverage of countries (only ten countries have published on the subject). Two important studies in tropical climates have been done: one on the Tucutu Reservoir in Pernambuco, Brazil (da Costa & da Silva, 2021), and the other in Indonesia, an on-site analysis of Lake Mahoni (Andini et al., 2022). Of the studies analyzed, most mention some kind of impact on the physical environment (48%), followed by the chemical environment (31%), and the least studied environment was the biotic (24%).

Due to the low number of studies - some parameters were analyzed in only one article - the evidence of changes is still weak and further research is needed. Regarding the physical environment parameters, water temperature and evaporation are the predominant parameters, being analyzed in 34.4% and 31% of the studies analyzed, respectively, in which all observed a reduction in the value of both. The Suspended Solids and Irradiation parameters were mentioned in approximately 7% of the studies, and a reduction in their concentration and incidence was also observed. Next, the parameters of Wind Speed, Dissolved Solids, Diffusivity and Magnetic Field are present in only 3% (a single article) of the studies analyzed.

Regarding the chemical environment, the most analyzed parameter was oxygen concentration, which was present in approximately 20% of the studies. There was a convergence of results, with all the studies that investigated oxygen concentration observing a reduction in its value. The parameters pH and concentration of biochemical oxygen demand were investigated in 7% of the articles, which also found a reduction. As for phosphorus, there was a divergence between the results, as two studies found an increase in the concentration of the parameter and another a decrease. The other parameters such as silicate, nitrate, nitrogen and ammoniacal nitrogen were analyzed in only one study each. The most commonly analyzed parameters in the biotic environment were biomass and chlorophyll (14 % and 10 % of the studies consulted, respectively), both of which were always found to be decreasing in value. About eutrophication, two studies (7%) mentioned a reduction. Two studies analyzed changes in aquaculture production following the installation of FPVs in farm ponds, one of which found an increase in production and the other a decrease.

Wei et al. (2025) carried out an interdisciplinary review of the literature on the environmental impacts of FPVs. Among the studies discussed are the effects on sediments, due to their resuspension because of the anchoring systems (Hooper et al., 2021). The restriction of gas exchange between water and air is also highlighted (H. M. Pouran et al., 2022). However, the impacts depend on the design of

the system, as well as the meteorological and hydrological conditions of the site (Hooper et al., 2021). One well-established impact is the reduction in evaporation due to the presence of FPVs (Pouran et al. (2022), Soltani et al. (2022) Lopes et al. (2020)). Scavo et al. (2020) made a comparison between models and measurements, achieving errors of less than 5%.

As for water quality, few studies involve in situ measurements. Lima et al. (2021) carried out measurements at Bomhofsplas lake in the Netherlands. The FPV covers an area of 18.25 ha, approximately 30% of the lake. The measurements focused on dissolved oxygen and water temperature, where they observed little variation between the areas with and without FPV. In both parameters, less variation was observed along the water column below the panels.

3.2 FPV MODELING

Another approach to studying the effects of floating photovoltaic systems is based on modeling the hydrodynamic and water quality conditions in lakes and reservoirs, simulating the presence of the module cover at the air-water interface. An example of an application is the study conducted in the Rapel reservoir in Chile, in which Haas et al. (2020) used three-dimensional numerical modeling with ELCOM-CAEDYM (Estuary, Lake, and Coastal Ocean Model - Computational Aquatic Ecosystem Dynamics Model), observing the growth of algae through the concentration of Chlorophyll-a with different percentages of coverage by modules. They represented the FPV in the model by reducing the incident radiation. The results showed that a cover of less than 40% of the reservoir had no significant effect on algae growth, while values above 60% resulted in their eradication. Coverage ranging from 40% to 60% proved ideal, allowing for controlled development. This study also considered the revenue generated by the hydroelectric plant, as the modules need to raise the minimum water level in the reservoir to prevent them from running aground. The results showed that coverage above 60% generates significant losses in hydroelectric power generation due to the need to maintain a higher minimum water level in the reservoir, reducing the flow used in power generation and increasing the flow through the spillway.

Abdelgaied et al. (2023) observed that covering shallow areas of Lake Nasser in Egypt was efficient and economical regarding water evaporation in the reservoir. Evaporation estimates were made using aerodynamic methods, using the Harbeck equation (Rosenberry et al., 2007). This study considered coverages of 25%, 50%, 75% and 100% of the reservoir, and estimated the volumes of water that would be maintained due to the reduction in evaporation and the energy produced by the modules, in each of the scenarios. The FPV was represented considering the irradiation balance due to the coverage. The study indicated that the use of FPVs can help increase water availability and energy production, especially in arid and semi-arid regions.

Scavo et al. (2020) analyzed Lake Lentini in Italy using evaporation models such as Penman-Monteith (1948), Valiantzas (2006), Hargreaves & Allen (2003) and others, and proposed evaporation models based on linear regression and design of experiments (DoE) methods. The results showed that

not only did the percentage of surface covered influence the amount of water evaporation, but also that the characteristics of the floating arrangement are of significant relevance. In addition, with an optimized arrangement, i.e. positioned in areas of greatest evaporation and with the right spacing, it is possible to reduce evaporation by up to 49% with 30% of the reservoir surface covered.

Exley et al. (2021) studied the potential effects of installing an FPV on Lake Windemere in England. Using the MyLake model (Saloranta & Andersen, 2004), they simulated scenarios varying the coverage of the modules from 0 to 100% of the lake surface, based on a reduction in incident radiation and wind speed. Their results did not show a linear variation, being dependent on the design of the system and the coverage. However, most of them showed a reduction in water temperature and a reduction in thermal stratification.

Using the Xiangjiaba reservoir (China) as a case study, Ji et al. (2022) studied the potential impact of installing a floating system in the lake area. Using the CE-QUAL-W2 model and applying reductions in incident radiation and wind speed, their results showed reductions in water temperature and relative stability of the water column.

Yang et al. (2022a) used ELCOM-CAEDYM to simulate a hypothetical installation of an FPV covering 30% of the Poyan Reservoir, in Singapore. The representation of FPV was made by a reduction of wind speed and incident radiation. They analyzed several water quality parameters, including dissolved oxygen, chlorophyll-a, total organic carbon, nitrogen, phosphorus, temperature and stability (Richardson number). After calibration with measured data on a pilot installation, the simulations showed an increase in the water column stability, reduced wind mixing and, consequently, reduced dissolved oxygen concentration.

Ilgen et al. (2023) recently quantified the impacts of an FPV on Lake Mainwald (Germany), assessing water temperature, energy balance and water column stratification. Using water temperature data measured over three months, they calibrated a hydrodynamic model of the lake with modules using GLM to simulate expansion scenarios, also representing the FPV by reducing wind speed and radiation. Their results showed less stratification during the summer, and the reduction in water temperature followed a non-linear relationship with the increase in panel coverage area.

Liu et al. (2024) have constructed a numerical model to reflect the water energy balance in open water and under FPV coverages based on measured data. The study was developed in Hauian, China, and was able to represent the energy balance characteristics with a correlation coefficient of 0.80.

Table 3-1 shows a summary of the cited studies, with the characteristics of the sites. Considering the research and methods mentioned above, the limitations in the way FPVs are represented are noticeable. One-dimensional modeling, although capable of representing stratification, disregards the hydrodynamics of lakes, which can have a significant influence on the effects of coverage. Two-dimensional vertical models disregard horizontal interactions, limiting the representation of the systems and thus their impact. Without representing lateral heat exchange, it is difficult to represent the real state

of water temperature throughout the area. Thus, developing a three-dimensional numerical model is still essential to gain a deeper understanding of heat transfer processes and to define the lateral extent of the FPV's impact more clearly (Liu et al., 2024).

In this study, a 3D modeling is proposed considering the meteorological variables varying in time and space, being able to apply the estimated reduction in wind speed and solar radiation reaching the water surface. The aim of this approach was to get as close to the reality of these structures as possible, since most floaters are not completely blocking the wind and the radiation reaching the water surface in the whole area of the systems.

In addition, two study areas were considered, one being a reservoir in a subtropical climate and the other a gravel pit lake in a temperate climate. These two environments have different characteristics, since one has the influence of surface water reaching its area, while the other has a predominantly groundwater contribution. The difference in climate may also impact the effects of the FPV since temperate climates have well-defined seasons, affecting the amount of rainfall and solar radiation incident on the lake, unlike subtropical climates.

.

Table 3-1. Studies involving modeling with floating photovoltaic systems.

Reference	Location	Lake area/volume	FPV: potential or existent	% covered area	Model used	Type of modeling	Water quality modeling	FPV representation	Calibration
Liu et al. (2024)	Huainan City (China)	4.5 km²	Existent	8,16%	-	Energy balance	No	Simulation of net heat flux with monitoring data	-
Ilgen et al. (2023)	Lake Maiwald (Germany)	0.4 km²	Existent	2,10%	General Lake Model (GLM)	1DV	No	Reduced incident radiation and wind speed	Calibrated with temperature data (3 months of measurements)
Q. Ji et al. (2022)	Xiangjiaba hydropower (China)	5.2 km²	Potential	0 a 100%	Ce-Qual-W2	2DV	No	Reduced incident radiation and wind speed	Based on pre-calibrated model
Yang et al. (2022b)	Tengeh and Poyan Reservoirs (Singapore)	1.4 km²	Installed / Hypothetical	0,7% / 30%	ELCOM-CAEDYM	3D	Yes	Surface fully covered (no space between panels – zero wind condition)	Measured data on prototype (1 ha)
Abdelgaied et al. (2023)	Lake Nasser (Egypt)	6500 km², 162 Mm³	Potential	25 a 100%	*bulk aerodynamic method* (estimativa de perdas por evaporação)	-	No	Irradiation balance	-
Exley et al. (2021)	Lake Windemere (England)	6.7 km²	Potential		MyLake	1DV	No	Reduced incident radiation and wind speed	-
Bontempo Scavo et al. (2020)	Lake Lentini (Italy)	12 km²	Potential	0 a 50%	Estimating evaporation losses	-	No	% covered area	-
Haas et al. (2020)	Rapel Reservoir (Chile)	400 Mm³	Potential	0 a 100%	ELCOM-CAEDYM	3D	Yes. Focus on Chlorophyll-a	Reduced incident radiation	Based on pre-calibrated model

4 MATERIALS AND METHODS

This thesis aimed to assess the influence of FPVs on the hydrodynamics, temperature and water quality of lakes and reservoirs. To this end, two case studies were used, in which field monitoring, data analysis and computer modeling were developed. This chapter presents the software used, as well as characterizing the two case studies and the monitoring and modelling strategies adopted.

4.1 HYDRODYNAMIC AND WATER QUALITY MODELING SOFTWARE

The model used was Delft3D®, software developed by Deltares. This is a multidimensional model (2D or 3D) that simulates hydrodynamics and transport phenomena of unsteady flows (Deltares, 2025a). It has a water quality module that simulates various components, from conservative substances to dissolved oxygen, BOD, nutrients, macrophytes, bacteria, and algae, among others.

The Delft3D-FLOW hydrodynamic module simulates unsteady, two-dimensional (vertically averaged) and/or three-dimensional flows, as well as the transport of constituents due to meteorological, tidal, and river discharge forces, including density effects resulting from temperature and salinity gradients, and sediment transport. This module provides the hydrodynamic conditions used by the other modules and is the first step in developing any simulation with the Delft3D program.

The equations that describe free-surface flows are based on fundamental physical conservation principles: conservation of mass (equation (4-1) and conservation of momentum (equations (4-2, (4-3, and (4-4). In addition, these flows are capable of transporting substances and/or thermal energy. Delft3D-FLOW simulates the transport of mass and heat using the advection-diffusion equation, presented in the next section (equation (4-5). The equations presented below correspond to the Reynolds-averaged Navier-Stokes equations (RANS), adapted for shallow water conditions and incorporating the incompressible flow and hydrostatic assumptions (Deltares, 2025a).

$$\frac{\partial u}{\partial x}+\frac{\partial v}{\partial y}+\frac{\partial w}{\partial z}=0 \tag{4-1}$$

$$\frac{\partial u}{\partial t}+u\frac{\partial u}{\partial x}+v\frac{\partial u}{\partial y}+w\frac{\partial u}{\partial z}-fv=g\frac{\partial H}{\partial x}-\frac{1}{\rho}\frac{\partial P}{\partial x}+v_H\left(\frac{\partial^2 u}{\partial x^2}+\frac{\partial^2 u}{\partial y^2}\right)+\frac{\partial}{\partial z}\left(v_V\frac{\partial u}{\partial z}\right) \tag{4-2}$$

$$\frac{\partial v}{\partial t}+u\frac{\partial v}{\partial x}+v\frac{\partial v}{\partial y}+w\frac{\partial v}{\partial z}+fu=g\frac{\partial H}{\partial y}-\frac{1}{\rho}\frac{\partial P}{\partial y}+v_H\left(\frac{\partial^2 v}{\partial x^2}+\frac{\partial^2 v}{\partial y^2}\right)+\frac{\partial}{\partial z}\left(v_V\frac{\partial v}{\partial z}\right) \tag{4-3}$$

$$\frac{\partial P}{\partial z}=\rho(x,y,z)g \tag{4-4}$$

Where x, z, and y are the spatial coordinates; t is the time; u, v, and w are the velocities in x, y, and z directions, respectively; f is the Coriolis parameter[2]; g is the acceleration due to gravity; H is

[2] Coriolis parameter is $f = 2\Omega \sin\theta$ where Ω is The rotation rate and θ is the latitude.

the water depth (m); P is the hydrostatic pressure; v_H and v_V are the horizontal and vertical eddy viscosity, respectively.

4.1.1 HYDRODYNAMIC MODEL SETUP

To perform a simulation in the Delft3D model, a series of settings are required. A flowchart of the model setup is presented in Figure 4-1, and the main components are explained as following.

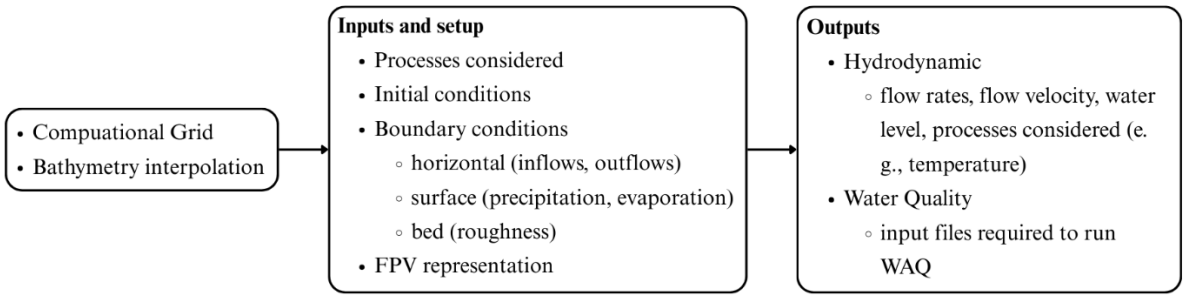

Figure 4-1. Flowchart of the hydrodynamic model setup.

- Computational grid

To solve the governing equations, the study area must be covered by a computational grid, assumed to be orthogonal and well-structured. The model supports two types of vertical coordinates: σ-grid (boundary-fitted) and Z-grid (strictly horizontal). In the first type, the number of vertical layers is constant throughout the domain, regardless of the depth of the water column, so the layer thickness is not uniform. This type of grid is commonly used for near-bed area representations, such as sediment transport. The Z-grid features horizontal coordinate lines that remain almost parallel to density interfaces in areas with steep bottom slopes. This design helps minimize artificial mixing of scalar properties like salinity and temperature, which is important in this study. Therefore, the Z-grid is used.

Once the computational grid has been defined, the bathymetry within it is interpolated using the grid cell averaging method. This is an iterative process in which grid configurations and bathymetry interpolations are tested until a stable and representative model is obtained.

- Processes modeled

Among the processes available in the hydrodynamic model, this study considered the Wind and Temperature processes. It is therefore necessary to provide basic parameters for the simulation.

In the case of wind, the wind drag coefficients must be provided, as well as the timeseries for wind speed and direction. For temperature modeling, there are five heat transfer models available. In this study, the Ocean model was used, which has been calibrated for the North Sea and has been successfully applied to large lakes (Deltares, 2025a). Input data includes Secchi depth, Dalton number for evaporative heat flux, Stanton number for heat convection, and time series of relative humidity, air temperature, cloud cover and solar radiation.

- Initial conditions

Initial conditions can be constant values, map files, initial condition files (with water level, velocities in the x and y directions, and the variables dependent on the processes considered, such as temperature), or previous simulation results (restart-files). In this study, constant initial conditions were used and the model's warm-up period was analyzed.

- Boundary conditions and Source and Sink terms

The model allows the use of horizontal boundary conditions, which can be discharge data, water level, current, among others. It is also possible to insert flow inputs or sinks into the model by means of discharges. In this study, both options were used and will be indicated in each case study.

With regard to bed boundary conditions, the roughness formulas available are Manning, Chezy, White-Colebrook, and Z0. In this study, Manning was used for both models.

In terms of surface boundary conditions, the processes of evaporation and precipitation were included. Precipitation rate and rain temperature data are required, while evaporation rate can be entered as an input or calculated by the model. This study considers the effects of cells on evaporation, so the option of calculating evaporation was used. This processes are added in the additional parameters section.

- FPV representation

There are two possible ways of representing FPVs in this model: by means of floating structures (available in the software) and by means of time series files with spatial variation in weather conditions (e.g. solar radiation and wind).

In the hydrodynamic module, it is possible to include floating structures (Figure 4-2) positioned in cells of the computational grid. It is possible to change the position and height (H-h in the figure) underwater of this floating structure in order to achieve the best representation of the system. Delft3D understands that this structure alters evaporation E (disregarding it in the covered region) and the action of wind W in the covered region (disregarding its effects). However, it does not alter the effects of precipitation P, with the water being infiltrated on site, nor the formation of vertical turbulence, and there is no friction between the structure and the runoff (DELTARES, 2025a). These conditions were considered sufficient to simulate the presence of the modules in a water body, despite being a conservative approach. However, this approach is not compatible with the water quality module.

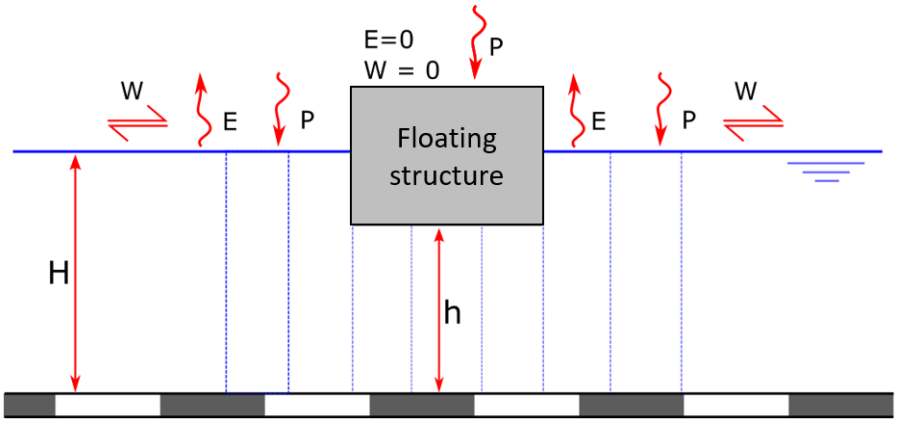

Figure 4-2. Schematic figure on the interpretation of the Delft3D software and floating structures. E: evaporation, P: precipitation, W: friction and wind speed, H: height of the water column, h: height of the water column below the structure.

Another option is to define files of meteorological forces (air temperature, cloudiness, solar radiation, relative humidity, wind speed) varying in time and space to represent the floating system (Figure 4-3). Based on observed values of the variables, this reduction can be applied to the region of the FPV, like the example of solar radiation on Figure 4-4. These inputs must be built with some offline program (in this study, a python script was used) and added as additional parameters in the model setup. See Delft3D Flow User Manual for detailed information (Deltares, 2025a).

Considering that most FPV array designs do not fully cover the surface of the water in the area of the structure, the latter approach is considered to be closer to reality. It was therefore decided to use these spatialized files to conduct the simulations in this study.

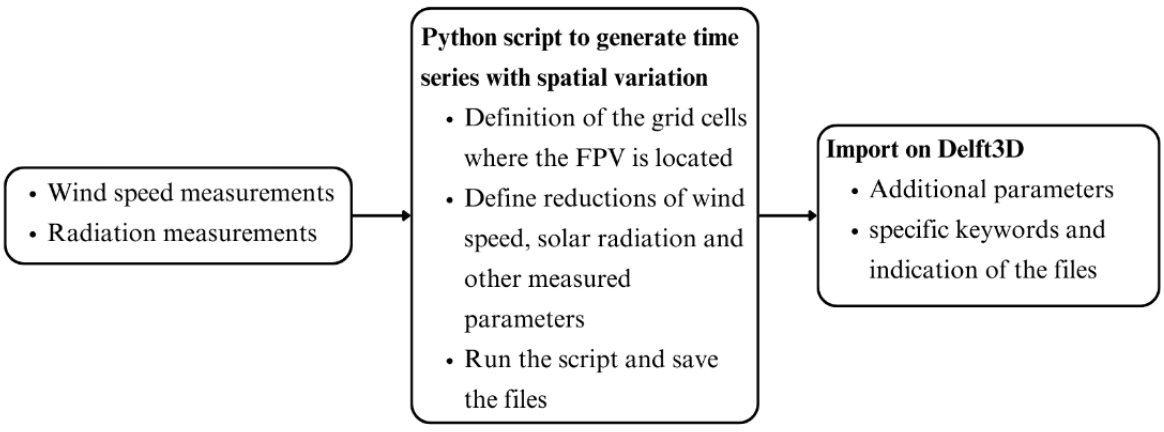

Figure 4-3. Flowchart of the implementation of FPV coverage in the hydrodynamic module of Delft3D.

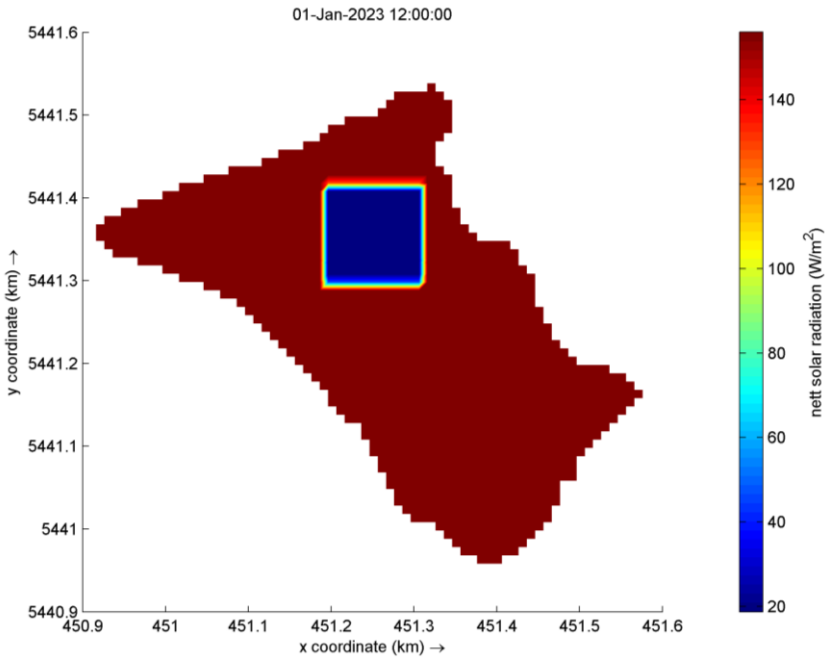

Figure 4-4. Solar radiation time- and space-varying input of Delft3D-FLOW, showing an specific time as example. The region of FPV is the one in blue, with lower radiation.

4.1.2 WATER QUALITY MODEL SETUP

The water quality module is available on the same interface, but has different configurations to the hydrodynamic one. A flowchart is shown in Figure 4-5 and the items are detailed below.

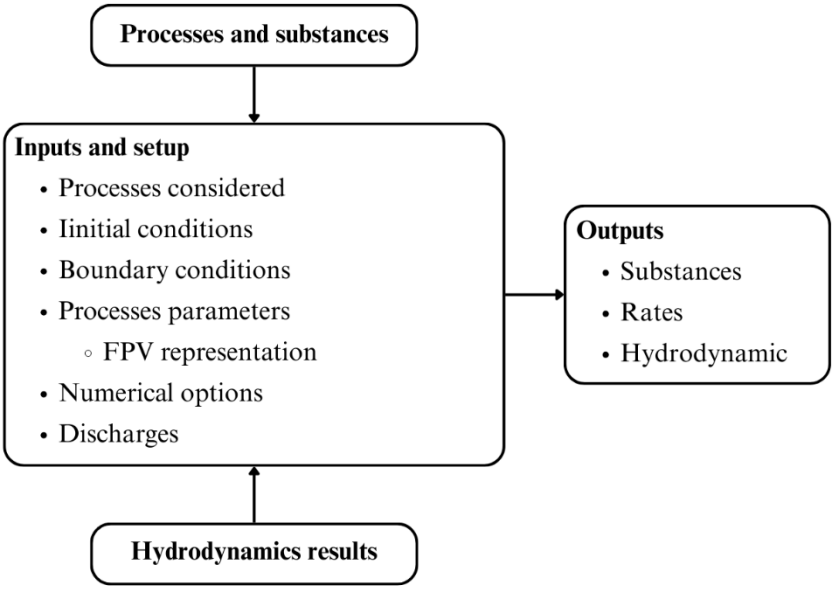

Figure 4-5. Flowchart of the water quality model setup.

- Computational grid

To configure the water quality model, the results of the hydrodynamic model must first be coupled. By importing the files exported in the previous module, the water quality model incorporates

the computational grid, water levels, flows and velocities, among other parameters. There is an aggregation option for the grid, in which the horizontal and/or vertical resolution can be changed for the quality model, but this was not used in this study. Therefore, the computational grid is the same as that used in the hydrodynamic module.

- Processes and substances

The water quality substances available are wide-ranging and include tracers (conservative and decaying), dissolved oxygen, nutrients (such as phosphorus and nitrogen), bacteria, algae, metals, vegetation, among others. It is a two- or three-dimensional model used to represent water quality in natural and artificial environments, by solving the advection-diffusion-reaction equations (eq. (4-5)) for a computational grid predefined by Delft3D-FLOW (Deltares, 2025b).

$$\frac{\partial C}{\partial t} + v_x \frac{\partial C}{\partial x} - D_x \frac{\partial^2 C}{\partial x^2} + v_y \frac{\partial C}{\partial y} - D_y \frac{\partial^2 C}{\partial y^2} + v_z \frac{\partial C}{\partial z} - D_z \frac{\partial^2 C}{\partial z^2} = S + f_R(C,t) \quad (4\text{-}5)$$

Where C is the concentration of a substance; t is the time; v is the velocity in x, y, and z directions; D is the dispersion coefficient in x, y, and z directions; S are the discharges or loads (additional inflows of water or mass that are not present in the hydrodynamic module); and f_R are the reaction terms (processes).

Depending on the substances desired, it is possible to select the processes to be considered or not in the model. The software has two groups, BLOOM (ECO) and DYNAMO (WAQ), which differ in how algae are considered (Deltares, 2025b). As algae were not considered in this study, the details of each option will not be explored, it is only indicated that ECO was used in order to complement the model in future stages. Detailed information can be checked in the user manual (Deltares, 2025b).

Water quality modeling, however, is a multi-parameter problem, where even calibrated models may have limitations in doing clear cause-impact relationships. As an intermediate step, this thesis uses additional, innovative methods to improve the analysis of the effects of FPVs on transport and mixing (hydrodynamics) and relations to potential substance transport (water quality) by using concepts of residence time and tracers under the FPV.

This module allows to calculate the local residence time (**4-6**) in each computational cell, considering only the advective transport, derived from the hydrodynamic module (FLOW). In this study, a tracer was placed in a cell below the FPV, and released into the surface layer, to evaluate the overall transport and mixing characteristics.

$$RT = \frac{Volume}{\sum_{exchanges} |Flow|/2} \quad (4\text{-}6)$$

Where RT is the residence time, in s; Volume is the water volume of a segment (grid cell), in m^3; Flow is the water flow, in m^3/s.

In addition to the tracers, dissolved oxygen was modeled. A complete water quality model involves several substances, as well as complex physical and chemical processes that require a robust amount of data to feed them. In a simplified way, this study isolated the physical process of reaeration in order to assess the effects of FPV on this process. In other words, only water temperature and wind influence dissolved oxygen concentrations. No sources of oxygen consumption or production were considered. The reaeration rate is calculated from the following equations.

$$Rrear = klrear\ x\ {(Coxs - \max(Cox, 0.0))}/{H} \quad (4\text{-}7)$$

$$Coxs = (a - bT + (cT)^2 - (dT)^3) \quad (4\text{-}8)$$

$$klrear = klrear_{20}\ x\ tcrear^{(T-20)} \quad (4\text{-}9)$$

$$klrear_{20} = \left(\frac{a\ x\ v^b}{H^c}\right) + (d\ x\ W^2) \quad (4\text{-}10)$$

Where Rrear is the reaeration rate, in gO_2/m3/d; klrear is the reaeration transfer coefficient in water, in 1/d; Coxs is the saturation concentration of dissolved oxygen, in gO_2/m^3; Cox is the actual dissolved oxygen concentration, in gO_2/m3; H is the depth of water column, in m; a, b, c and d are coefficients with different values for each reaeration option; T is the water temperature, in °C; $klrear_{20}$ is the reaeration transfer coefficient at reference temperature 20°C, in m/d; tcrear is the temperature coefficient for the transfer coefficient; v is the flow velocity, in m/s; W is the wind speed at 10 m height, in m/s.

In this study, two reaeration options were chosen, since the environments are classified in different ways. One of them is characterized by a lake in a temperate climate, with no significant surface velocity, opting for a ratio of coefficients calibrated in studies of lakes in the Netherlands (Banks & Herrera (1977) apud Deltares (2025b)). In this case, the flow velocity is disregarded (b = 0).

The other case study involves a tropical lake, where the use of another formulation is recommended, which varies in relation to the dependence on wind speed and temperature, as well as including the effects of rain (Guérin et al. (2007) apud Deltares (2025b)).

$$klrear = \left(e\ x \exp(b_1\ x\ W^{b2}) + (c_1\ x\ P^{c2})\right)\ x\ f\ sc \quad (4\text{-}11)$$

$$fsc = \left(\frac{Sc}{Sc_{20}}\right)^{-0.67} \quad (4\text{-}12)$$

$$Sc = d_1 - d_2 xT + d_3 xT^2 - d_4 xT^3 \quad (4\text{-}13)$$

Where e, b1,b2, c1, c2 are coefficients; P is the precipitation, e.g. rainfall, in mm/h; fsc is a function of Schmidt number, where the temperature is taken into account. Detailed formulation can be checked in Deltares (2025b).

- Initial conditions

Initial conditions can be constant values or map files, or previous simulation results, as well as the hydrodynamic moule. In this study, constant initial conditions were used and the model's warm-up period was analyzed.

- Boundary conditions and Source and Sink terms

The model allows to import the boundary conditions from hydrodynamic model. However, concentration for every substance modeled should be designated to each boundary. In this study, besides the hydrodynamic ones, a discharge was placed below the FPV to place a tracer and analyze the mixing processes. The concentration of this tracer was high (10^5 kg/m³) and the flow rate was low (0.00001 m³/s) so it would not influence the hydrodynamics.

- Processes parameters and FPV representation

In the WAQ module, depending on the processes selected, several parameters must be defined. On this tab, the water temperature must be imported from the hydrodynamic results. For this study, it is also selected the formulation of reaeration, coefficients, and decayable rates.

It is also in this tab that the FVP representation is defined. Spatialized wind speed time series files must also be inserted here to represent the FPV. It should be noted that the spatialized files have different configurations for the hydrodynamic module and the water quality module. Therefore, new files were generated in a second python script and inserted into the wind speed parameter.

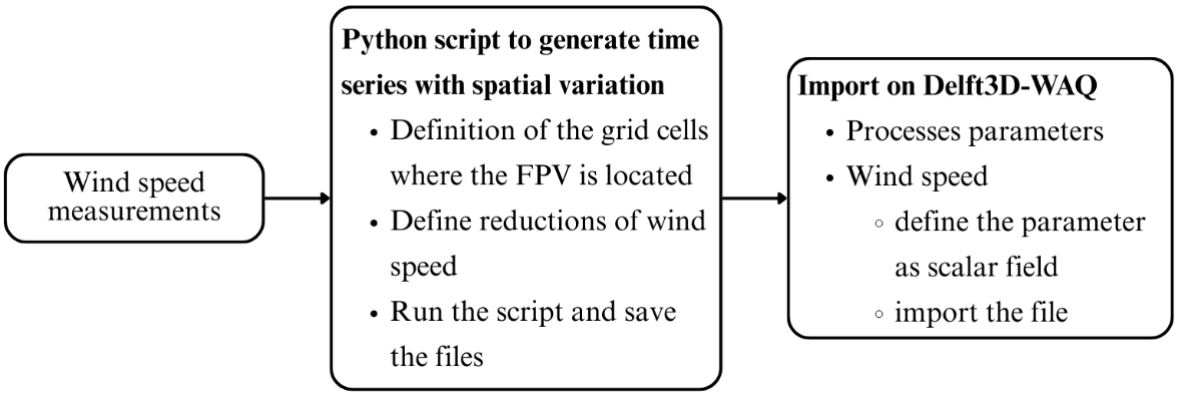

Figure 4-6. Flowchart of the implementation of FPV coverage in the water quality module of Delft3D.

4.2 CASE STUDIES

For the development of this research, two case studies were considered. In 2022, the FotoÁgua (SANEPAR, 2023) project began, focusing on the Passaúna reservoir in Brazil, which has a pilot FPV system installed. During this project, the thesis candidate took part in several field campaigns, in which surveys were carried out with mobile and fixed sensors and water was collected for laboratory analysis.

During a 12 month research stay at the KIT (Karlsruhe Institute of Technology, department of Water Quality Management, in Germany), field campaigns were also carried out to monitor a gravel pit lake with an operational FPV installation. Five field campaigns were carried out with mobile sensors, in addition to the installation of fixed temperature and dissolved oxygen sensors.

The aim of these two case studies was to investigate the impacts of FPV on water bodies with distinct characteristics, also set in different climatic conditions. More details on each case study are presented in the following sections.

4.2.1 FPV ON A GRAVEL PIT LAKE – LEIMERSHEIM, GERMANY

The gravel pit lake near Leimersheim (latitude 49.123, longitude 8.332) is located in southwestern Germany in the Upper Rhine Valley west of the Rhine River. The lake is one of several gravel pit lakes in the Upper Rhine Valley that are actively excavated. The FPV system (Solarpark) is in the northern part of the lake. The first part of the system, with a capacity of 750 kWp, was commissioned in autumn 2020, and the second part, with an additional 750 kWp, in autumn 2021. This procedure was prescribed by the German Renewable Energy Act, as at the time of construction only systems with an installed capacity of less than 750 kWp could be built without a tender.

The annual electric yield of the 1.5 MWp FPV system is 1.7 GWh, which is either transferred directly to the adjacent gravel plant or fed into the public grid. The gravel plant can thus cover 20-30% of its electricity consumption with the electricity from the FPV system. It consists of 3,744 modules arranged over 8% of the lake's total surface area of 19.5 ha (Figure 4-7). The mean lake depth is 9.3 m while the maximum depth is 19 m and the total lake volume is 1.7×10^6 m^3.

There are no tributaries reaching the lake, so the only contributions are groundwater and rain. The quarry is still in operation, and some of the water is removed for washing and returned to the shore, with its influence on the variation in the lake level being insignificant.

Figure 4-7. Gravel pit lake near Leimersheim, Germany (Source: Stephan Hilgert, LimKnow GmbH).

4.2.1.1 MONITORING STRATEGY

Regarding the meteorological effects, the FPV system is anticipated to decrease both the amount of irradiance reaching the lake and the near-surface wind speeds (Exley et al. (2021), Yang et al. (2022a), Ilgen et al. (2023)). Reducing irradiance could lead to less energy entering the lake, potentially lowering surface water temperatures and creating a more unstable thermal stratification. Conversely, reduced wind shear might result in a more stable thermal stratification with warmer water temperatures. Consequently, these opposing effects may influence the lake's mixing regime and are largely dependent on the design of the FPV system.

A monitoring setup was established to accurately measure these key factors and incorporate them into a model representing the FPV system. Figure 4-8 illustrates a climate station (WS510-UMB, Lufft) positioned at the northern boundary of the system. This station records global horizontal irradiance (GHI) (W/m²), wind speed (m/s) and direction (°), relative humidity (%), atmospheric pressure (hPa), and air temperature (°C).

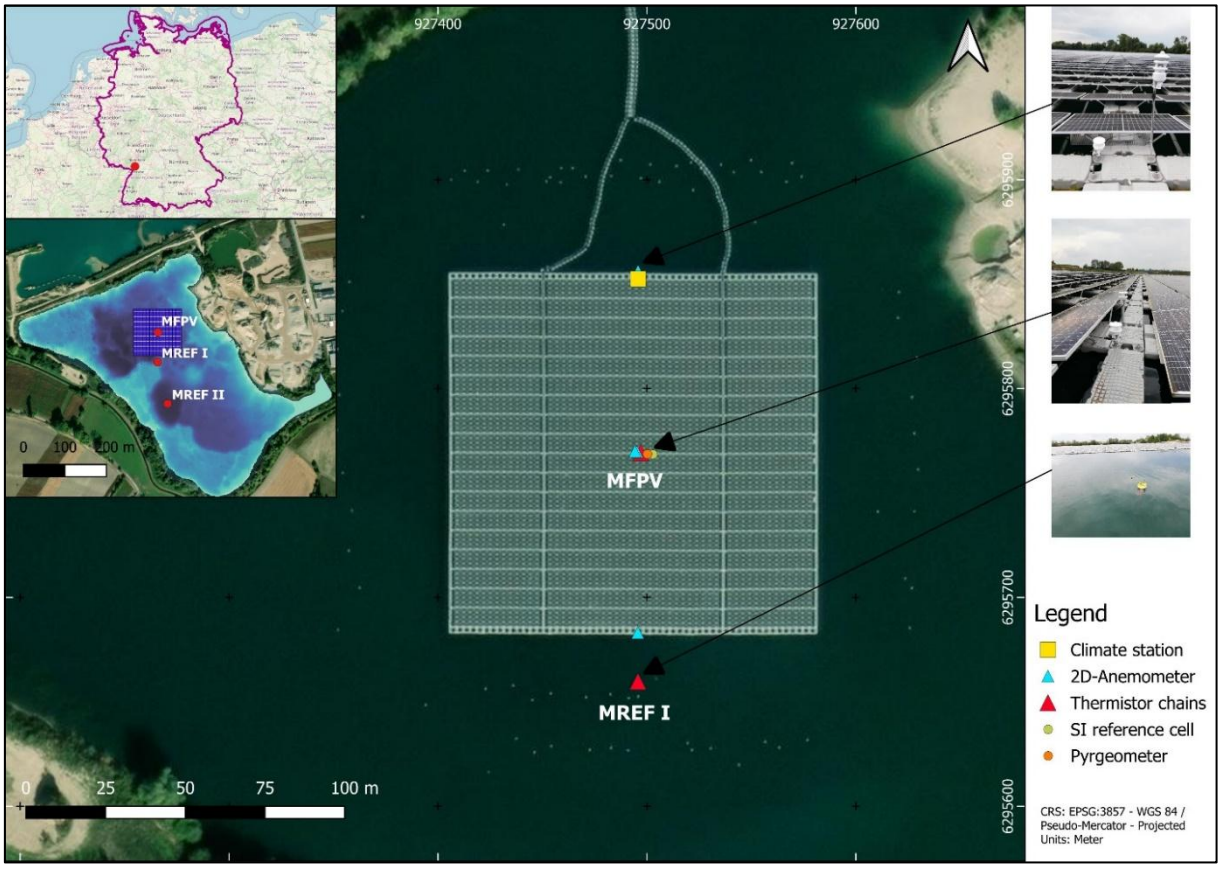

Figure 4-8. Climate station and monitoring points at the gravel pit lake (Ilgen et. al, 2025, APPENDIX B).

Additionally, 2D ultrasonic anemometers (WS200-UMB, Lufft) were placed at various locations, including the edges and center of the system, to measure near-surface wind speeds. The anemometers at the system's edges were positioned at the height of the upper edge of the solar panels, while the two central anemometers were set at different elevations: one above the top of the solar panel and the other as close to the water surface as feasible. These devices have a wind direction measurement accuracy of ±3° and a wind speed accuracy of ±0.3 m/s or ±3% within the 0-35 m/s range. By analyzing wind speeds at various heights, the impact of the FPV system on wind reduction could be assessed. Long-wave radiation measurements were taken at the system's center using a pyrgeometer (SGR3, Kipp & Zonen). A thermistor chain, measuring 10 meters in length with sensors spaced 50 cm apart, was used to record water temperatures at different depths at the FPV measurement point (MFPV). An additional chain was mounted on a buoy and deployed in open water at the reference point (MREF I). The thermistors had an accuracy of ±0.1°C.

The reduction in irradiance caused by the FPV system was calculated using the Radiance raytracing model (Ilgen et. al, 2025, APPENDIX B). Radiance is a commonly utilized tool for simulating how various objects affect the path of light from different sources. It accounts for specular, diffuse, and directional diffuse reflections and transmissions in any configuration, even with complex curved geometries (Ward, 1994). The model tracks light paths through image plane pixels and simulates

interactions with virtual objects, with highly customizable material properties. It produces outputs such as shading rates, light availability, and spatial distribution through a grid of virtual sensors. In photovoltaics, it is frequently applied in agrivoltaics alongside crop yield simulations.

Water quality was assessed using two YSI-EXO2 multiparameter probes during measurement campaigns at MFPV, MREF I, and MREF II (Figure 4-8). Measurements were taken at 1-meter depth intervals throughout the entire depth of each sampling site. The first set of measurements used in this study's statistical analysis was recorded on May 9, 2023, and the final set on July 9, 2024. Throughout the 14 months, measurements were collected on 17 different days, focusing on the vegetation and transitional periods of the mixing regime. During winter, measurements were taken regularly but at wider intervals due to isothermal conditions resulting from lake turnover, with little variation observed between winter readings. These measurements were analyzed statistically and combined with water temperature data from thermistor chains to calibrate the hydrodynamic model.

Two temperature and dissolved oxygen loggers (miniDOT, PME) were also deployed at MPFV and MREF I. Both loggers were placed at a 1-meter depth and set to record data every 15 minutes. The first data were recorded on September 5, 2023, and the final on January 9, 2024. The data from these loggers were analyzed statistically and compared with the YSI-EXO2 results and the modeling outcomes.

4.2.1.2 MODELING STRATEGY

Following the principal model setup strategy (item 4.1.1) a regular computational grid was created to represent the lake, using the Z-model (Deltares, 2025a). This grid had a resolution of 10 m x 10 m covering the lake area, with 20 vertical layers (Figure 4-9), defined after sensitivity analysis.

Initial conditions for the hydrodynamic and the water quality model were constant values. This lake had no horizontal boundary conditions, since it is a gravel pit lake with no tributaries. Although the quarry is still in operation, so that a quantity of water is removed for washing and returned to the lake, its influence is considered insignificant. As surface boundaries, precipitation and evaporation are considered. A tracer was placed below the FPV (MFPV point) at the surface to analyze the advection transport and local residence time. Further model parameters are specified at Table 7-1 and Table 7-2 on APPENDIX C.

Figure 4-9. Computational grid of the lake simulations, with 10 x 10m resolution, and location of the FPV (Solarpark). Satellite image from 2025.

Different lake cover scenarios were simulated. For the calibration, the actual FPV coverage of the lake was considered (8% of the total area) and the calibrated points were MFPV and MREFI. This calibration was based on temperature profile data and surface dissolved oxygen concentration (1 m below surface).

The scenarios considered were no cover (0), the current cover (8% of the lake area), 15% (maximum allowed by German legislation), 50% and 90%. The aim was mainly to assess changes in temperature, evaporation, and dissolved oxygen.

Table 4-1. Simulation scenarios for the gravel pit lake simulation.

Scenario	Coverage (%)	Coverage (area, ha)
0	0	0
8	8 (actual)	1.6
15	15 (expanded – maximum allowed in Germany)	2.9
30	50 (expanded)	9.7
90	90 (technical maximum)	17.5

Representation of FPVs in model setup

As described in chapter 4.1.1, files of meteorological forces varying in time and space were created to represent the floating system. Based on the observed values of reduction in wind speed and radiation, this reduction was applied to the region of the FPV, like shown in Figure 4-10. Files of air temperature, cloudiness, relative humidity, solar radiation, wind speed in x direction, and wind speed in y direction were made, with reduction coefficients only in the last three based on measurement results.

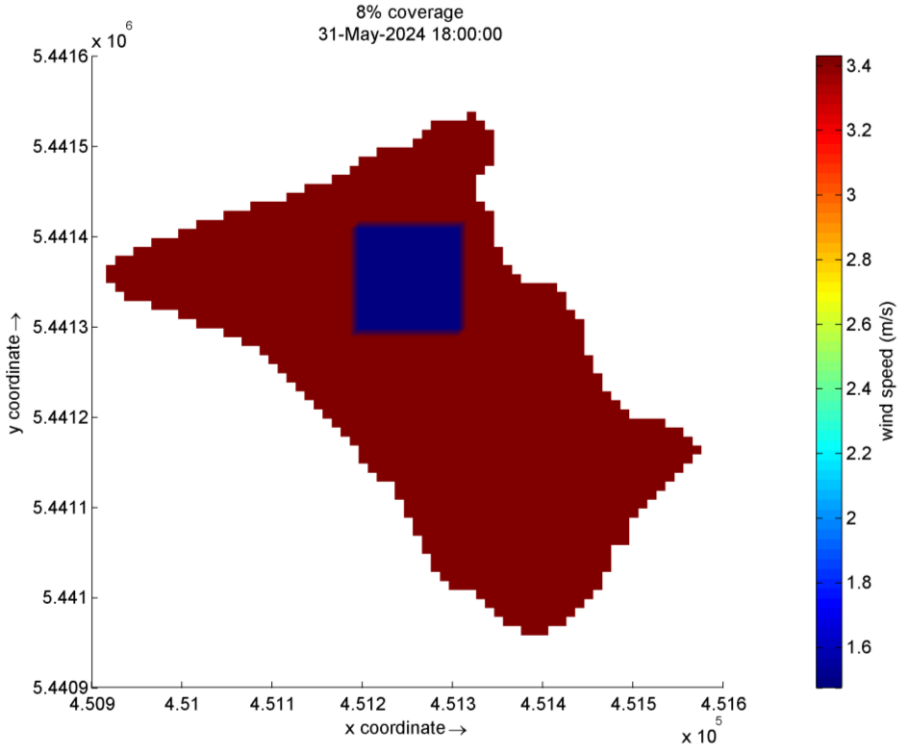

Figure 4-10. Wind speed time- and space-varying input of Delft3D-FLOW example for scenario 8 (8% coverage), here shown for May 31st at 6 p.m.

The modeling period spans from January 1, 2023, to June 30, 2024 for hydrodynamics, and from June 1st, 2023 to June 1st, 2024 for water quality modeling. For the time frame of January 1, 2023, to August 12, 2023, meteorological datasets from NASA's Prediction of Worldwide Energy Resources (POWER) project were used. POWER provides solar and meteorological data to meet the needs of sectors like agriculture, renewable energy, and energy-efficient buildings (NASA, 2023). From August 12, 2023, onwards until the end of the modeling period, meteorological data were sourced from the climate station installed on the FPV system. The variables used for the models include shortwave radiation, longwave radiation, air temperature, wind speed, wind direction, relative humidity, rain, and snow. Since no precipitation measurements were taken directly from the FPV system, data for rain and snow were obtained from a nearby climate station (ID: 05906) managed by the German Meteorological Service. Figure 4-11 displays the meteorological time series used as input for the models. The same station from the German Meteorological System only had monthly cloud cover data for a period prior

to the modeling. It was therefore decided to adopt monthly average values from this period of data. A wind rose is presented in Figure 4-12 to indicate the wind characteristics during the simulation period.

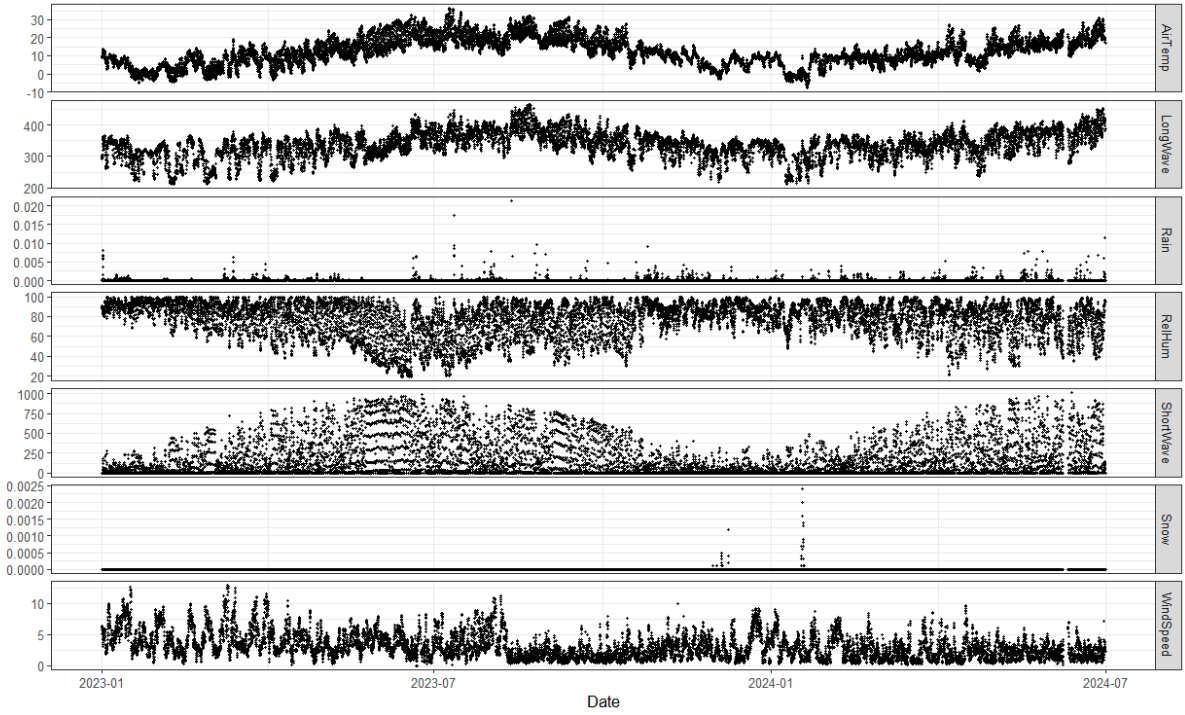

Figure 4-11. Meteorological time series that was used as input for the model.

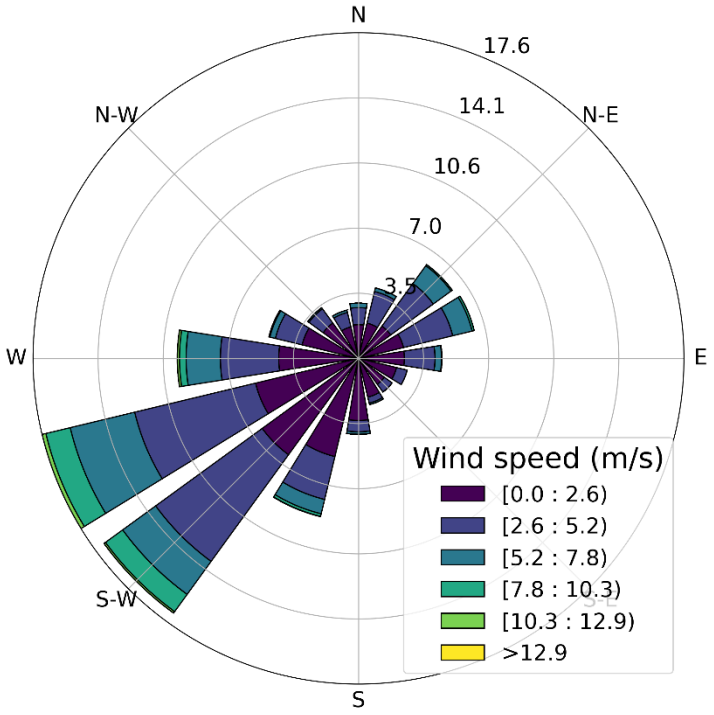

Figure 4-12. Wind rose of the simulation period.

4.2.2 FPV PILOT PLANT ON PASSAÚNA RESERVOIR – CURITIBA, BRAZIL

The Passaúna reservoir, is located in a humid subtropical climate region in the city of Curitiba, Brazil. This reservoir has approximately 9 km² of flooded area, with a maximum depth of 17.5 m and an average of 8.3 m, 59 hm³ of volume, and its main purpose is public drinking water supply (SANEPAR, 2023). Its estimated residence time is 292 days (Marcon et al., 2019). The average water intake, from 2020 to 2024, was 1.4 m³/s. The average river inflow (main tributary) is 1.5 m³/s, maximum 26.4 m³/s, and the average precipitation was 1426 mm/year for the same period. The watershed in which it is located covers approximately 152 km², with land use predominantly of forest remnants, cultivated areas, pastures, and urbanized regions.

Several studies have been conducted in this reservoir, involving sediment analysis (Sotiri et al., 2021) and phosphorus exchange between sediment and water (Carneiro et al., 2016), reservoir eutrophication modeling (Gobbi & Kruk, 2003), phosphorus load analysis from the catchment (Sotiri et al., 2022), as well as analysis of the effects of dimensionality on the performance of hydrodynamic models (Ishikawa et al., 2022a), hydrodynamics and mixing mechanisms (Ishikawa et al., 2021) and hydrodynamic drivers for nutrient and phytoplankton dynamics (Ishikawa et al., 2022b).

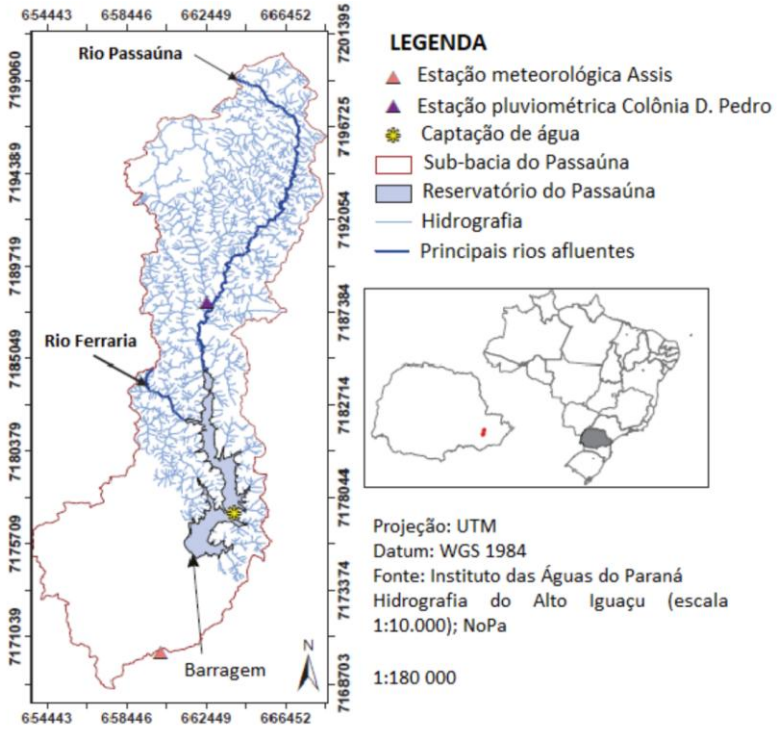

Figure 4-13. Passaúna reservoir location (SANEPAR, 2023).

Regarding FPV, a pilot floating photovoltaic system was installed on this reservoir, close to its intake point. This pilot project has a maximum capacity of 130 kWp, covering an area of approximately 1,200 m² (0.01% of the total area).

To understand and analyze the impacts on the hydrodynamics and water quality of the reservoir, the FotoÁgua Project – Effects of floating photovoltaic systems on transfer processes at the air-water interface and changes to water quality – was developed in partnership with *Companhia de Saneamento do Paraná* (SANEPAR). The project lasted a year and involved the development of a monitoring system, field campaigns, data processing, and computational modeling.

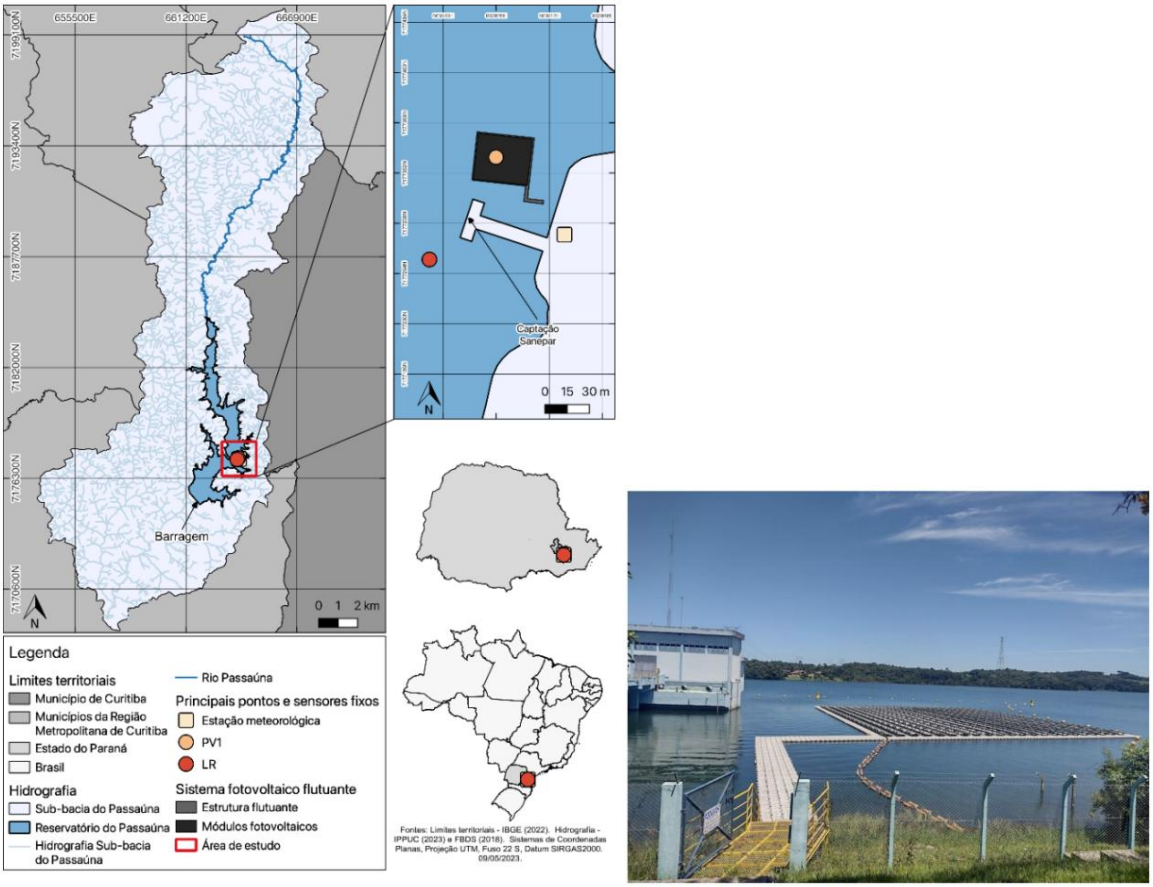

Figure 4-14. FPV pilot plant on Passaúna Reservoir.

4.2.2.1 MONITORING STRATEGY

The monitoring strategy (Figure 4-15) focused on two main locations, one in the center of the FPV system (PV1), and another located outside the system, considered to be a reference point without influence from it (Lake Reference, LR).

The monitoring system had fixed continuous monitoring sensors (Table 4-2) on the surface and bottom of these two main points. Monthly field campaigns were also conducted (Table 4-2), taking in situ measurements and collecting samples for laboratory analysis. Meteorological data (wind speed and direction, humidity, solar radiation) was obtained from a SANEPAR weather station, located at approximately 40 m from the FPV.

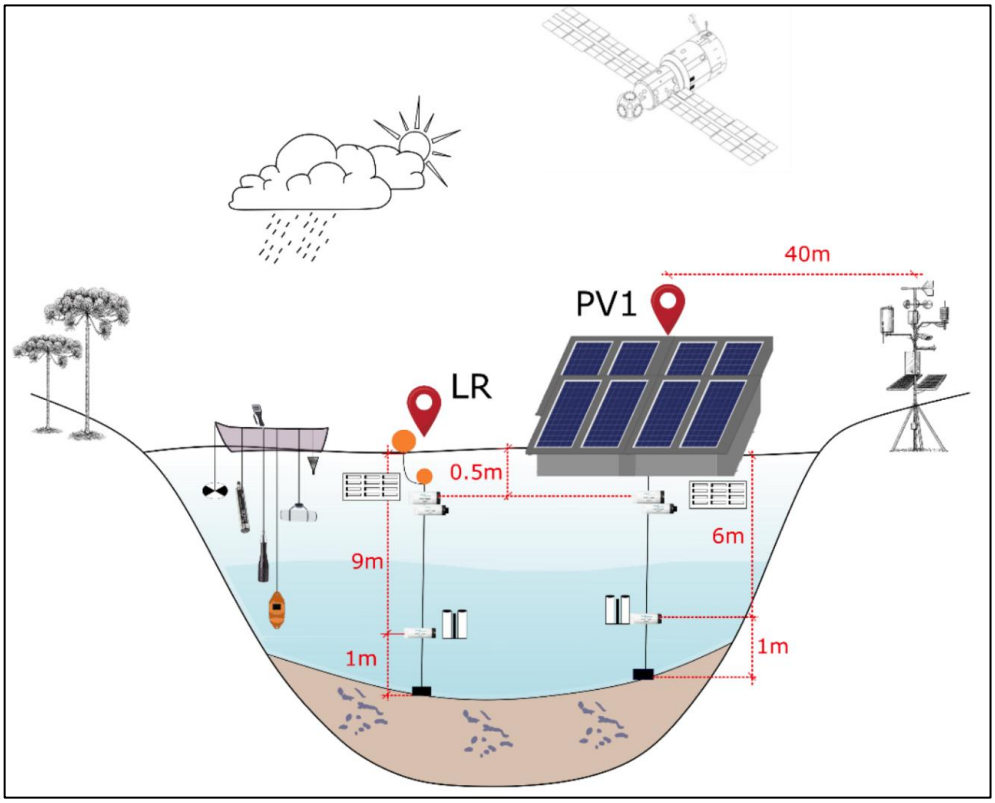

Figure 4-15. Simplified monitoring scheme for the Passaúna reservoir. Location of LR and PV1 points, and the dissolved oxygen sensors below them (0.5 m below surface and 6 m deep below PV1, 9 m deep below LR).

Table 4-2. Monitoring parameters and their frequency. All parameters were monitored at PV1 and LR.

Parameters	Monitoring
Temperature	Fixed
Dissolved oxygen	Fixed
Solar radiation	Fixed
Meteorologic station	Fixed
Secchi disk	Monthly
pH	Monthly
Conductivity	Monthly
Nitrate	Monthly
Redox potential	Monthly
Dissolved Organic Carbon	Monthly
Clorophyll-a	Monthly
Phytoplankton	Monthly
Total phosphorus	Monthly

4.2.2.1.1 FIXED CONTINUOUS MONITORING

The continuous monitoring system had four temperature and dissolved oxygen sensors (miniDOT), located on the surface (0.5 m deep) and bottom (6 m PV1, 8 m LR) of the two main points, and two photosynthetically active radiation sensors (miniPAR) located on the surface. In addition, there were previously installed sensors for measuring water temperature (model PT100, with a measurement range of -10 to 120°C, Class A). The sensor's accuracy is as follows: ± 0.15 + (0.002*t*)°C, where *t* is the absolute temperature value in °C (LIOHM, 2019), and for measuring the temperature of the panels.

The fixed sensor system also incorporates sensors from Sanepar's weather station, which is approximately 40 meters from the FPV. This automated station is equipped with the following sensors: a MeteoTemp RH+T 2-in-1 waterproof thermo-hygrometer for measuring air temperature and relative humidity (BARANI DESIGN, 2017a); a MeteoWind 2 anemometer for wind speed and direction (BARANI DESIGN, 2017b); and an MS-80 pyranometer for solar radiation measurement (EKO, 2020).

The weather station records meteorological parameters such as air temperature (°C), relative humidity (%), horizontal and inclined solar radiation at 15° (W/m^2) within a wavelength range of 285 nm to 3000 nm, wind speed (m/s), and wind direction (°). The 15° inclined solar radiation measurement corresponds to the tilt angle of the floating photovoltaic modules.

Temperature profilers (Vemco Minilog II-T Temperature Data Loggers) were deployed after the miniDOT and miniPAR sensors at PV1 and LR, with a time resolution of 1 minute. Apart from the sensor placed in the air beneath the FPV at PV1, the depth levels for both PV1 and LR were 0.25 m, 0.75 m, 1 m, 1.5 m, and 2 m. These temperature profilers offer a resolution of 0.01°C and an accuracy of ±0.1°C for temperatures ranging from -5°C to 35°C.

4.2.2.1.2 MONTHLY MONITORING

The monthly monitoring system involved 3 sensors (two multiparameter sensors, Horiba U-50-434 and Trios Opus, and a CTD), together with Secchi disk measurements. At each monthly campaign, measurements were taken meter by meter, as well as surface and bottom samples at points PV1 and LR.

Chlorophyll-a, total phosphorus and carbon analyses were carried out on the samples collected. Specific samples were also collected to characterize the composition of the phytoplanktonic and zooplanktonic communities.

4.2.2.2 MODELING STRATEGY

During the MuDak-WRM project in 2018 and 2019, a three-dimensional mathematical model was developed for the Passaúna reservoir that showed good results in terms of water temperature and flow velocity when compared to measured values, despite limitations in terms of energy dissipation

processes (Ishikawa et al., 2022). The computational grid is curvilinear, with cell sizes varying between 10 m and 100 m, with an average resolution of 79 m; it has 20 vertical layers (Z-model), and uses a k-ε turbulence model.

Based on the previous studies, the calibrated model from (Ishikawa et al., 2022) was adjusted for the modelling purpose of representing the floating photovoltaic system. This work was done in collaboration with the FotoÁgua Team, and also based on initial studies from a master student (Bonfim, 2024). Adjustments were made mainly to the grid, to represent the floating structures, but also extensions to the boundary conditions, to include the newly monitored periods.

Initial conditions for the hydrodynamic and the water quality model were constant values. Four horizontal boundary conditions were considered, being: a main tributary inflow; two secondary tributary inflows; water level at the dam. Two sinks were considered, the water intake (measured) and the groundwater contribution (obtained by water balance). As surface boundaries, precipitation and evaporation are considered. A tracer was placed below the FPV, at the surface layer, to analyze the advection transport and local residence time. Further model parameters are specified at Table 7-3 and Table 7-4, APPENDIX C.

FPV representation

As mentioned in chapter 4.1.1, Delft3D makes it possible to use two approaches to simulate the coverage of the reservoir caused by the FPV modules. Base on the calibrated model, two scenarios were carried out with photovoltaic modules for one year of measurements, from August 1st, 2022, to August 1st, 2023, in order to analyze the effects of inserting FPVs. The Pilot scenario represents the current pilot project. To simulate this scenario correctly, it was necessary to refine the computational grid horizontally, thus allowing such a small percentage coverage to be obtained in relation to the entire reservoir. The Expanded scenario simulates an expansion scenario for the FPV, occupying a larger area of the reservoir. Table 4-3 presents the scenarios analyzed and their coverage areas, while Figure 4-16 shows the computational grid for two scenarios and the actual structure using satellite imagery.

In terms of area, while the covered area of the real pilot project is approximately 1,200 m², in the simulated Pilot scenario the covered area was 1,140 m², and in the Expanded scenario it was 516,934 m². In relation to the total area of the reservoir, this is 0.01% and 6.15%, respectively. The submerged depth of the floating structure was 0.3 m, similar to that of the real structure, in both scenarios.

Table 4-3. Simulation scenarios for the Passaúna reservoir.

Scenario	Coverage (%)	Coverage (area, ha)
Base	0	0
Pilot	0.01 (actual)	1.1
Expanded	6.15 (expanded)	51.7

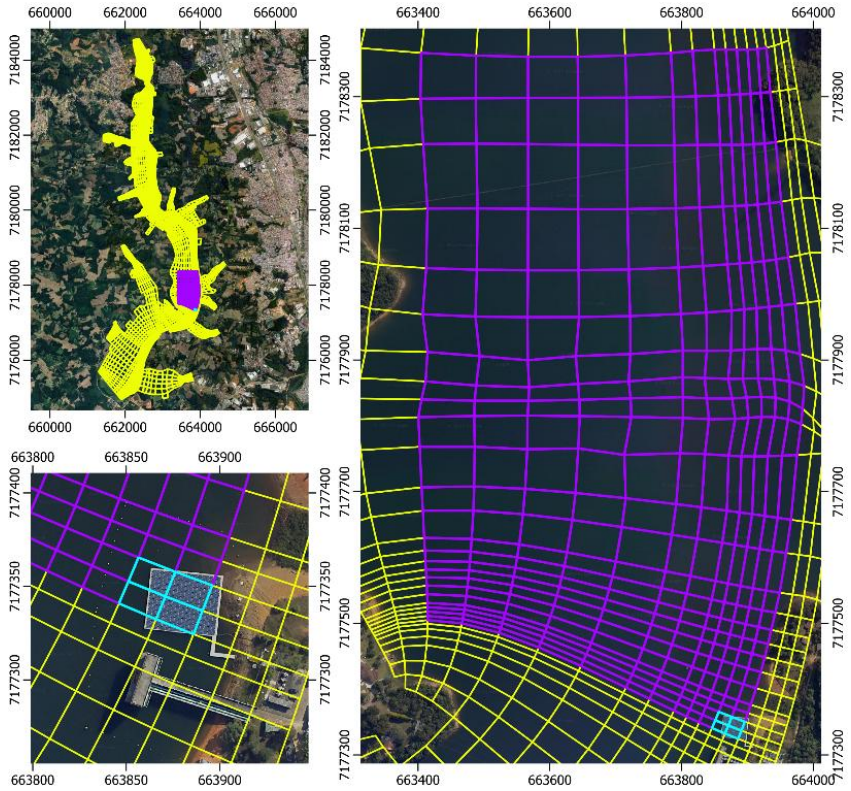

Figure 4-16. Location of floating structures on the modeling grid. Yellow represents the computational grid, in blue is the Pilot scenario (0.01% coverage), and in purple the Expanded scenario (6% coverage).

However, this approach does not allow coupling with the water quality model afterward (Deltares, 2025a). Therefore, the approach used to model the gravel pit lake in Germany was also tested for the Passaúna Reservoir. The Pilot and Expanded scenarios were simulated in order to model temperature and dissolved oxygen, and analyze their behavior in the tropical reservoir. To do this, a three-month period was simulated, from October 2022 to January 2023, considering the parameters calibrated in the previous model. The meteorological data is listed in Figure 4-17, and the flow rate of the main tributary, as well as its temperature, is presented in Figure 4-18. A wind rose is presented in Figure 4-19, to illustrate the wind characteristics during the simulation period.

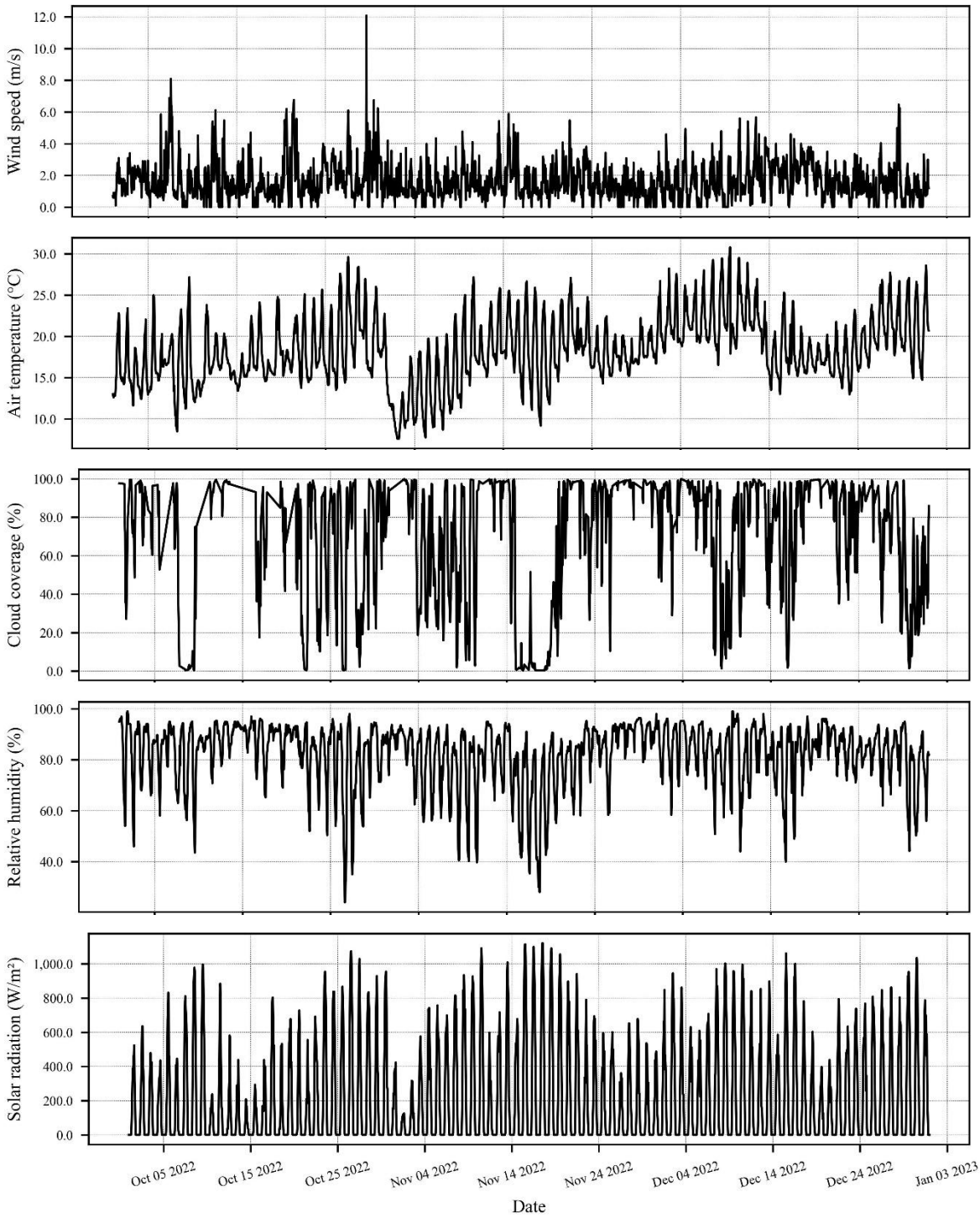

Figure 4-17. Meteorological data from Sanepar meteorological station used as input in the Delft3D model for the period of simulation (01/10/2022 to 01/01/2023).

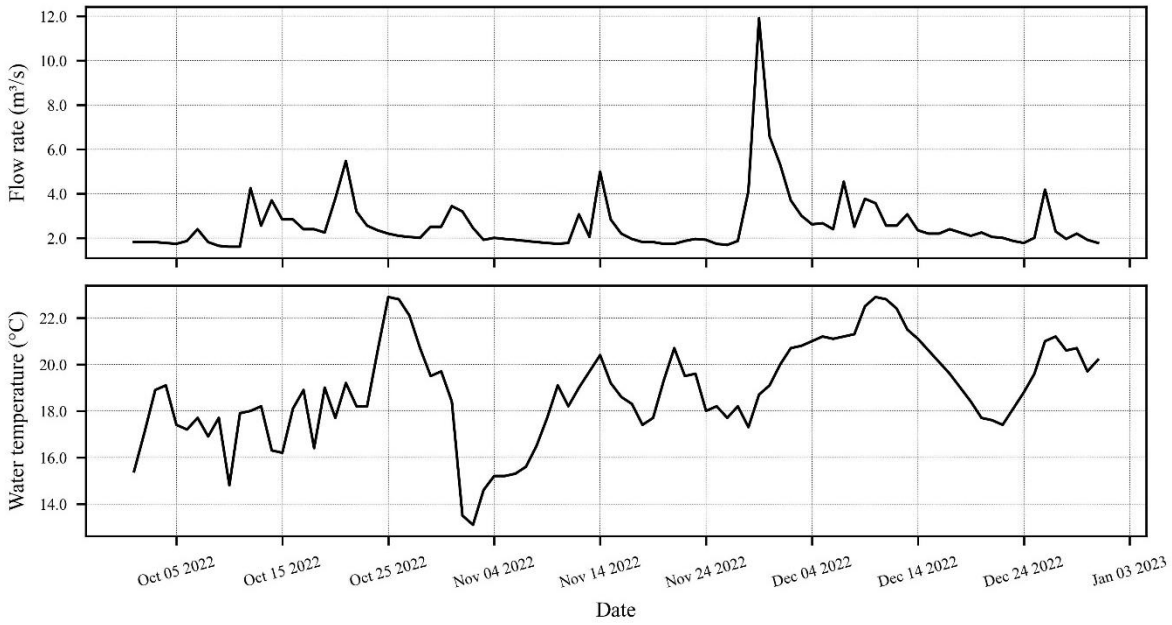

Figure 4-18. Flow rate and water temperature of the main tributary used as input in the Delft3D model for the period of simulation (01/10/2022 to 01/01/2023).

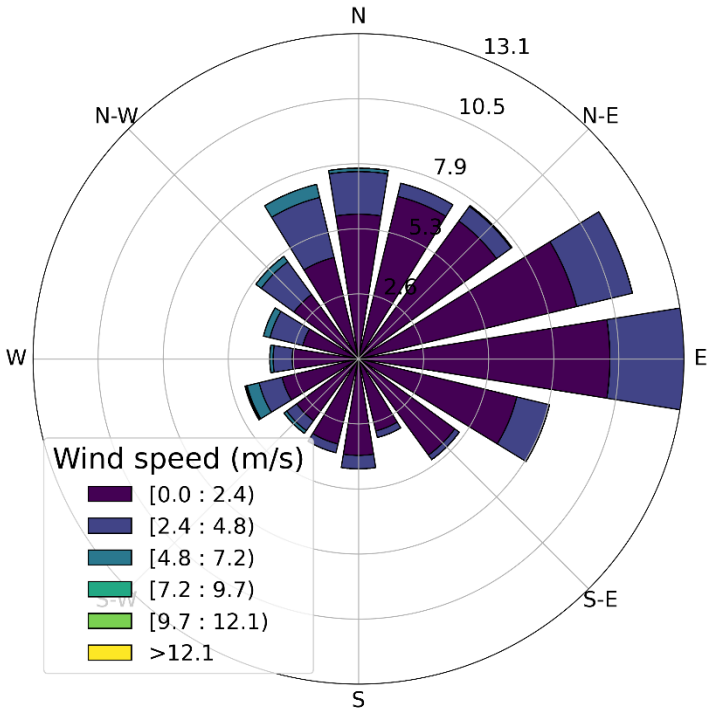

Figure 4-19. Wind rose of the simulation period for Passaúna reservoir.

4.3 MODELING ANALYSIS

Basic metrics were used to analyze the calibration of the models, including the Nash-Sutcliffe coefficient (NSE (4-14)), RMSE (4-15), correlation coefficient r (4-16) e bias (4-17). The calibration focused on the variables water temperature and dissolved oxygen.

$$NSE = 1 - \frac{\sum_{t=1}^{T}(A_o^t - A_m^t)^2}{\sum_{t=1}^{T}(A_o^t - \overline{A_o})^2} \quad (4\text{-}14)$$

$$RMSE = \sqrt{\frac{1}{n}\sum_{i=1}^{n}(A_o - A_m)^{\mathbf{2}}} \quad (4\text{-}15)$$

$$r = \frac{\sum_{i=1}^{n}(A_{o,i} - \overline{A_o})(A_{m,i} - \overline{A_m})}{\sqrt{\sum_{i=1}^{n}(A_{o,i} - \overline{A_o})^2 \sum_{i=1}^{n}(A_{m,i} - \overline{A_m})^2}} \quad (4\text{-}16)$$

$$Bias = \frac{1}{n}\sum_{i=1}^{n}(A_{m,i} - A_{o,i}) \quad (4\text{-}17)$$

Where A_o is the observed variable, A_m is the modeled, $\overline{A_o}$ is the mean of observed variable values, and $\overline{A_m}$ is the mean of modeled variable values.

Finally, the model results are also compared concerning the hydrodynamics in the lake quantifying the impact of an increasing FPV occupancy. To compare coverage scenarios, the time series and averages of the variables were evaluated. The mean lake surface water temperature (*LSWT*), Schmidt stability (S_t) and thermocline depth (*TD*) were used to assess the impact on the hydrodynamic conditions. S_t and *TD* are quantified using the R package rLakeAnalyzer (Winslow et al., 2022). In addition, to assess the effect on mixing, the behavior of tracers and residence time under the FPVs were compared.

The stability index S_t represents the amount of energy needed to mix the entire water column to uniform temperature without affecting the amount of internal energy, while the internal energy is the thermal energy stored in the water column (Schmidt (1928); IDSO (1973)). If $S_t > 0$, stratified conditions and the formation of a thermocline can be assumed. *TD* is calculated as the depth at which the maximum water density difference occurs, provided the water temperature is above 4.0 °C and the water density difference between the surface and bottom layers exceeds 0.1 kg/m³ (Ladwig et al., 2021).

5 RESULTS AND DISCUSSION

Results are presented separately for each study area. At the end of the chapter, there is a discussion with a general comparison of the data and the systems.

5.1 GRAVEL PIT LAKE – LEIMERSHEIM

5.1.1 MONITORING

Continuous wind measurements at the FPV system showed a significant (57%) decrease in wind speed beneath the installation. This reduction became more pronounced for higher wind speeds, demonstrating a stronger effect at higher velocities. Winds from the south, which directly impacted the southward-facing foundations of the array, led to a greater reduction in wind speed compared to winds from the north.

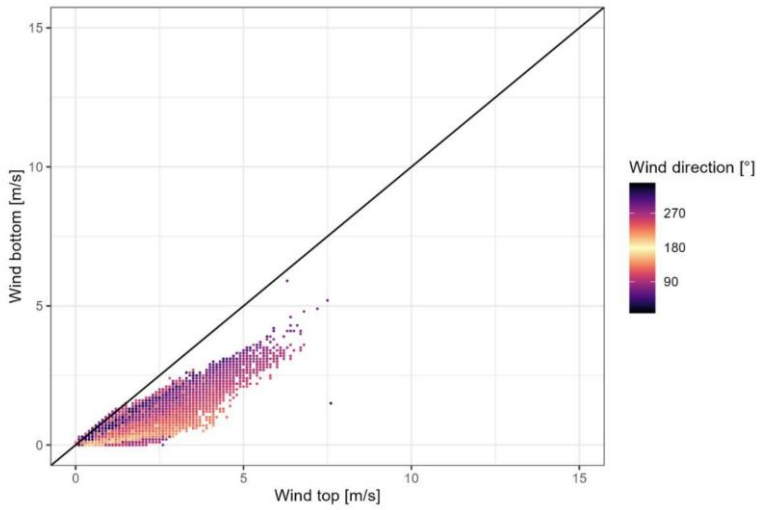

Figure 5-1. Comparison of wind speed recorded above (Wind top) and below (Wind bottom) the PV modules (but still above the water surface) based on wind Direction (Ilgen et. al, 2025, APPENDIX B).

Radiance calculations indicated an 88% reduction in solar irradiance reaching the water body below the panels. While certain areas, such as along cable routes and at the edges of the array, experienced little to no shading, significant shading was observed beneath the modules and substructure. These results are higher than those found in another lake in the Upper Rhine region, which showed a 23% reduction in wind and a 73% reduction in radiation (Ilgen et al., 2023).

Additionally, a 36% decrease in k_w (light extinction coefficient) was recorded under the FPV array, suggesting lower light extinction. This reduction implies a potential decline in suspended particles and dissolved substances that would otherwise increase turbidity and light scattering. One possible explanation for the reduced turbidity and particle concentration beneath the FPV system is filtration by mussels colonizing the structure. After these results, Table 5-1 provides a summary of the key input parameters used in hydrodynamic model to assess FPV impacts.

Table 5-1. Parameters adjusted to represent FPV in Delft3D.

Parameter	Without FPV	With FPV	Reduction (%)
Scaling factor for shortwave radiation	1	0.12	88
Scaling factor for wind speed	1	0.43	57

Table 5-2 presents a summary of water quality data collected from the lake. The measurements from MREF I and MREF II were averaged (MREF) and compared with those taken beneath the FPV system (MFPV). Statistical t-tests were conducted to assess whether the differences in water quality variables were statistically significant.

Table 5-2. Statistical analysis of water quality data collected using a multi-parameter probe. The average values of measurements taken beneath the FPV system (MFPV) are compared to those recorded in open water (MREF), with the standard deviation presented in brackets. The p-value is derived from t-tests and is indicated alongside significance levels: $p \leq 0.1$ (*), $p \leq 0.05$ (**), and $p \leq 0.01$ (***). (Ilgen et. al, 2025, APPENDIX B).

Variable	MFPV	MREF	p-value	Significance
Water temperature (°C)	14.28 (±5.57)	14.20 (±5.83)	0.856	
Dissolved oxygen (mg/L)	9.22 (±1.83)	9.60 (±1.7)	0.011	**
Oxygen saturation (%)	89.44 (±16.43)	92.84 (±13.91)	0.010	***
Specific conductivity (µS/cm)	595.70 (±76.33)	594.00 (±27.45)	0.737	
pH (-)	8.17 (±0.45)	8.14 (±0.39)	0.402	
Redox potential (mV)	172.13 (±53.91)	164.42 (±54.26)	0.095	*
Nitrate (mg/L)	0.16 (±0.18)	0.21 (±0.20)	0.011	**
Turbidity (NTU)	1.93 (±3.58)	2.39 (±4.21)	0.161	
Phycocyanin (µg/L)	0.05 (±0.14)	0.04 (±0.05)	0.508	
Chlorophyll-a (µg/L)	1.03 (±0.85)	1.08 (±1.00)	0.541	
Dissolved organic carbon (mg/L)	1.68 (±0.31)	1.68 (±0.30)	0.959	

Unlike the results of Nobre et al. (2025), differences in water temperature between MFPV and MREF were minimal and not statistically significant. However, it should be noted that the average coverage of the lakes analyzed was 49.1%, while in Leimersheim the coverage is 8%.

In contrast, both dissolved oxygen concentrations and saturation levels showed a notable decline, like observed by Wang et al. (2022) on experimental sites. Nutrient levels, particularly nitrate concentrations, exhibited slight reductions, though values were close to the detection limit. However, along with the lower turbidity observed beneath the FPV system, this reduction may suggest an influence of mussel filtration. Specific conductivity and pH levels reflected the presence of calcareous sediments, characteristic of the Upper Rhine Valley. Additionally, the relatively low concentrations of chlorophyll-a and nitrate indicated an oligotrophic trophic state.

The temperature and DO profiles over 5 monitoring campaigns are shown in Figure 5-2. It is possible to observe stratification in the September and October campaigns (Figure 5-2a), with little variation in temperatures between the MFPV (PV in the graph) and MLREF (LR in the graph) points.

The results of DO, on the other hand, shows greater variations between points, especially on the surface (Figure 5-2b).

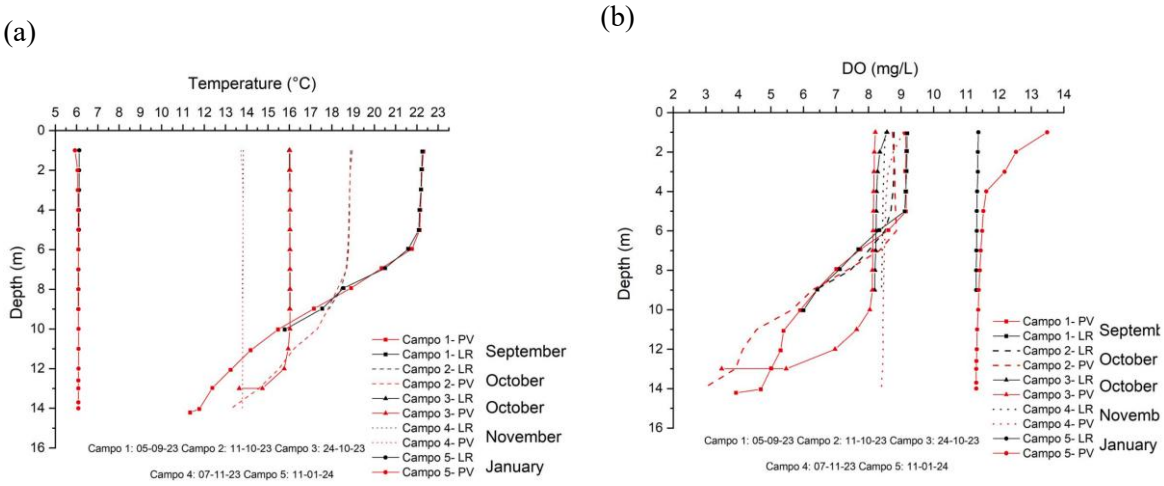

Figure 5-2. Vertical profiles of five field campaigns. (a) Temperature; (b) DO.

Figure 5-3 shows the results of continuous monitoring with the oxygen sensors (miniDOT). The time series shows instabilities at the start of the measurements (Figure 5-3a), which were fixed after the second campaign, when a copper cover device was installed to prevent biofilm from forming around the sensor. The average DO below the panels was 8.06 mg/L, while in the LR it was 8.57 mg/L (Figure 5-3b). The boxplots and averages were generated excluding the instability period.

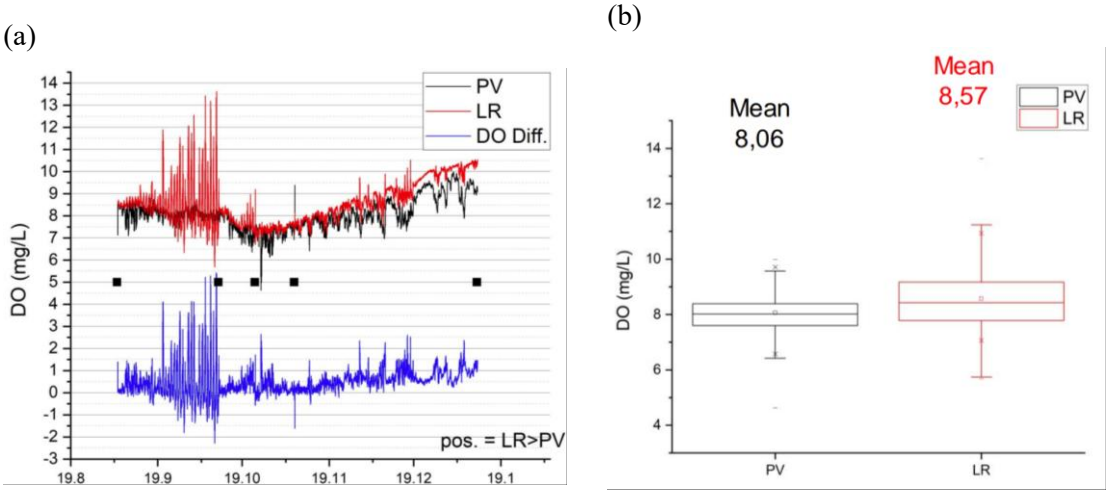

Figure 5-3. Time Series and Boxplots of oxygen sensor data, where LR is the MREF point and PV is the MFPV point. The black dots mark the dates of field campaigns.

During the field campaigns, mussels were found on the floaters (Figure 5-5 and Figure 5-6). These organisms were not analyzed in this study, but their existence is relevant for the discussion of the results.

Figure 5-4. Mussels attached to the floaters of the FPV system. Photo taken with Underwater ROV (Deep Trekker[3]) during a field campaign.

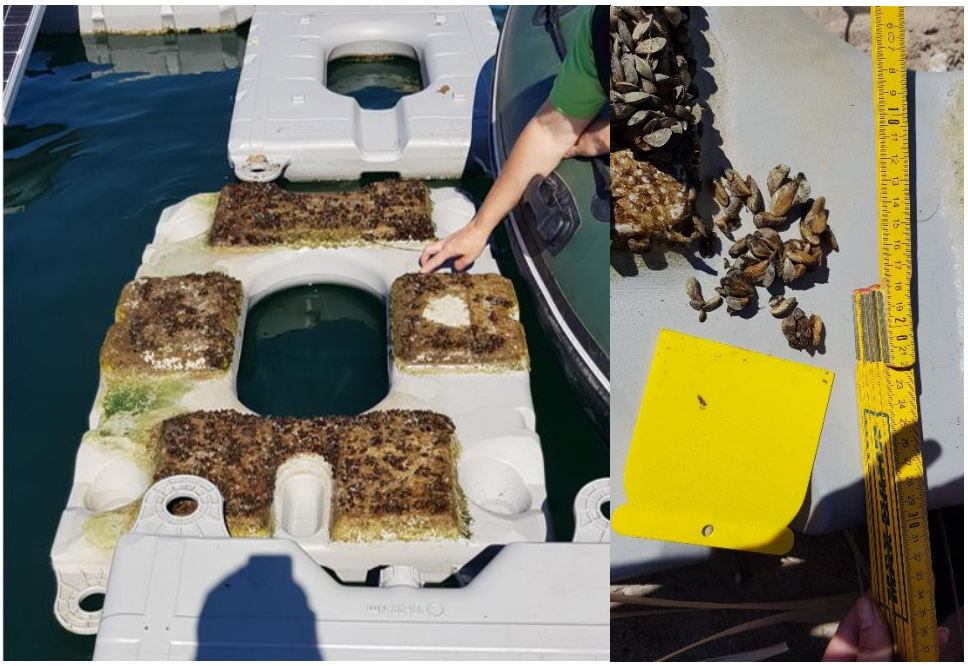

Figure 5-5. Mussels found below the FPV, attached to the floaters and their removal for laboratory analysis.

5.1.2 MODELING

5.1.2.1 Calibration

The model's calibration focused on matching simulated temperature and dissolved oxygen profiles to the monitored ones. Therefore parameters, such as wind drag coefficients, Dalton and Stanton numbers, were modified to improve the correlation. Figure 5-6 shows the time series of the temperature

[3] https://www.deeptrekker.com/products/underwater-rov

modeling (continuous lines) compared to the measurements (dots) at the different depths. The calibration metrics are shown in Table 5-3.

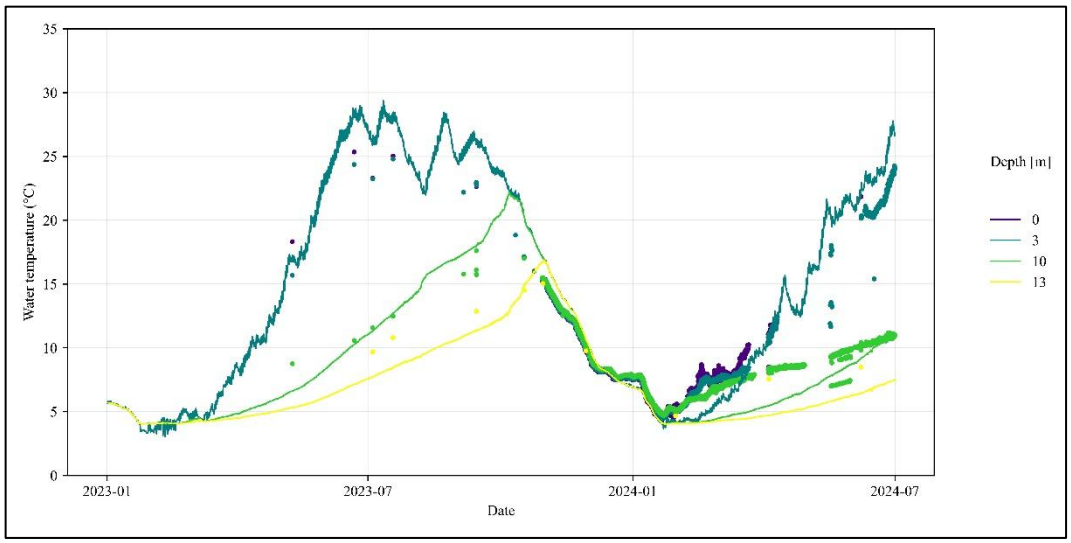

Figure 5-6. Observed temperature (dots) and modeled temperatures (continuous lines) from 01/01/2023 to 30/06/2024 at MREF I for four different depths.

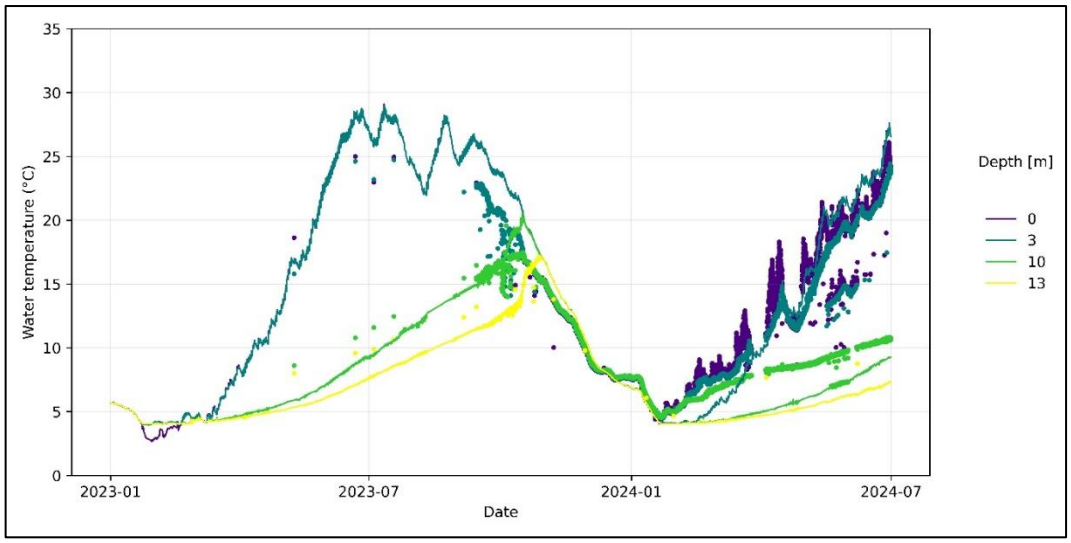

Figure 5-7. Observed temperature (dots) and modeled temperatures (continuous lines) from 01/01/2023 to 30/06/2024 at MFPV for four different depths.

Table 5-3. Metrics obtained in the temperature calibration for the MREFI and MFPV points, on the surface (0 m depth) and closer to the bottom (10 m depth).

Point	Depth (m)	RMSE (°C)	NSE	R	Mean bias (°C)	MAE (°C)
MREFI	0	1.41	0.74	0.96	-0.61	1.17
	10	1.64	0.50	0.96	-1.08	1.40
MFPV	0	2.12	0.84	0.97	-0.21	1.66
	10	1.84	0.69	0.97	-0.65	1.55

After the temperature calibration, the water quality model was calibrated for dissolved oxygen by changing the reaeration formula, and reaeration transfer coefficient in water to achieve the best match

between the monitoring and simulated data. It is important to highlight that, in this thesis, the focus was on analyzing the influence of FPV on the physical process of reaeration. Therefore, DO was calibrated for this scenario and, subsequently, the impact of panel coverage expansion was evaluated. Figure 5-8 shows the results for DO at the MREFI point, Figure 5-9 for the MFPV point, while the Table 5-4 presents the obtained metrics.

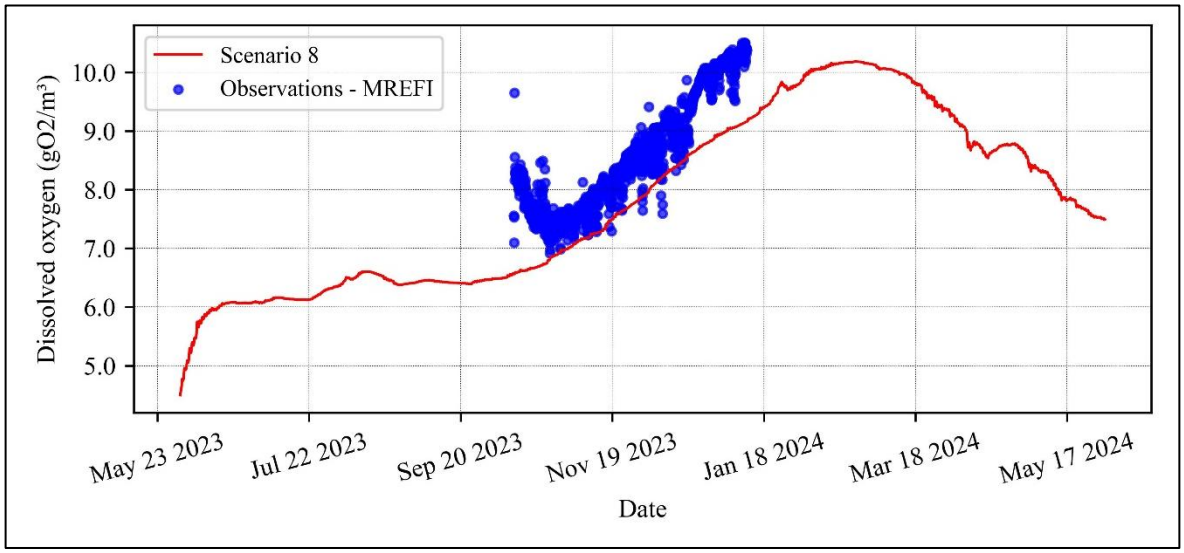

Figure 5-8. Observed temperature (dots) and modeled temperatures from 01/06/2023 to 01/06/2024, 1 m below surface, at MREFI.

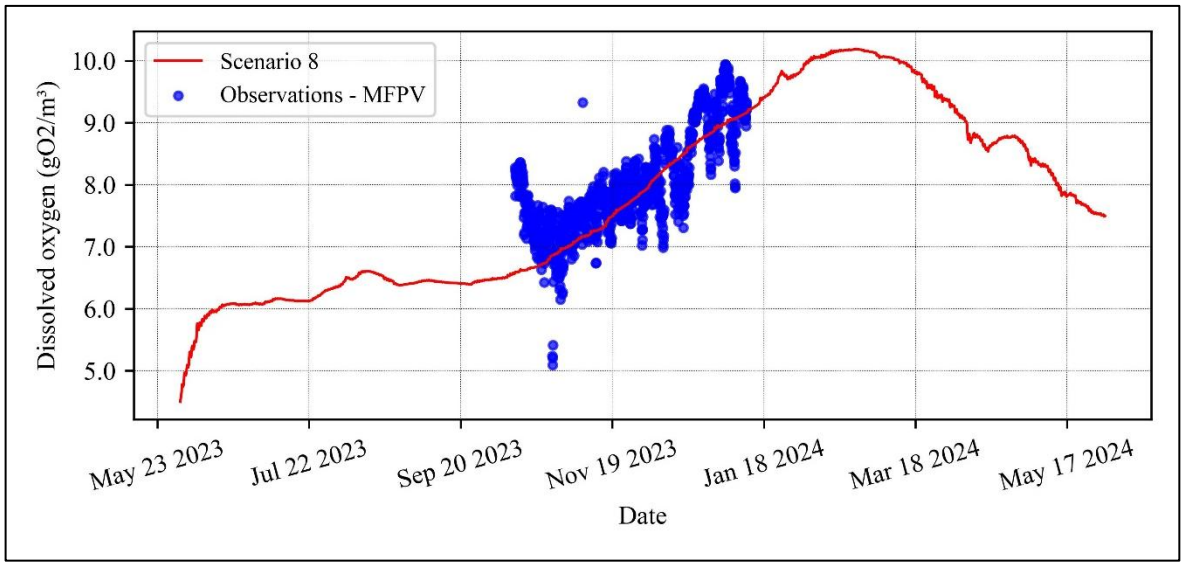

Figure 5-9. Observed temperature (dots) and modeled temperatures from 01/06/2023 to 01/06/2024, 1 m below surface, at MFPV.

Table 5-4. Metrics obtained in the DO calibration for the MREFI and MFPV points.

Point	Depth (m)	RMSE (g/m³)	NSE	r	Bias (°C)	MAE (°C)
MREFI	1	0.86	0.24	0.93	-0.78	0.78
MFPV	1	0.55	0.54	0.81	-0.23	0.44

5.1.2.2 Scenarios

To assess the impact of different areas of FPV coverage on the lake, the results of water temperature, horizontal velocity, total evaporation, residence time, tracer concentration and, finally, dissolved oxygen were analyzed. The average lake surface temperature (LSWT), Schmidt Stability (St), thermocline depth (TD), and lake's total evaporation were first analyzed for the entire hydrodynamic simulation period (Table 5-5).

Table 5-5. Summary of variations between scenarios (average over time), for the total period of simulation (01/01/2023 to 30/06/2024) at MFPV.

FPV occupancy (%)	LSWT (°C)	St (J/m²)	TD (m)	Lake's total evaporation* (x1000 m³)	Water savings (x1000 m³)	Water savings (%)
0	14.45	176.48	6.98	126.38	-	-
8	14.26	176.87	7.25	126.42	0.04	0.03
15	13.57	166.65	6.91	107.55	18.83	14.9
50	11.31	122.37	5.37	52.89	73.49	58.15
90	4.63	21.26	3.02	2.73	123.65	97.84

*To calculate total evaporation, the time series of evaporation rates for each cell were added together and multiplied by its area (100 m²).

St decreases significantly with increasing coverage, as observed by Ilgen et al. (2023) and Ji et al. (2022). A decrease in this parameter indicates that thermal stratification is weaker, favoring mixing of the water column. When 90% of the lake is covered, St decreases by 88%, approaching a mixed system. In line with this, TD becomes shallower as coverage increases. This indicates that the transition between warmer and colder waters occurs closer to the surface, which can impact nutrient circulation and affect ecological patterns. In terms of total evaporation, water retention in the reservoir is quite significant as coverage increases.

The other parameters were then analyzed for the period from June 1st, 2023 to June 1st, 2024, a period for which water quality was also simulated. A summary of the results is shown in Table 5-6, while a detailed analysis is done parameter by parameter as following, focusing on the differences between scenarios. The parameters time series are shown in APPENDIX D.

Table 5-6. Summary of time averaging differences between the simulated scenarios, with the standard deviation presented in brackets, from 01/06/2023 to 01/06/2024.

Parameter	Time averaging differences between scenarios			
	0 – 8	**0 – 15**	**0 – 50**	**0 - 90**
Actual DO saturation (%)	1.40(±1.75)	1.83(±1.74)	2.58(±1.90)	4.31(±4.86)
Dissolved oxygen (g/m³)	0.07(±0.11)	-0.03(±0.15)	-0.39(±0.37)	-1.72(±0.47)
Horizontal velocity (cm/s)	-0.58(±0.6)	-0.55(±0.62)	-0.25(±0.40)	-0.02(±0.22)
Reaeration rate (1/d)	0.75(±1.23)	0.96(±1.24)	1.26(±1.26)	1.40(±1.27)
Residence time (h)	1.87(±4.86)	1.54(±5.15)	0.85(±5.48)	-4.74(±11.38)
Saturation concentration (g/m3)	-0.06(±0.15)	-0.19(±0.20)	-0.63(±0.31)	-2.17(±0.60)
Surface temperature (°C)	0.18(±0.57)	0.92(±0.68)	3.35(±1.31)	11.12(±4.27)

Parameter	Time averaging differences between scenarios			
	0 – 8	**0 – 15**	**0 – 50**	**0 - 90**
Total Evaporation rate (m³/h)	1.32(±2.22)	2.26(±2.84)	6.84(±6.56)	11.74(±11.20)
Tracer concentration (g/m³)	0.01(±0.01)	0.03(±0.03)	0.04(±0.11)	-0.33(±0.46)
Turbulent energy (m²/s²)	-0.35(±0.72)	-0.32(±0.72)	0.14(±0.62)	0.61(±0.55)

Temperature

The temperature results at the MFPV point show a gradual reduction in surface temperature as FPV occupancy increases (Figure 5-10). Up to 15% coverage, this decrease in temperature is slower (Figure 5-11), not reaching 1°C of variation between the averages for the period. When it reaches 50%, this decrease becomes more significant, varying by almost 20°C in the 90% scenario.

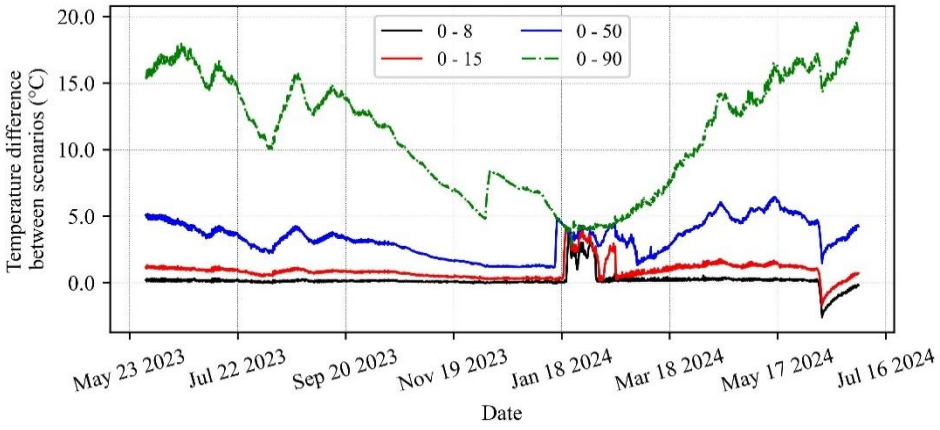

Figure 5-10. Surface temperature differences at the MFPV point between the base scenario (0) and the coverage scenarios, from 01/06/2023 to 01/06/2024.

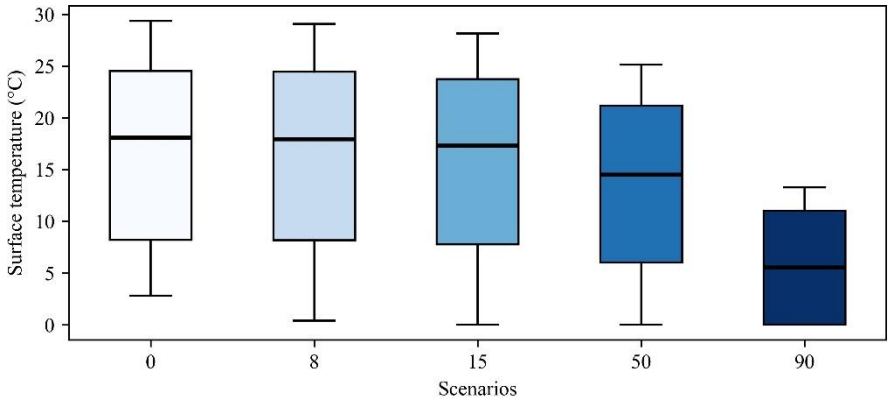

Figure 5-11. Boxplots of the surface temperature series considering the scenarios analyzed, from 01/06/2023 to 01/06/2024.

The maps show that the covered region has a lower temperature than the uncovered region. In scenario 15, variations of more than 0.5°C are observed between MFPV and MREFII (Figure 5-12c), while in scenario 8 they do not reach 0.5°C (Figure 5-12b). From 50% onwards, average temperatures become more homogeneous and are reduced throughout the lake.

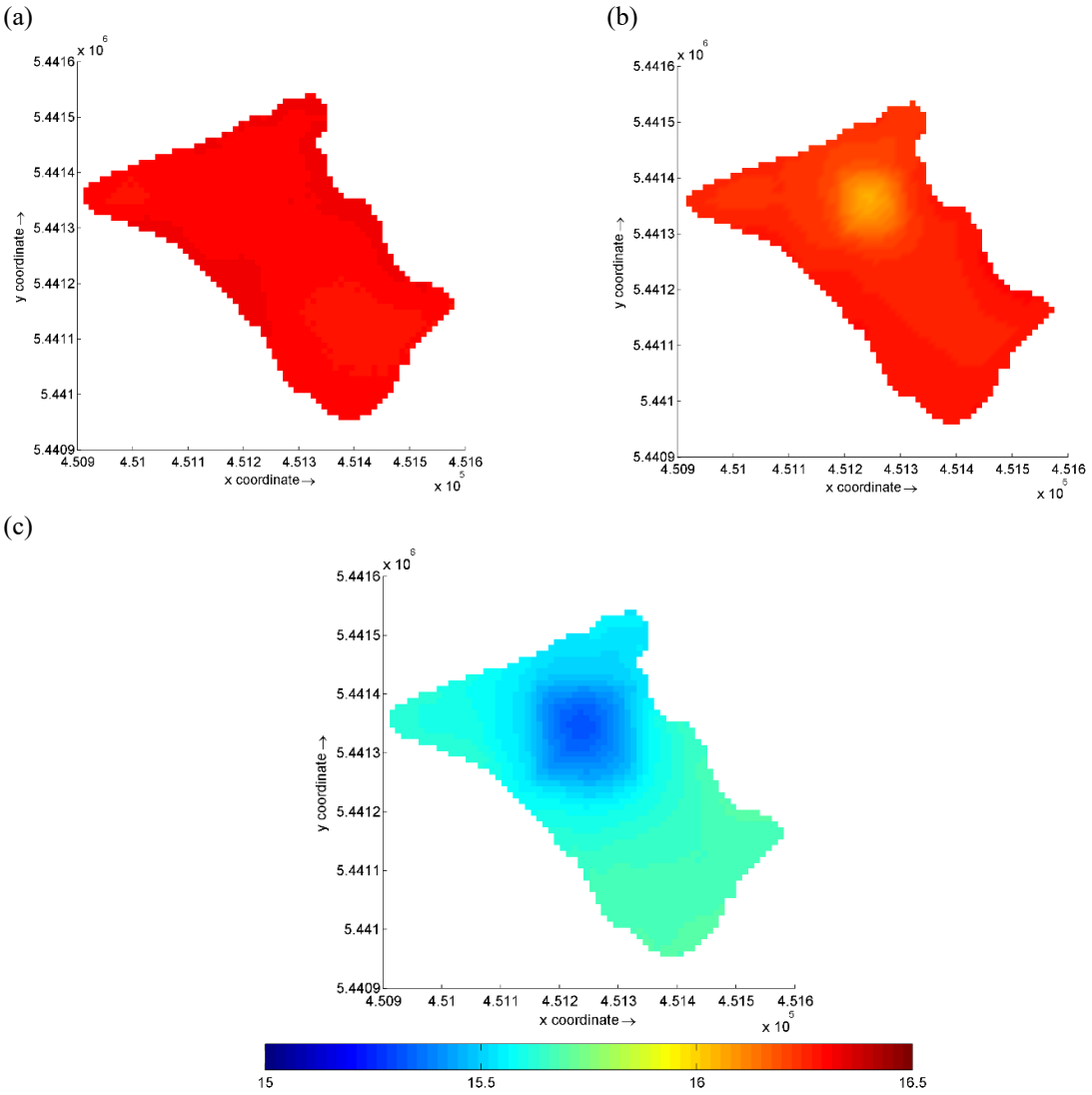

Figure 5-12. Mean surface temperature for scenarios (a) 0, (b) 8, and (c) 15, from 01/06/2023 to 01/06/2024.

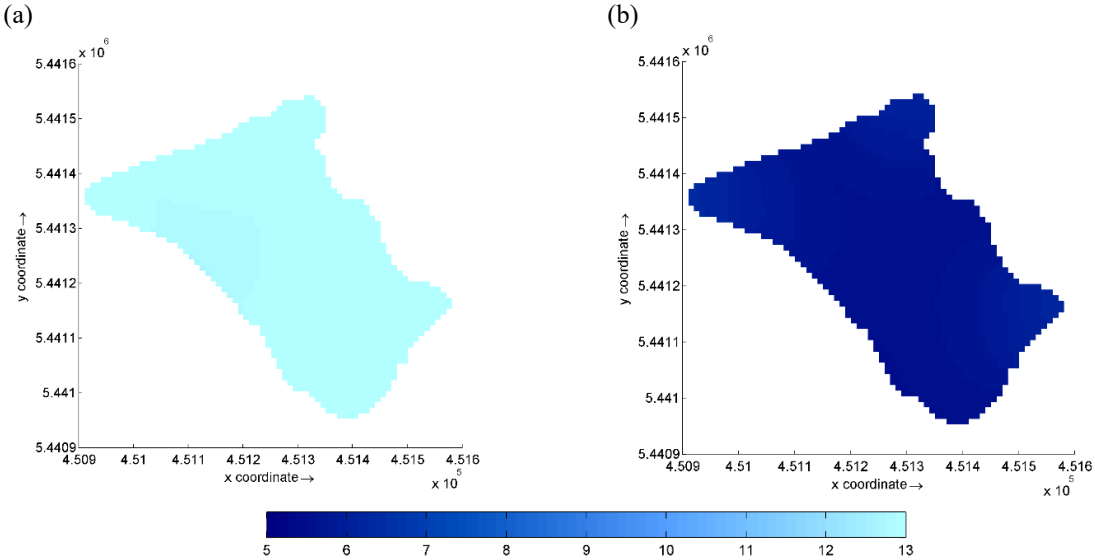

Figure 5-13. Mean Surface temperature for scenarios (a) 50 and (b) 90, from 01/06/2023 to 01/06/2024.

When looking at the temperature profiles, one can see that the thermocline gets shallower and the stratification gets weaker as the coverage increases, as mentioned earlier. Similar results were found by Ilgen et al. (2023) while modeling lake Maiwald (Germany). This effect is mainly caused by the blocking of solar radiation (Figure 5-14). It shows that with 90% coverage, the temperature differences are smaller, and stratification is only observed in the summer of 2023, remaining mixed at the beginning of the second half of 2024.

The difference between the temperature profiles is shown in Figure 5-15, where the impact on stratification and the reduction in temperature is more evident. The greatest differences can be seen initially at the height of the thermocline (Figure 5-15b and Figure 5-15c), until they become significant throughout the epilimnion in scenario 90 (Figure 5-15d).

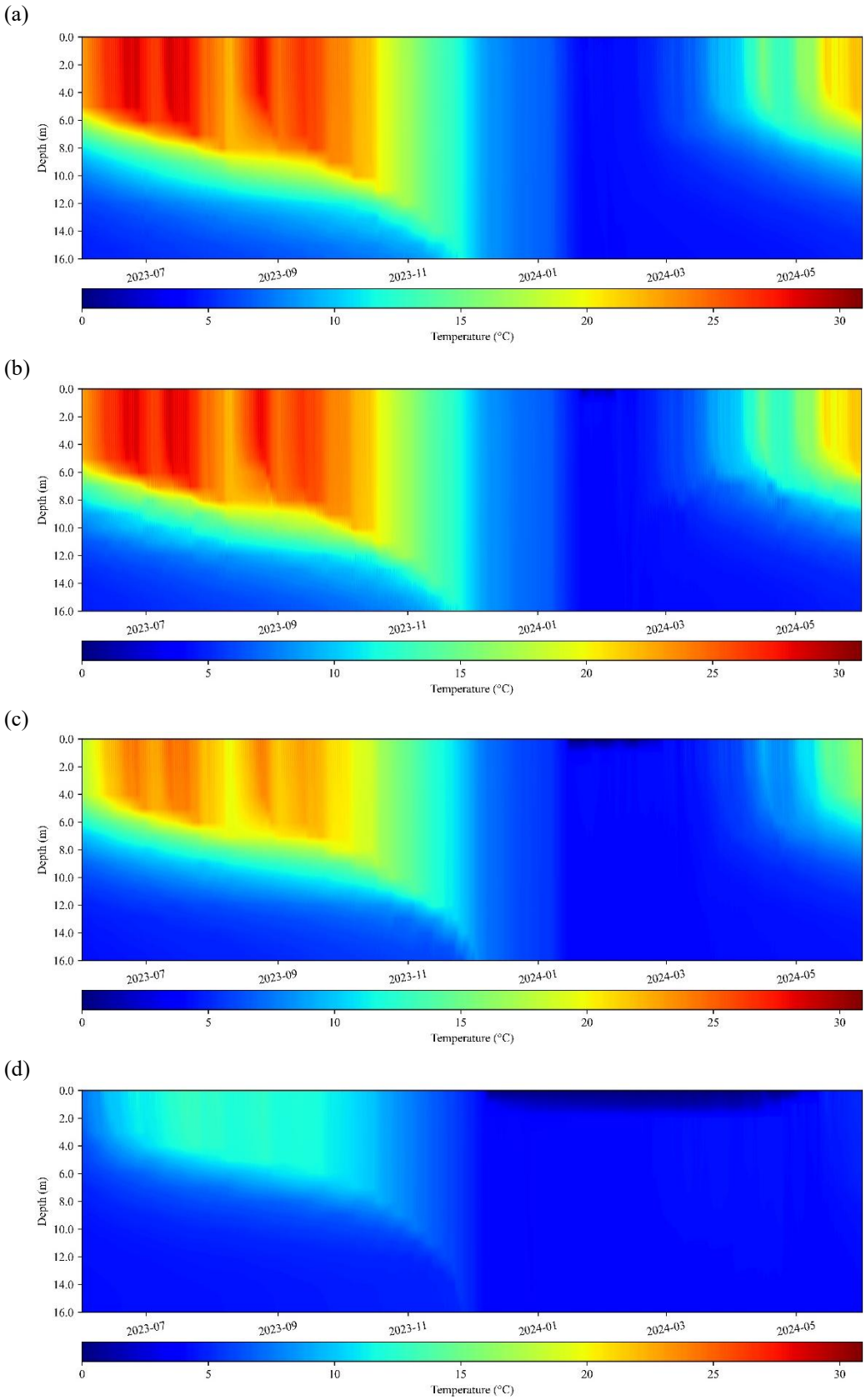

Figure 5-14. Temperature profiles, at MFPV point, for scenarios (a) 0 , (b) 8, (c) 50, (d) 90, from 01/06/2023 to 01/06/2024.

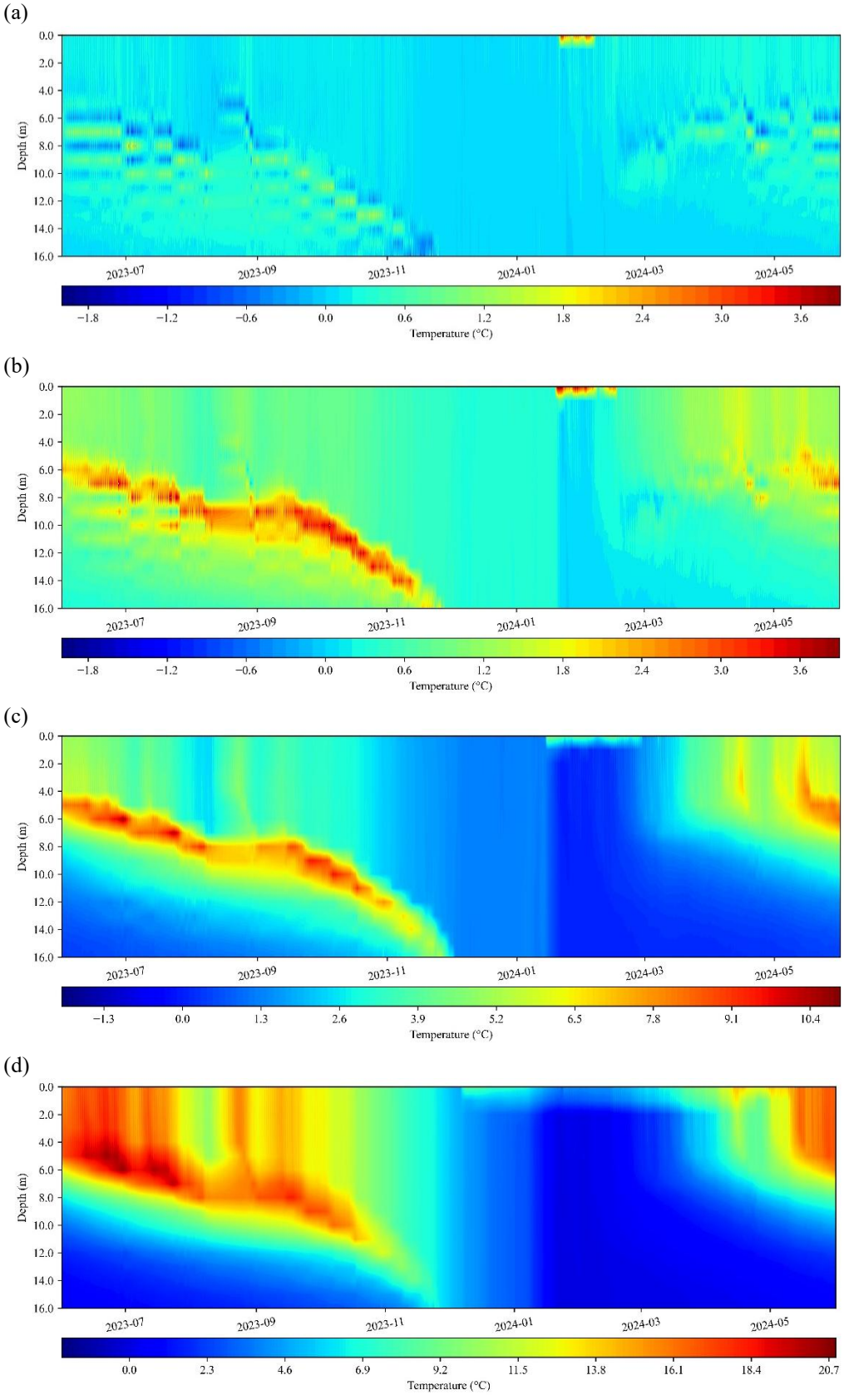

Figure 5-15. Temperature profiles differences, at MFPV point, between scenarios (a) 0 - 8, (b) 0 - 15, (c) 0 - 50, (d) 0 – 90, from 01/06/2023 to 01/06/2024. The color legends have different limits to enable visualization.

Evaporation rate

To obtain the total evaporation rate, the rates for each computational cell were added together and multiplied by their area (100 m²). As seen in several studies (Scavo et al., 2020; Aminzadeh et al., 2018; Ilgen et al., 2023), the evaporation rate decreases as the lake coverage grows (Figure 5-16). Also its variation over time decreases (Figure 5-17). Spatially, there are differences in evaporation rates not only below the FPV, but also in other regions of the lake (Figure 5-18). As seen in the previous results, the presence of the FPV leads to changes in temperature (Figure 5-12 and Figure 5-13), even if they are small, throughout the entire area of the lake. This dynamic also has an impact on evaporation, which is dependent on water surface temperature.

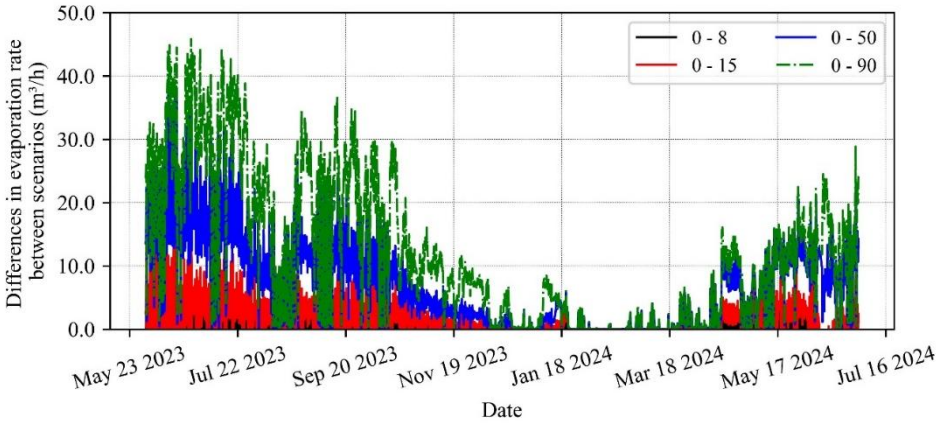

Figure 5-16. Differences in the lake's total evaporation rate between the base scenario (0) and the coverage scenarios, from 01/06/2023 to 01/06/2024.

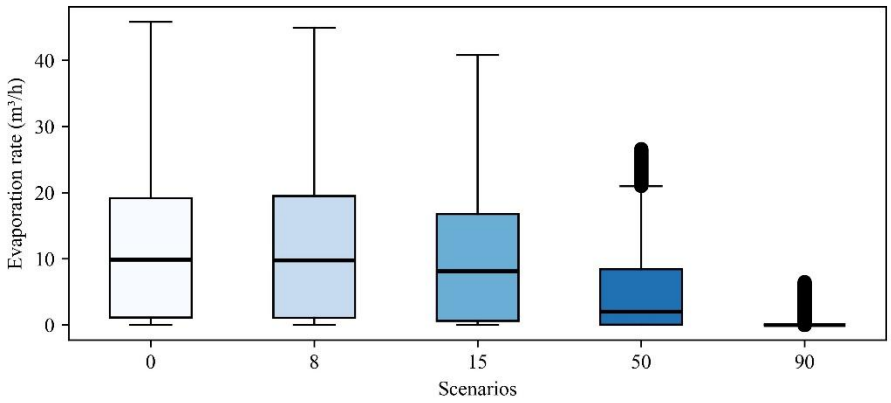

Figure 5-17. Boxplots of the total evaporation rate for the analyzed scenarios, from 01/06/2023 to 01/06/2024.

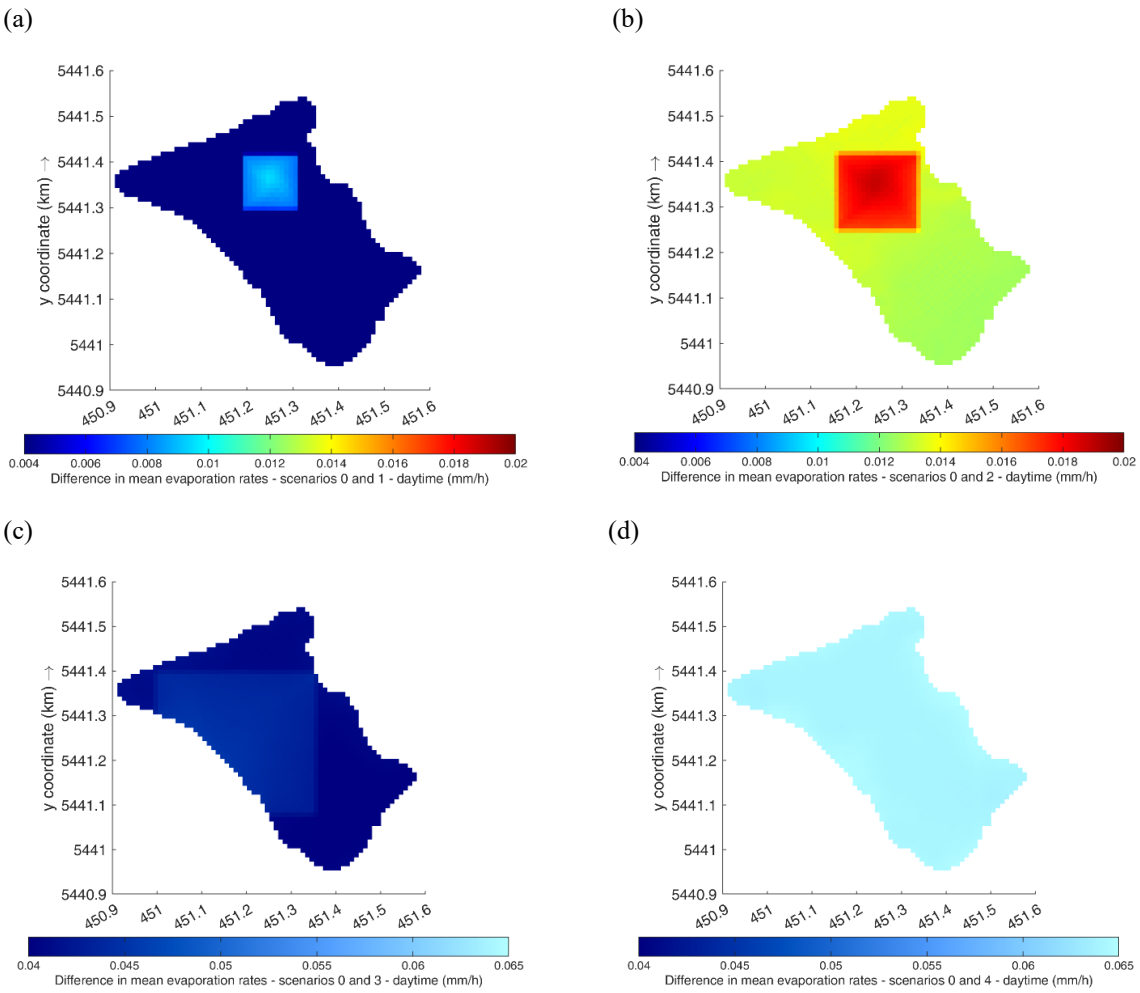

Figure 5-18. Difference between mean evaporation rates during the day for scenarios (a) 0-8, (b) 0-15, (c) 0-50, and (d) 0-90, from 01/06/2023 to 01/06/2024. The color legends have different limits to enable visualization.

Unlike what was observed by Assouline et al. (2011), on this lake there is a linear relationship between the percentage of area covered and the water savings (Figure 5-19). However, their study was focused on larger reservoirs.

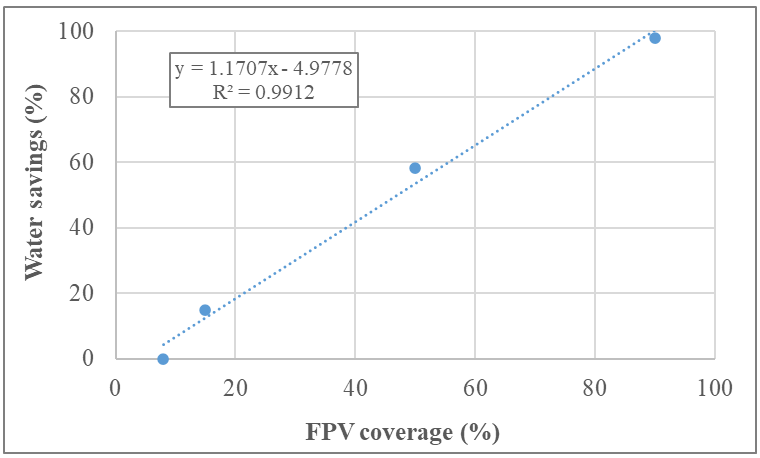

Figure 5-19. Linear relationship between water savings and FPV occupancy in the gravel pit lake simulations, considering 8%, 15%, 50% and 90% coverages.

Horizontal Velocity and Turbulent Energy

The horizontal velocity differences are shown in Figure 5-20. From the 8% to the 50% scenario, there are negative differences compared to the base scenario, indicating that there is an increase in surface velocity at the MFPV point. However, from 8% onwards, as coverage increases, there is a reduction in the magnitude of the horizontal velocity. The same behavior is observed in the variations in the velocity magnitude over time (Figure 5-21).

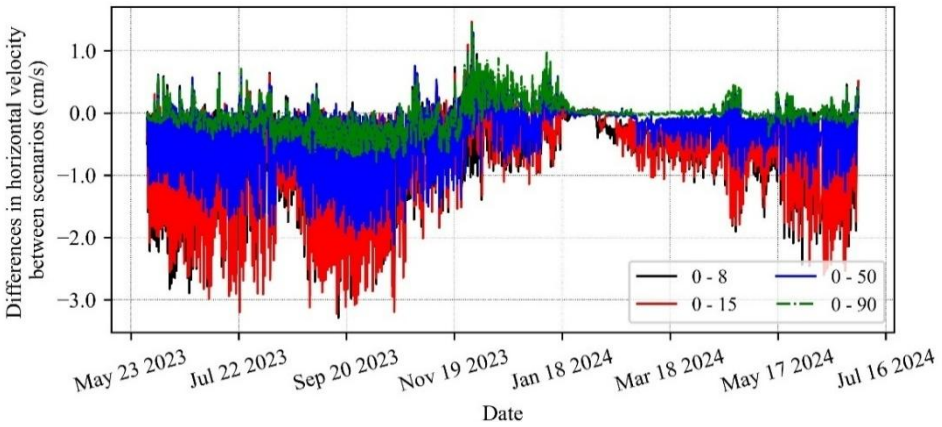

Figure 5-20. Differences in horizontal velocity magnitude at the MFPV point between the base scenario (0) and the coverage scenarios.

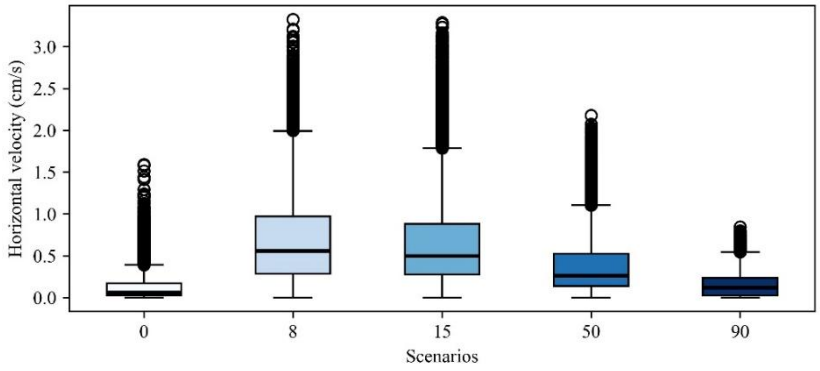

Figure 5-21. Boxplots of the horizontal velocity series considering the scenarios analyzed, from 01/06/2023 to 01/06/2024.

Looking at the maps, in intermediate coverages, the horizontal velocity increases in the FPV region (Figure 5-22). The hypothesis is that the velocities grow due to the flow generated by the temperature differences observed in these scenarios (Figure 5-23). On the other hand, in the larger coverages (scenario 90), where temperatures remain more homogeneous in space, this flow is not observed. From an estimate of the velocity generated by the difference in density (difference in water temperature), it is possible to assess the magnitude of these flow velocities (5-1). The results show the magnitude of up to 2.8 cm/s.

$$v = \sqrt{2g'h} \tag{5-1}$$

$$g' = g\frac{\Delta\rho}{\rho} \tag{5-2}$$

Where v is the flow velocity, h is the height between the temperature differences, g is the gravitational acceleration, ρ is the fluid density, Δρ is the difference between fluid densities.

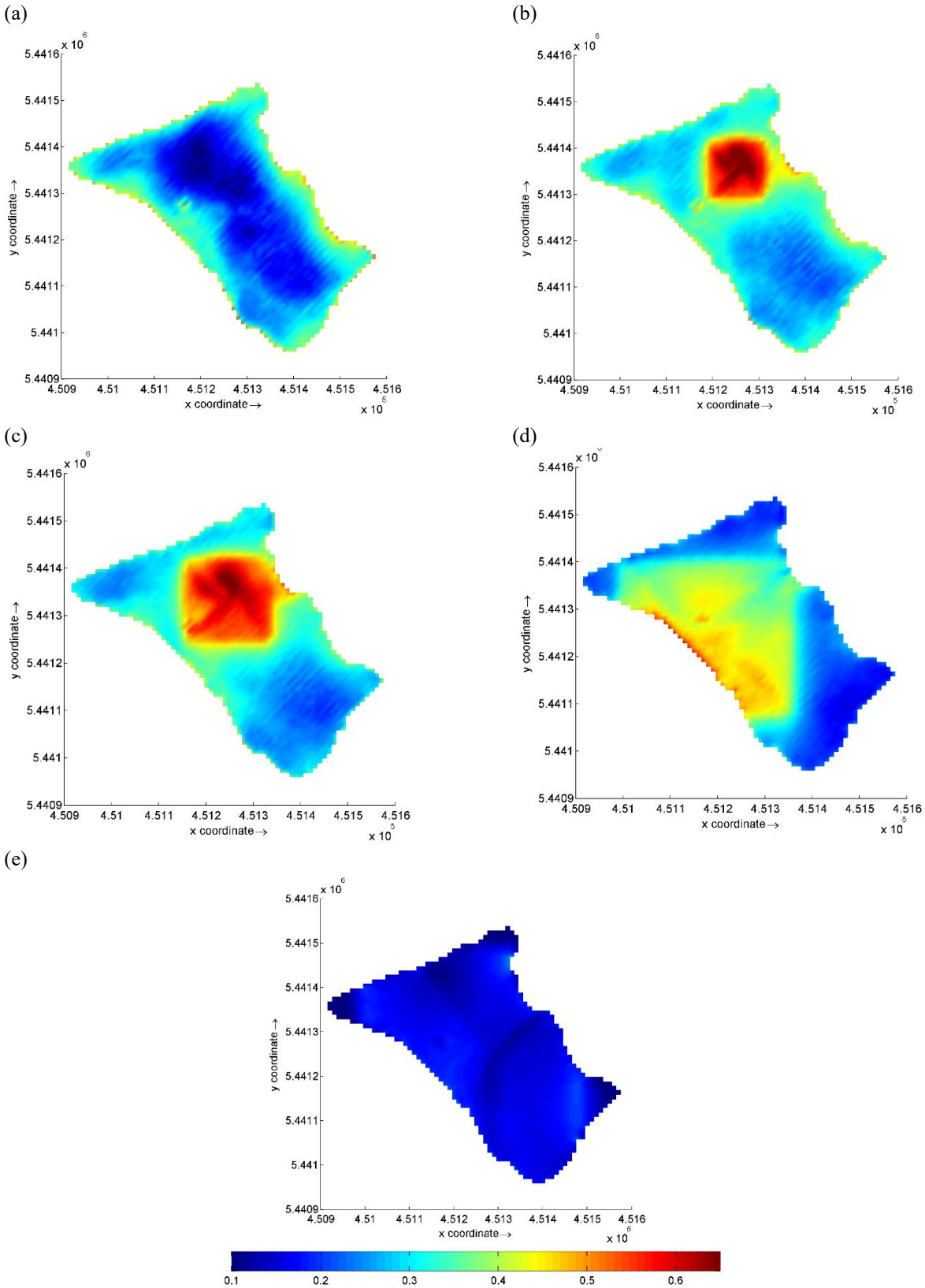

Figure 5-22. Mean horizontal velocities, in cm/s, for scenarios (a) 0, (b) 8, (c) 15, (d) 50, and (e) 90, from 01/06/2023 to 01/06/2024.

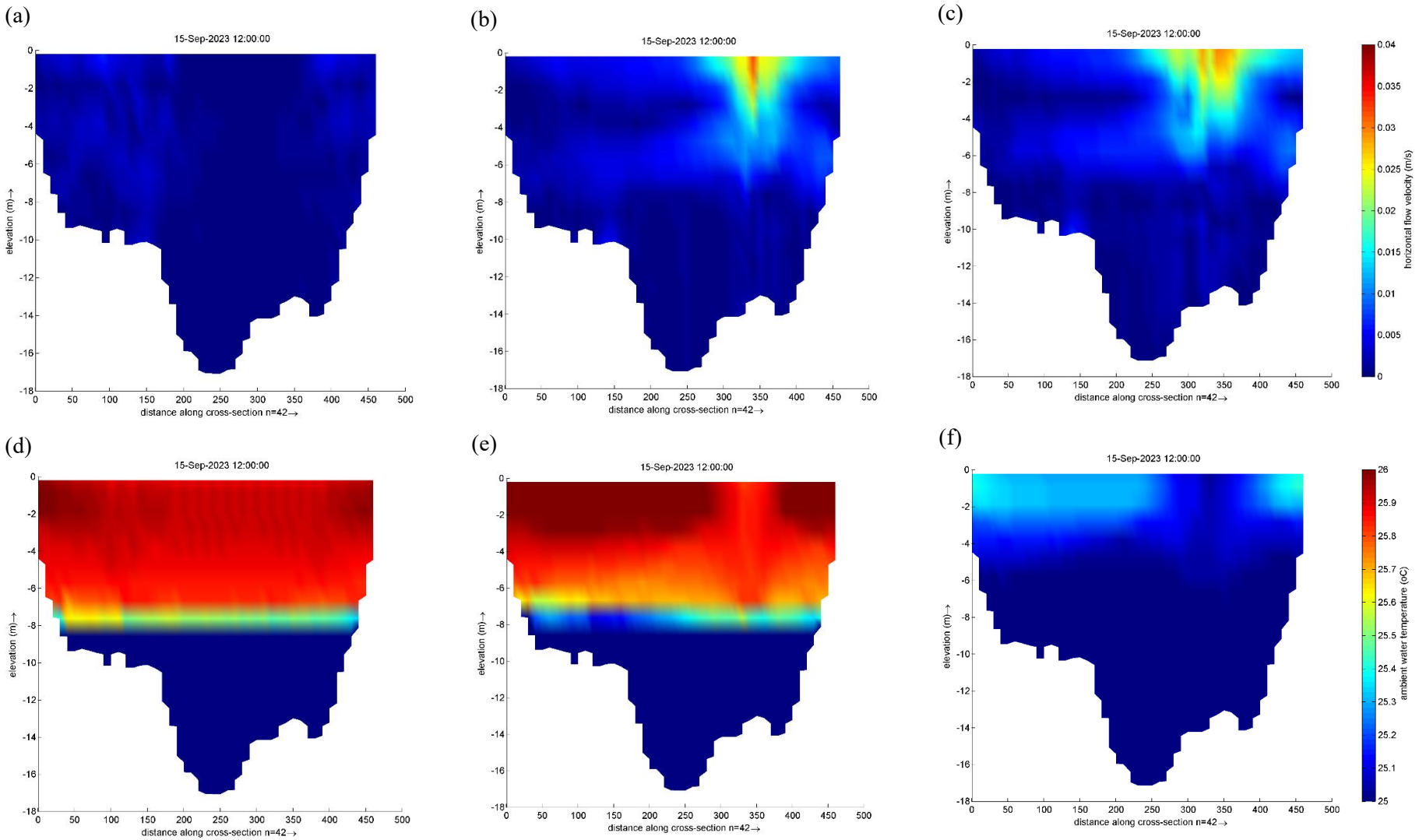

Figure 5-23 – Velocity (top row) and temperature (bottom row) in a cross section of the lake for scenarios 0 (left), 8 (center), and 15 (right), on 15/09/2023. Visualization of the generation of the velocity field due to the temperature difference .

Regarding turbulent energy, following the velocity behavior, from 8% to 90% it decreases as the area covered by FPV increases, showing that there is less vertical mixing and water circulation (Figure 5-24, Figure 5-25). These results are in accordance with Yang et al. (2022b), that observed a reduction in mixing energy with 30% lake cover. This can reinforce stagnation in deeper layers, altering the distribution of nutrients.

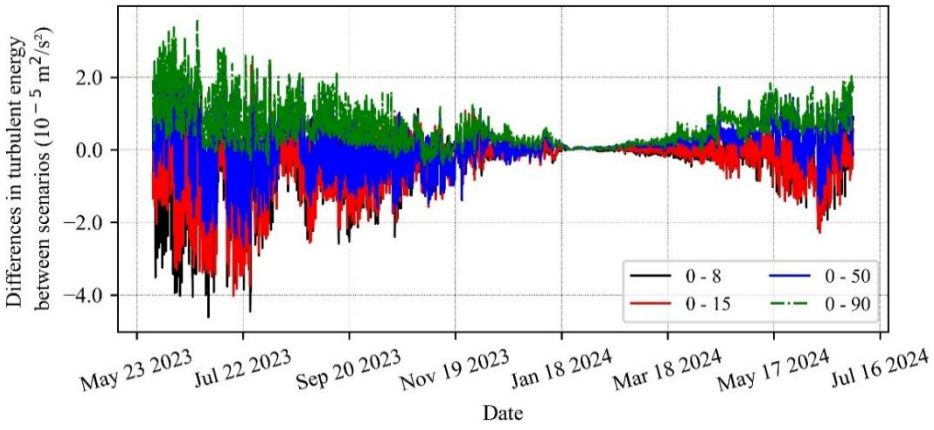

Figure 5-24. Differences in turbulent energy at the MFPV point between the base scenario (0) and the coverage scenarios, from 01/06/2023 to 01/06/2024.

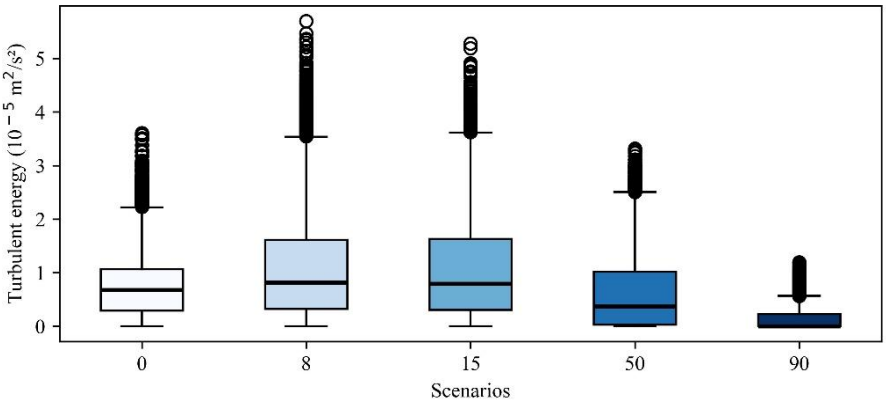

Figure 5-25. Boxplots of turbulent energy series considering the analyzed scenarios, from 01/06/2023 to 01/06/2024.

Residence Time

The residence time indicates the average time that a particle of water remains in the system before it is renewed. As it shows, up to 15% coverage, velocities increase and water circulation accelerates in the MFPV region, so the residence time in this area decreases (Figure 5-26). Between 15% and 50%, coverage effects begin to reduce circulation, increasing residence time. At 90%, this circulation is drastically reduced, as seen above, impacting the residence time, which almost triples its value. According to Olsson et al. (2022), reducing annual residence time can shorten and weaken thermal stratification.

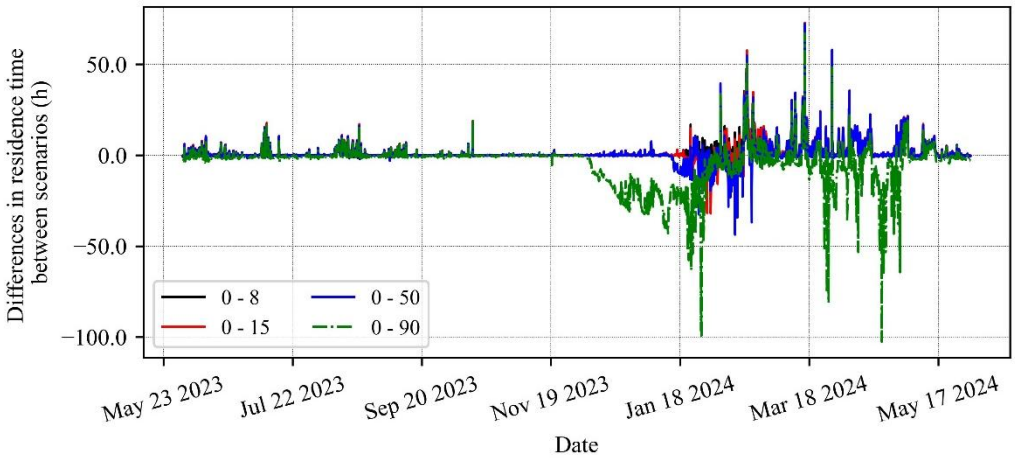

Figure 5-26. Differences in residence time at the MFPV point between the base scenario (0) and the coverage scenarios, from 01/06/2023 to 01/06/2024.

Tracer concentration

As seen in the behavior of the velocity, the transport of the tracer is more effective, increasing the difference in concentration between the MFPV and MREFII points (Figure 5-27). From 8% to 90%, as coverage increases, this difference rises, indicating a reduction in circulation in the covered region, affecting the tracer's dispersion.

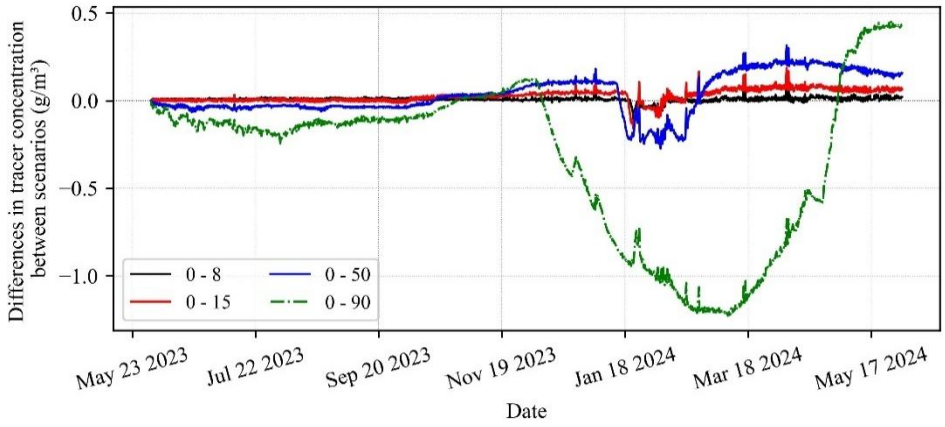

Figure 5-27. Differences in tracer concentration at the MFPV point between the base scenario (0) and the coverage scenarios, from 01/06/2023 to 01/06/2024.

Analyzing the concentration profile at the MFPV point (Figure 5-28) mixing in the water column is also affected, more significantly from 50% coverage onwards, as we see that convection is affected. When it reaches 90% coverage, the tracer accumulates on the surface, up to a depth of 2m (Figure 5-28e).

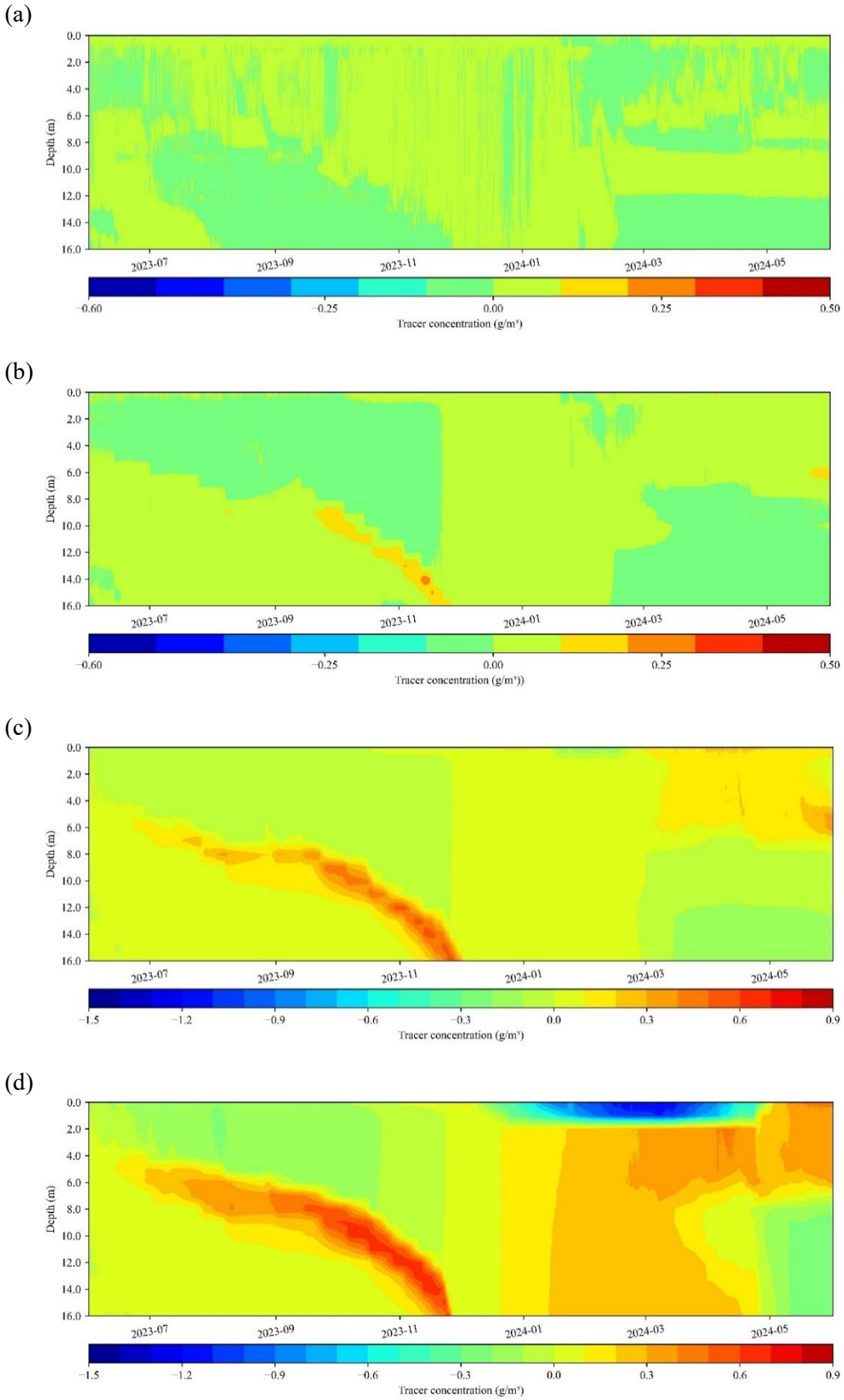

Figure 5-28. Tracer profiles differences, at MFPV point, between scenarios (a) 0 - 8, (b) 0 - 15, (c) 0 - 50, (d) 0 – 90, from 01/06/2023 to 01/06/2024. The color legends have different limits to enable visualization.

Dissolved oxygen

DO concentration increases as FPV coverage grows (Figure 5-29a), although the reaeration rate declines drastically between scenarios (Figure 5-30), falling by 76% in scenario 90 compared to the base scenario (Table 5-2). The saturation concentration rises (Figure 5-29b), as a function of its relationship with temperature (eq (4-8)), as its reduction increases the oxygen retention capacity. This relationship is illustrated by Chapra (2008) who shows that oxygen saturation decreases with rising temperature and vice versa (Figure 5-31). However, the relative oxygen saturation diminishes, in line with the measurements (Table 5-2).

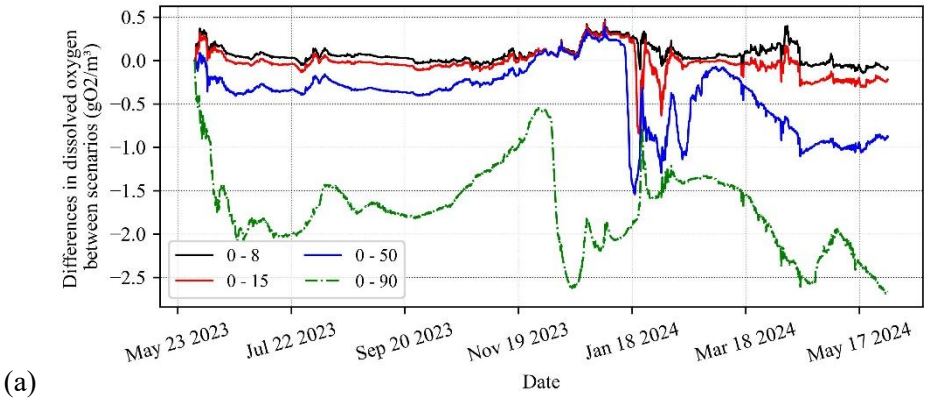

(a)

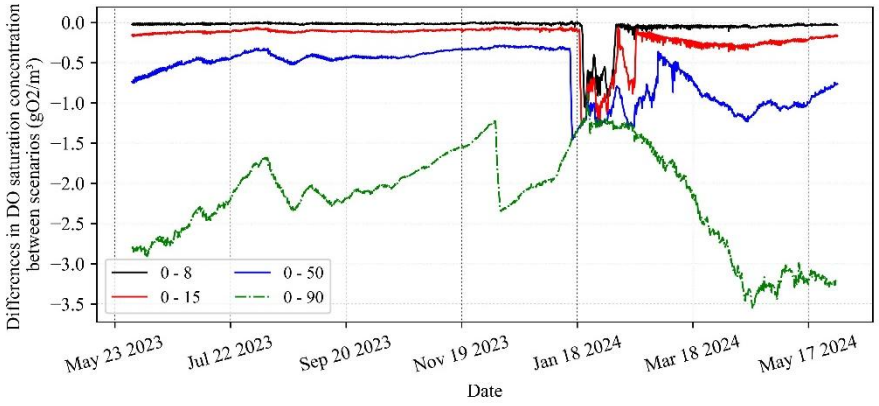

(b)

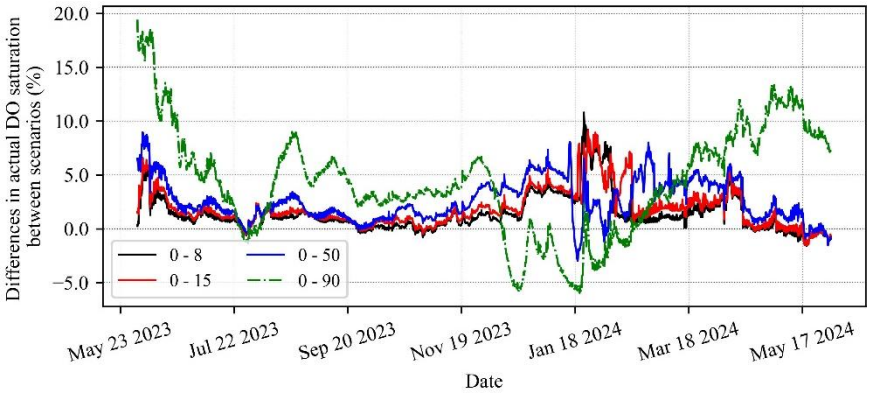

(c)

Figure 5-29. Differences in (a) DO, (b) DO saturation concentration, and (c) Actual DO saturation at the MFPV point between the base scenario (0) and the coverage scenarios, from 01/06/2023 to 01/06/2024.

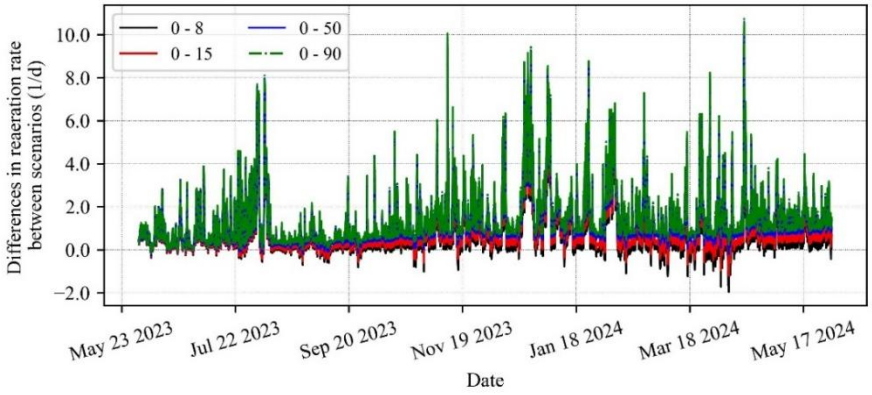

Figure 5-30. Differences in reaeration rate at the MFPV point between the base scenario (0) and the coverage scenarios, from 01/06/2023 to 01/06/2024.

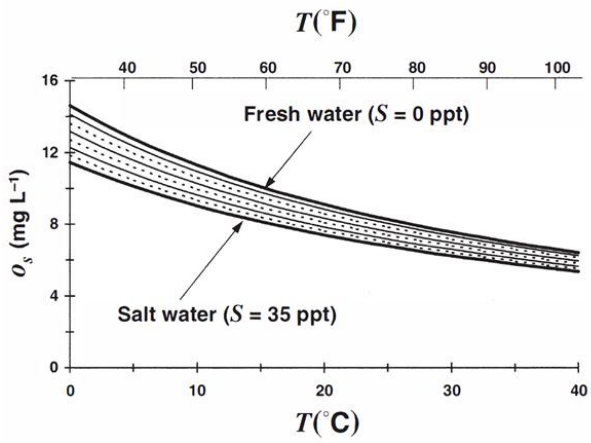

Figure 5-31. Relationship between oxygen saturation, temperature, and salinity (Chapra, 2008).

The variations between the scenarios (Figure 5-32) do not differ significantly until scenario 50, with the median remaining close to 7.5 g/m³. In the 90% scenario, values rise, with the median exceeding 8 g/m³. Looking at the profiles (Figure 5-33), the same behavior is highlighted, as a function of temperature. Up to scenario 15, it follows the pattern of thermal stratification. In scenarios 50 and 90, there is an increase in concentration in the upper layers, up to 4 m (Figure 5-33e).

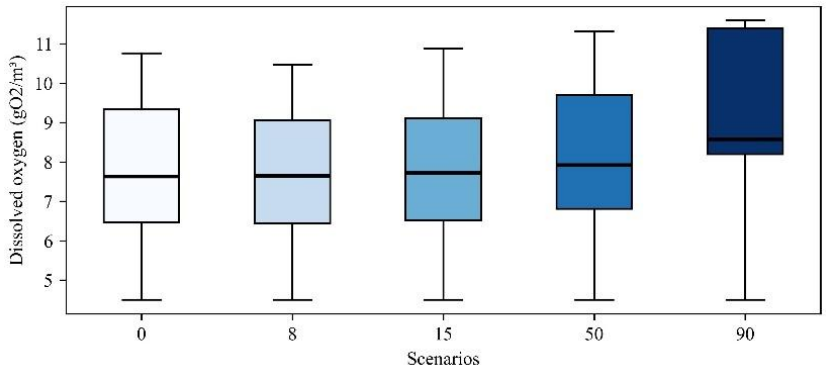

Figure 5-32. Boxplots of the dissolved oxygen concentration series considering the scenarios analyzed, from 01/06/2023 to 01/06/2024.

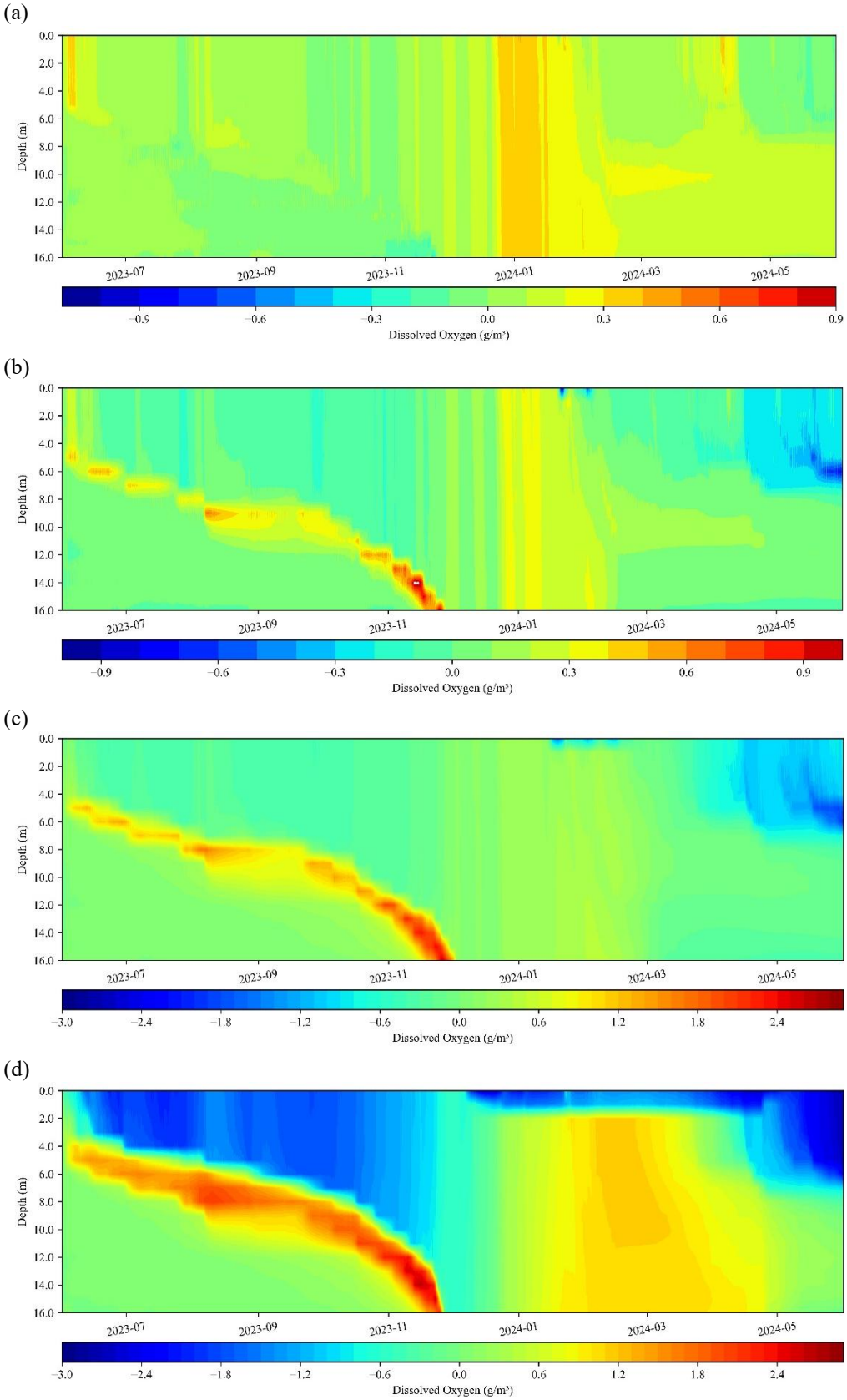

Figure 5-33. Dissolved oxygen concentration profiles differences, at MFPV point, between scenarios (a) 0 - 8, (b) 0 - 15, (c) 0 - 50, (d) 0 - 90, from 01/06/2023 to 01/06/2024. The color legends have different limits to enable visualization.

These results only represent the isolation of the reaeration process, disregarding oxygen consumption and production processes. In this way, the relationship with temperature dominates the reactions, increasing dissolved oxygen, unlike what was observed in the measurements. For a better understanding of the impacts on DO, other processes such as photosynthesis, respiration, oxygen consumption for the decomposition of organic matter, among others, should be added to the model.

5.2 PASSÚNA RESERVOIR

Several variables were monitored throughout 2022 and 2023, as shown in section 4.2.2. In this thesis, however, the analyses focused on temperature and dissolved oxygen. The modeling results are analyzed for surface temperature, evaporation rates, horizontal velocities, turbulent energy, residence time, tracer concentration, and dissolved oxygen.

5.2.1 MONITORING

Figure 5-34 and Figure 5-35 comparatively show the time series for the years 2022 and 2023 of the surface temperature (ST) and surface dissolved oxygen (SDO) variables for points PV1 and LR, measured at 0.50 m below the surface by the miniDOT sensors. In general, no significant differences were observed in surface water temperatures between both points, as well as observed by Bax et al. (2023), also in a pilot power plant.

Dissolved oxygen, on the other hand, showed higher concentrations at point LR when compared to point PV1. This can be associated with greater contact between the reservoir surface and the atmosphere at point LR and greater wind action (reaeration), resulting from less interference from the floating photovoltaic system (SANPEAR, 2023).

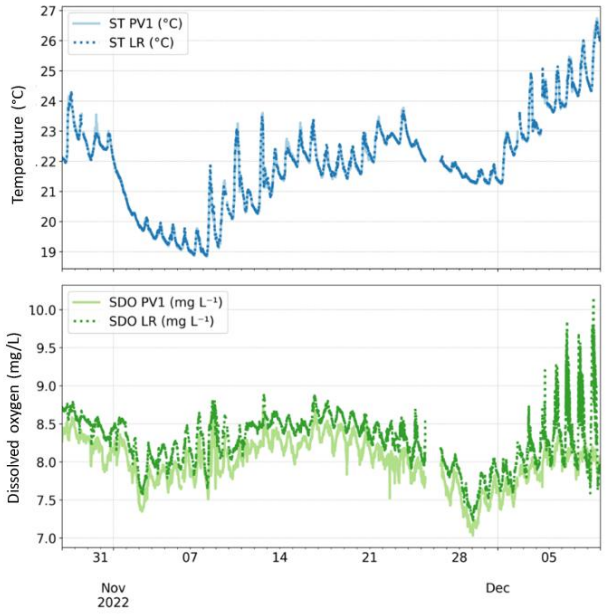

Figure 5-34. Time series (2022) for surface temperatures (ST, top graph) and surface dissolved oxygen (SDO, bottom graph). The ST series are similar between points PV1 and LR. The SDO series for point LR showed higher dissolved oxygen concentrations compared to the SDO series for point PV1 (SANEAR, 2023).

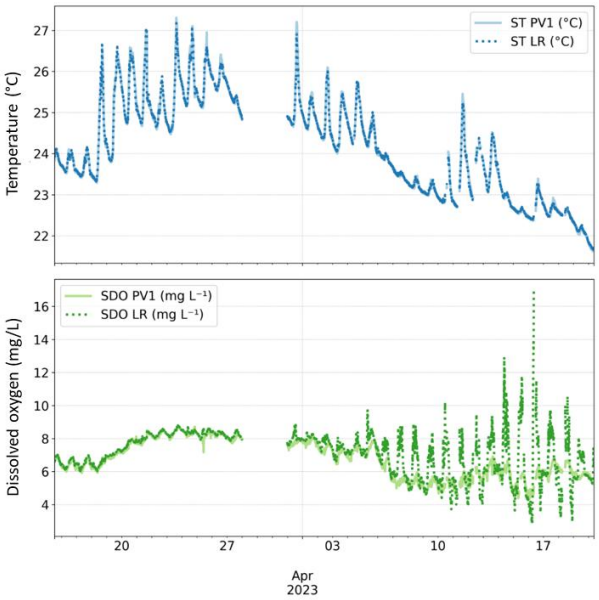

Figure 5-35. Time series (2023) for surface temperatures (ST, top graph) and dissolved oxygen at the surface (SDO, bottom graph). As with the year 2022, the STs were similar, with no significant differences between points PV1 and LR. The SDO for the 2023 period showed greater differences from around April 5, 2023, onwards, with a higher concentration of dissolved oxygen at the LR point (SANEAR, 2023).

Figure 5-35 illustrates that SDO LR exhibited greater amplitude in variations compared to SDO PV1, particularly from April 5, 2023, onward. During the period from March 15 to April 20, SDO PV1 was more stable than SDO LR. Emphasis was placed on describing the variables of surface temperature (ST PV1 and ST LR) and surface dissolved oxygen (SDO PV1 and SDO LR), for direct comparison of the effects of FPV on water temperature and the concentration of dissolved oxygen in the water (Figure 5-36, Figure 5-37).

The distributions shown in the histograms, as well as the box-plots of the series, are very similar to each other for the temperatures. The mean and standard deviation for ST PV1 was 22.91 °C ± 1.81 °C, and for ST LR, 22.92 °C ± 1.79 °C. These values are very close, with a difference of just over 0.01 °C for the LR point. The minimum values observed for ST PV1 and ST LR were 18.83 °C and 18.86 °C, respectively, and the maximum values were 27.31 °C and 27.24 °C. The medians, considered to be measures resistant to extreme values (anomalies/outliers), were the same at 22.83 °C for both points ST PV1 and ST LR. Thus, it can be seen that the greatest differences observed were associated with the maximum surface temperature values between each point, but values that are still within the sensor's error range

(a)

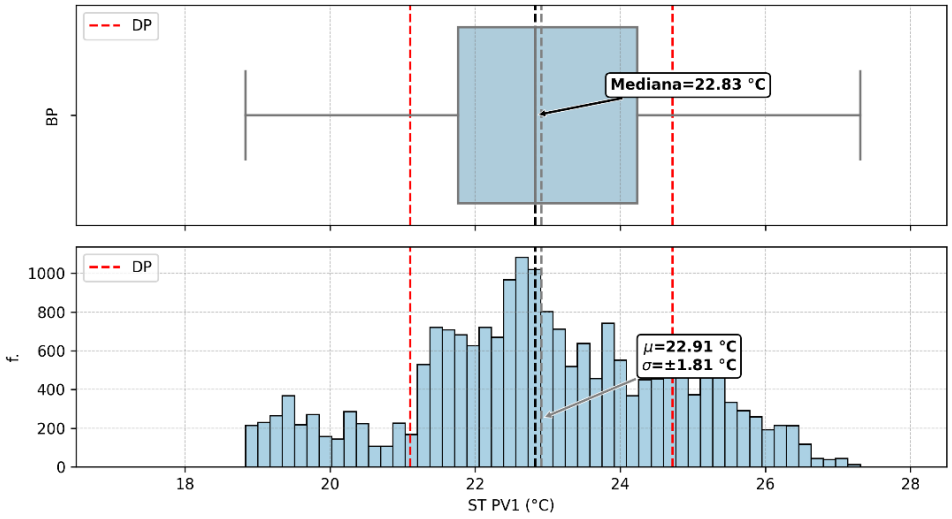

(b)

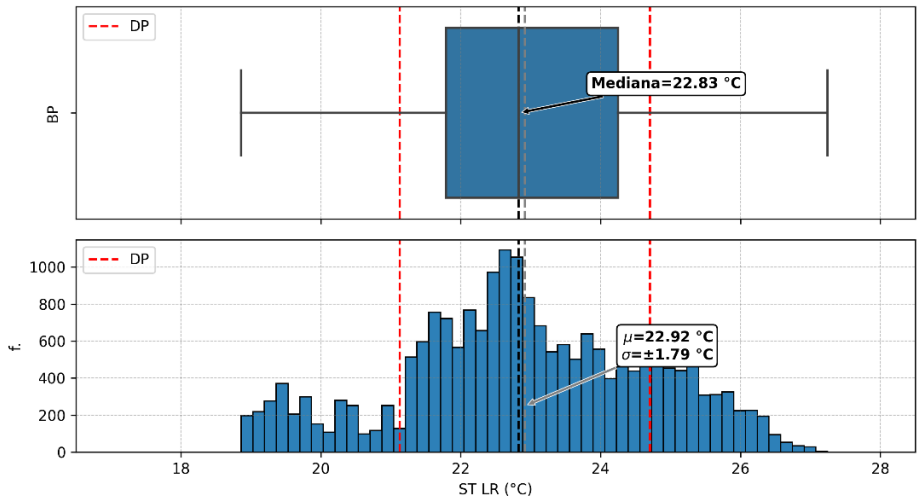

Figure 5-36. Composition of histograms, boxplots and notations of mean, standard deviation and median of surface water temperature data (a) ST PV1 and (b) ST LR (SANEPAR, 2023).

The maximum concentration observed throughout the entire period (October 2022 to April 2023) were 16.94 mg/L for SDO LR and 8.76 mg/L for SDO PV1, with minimum of 4.34 mg/L and 2.80 mg/L, respectively (Figure 5-37). The averages for SDO PV1 and SDO LR were 7.46±0.99 mg/L and 7.76±1.07 mg/L, respectively. Based on the values obtained, a higher concentration of dissolved oxygen can be seen at the LR point, as well as a greater variation in the extreme values of minimum and maximum.

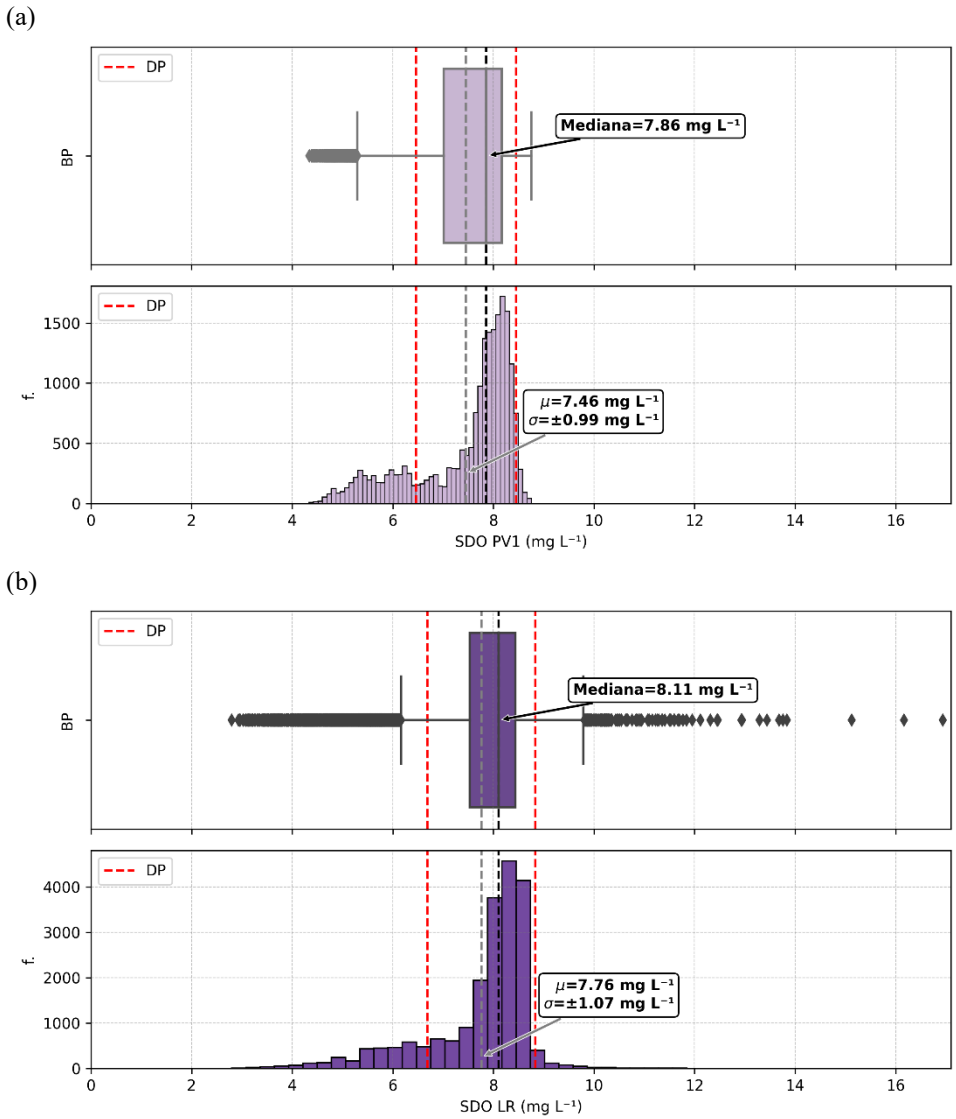

Figure 5-37. Composition of histograms, boxplots and notations of mean, standard deviation and median of surface water temperature data (a) SDO PV1 and (b) SDO LR (SANEPAR, 2023).

Statistical t-tests were conducted to assess whether the differences in the variables were statistically significant (Table 5-7). The surface temperature series showed no statistical difference between PV1 and LR (p-value = 0.889). On the other hand, the surface DO series showed a statistical difference with 99% significance (p-value = 0.001).

Table 5-7. Statistical analysis of temperature and dissolved oxygen from miniDOT data (October 2022 to April 2023). The average values of measurements taken beneath the FPV system (PV1) are compared to those recorded in open water (LR), with the standard deviation presented in brackets. The p-value is derived from t-tests and is indicated alongside significance level p ≤ 0.01 (*).

Variable	PV1	LR	p-value	Significance
Water temperature (°C)	22.91 (±1.81)	22.92 (±1.79)	0.889	
Dissolved oxygen (mg/L)	7.46 (±0.99)	7.76 (±1.07)	0.001	*

Table 5-8 provides a summary of the key input parameters used in the hydrodynamic model to assess FPV impacts on Passaúna Reservoir. The scaling factor for shortwave radiation was estimated from miniPAR monitoring results (SANEPAR, 2023). As the wind reduction below the structure in Passaúna was not evaluated, it was decided to use the same reduction factor as that used in the Leimersheim lake, as this value is within the range found in the literature (Ilgen et al., 2023).

Table 5-8. Parameters adjusted to represent FPV in Delft3D.

Parameter	Without FPV	With FPV	Deviation (%)
Scaling factor for shortwave radiation	1	0.10	90
Scaling factor for wind speed	1	0.43	57

5.2.2 MODELING

5.2.2.1 Calibration

Based on the model calibrated during the FotoÁgua project, a new simulation was carried out, varying the approach to representing the coverage of the panels, as explained in chapter 4.2.2. In order to check that the calibration is valid in this new simulation, the levels (Figure 5-38) and temperatures (Figure 5-39, Figure 5-40) were compared to the measurements at PV1.

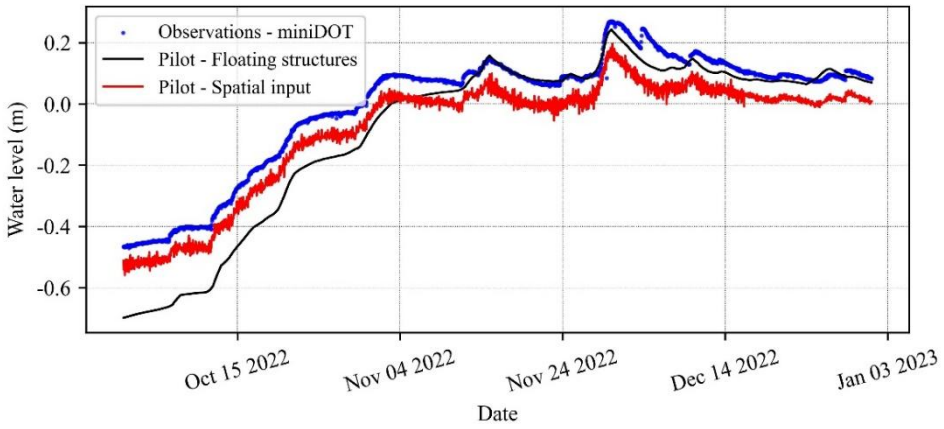

Figure 5-38. Water level at the intake location. Observations in blue, results from FotoÁgua model in black, and from the Spatial varying model in red.

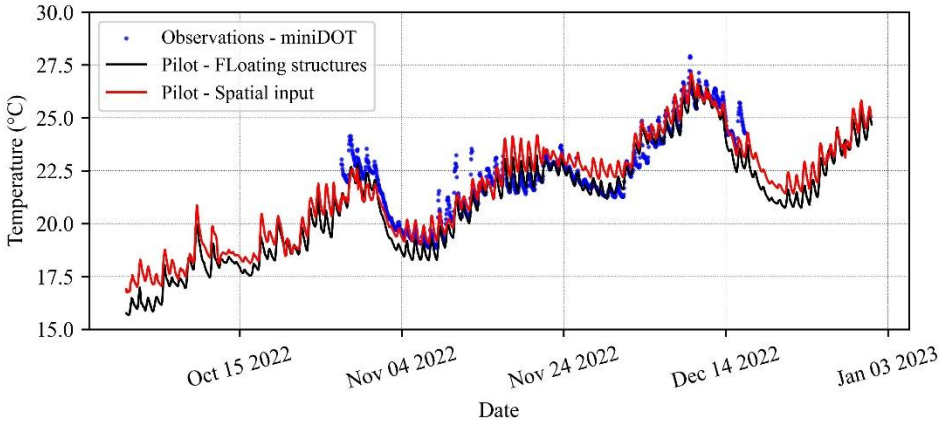

Figure 5-39. Surface temperature at PV1 (0.5 m below surface). Observations in blue, results from FotoÁgua model in black, and from the Spatial varying model in red.

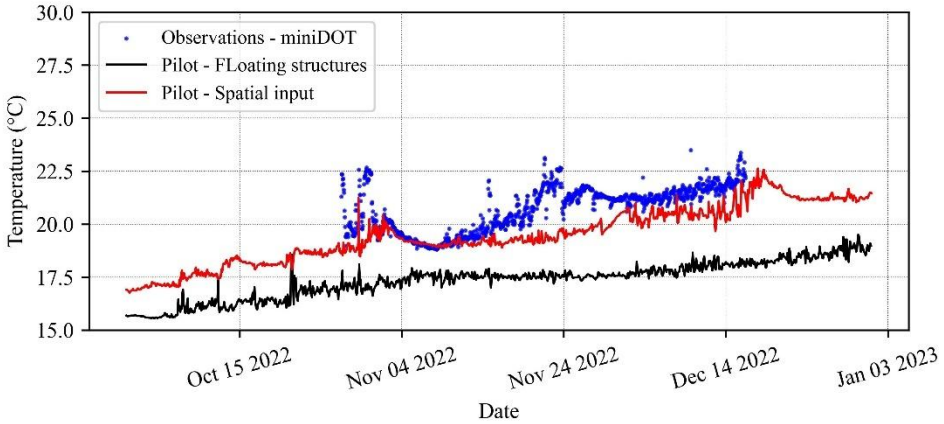

Figure 5-40. Bottom temperature at PV1 (6 m below surface). Observations in blue, results from FotoÁgua model in black, and from the Spatial varying model in red.

After checking the temperatures, the calibration was analyzed for dissolved oxygen, at the surface (Figure 5-41) and at the bottom (Figure 5-42), at PV1. The calibration metrics are shown in Table 5-9.

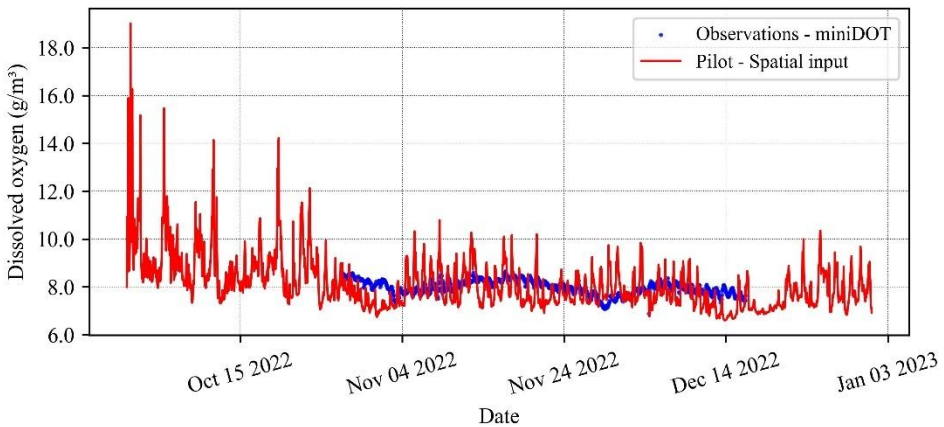

Figure 5-41. Surface dissolved oxygen at PV1 (0.5 m below surface). Observations in blue, results from FotoÁgua model in black, and from the Spatial varying model in red.

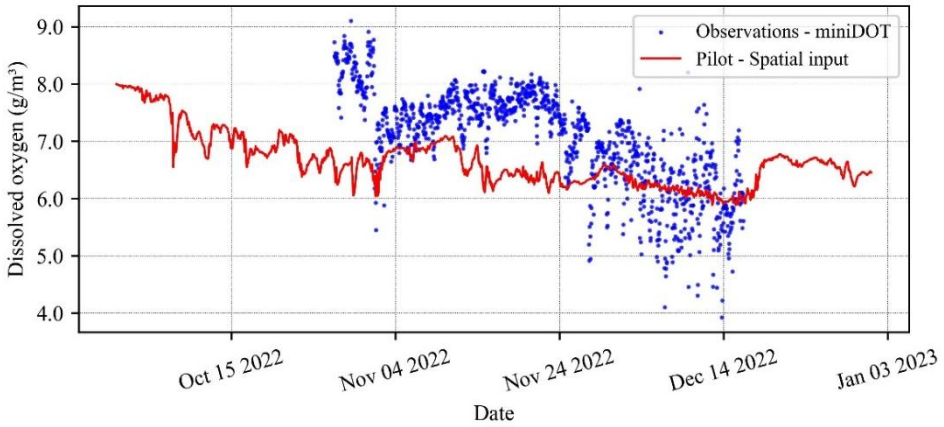

Figure 5-42. Bottom dissolved oxygen at PV1 (6 m below surface). Observations in blue, results from FotoÁgua model in black, and from the Spatial varying model in red.

Table 5-9. Statistics obtained from the calibration of water level, temperature and dissolved oxygen at point PV1. Surface: 0.5 m below surface; Bottom: 6 m below surface.

Parameter	RMSE	NSE	MAE	Bias	r
Water Level (m)	0.08	0.83	0.08	-0.08	0.99
Surface temperature (°C)	0.79	0.84	0.64	0.15	0.92
Bottom temperature (°C)	1.32	-0.54	1.04	-1.02	0.61
Surface DO (g/m³)	0.76	-5.54	0.65	-0.51	0.23
Bottom DO (g/m³)	0.99	-0.27	0.83	-0.62	0.51

In general, the model is capable to represent the parameter analyzed. It tends to underestimate dissolved oxygen concentrations, as well as bottom temperature, while it tends to overestimate surface temperature. Although in absolute values there are differences of up to 1°C, the temperature behavior is satisfactorily represented over time.

5.2.2.2 Scenarios

To analyze the scenarios, the maps were cut to make it easier to see the variations. A region of approximately 2.5 km² was considered, including the FPV expansion region and areas without significant influence from the panels. All the time series were extracted from a point in the center of the expanded coverage (named Cell Cover), making it possible to compare coverage vs. non-coverage. A summary of the main results between the scenarios is presented in Table 5-10.

Table 5-10. Summary of differences between scenarios (average over time), with the standard deviation presented in brackets, for the total period of simulation (01/10/2022 to 01/01/2023).

Parameter	Pilot - Expanded
Actual DO saturation (%)	0.2(±0.74)
Dissolved oxygen (g/m³)	-0.03(±0.05)
Horizontal velocity (cm/s)	0.13(±1.67)
Reaeration rate (1/d)	2.33(±4.64)
Residence time (h)	0.07(±1.38)
Saturation concentration (g/m³)	-0.05(±0.03)
Shmidt Stability (J/m²)	4.77(±5.21)
Surface temperature (°C)	0.34(±0.25)

Parameter	Pilot - Expanded
Thermocline depth (m)	-0.26(±1.7)
Total Evaporation rate (m³/h)	68.51(±48.20)
Tracer concentration (g/m³)	0.19(±0.43)
Turbulent energy (m²/s²)	1.44E-05(±2.71E-05)

Temperature

The average surface temperature drops slightly between the pilot and expanded scenarios (Figure 5-43), decreasing by around 1.6%. The temperature variations follow the two scenarios, with no significant differences (Figure 5-44). Like highlighted by Ji et al. (2022), reservoirs are different from lakes, with the temperature being highly influenced by inflow water temperatures.

Spatially, there is a slight temperature variation in the region near the panels (Figure 5-45), which does not reach 0.5°C. Looking at a cross-section that cuts through the region of the panels, it is possible to see a modest reduction in temperature that occurs up to a depth of approximately 4 m (Figure 5-46).

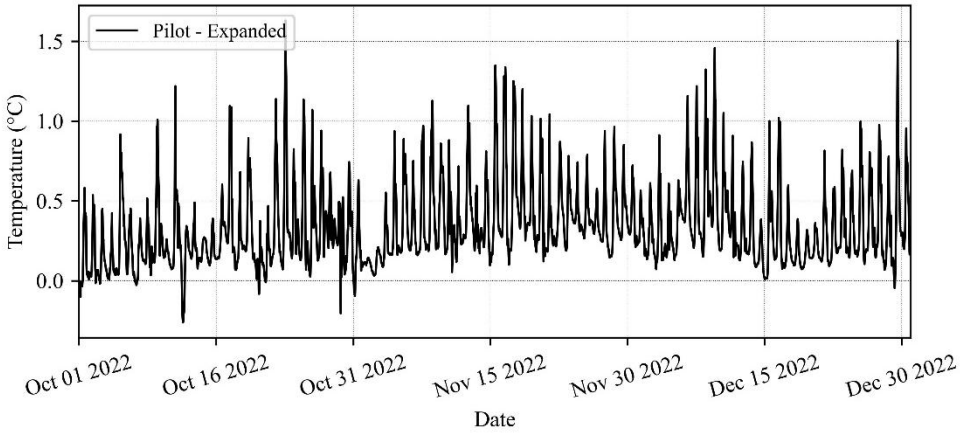

Figure 5-43. Difference of surface temperature between the Pilot - Expanded scenarios, from 01/10/2022 to 01/01/2023.

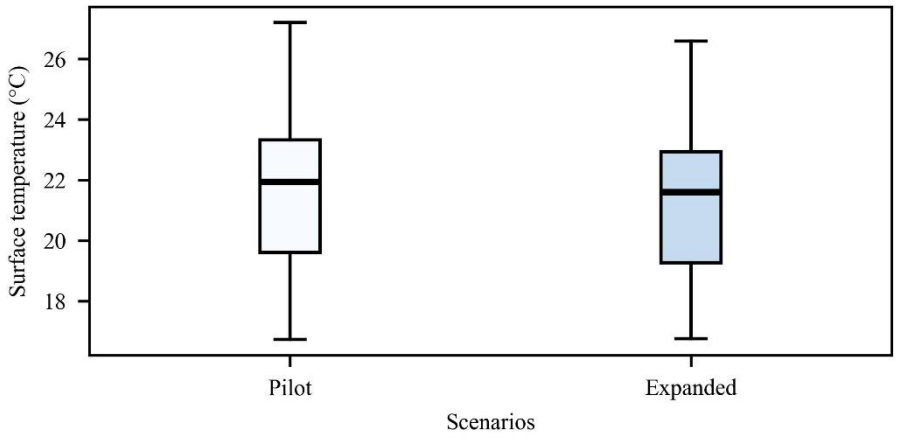

Figure 5-44. Boxplots of the Surface temperature, from 01/10/2022 to 01/01/2023.

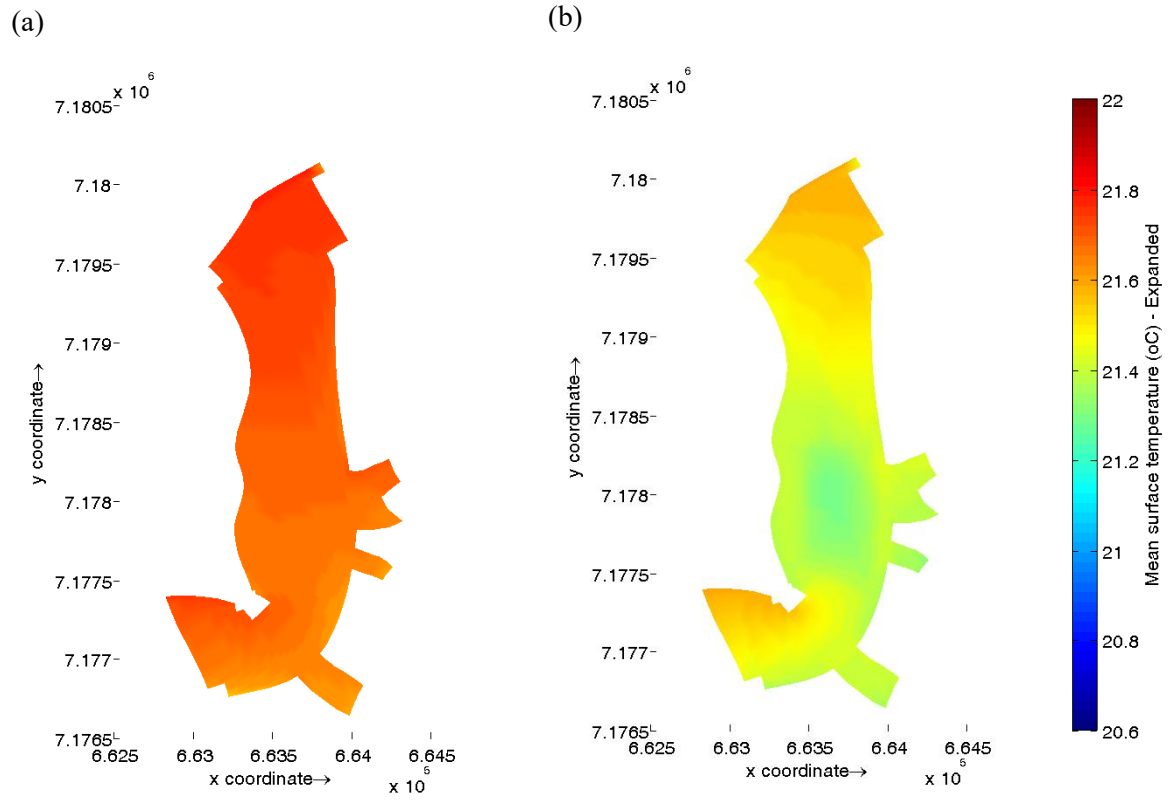

Figure 5-45. Mean Surface temperatura for scenarios (a) Pilot and (b) Expanded, from 01/10/2022 to 01/01/2023.

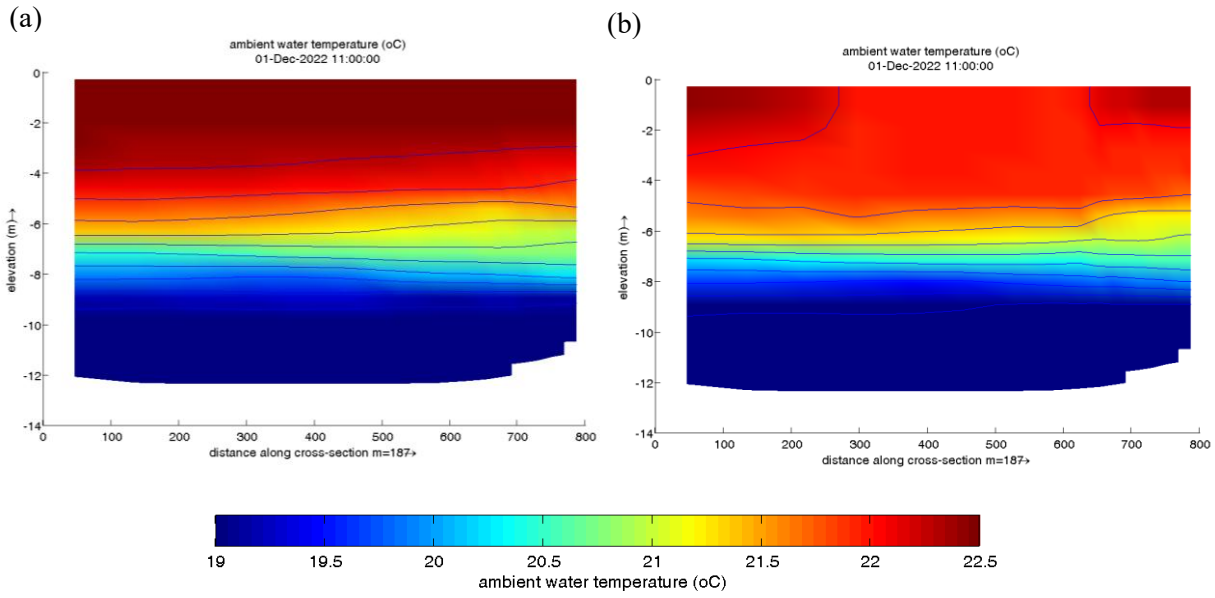

Figure 5-46. Temperature in a cross section at the FPV cover for scenarios (a) Pilot and (b) Expanded, at 01/10/2022 11 a.m.

Looking at the temperature profiles (Figure 5-47, a and b), one can see that the panels have little influence on stratification (Figure 5-47c), as shown by the variation in the depth of the thermocline at Table 5-10 (~0.26 m).

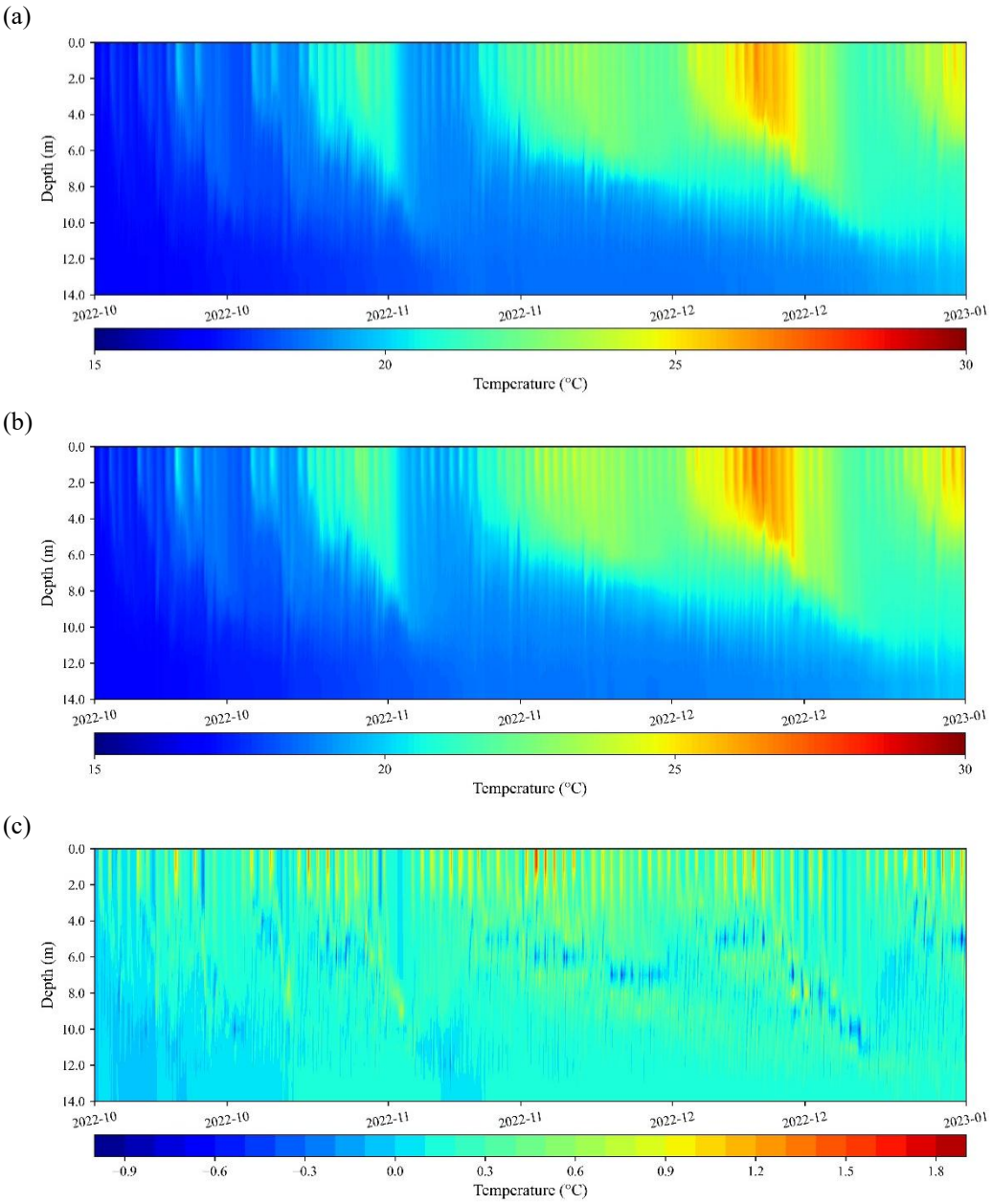

Figure 5-47. Temperature profiles, at Cell Cover point, for scenarios (a) Pilot , (b) Expanded, and temperature profiles difference (c) Pilot - Expanded, from 01/10/2022 to 01/01/2023.

Evaporation rate

The average difference in evaporation rates between the pilot and expanded scenarios is 68.5 m³/h, with a reduction of approximately 14% in evaporation due to the coverage (Figure 5-48). These differences in evaporation are accentuated in the daytime, as can be seen in Figure 5-50. As for the gravel pit lake, total evaporation rates were obtained by the sum of the rates for each cell times the average cell area.

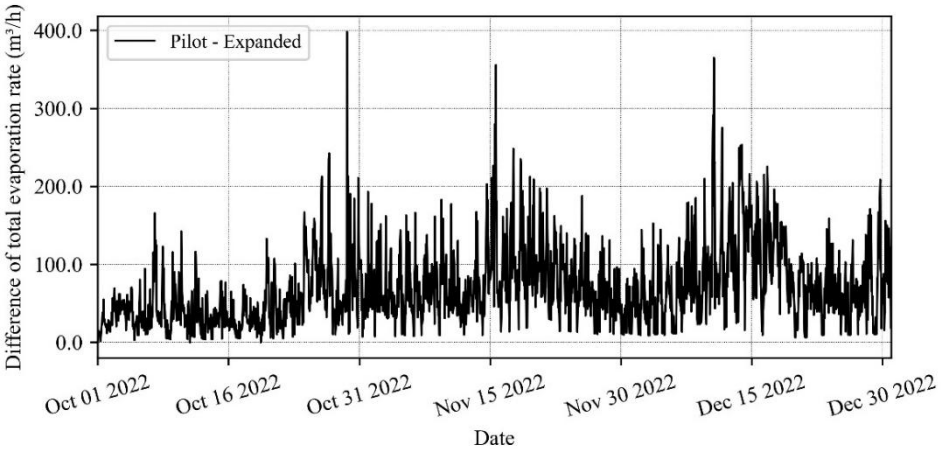

Figure 5-48. Difference of evaporation rates between the Pilot - Expanded scenarios, from 01/10/2022 to 01/01/2023.

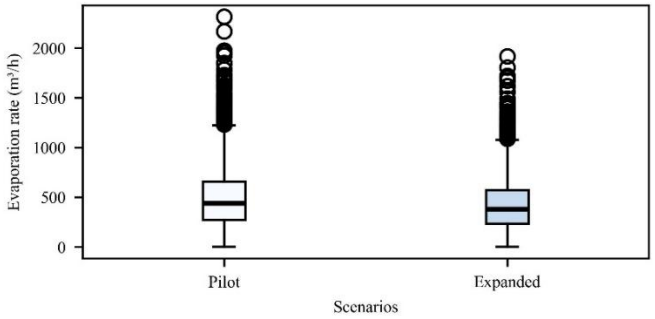

Figure 5-49. Boxplots of the evaporation rate time series for the analyzed scenarios, from 01/10/2022 to 01/01/2023.

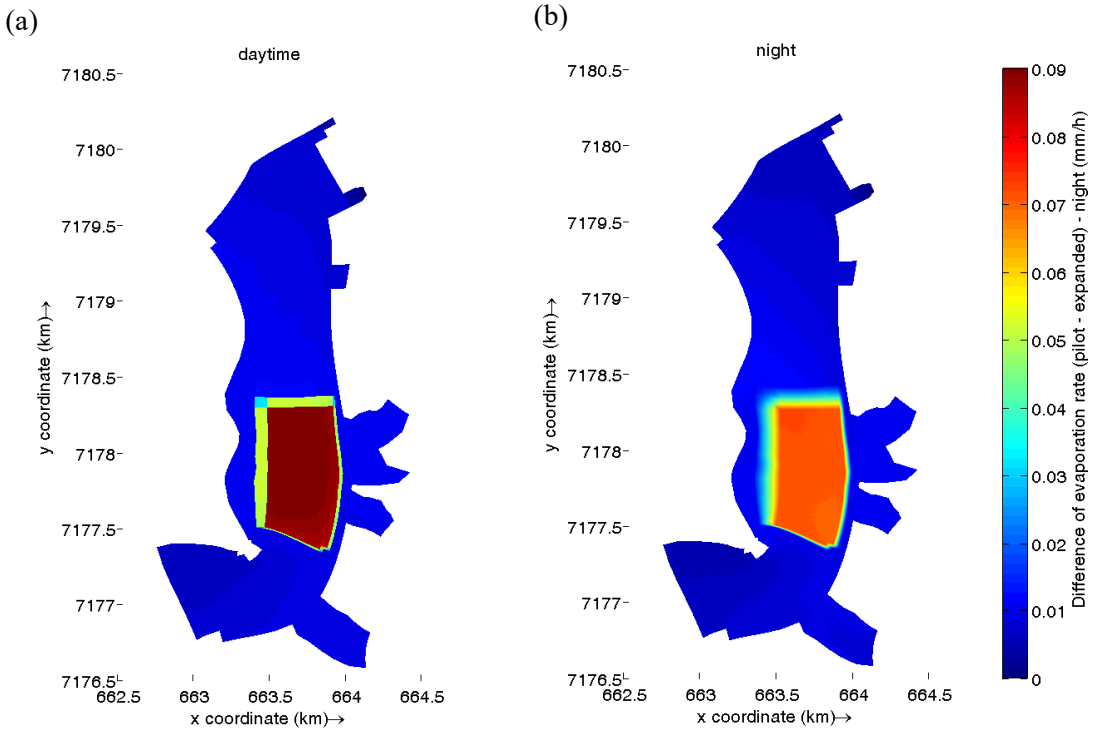

Figure 5-50. Difference between the mean evaporation rate, Pilot – Expanded, during the day (a) and the night (b), in mm/h, from 01/10/2022 to 01/01/2023.

Horizontal velocity and Turbulent Energy

As seen in Table 5-10, where the variation in average horizontal velocity is in the order of 0.1 cm/s, there is little variation in the velocities (around a 5% reduction) due to the reduction in wind speed in the region of the panels (Figure 5-51, Figure 5-52). Spatially, no significant variation can be observed in the time average (Figure 5-53). Selecting a moment of higher velocity at the Cell Cover point and looking at the cross-section (Figure 5-54), it shows a slight reduction in velocity in the region of the panels, with the impact occurring up to a depth of almost 2 m. However, the behavior of the timeseries averages indicates that at other times there is an increase in speed below the panels, so that there seems to exist no pattern.

Unlike the velocities, the difference in turbulent energy between the scenarios shows a reduction due to the coverage almost all period (Figure 5-55). Also its variation decreases in relation to the Pilot scenario (Figure 5-56). An average reduction of 43% is calculated at the Cell Cover point in the expanded scenario (Table 5-10).

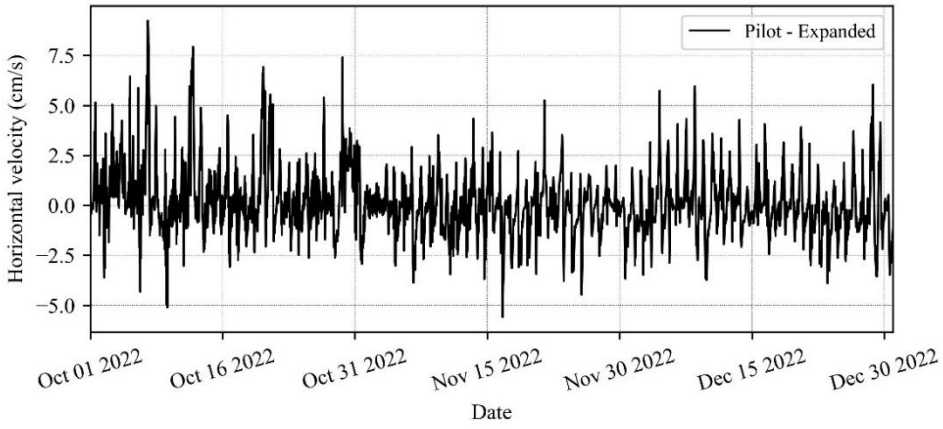

Figure 5-51. Difference of horizontal velocities between the Pilot - Expanded scenarios, from 01/10/2022 to 01/01/2023.

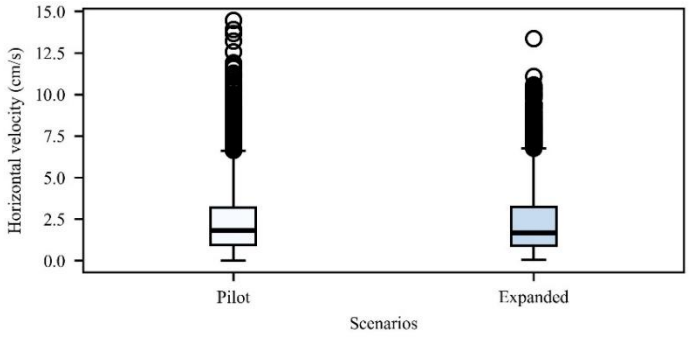

Figure 5-52. Boxplots of the horizontal velocity, from 01/10/2022 to 01/01/2023.

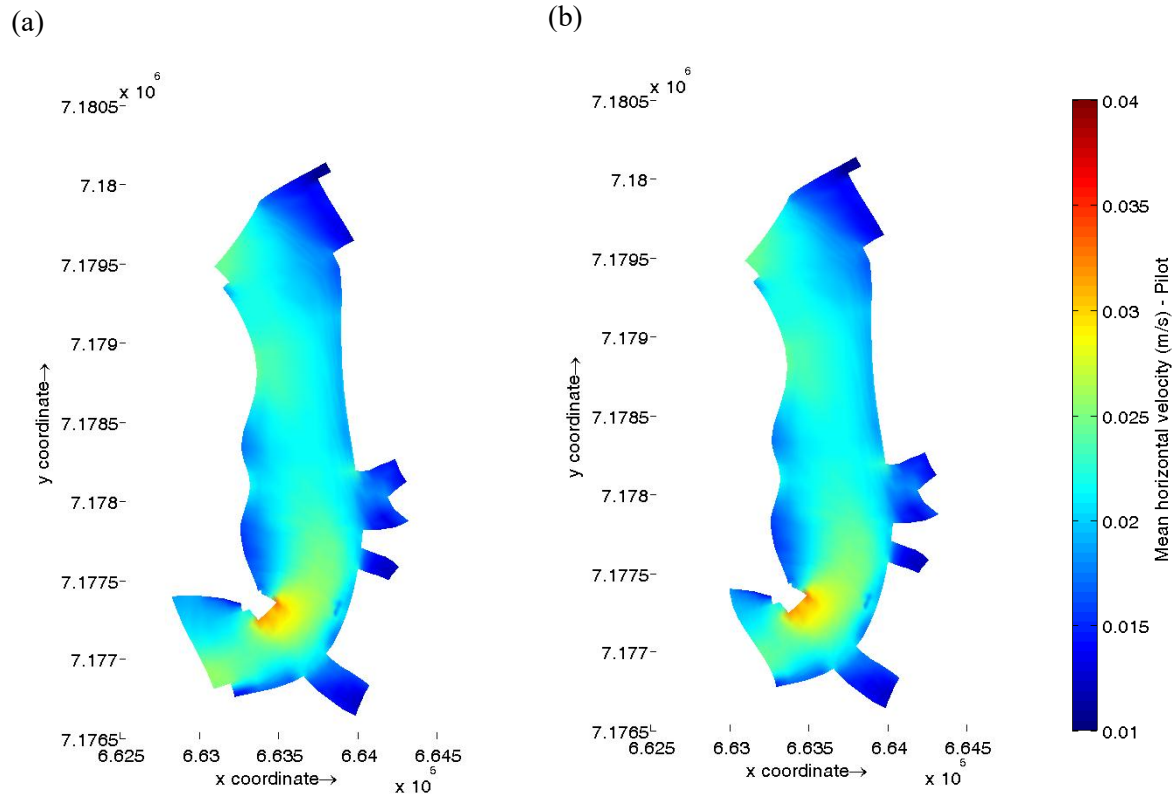

Figure 5-53. Difference between the mean horizontal velocity, Pilot – Expanded, during the day (a) and the night (b), from 01/10/2022 to 01/01/2023.

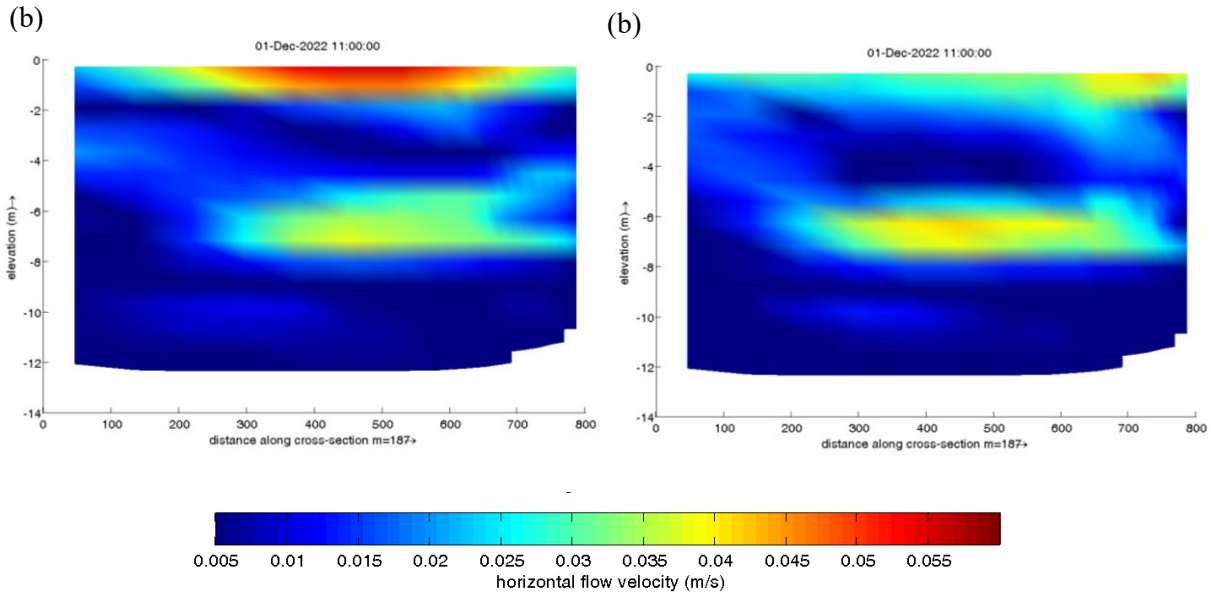

Figure 5-54. Horizontal velocity in a cross section at the FPV cover for scenarios (a) Pilot and (b) Expanded, at 01/12/2022 11 a.m.

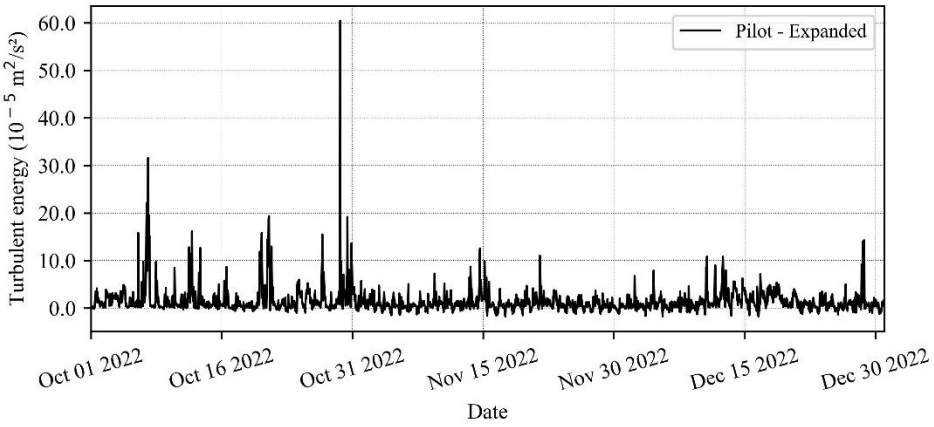

Figure 5-55. Difference of turbulent energy between the Pilot - Expanded scenarios, from 01/10/2022 to 01/01/2023.

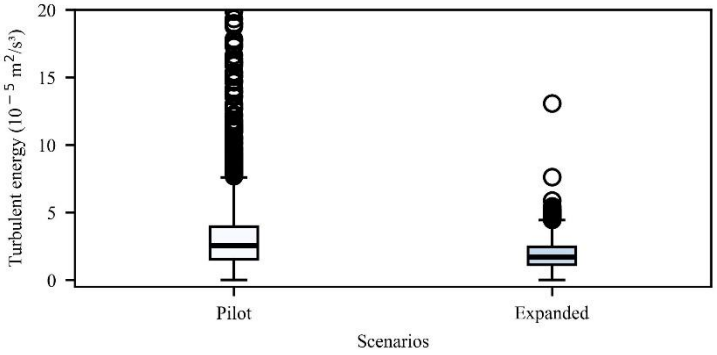

Figure 5-56. Boxplots of the turbulent energy, from 01/10/2022 to 01/01/2023.

Residence time

The average residence time decreases by around 6% in the region below the panels, and is in the order of 1 h (Table 5-10). As observed in the behavior of the velocities, the time series of the difference in residence time between the scenarios shows positive and negative moments (Figure 5-57), and the variation of the timeseries show similar results for both scenarios (Figure 5-58). This indicates that, at certain times, the coverage generates an increase and at others a reduction in RT.

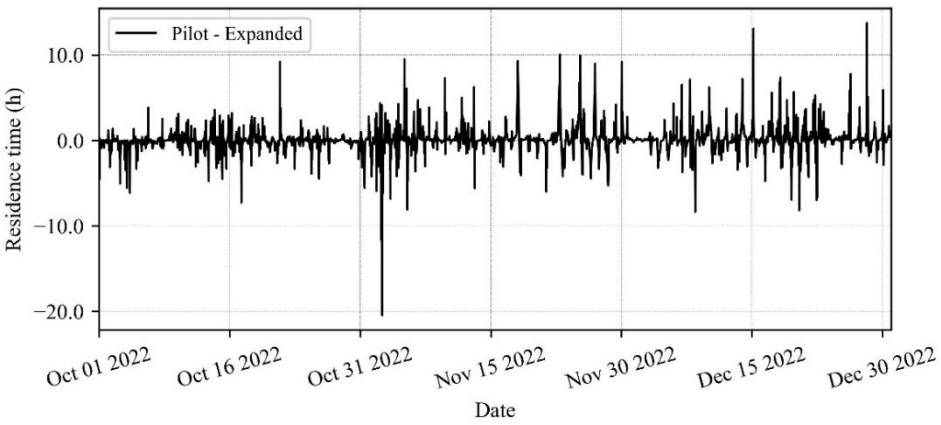

Figure 5-57. Difference of residence time between the Pilot - Expanded scenarios, from 01/10/2022 to 01/01/2023.

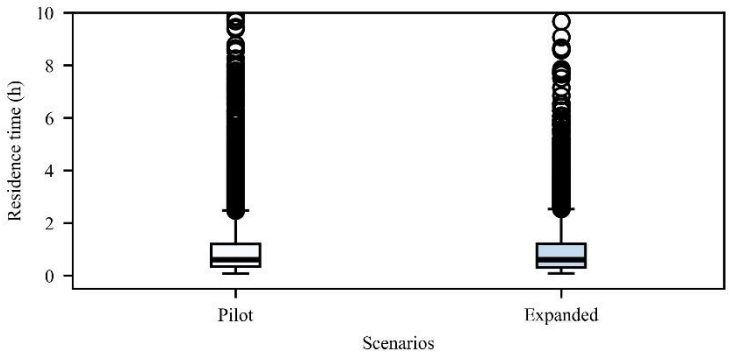

Figure 5-58. Boxplots of the residence time, from 01/10/2022 to 01/01/2023.

Tracer concentration

The tracer was released at the Cell Cover point, with a low flow rate that would not influence the hydrodynamics of the area (4.2.2.2). There is a reduction in the concentration of the tracer at the point just downstream, with an average decrease of approximately 12% (Figure 5-59, Figure 5-60).

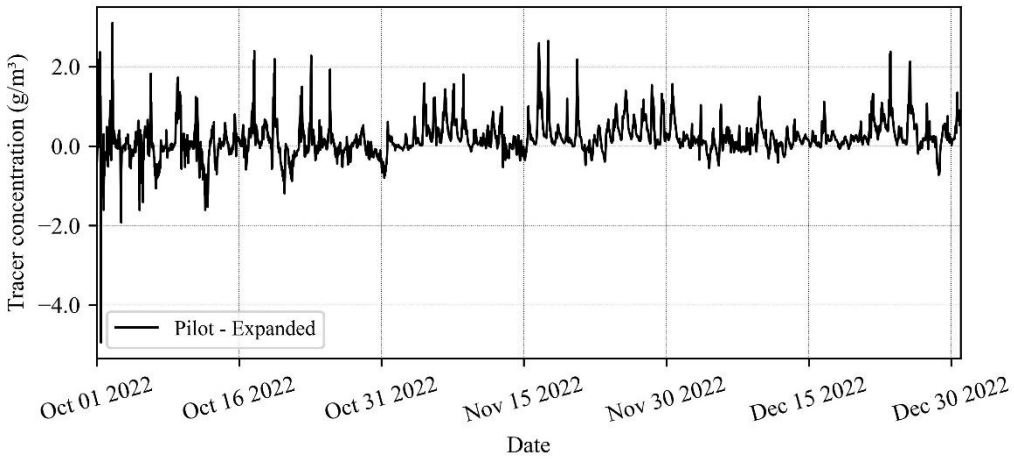

Figure 5-59. Difference of tracer concentration between the Pilot - Expanded scenarios, from 01/10/2022 to 01/01/2023.

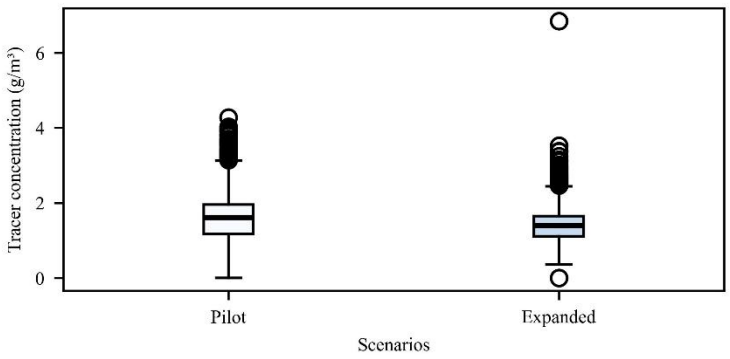

Figure 5-60. Boxplots of the tracer concentration, from 01/10/2022 to 01/01/2023.

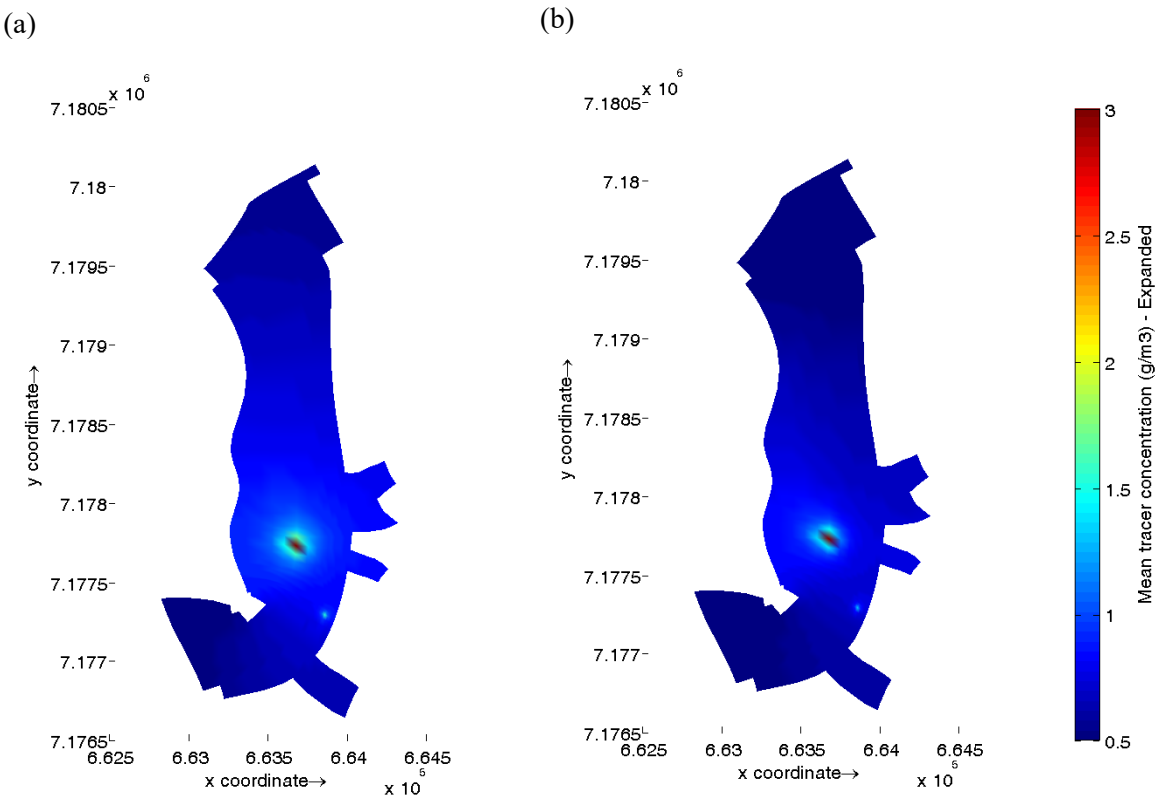

Figure 5-61. Mean tracer concentration for (a) Pilot, and (b) Expanded scenarios.

Dissolved oxygen

Surface DO concentration increases slightly with the presence of the panels (0.5%, Table 5-10) as shown in Figure 5-62. The variation in DO are similar between scenarios and over time series (Figure 5-63). Although there is a decrease in the reaeration rate (around 25.6%) with the presence of the panels (Figure 5-64), this behavior may be due to temperature reduction. The saturation concentration rises (~0.7%), and the oxygen saturation in the water reduces slightly (~0.2%). Looking at the profiles (Figure 5-65) at Cell Cover point, there are almost no variations.

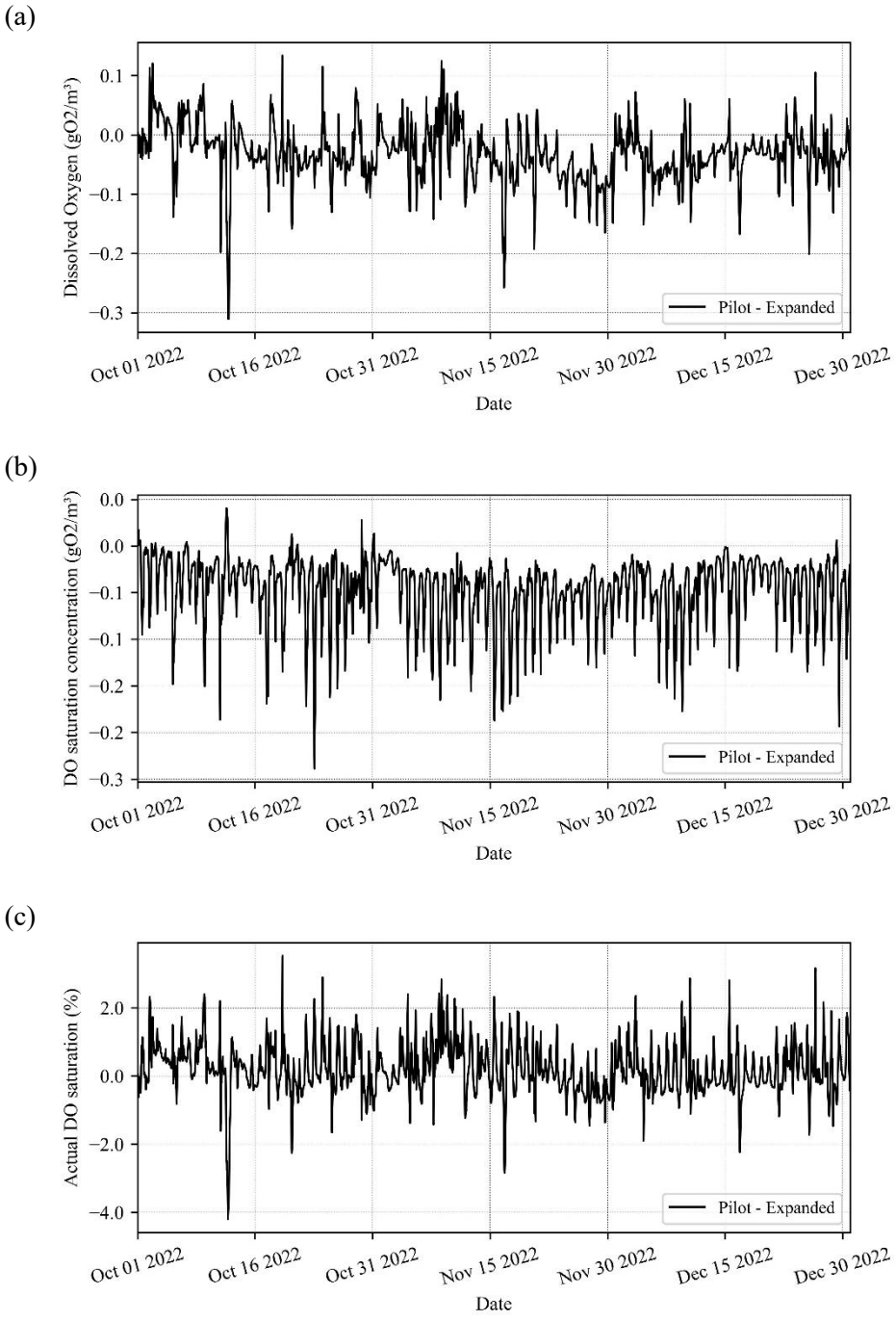

Figure 5-62. Differences in (a) DO, (b) DO saturation concentration, and (c) Actual DO saturation at the Cell Cover point between the Pilot and Expanded scenarios, from 01/10/2022 to 01/01/2023.

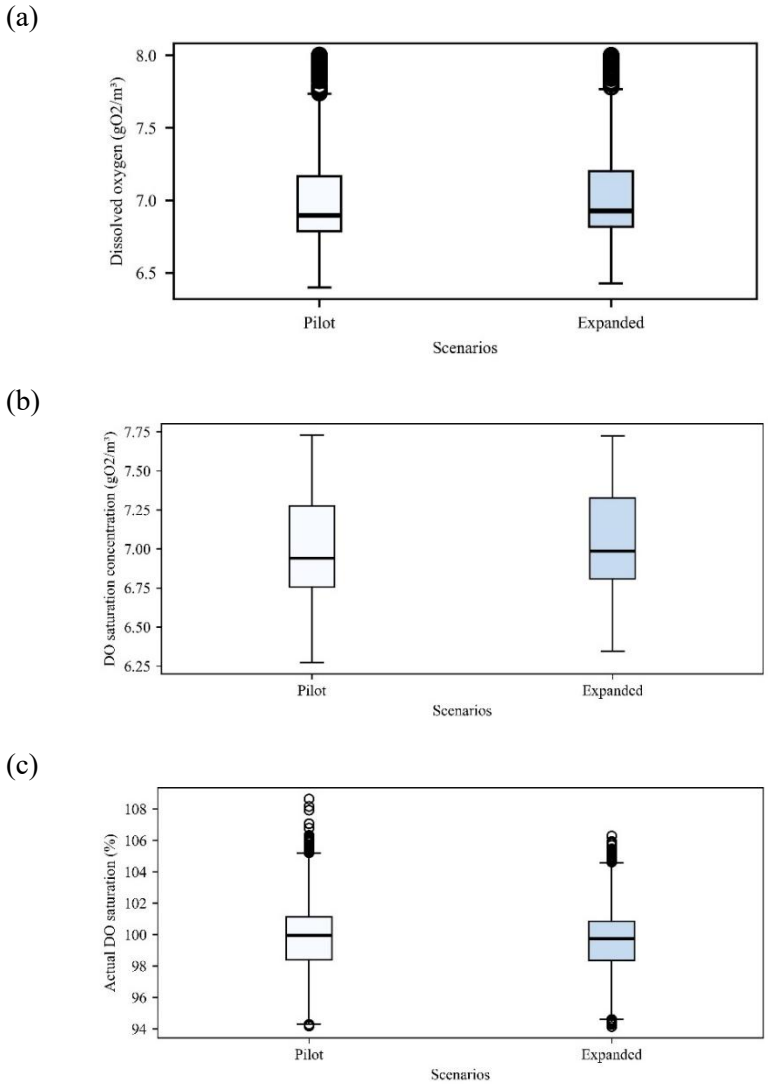

Figure 5-63. Boxplots of (a) DO, (b) DO saturation concentration, and (c) Actual DO saturation at the Cell Cover point, from 01/10/2022 to 01/01/2023.

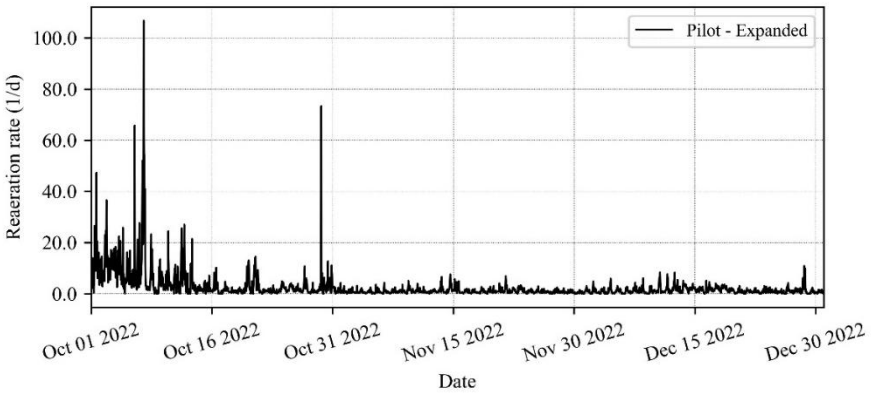

Figure 5-64. Reaeration rate resulting from Pilot and Expanded scenarios, from 01/10/2022 to 01/01/2023.

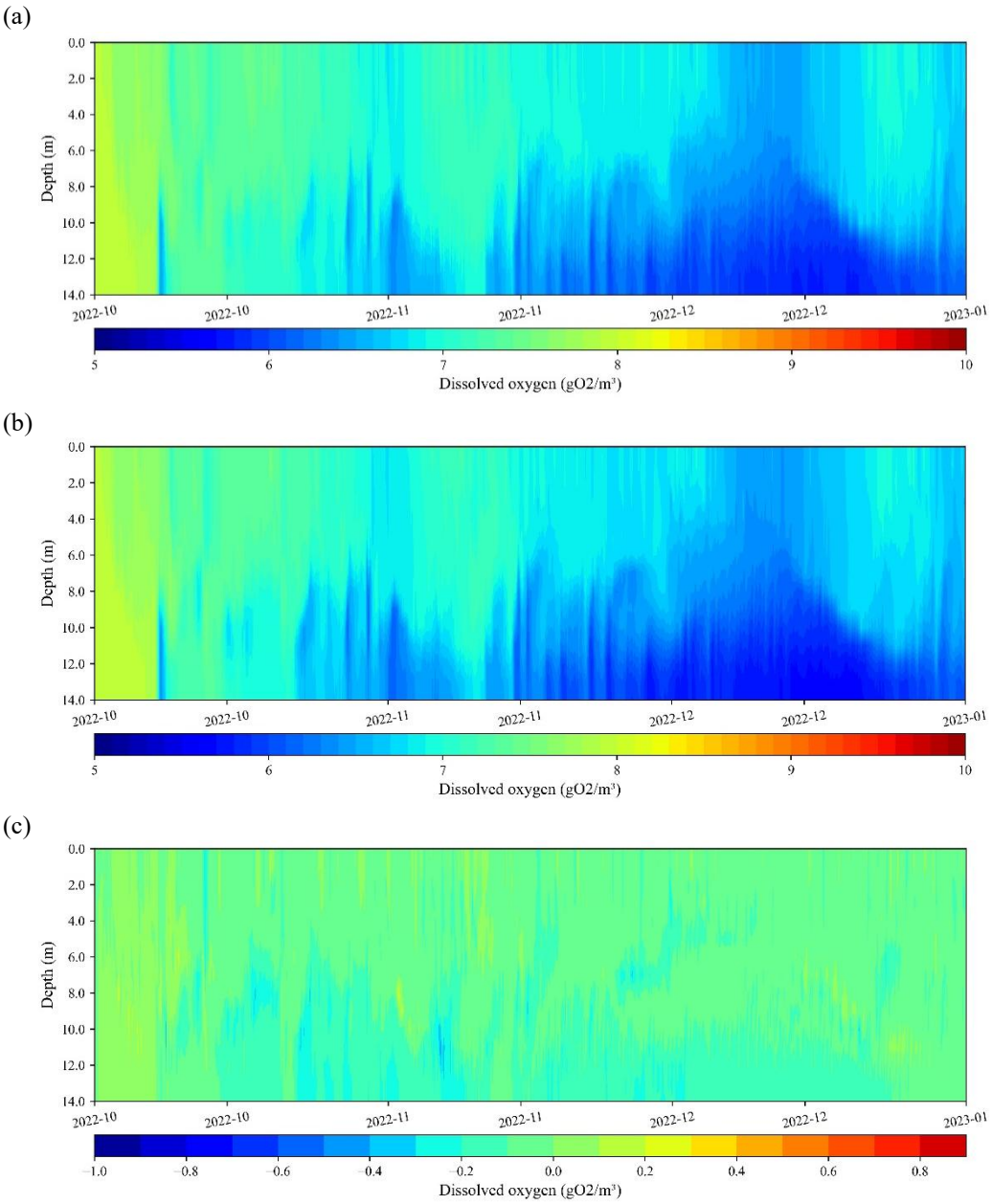

Figure 5-65. Dissolved Oxygen profiles, at Cell Cover point, for scenarios (a) Pilot , (b) Expanded, and DO profiles difference (c) Pilot - Expanded, from 01/10/2022 to 01/01/2023.

5.3 STUDY SITES COMPARISON

Germany's lake has a volume of approximately 1.7 hm³, around 2% of Passaúna's volume (59 hm³). Their maximum depths are similar, but the difference in flooded area is the same as their volume (Leimersheim: 19.5 ha and Passaúna: 900 ha). The thermocline depth in the current state is similar for the two sites (Leimersheim: 6.98 and Passauna 7.22 m), but the Schmidt Stability varies, being higher in Leimersheim (176.5 J/m²), decreasing by 77% in Passauna (58.1 J/m²). This indicates that the lake in Germany has a more stable stratification and is more resistant to water mixing than Passaúna. This may be due to various factors, including morphometry and climatic issues. Leimersheim has more transparent

water (Secchi depth reached 7 m in some periods, while Passaúna is around 2 m) and lower velocity than the Passaúna Reservoir.

Their main differences include the climate in which they are located, with Germany's climate being temperate, while the Passaúna region is subtropical, with average annual temperatures of 11.2°C and 18°C, respectively. Another important variation is that the Passaúna has tributary rivers, i.e. streams reaching the reservoir. In Leimersheim, a gravel pit lake, there is only an groundwater contribution, with no influence from surface flows on its hydrodynamics. Despite having some similar characteristics, these differences can have an impact on the hydrodynamics and, consequently, the water quality of these two environments in different ways (Goulart et al. (2024), APPENDIX A).

Within the monitoring periods analyzed, similar results were observed in terms of variation due to FPV. Both lakes showed no statistically significant difference in water temperature values due to FPV, like other studies with lower percentage of coverage (Bax et al. (2023), de Lima et al. (2021)), but they did in dissolved oxygen results. In terms of time average, both sites showed a slight reduction in DO below the panels (0.3 mg/L in Passaúna, 0.38 mg/L in Leimersheim). It should be noted that, in addition to the reduction in wind, there were mussels clinging to the floats at Leimersheim, which can influence the reduction in DO levels in the water.

In terms of modeling results, both models were able to represent water temperature. Regarding dissolved oxygen, the model was able to reproduce the trends over time in the calibration scenario, even though only the physical process of reaeration was considered. One possible reason is that both reservoirs are oligotrophic, unpolluted. However, it was unable to represent daily variability. The initial idea was to focus on the physical processes and, in the next steps, to add the processes of oxygen consumption and production, as well as nutrients and algae, which are essential for representing environments with a greater amount of organic matter.

Comparing scenario 8 (Leimersheim) with the Expanded scenario (Passaúna), which show a similar proportion of coverage, the reduction in surface temperature occurs to the same extent in both environments (up to 1.5%). These results are of the same order of magnitude as other modeling studies for low coverage (Ilgen et al. (2023), Exley et al. (2021)). As for dissolved oxygen, there is a reduction of less than 1% in Leimersheim, while there is a slight increase in concentration in Passaúna (0.5%). The saturation concentration varies in the same proportion in both cases (rises up to 0.7%), while the actual oxygen saturation in the water decreases in Leimersheim (~1.4%) and in Passaúna (~0.2%).

The results for horizontal velocity are the ones that show the greatest differences (Leimersheim increases velocity, while Passaúna reduces it by 5%), residence time (L reduces by 77%, P by 6%), and turbulent energy (L increases, Passaúna reduces it by 43%). Even though Passaúna has an inflowing surface flow, it is known that the current in the reservoir are mainly driven by wind (Ishikawa et al., 2021).

Another difference of greater magnitude is in the reaeration rate. Different formulations are used, in which the relationship with temperature and wind speed are considered in different ways (equations (4-7) a (4-13)). The formulation adopted for the temperate lake is more sensitive to wind variation: a 57% reduction in wind speed decreases the reaeration rate by 82% at Leimersheim, while the same reduction at Passaúna decreases the rate by 26%. It should be noted that, within the period of each modeling (which have different durations), winds of greater magnitude were observed in the German lake, reaching more than 10 m/s. In Passaúna, the speeds did not exceed 6m/s.

Considering the expansion scenarios in Leimersheim, the impacts of FPV vary according to coverage, affecting hydrodynamics and gas exchange processes. At low coverages (up to 15%), there is a slight cooling of the water surface (up to 0.9°C), a small decrease in dissolved oxygen saturation (up to 1.83%), and an increase in horizontal velocity, indicating the influence of temperature differences on circulation. The reaeration rate already shows a significant reduction (52% drop at 15% coverage). At moderate coverage (50%), the surface temperature drops more sharply (reduction of 3.35°C), the DO concentration increases slightly, but the actual DO saturation continues to decrease. Circulation becomes more restricted, with a reduction in horizontal velocity and a longer residence time. At high coverages (90%), the impacts are even more significant: the surface temperature drops dramatically (11.12°C reduction), the reaeration rate is reduced by 76%, and circulation is practically inhibited, reflected in the drop in turbulence and energy dissipation. In addition, the evaporation rate suffers an extreme reduction, reaching only 1.7% of the initial value. These results show that optimized coverage studies can be useful for water savings, like in semi-arid regions (da Costa & da Silva, 2021), as well as generating energy managing the impact.

Combining the results of both study sites (Figure 5-66), it is possible to see that the variation in the temperature is not linear, as shown by Exley et al. (2021). The same applies to DO concentrations, that show a non-linear increase (when considering only the reaeration process). In terms of circulation, there is a linear trend in the horizontal velocity and turbulent energy results with increasing FPV for Leimersheim (Figure 5-67). However, the Passaúna results deviate from that line, underlining what was said earlier about the impacts on circulation being stronger in the gravel pit lake. The hypothesis is that in the lake, these variations in velocity magnitude are caused by the difference in temperature, not by the wind. This is not the case in Passaúna, since temperatures do not vary much. It should be remember that although the variations in the lake are large (up to 450%), these velocities are in the mm/s range. Residence time and the tracer concentration show a weak linear tendency (Figure 5-68). In this case, the values for Passaúna show the same trend as those for Leimersheim (reduction with 6% coverage), although the magnitudes of the variations differ.

Regarding evaporation, the water savings for Leimersheim show a linear tendency as the FPV coverage grows (Figure 5-69). For a similar coverage proportion, Passaúna reservoir shows 14% reduction, while the lake shows 0.03%.

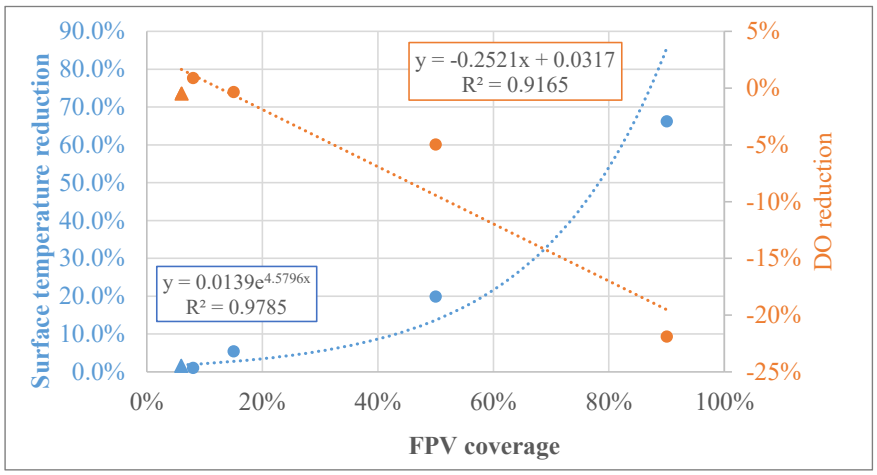

Figure 5-66. FPV coverage vs Surface Temperature reduction (blue) and vs Dissolved Oxygen reduction (orange) for Leimersheim (dots) and Passaúna (triangle).

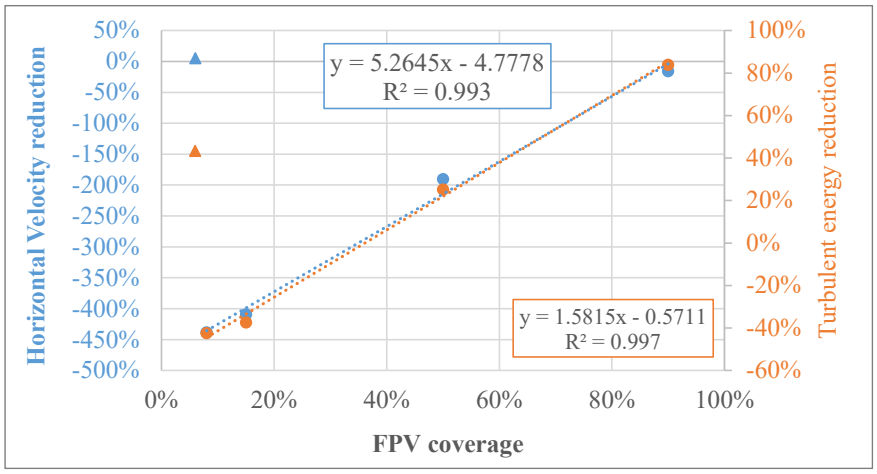

Figure 5-67. FPV coverage vs Horizontal velocity reduction (blue) and vs Turbulent energy reduction (orange) for Leimersheim (dots) and Passaúna (triangle). The tendency lines consider only Leimersheim results.

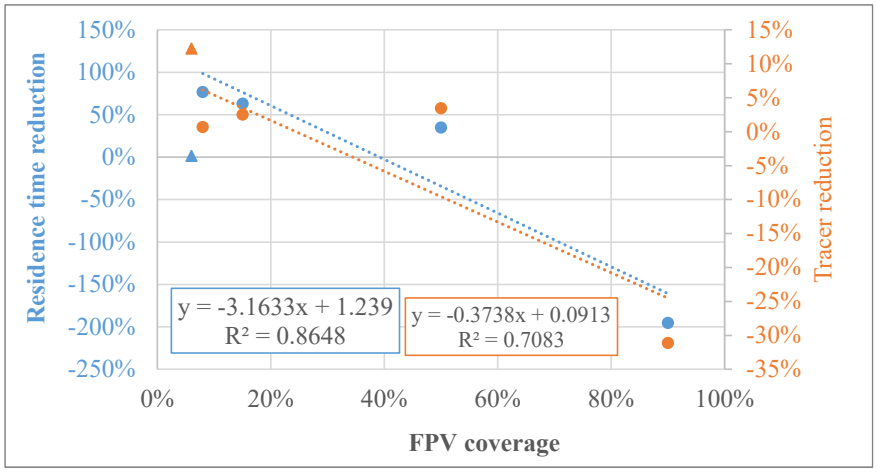

Figure 5-68. FPV coverage vs Residence Time reduction (blue) and vs Tracer Concentration reduction (orange) for Leimersheim (dots) and Passaúna (triangle). The tendency lines consider only Leimersheim results.

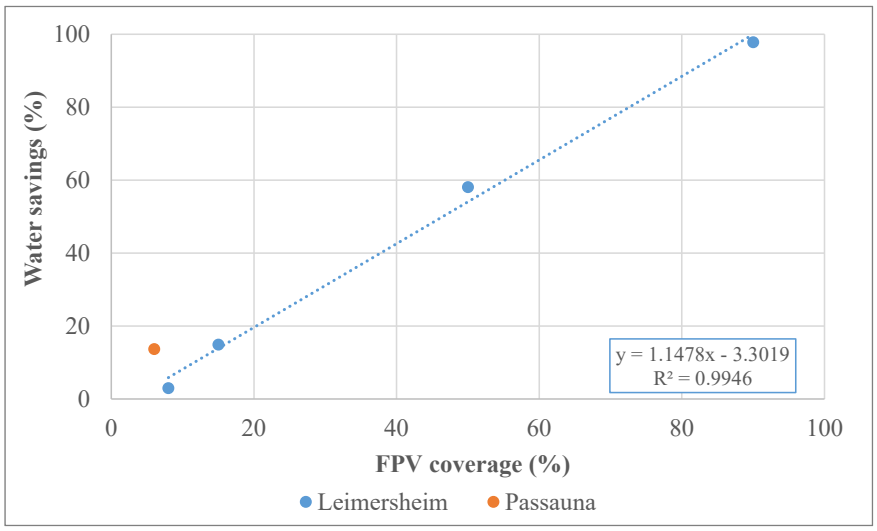

Figure 5-69. Water savings vs FPV coverage for Leimerisheim and Passaúna. Results show a linear tendency for the gravel pit lake.

By observing the variations in the lake's time series through the boxplots, it is possible to assume a natural variation in the parameters for scenario 0 (base) and analyze whether the variations of the other scenarios in relation to the base scenario fit (Figure 5-70).

The temperature results indicate that up to scenario 50, the variations observed in relation to the scenario without FPV are within natural variability (Figure 5-70a). However, from 90% onwards, the impacts exceed natural variability.

The opposite is true for horizontal velocity (Figure 5-70b). Scenarios in which there is an increase in speed show variations that exceed those assumed to be natural for the period. However, this does not seem to have a significant influence on the variations in residence time, which show the same behavior as temperature, where only scenario 90 exceeds the natural variability (Figure 5-70c). Regarding dissolved oxygen, all the scenarios were within the variability assumed to be natural (Figure 5-70d). For the Passaúna, all the results were within the range of natural variability (Figure 5-71).

Another useful analysis is that of heterogeneity (Figure 5-72). By considering a fixed point below the FPV and another outside the FPV for all scenarios, it is possible to assess how the variation between these two points changes for each scenario. In the case of the lake, the 90% scenario was disregarded because it covers practically the entire area.

Regarding surface temperature, the variation between points increases as coverage grows, showing a certain trend throughout the scenarios (Figure 5-72a). The maximum variations reach 1°C in scenario 50. The same occurs for dissolved oxygen (Figure 5-72d), but the extremes do not exceed the absolute value of 0.02 g/m³. The velocity results show an increase in variation in the scenario with the least coverage (8%), which decreases as coverage advances (Figure 5-72b). In scenario 50, they are close to the base scenario. For residence time, there was an increase in variability in all three scenarios, with maximum values exceeding 4 hours in scenario 15 (Figure 5-72c).

In the Passaúna reservoir, only the surface temperature and velocity results showed greater variability between covered and uncovered points in the expanded scenario (Figure 5-73). It is possible to observe a slight increase in the residence time results, with dissolved oxygen showing little variation. It should be noted that the series was not treated for outliers.

All these results show that the impacts of FPV are not linear and can vary significantly between different coverage ranges, as well as between different water bodies. This highlights the need for careful planning to minimize adverse effects on water quality and ecosystem dynamics.

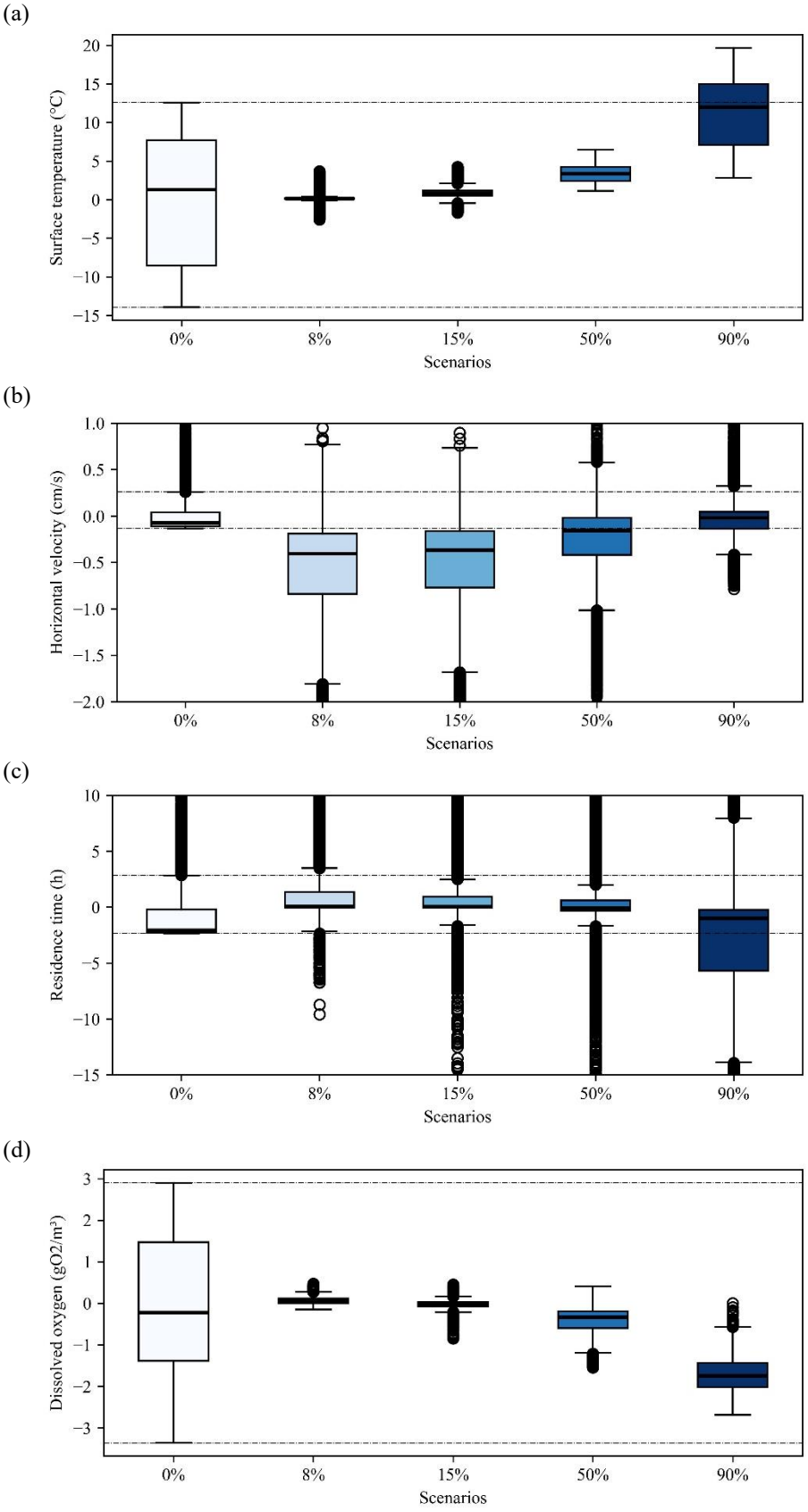

Figure 5-70. General effect of the FPV coverage for the gravel pit lake. Dotted lines are the natural variability (sc. 0). (a) surface temperature; (b) horizontal velocity; (c) residence time; and (e) DO concentration.

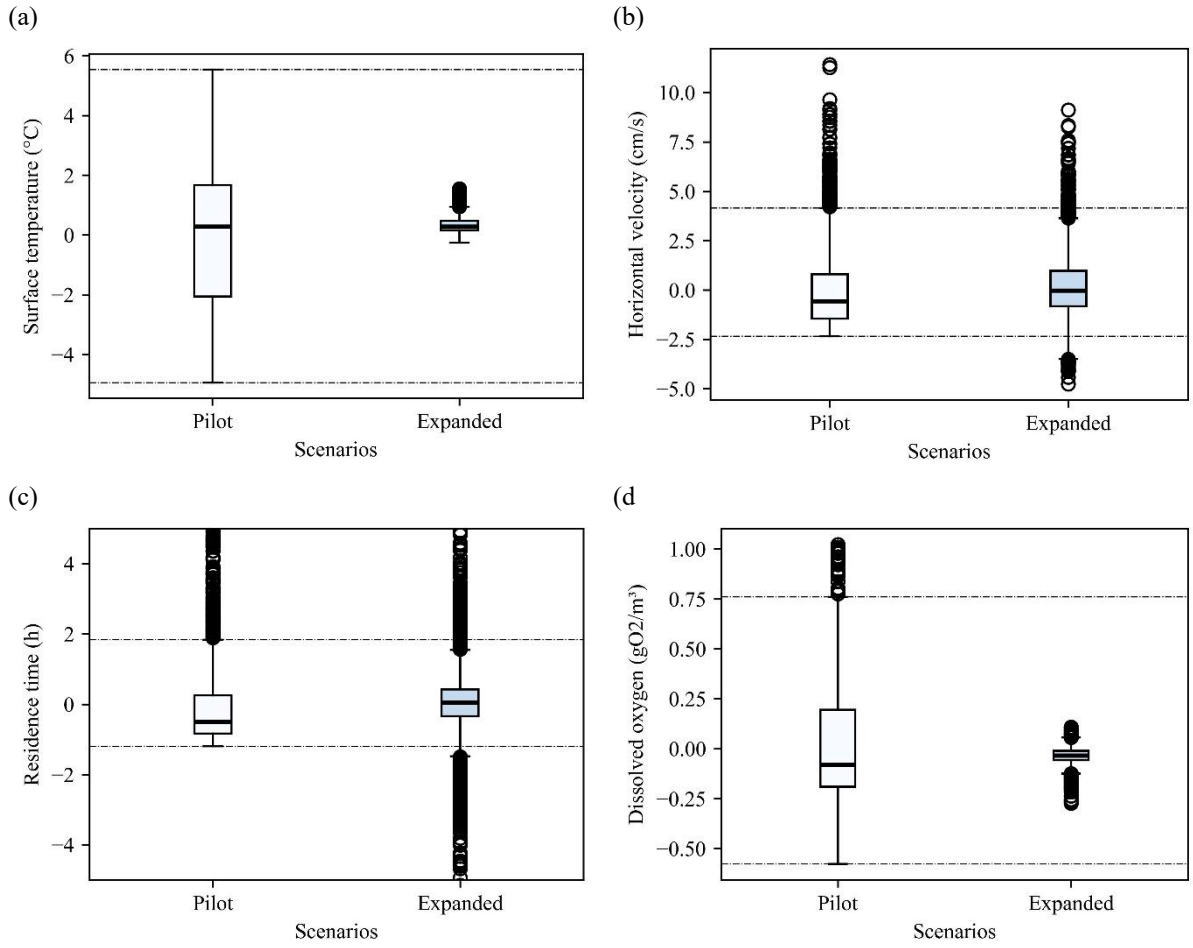

Figure 5-71. General effect of the FPV coverage for Passaúna reservoir. Dotted lines are the natural variability (Pilot sc.). (a) surface temperature; (b) horizontal velocity; (c) residence time; and (e) DO concentration.

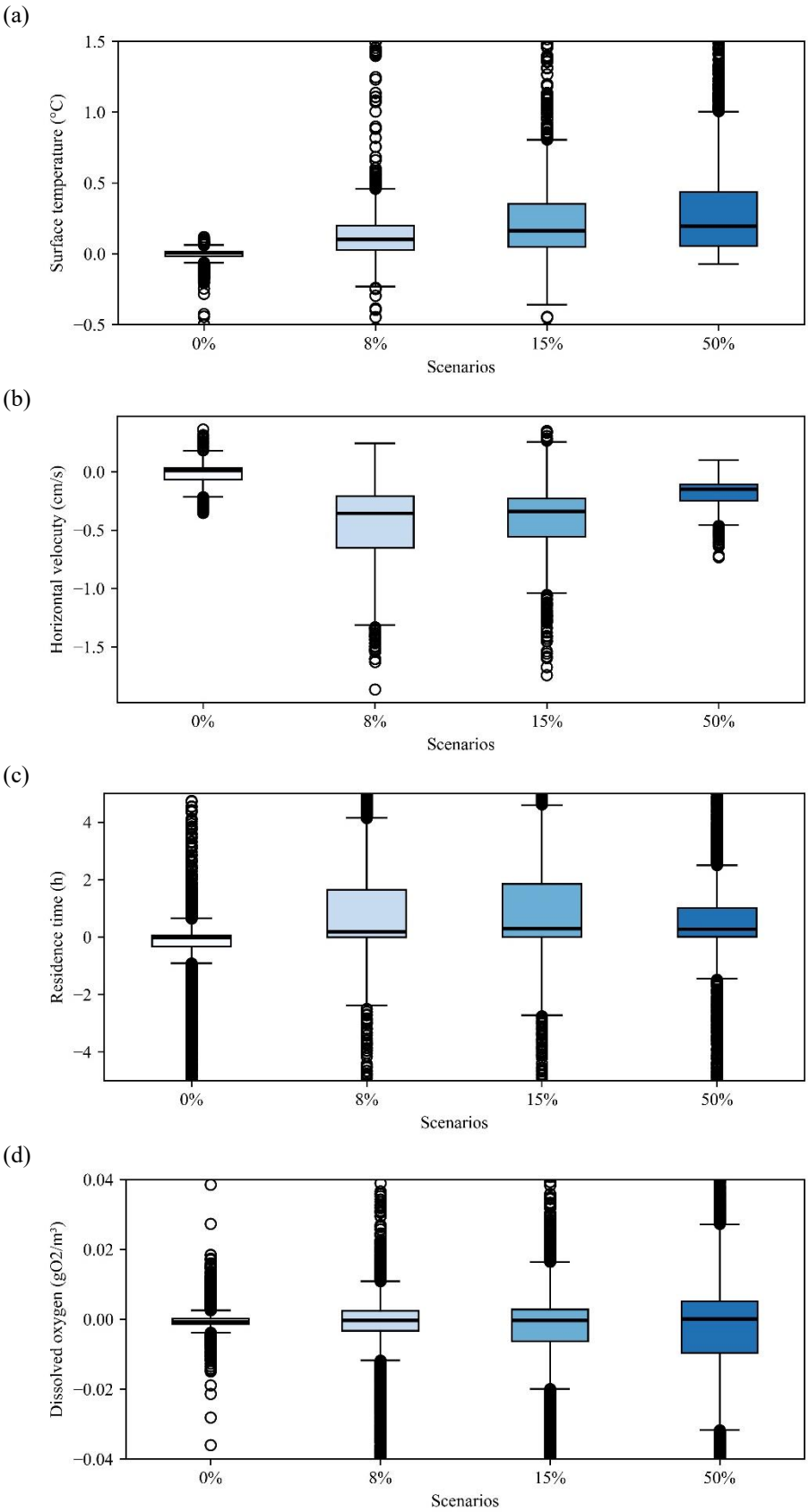

Figure 5-72. Spatial heterogeneity (REF-MFPV) of the simulated scenarios for the gravel pit lake. (a) surface temperature; (b) horizontal velocity; (c) residence time; and (e) DO concentration.

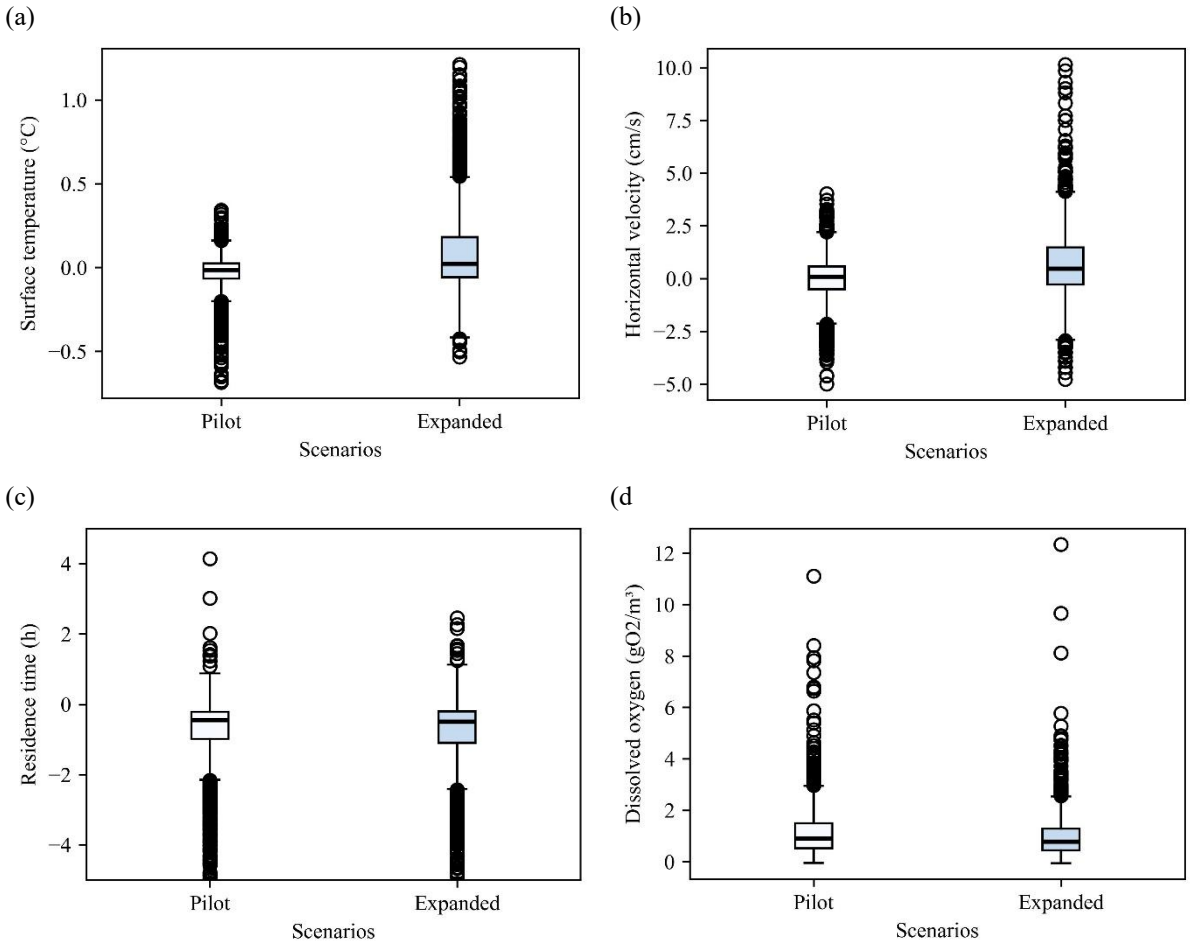

Figure 5-73. Spatial heterogeneity (LR-Cell Cover) of the simulated scenarios. (a) surface temperature; (b) horizontal velocity; (c) residence time; and (e) DO concentration.

6 CONCLUSIONS

This thesis presented monitoring results from two case studies with FPVs installed (8% coverage in Leimersheim, 0.01% in Passaúna), and expansion modeling scenarios in order to assess the impacts of these structures on the water body. The monitoring results showed that temperature did not differ significantly between points with and without panels. Dissolved oxygen results showed a slight reduction below the panels at both sites.

Computational modeling was used to analyze the possible impacts on advective transport and mixing effects of both case studies for scenarios with greater coverage. In the gravel pit lake, 5 scenarios were simulated (0%, 8%, 15%, 50% and 90%), while in the Passaúna reservoir only one expansion scenario was used (Pilot, Expanded).

The transport and mixing results differed between the two case studies. In the lake, there was an increase in velocities under the panels in the 8% coverage scenario, which diminished as coverage grew. However, up to scenario 50, there was an increase in velocities compared to the base scenario. Accordingly, there was an increase also in turbulent energy and a reduction in residence time up to scenario 50, and in tracer concentration, indicating that transport was enhanced. Observing the temperatures and thermal stratification, it can be seen that there is a reduction in surface temperature in the region of the panels. The hypothesis is that the difference in temperatures causes this rise in velocities magnitude, the averages of which are in the order of mm/s. In high coverage scenarios (90%), the impacts become even more pronounced, leading to a drastic temperature drop, and reduction in water movement, as indicated by lower horizontal velocities and turbulent energy.

The Passaúna reservoir showed the opposite effect. There was a drop in velocities with the expansion of the FPV, as well as a drop in turbulent energy. However, the mean residence time also decreased, but to a lesser extent (6%), as did the tracer concentration. One possibility is that, despite the decrease in velocities, the effect of the lower evaporation rates causes this reduction in concentration.

Based on these divergent results, the effect of the panels on advective transport seems to depend not only on the % of cover, but also on the characteristics of the water body. Despite the different behavior in terms of velocities, both sites showed a reduction in residence time and tracer concentration due to the presence of the panels.

With regard to dissolved oxygen, the results indicate that when considering only the reaeration process (without oxygen consumption or production), the behavior of the concentrations is very dependent on temperature. Although the reaeration rate decreases dramatically in the region of the panels (40.9% Leimersheim scenario 8, 25.6% in the expanded Passaúna), an increase in concentrations is observed as the coverage increases. Due to the reduction in temperature, the saturation concentration increases. In both cases, the model was able to represent the concentrations satisfactorily in the current scenarios only with the reaeration process. However, both the lake and the reservoir are oligotrophic environments, unpolluted and with little organic matter. This may not apply to other systems. Therefore,

this approach is recommended initially, for later analysis including oxygen consumption and production processes, such as respiration and photosynthesis.

Another critical impact of FPV is its effect on evaporation. At moderate levels (50%), water retention is already substantial, with a reduction of over 50% in total evaporation. This highlights the potential of FPV as a strategy for water conservation, particularly in regions where water scarcity is a concern. However, the reduction in evaporation also implies less latent heat loss, contributing to the observed changes in thermal dynamics within the water column.

These variations highlight the importance of site-specific assessments when implementing FPV systems. The same percentage of FPV coverage can yield different responses in distinct climatic and morphological conditions. For instance, while Leimersheim experienced a notable reduction in oxygen saturation, Passaúna showed a more stable oxygen profile, likely due to the influence of tributary inflows. Additionally, the influence of wind reduction played a more critical role in the temperate lake, affecting its reaeration rates more significantly than in the subtropical reservoir.

Careful planning is essential to minimize potential adverse effects on water quality and ecosystem functioning. The integration of hydrodynamic modeling proved to be an effective tool for predicting and analyzing FPV impacts, highlighting the need for site-specific calibration to ensure accurate assessments. Understanding how FPV interacts with water bodies under different environmental conditions can inform better management strategies, optimizing the benefits of renewable energy generation while mitigating potential ecological disturbances.

It should be noted that this study isolated the reaeration process, neglecting the biochemical processes that interfere with dissolved oxygen concentrations. Future investigations should focus on long-term monitoring of FPV systems, particularly their influence on nutrient cycling, sediment dynamics, and aquatic biological communities. In addition, complete water quality modeling, considering other processes such as nutrient circulation, primary production, respiration, among others, will allow for a more robust analysis of the impacts of FPV.

7 SCIENTIFIC CONTRIBUTIONS DURING DOCTORAL STUDIES

- Goulart, C. B., Carvalho, J. M., Bernardo, J. W. Y., Polli, B. A., Fernandes, C. V. S., Fuchs, S., Bleninger, T. (2024). A comprehensive reservoir segmentation for hydrodynamics and water quality assessment. Revista Brasileira de Recursos Hídricos. https://doi.org/10.1590/2318-0331.292420240079.
- Ferreira, E. M., Bueno, R. C., Goulart, C. B., Fernandes, C. V. S., Bleninger, T. (2024) Influência da capacidade de armazenamento de calor nas estimativas de evaporação de lagos. In II FluHidros - Simpósio Nacional de Mecânica dos Fluidos e Hidráulica e XVI ENES - Encontro Nacional de Engenharia de Sedimentos. Curitiba, Brazil.
- Acosta, E. A., Kishi, R. T., Souza, M. L., Pereira, G. H. A., Bleninger, T. B., Fernandes, C. V. S., Goulart, C. B., Carvalho, J. M., & Polli, B. A. (2024). A WEB-GIS for decision-making to achieve water quality standards of water bodies through collaborative watershed modeling. Revista Brasileira de Recursos Hídricos. https://doi.org/10.1590/2318-0331.282320230038
- Becker, A. C. C., Carvalho, J. M., Goulart, C. B., Ferreira, A. H. R., Polli, B. A., Ferreira, D. M., Bernardo, J. W. Y., Bleninger, T. B., & Fernandes, C. V. S. (2023). Zero-dimensional modelling as tool for reservoir water quality planning and management. Revista Brasileira de Recursos Hidricos, 28. https://doi.org/10.1590/2318-0331.282320220115
- Goulart, C. B., Carvalho, J. M., Bonfim, A. L. D. S., Maranhão, U., Bernardo, J. W. Y., Chadanowicz, A., & Bleninger, T. (2023). Estratégia Para Zoneamento De Reservatórios: Uhe Jurumirim. Anales Del XXX Congreso Latinoamericano de Hidráulica – VOLÚMEN 6 A – AGUA, AMBIENTE Y SOCIEDAD DEL CONOCIMIENTO, 187–197.
- Santos, B. K. L., Ferreira, E. M., Bueno, R. C., Goulart, C. B., Fernandes, C. V. S., Bleninger, T. (2023). Diferencas entre métodos de cálculo global e modelagem 3D de evaporacao de lagos e reservatórios. In XXV Simpósio Brasileiro de Recursos Hídricos. Aracajú, Brazil.

REFERENCES

Abdelal, Q. (2021). Floating PV; An assessment of water quality and evaporation reduction in semi-arid regions. *International Journal of Low-Carbon Technologies*, *16*(3), 732–739. https://doi.org/10.1093/ijlct/ctab001

Abdelgaied, M., Kabeel, A. E., Zeleňáková, M., & Abd-Elhamid, H. F. (2023). Floating Photovoltaic Plants as an Effective Option to Reduce Water Evaporation in Water-Stressed Regions and Produce Electricity: A Case Study of Lake Nasser, Egypt. *Water*, *15*(4), 635. https://doi.org/10.3390/w15040635

Alexander, C., & Robinson, M. (2006). *Quantifying the ecologicalsignificance of marsh shading: the impact of private recreationaldocks in coastal Georgia. Final report* .

Aminzadeh, M., Lehmann, P., & Or, D. (2018). Evaporation suppression and energy balance of water reservoirs covered with self-assembling floating elements. *Hydrology and Earth System Sciences*, *22*(7), 4015–4032. https://doi.org/10.5194/hess-22-4015-2018

Andini, S., Suwartha, N., Setiawan, E., & Ma'arif, S. (2022). Analysis of Biological, Chemical, and Physical Parameters to Evaluate the Effect of Floating Solar PV in Mahoni Lake, Depok, Indonesia: Mesocosm Experiment Study. *Journal of Ecological Engineering*, *23*(4), 201–207. https://doi.org/10.12911/22998993/146385

Assouline, S., Narkis, K., & Or, D. (2011). Evaporation suppression from water reservoirs: Efficiency considerations of partial covers. *Water Resources Research*, *47*(7). https://doi.org/10.1029/2010WR009889

Bahaidarah, H., Subhan, A., Gandhidasan, P., & Rehman, S. (2013). Performance evaluation of a PV (photovoltaic) module by back surface water cooling for hot climatic conditions. *Energy*, *59*, 445–453. https://doi.org/10.1016/j.energy.2013.07.050

Banks, R. B., & Herrera, F. F. (1977). Effect of wind and rain on surface reaeration. *J. Environ. Eng. Div (ASCE)*, *103*, 489–504.

BARANI DESIGN. (2017a). *MeteoTemp RH+T+P sensor*. https://www.baranidesign.com/meteotemp-rht

BARANI DESIGN. (2017b). *MeteoWind 2 wind sensor*. https://www.baranidesign.com/meteowind2-anemometer

Bax, V., van de Lageweg, W. I., Hoosemans, R., & van den Berg, B. (2023). Floating photovoltaic pilot project at the Oostvoornse lake: Assessment of the water quality effects of three different system designs. *Energy Reports*, *9*, 1415–1425. https://doi.org/10.1016/j.egyr.2022.12.080

Becker, A. C. C., Carvalho, J. M., Goulart, C. B., Ferreira, A. H. R., Polli, B. A., Ferreira, D. M., Bernardo, J. W. Y., Bleninger, T., & Fernandes, C. V. S. (2023). Zero-dimensional modelling as tool for reservoir water quality planning and management. *Revista Brasileira de Recursos Hidricos*, *28*. https://doi.org/10.1590/2318-0331.282320220115

Benyahya, L., St-Hilaire, A., Quarda, T. B. M. J., Bobée, B., & Ahmadi-Nedushan, B. (2007). Modeling of water temperatures based on stochastic approaches: case study of the Deschutes River. *Journal of Environmental Engineering and Science*, *6*(4), 437–448. https://doi.org/10.1139/s06-067

Bernardo, J. W. Y. (2018). *LINKING WATER QUALITY TO RESIDENCE TIME AND DIMENSIONLESS NUMBERS IN A STRATIFIED , DENDRITIC RESERVOIR DURING INTENSE INFLOW EVENTS* [Doctoral Thesis]. UNIVERSIDADE FEDERAL DO PARANÁ.

Bonalumi, M., Anselmetti, F. S., Wüest, A., & Schmid, M. (2012). Modeling of temperature and turbidity in a natural lake and a reservoir connected by pumped-storage operations. *Water Resources Research*, *48*(8). https://doi.org/10.1029/2012WR011844

Bonfim, A. L. de S. (2024). *MODELAGEM HIDRODINÂMICA E TÉRMICA PARA DIFERENTES FRAÇÕES DE COBERTURA DE SISTEMA FOTOVOLTAICO FLUTUANTE NO RESERVATÓRIO PASSAÚNA*. Universidade Federal do Paraná.

Bontempo Scavo, F., Tina, G. M., Gagliano, A., & Nižetić, S. (2020). An assessment study of evaporation rate models on a water basin with floating photovoltaic plants. *International Journal of Energy Research*, *45*(1), 167–188. https://doi.org/10.1002/er.5170

Carneiro, C., Kelderman, P., & Irvine, K. (2016). Assessment of phosphorus sediment–water exchange through water and mass budget in Passaúna Reservoir (Paraná State, Brazil). *Environmental Earth Sciences*, *75*(7). https://doi.org/10.1007/s12665-016-5349-3

Cathcart, T. P., & Wheaton, F. W. (1987). Modeling temperature distribution in freshwater ponds. *Aquacultural Engineering*, *6*(4), 237–257. https://doi.org/10.1016/0144-8609(87)90021-5

CETESB. (2024, April 30). *Usina fotovoltaica flutuante na Billings obtém LO*. Https://Cetesb.Sp.Gov.Br/Blog/2024/04/30/Usina-Fotovoltaica-Flutuante-Na-Billings-Obtem-Lo/.

Chapra, S. (2008). *Surface Water-Quality Modeling* (1st ed., Vol. 1). Waveland press, INC.

Choi, H., Ryu, I., Park, M., Song, Y., Yu, S., & Kim, S. (2020). Analysis of the water circulation structure in the Paldang Reservoir, South Korea. *Applied Sciences (Switzerland)*, *10*(19). https://doi.org/10.3390/app10196822

Clark, E. R., Harman, J. P., & Forster, J. R. M. (1985). Production of metabolic and waste products by intensively farmed rainbow trout, *Salmo gaivdnevi* Richardson. *Journal of Fish Biology*, *27*(4), 381–393. https://doi.org/10.1111/j.1095-8649.1985.tb03187.x

Cole, T. M., & Wells, S. A. (2013). *CE-QUAL- W2: A Two-Dimensional, Laterally Averaged, Hydrodynamic and Water Quality Model* (3.7.1). Portland State University.

COX, B. (2003). A review of currently available in-stream water-quality models and their applicability for simulating dissolved oxygen in lowland rivers. *The Science of The Total Environment*, *314–316*, 335–377. https://doi.org/10.1016/S0048-9697(03)00063-9

da Costa, L. C. A., & da Silva, G. D. P. (2021). Save water and energy: A techno-economic analysis of a floating solar photovoltaic system to power a water integration project in the Brazilian semiarid. *International Journal of Energy Research*, *45*(12), 17924–17941. https://doi.org/10.1002/er.6932

da Rocha Santos, F., D'Angela Mariano, J., Sestrem Junior, J. A., & Junior, J. U. (2019). Analysis of solar photovoltaic energy potential in Brazilian hydroelectric reservoirs through floating panels. *Brazilian Archives of Biology and Technology*, *62*(specialissue). https://doi.org/10.1590/1678-4324-SMART-2019190012

de Lima, R. L. P., Paxinou, K., Boogaard, F. C., Akkerman, O., & Lin, F. Y. (2021). In-situ water quality observations under a large-scale floating solar farm using sensors and underwater drones. *Sustainability (Switzerland)*, *13*(11). https://doi.org/10.3390/su13116421

Deltares. (2025a). *Delft3D 3D/2D modelling suite for integral water solutions Hydro-Morphodynamics* (4.05). Deltares systems. https://oss.deltares.nl/web/delft3d/manuals

Deltares. (2025b). *Delft3D-WAQ 3D/2D modelling suite for integral water solutions Technical Reference Manual Processes Library Description* (5.01). Deltares systems. https://oss.deltares.nl/web/delft3d/manuals

EKO. (2020). *Pyrnometer MS-80*. https://www.eko-instruments.com/eu/categories/products/pyranometers/ms-80-pyranometer

Empresa de pesquisa energética - EPE. (2021). *Balanço Energético Nacional 2021*.

Exley, G., Armstrong, A., Page, T., & Jones, I. D. (2021). Floating photovoltaics could mitigate climate change impacts on water body temperature and stratification. *Solar Energy*, *219*(October 2020), 24–33. https://doi.org/10.1016/j.solener.2021.01.076

Gobbi, M., & Kruk, N. (2003). Implementação de Um Modelo para Simular a Eutrofização do Reservatório do Passaúna - Curitiba-PR. *Revista Brasileira de Recursos Hídricos*, *8*(3), 59–69. https://doi.org/10.21168/rbrh.v8n3.p59-69

Gonçalves, L. de A., Faria, L., Mannich, M., Coelho, M., Rigotti, J. A., Bleninger, T., & Vitule, J. R. S. (2025). A Systematic Review of Floating Photovoltaic Plant Environmental Impacts. *Journal of Sustainable Development*, *18*(1), 94. https://doi.org/10.5539/jsd.v18n1p94

Gonzalez Sanchez, R., Kougias, I., Moner-Girona, M., Fahl, F., & Jäger-Waldau, A. (2021). Assessment of floating solar photovoltaics potential in existing hydropower reservoirs in Africa. *Renewable Energy*, *169*, 687–699. https://doi.org/10.1016/j.renene.2021.01.041

Goulart, C. B., Carvalho, J. M., Bernardo, J. W. Y., Polli, B. A., Fernandes, C., Fuchs, S., & Bleninger, T. (2024). A comprehensive reservoir segmentation for hydrodynamics and water quality assessment. *Revista Brasileira de Recursos Hidricos*, *29*. https://doi.org/10.1590/2318-0331.292420240079

Guérin, F., Abril, G., Serça, D., Delon, C., Richard, S., Delmas, R., Tremblay, A., & Varfalvy, L. (2007). Gas transfer velocities of CO2 and CH4 in a tropical reservoir and its river downstream. *Journal of Marine Systems*, *66*(1–4), 161–172. https://doi.org/10.1016/j.jmarsys.2006.03.019

Haas, J., Khalighi, J., de la Fuente, A., Gerbersdorf, S. U., Nowak, W., & Chen, P. J. (2020). Floating photovoltaic plants: Ecological impacts versus hydropower operation flexibility. *Energy Conversion and Management*, *206*(December 2019). https://doi.org/10.1016/j.enconman.2019.112414

Hargreaves, G. H., & Allen, R. G. (2003). History and Evaluation of Hargreaves Evapotranspiration Equation. *Journal of Irrigation and Drainage Engineering*, *129*(1), 53–63. https://doi.org/10.1061/(ASCE)0733-9437(2003)129:1(53)

Haugwitz, F. (2020, September 22). Floating solar PV gains global momentum. *Https://Www.Pv-Magazine.Com/2020/09/22/Floating-Solar-Pv-Gains-Global-Momentum/*.

Hipsey, M. R., Bruce, L. C., Boon, C., Busch, B., Carey, C. C., Hamilton, D. P., Hanson, P. C., Read, J. S., de Sousa, E., Weber, M., & Winslow, L. A. (2019). A General Lake Model (GLM 3.0) for linking with high-frequency sensor data from the Global Lake Ecological Observatory Network (GLEON). *Geoscientific Model Development*, *12*(1), 473–523. https://doi.org/10.5194/gmd-12-473-2019

Hogeboom, R. J., Knook, L., & Hoekstra, A. Y. (2018). The blue water footprint of the world's artificial reservoirs for hydroelectricity, irrigation, residential and industrial water supply, flood protection, fishing and recreation. *Advances in Water Resources*, *113*, 285–294. https://doi.org/10.1016/j.advwatres.2018.01.028

Hooper, T., Armstrong, A., & Vlaswinkel, B. (2021). Environmental impacts and benefits of marine floating solar. *Solar Energy*, *219*, 11–14. https://doi.org/10.1016/j.solener.2020.10.010

IDSO, S. B. (1973). On the concept of lake stability1. *Limnology and Oceanography*, *18*(4), 681–683. https://doi.org/10.4319/lo.1973.18.4.0681

Ilgen, K., Schindler, D., Wieland, S., & Lange, J. (2023). The impact of floating photovoltaic power plants on lake water temperature and stratification. *Scientific Reports*, *13*(1), 7932. https://doi.org/10.1038/s41598-023-34751-2

IRENA. (2018). Renewable Power Generations Costs. In *International Renewable Energy Agency*.

Ishikawa, M., Bleninger, T., & Lorke, A. (2021). Hydrodynamics and mixing mechanisms in a subtropical reservoir. *Inland Waters*, *11*(3), 286–301. https://doi.org/10.1080/20442041.2021.1932391

Ishikawa, M., Gonzalez, W., Golyjeswski, O., Sales, G., Rigotti, J. A., Bleninger, T., Mannich, M., & Lorke, A. (2022). Effects of dimensionality on the performance of hydrodynamic models for stratified lakes and reservoirs. *Geoscientific Model Development*, *15*(5), 2197–2220. https://doi.org/10.5194/gmd-15-2197-2022

Ishikawa, M., Gurski, L., Bleninger, T., Rohr, H., Wolf, N., & Lorke, A. (2022). Hydrodynamic Drivers of Nutrient and Phytoplankton Dynamics in a Subtropical Reservoir. *Water (Switzerland)*, *14*(10). https://doi.org/10.3390/w14101544

Ji, Q., Li, K., Wang, Y., Feng, J., Li, R., & Liang, R. (2022). Effect of floating photovoltaic system on water temperature of deep reservoir and assessment of its potential benefits, a case on Xiangjiaba Reservoir with hydropower station. *Renewable Energy*, *195*, 946–956. https://doi.org/10.1016/j.renene.2022.06.096

Ji, Z.-G. (2008). *HYDRODYNAMICS AND WATER QUALITY: MODELING RIVERS, LAKES, AND ESTUARIES*. Wiley Interscience.

Khalifeh Soltani, S. R., Mostafaeipour, A., Almutairi, K., Hosseini Dehshiri, S. J., Hosseini Dehshiri, S. S., & Techato, K. (2022). Predicting effect of floating photovoltaic power plant on water loss through surface evaporation for wastewater pond using artificial intelligence: A case study. *Sustainable Energy Technologies and Assessments*, *50*(November 2021), 101849. https://doi.org/10.1016/j.seta.2021.101849

Ladwig, R., Hanson, P. C., Dugan, H. A., Carey, C. C., Zhang, Y., Shu, L., Duffy, C. J., & Cobourn, K. M. (2021). Lake thermal structure drives interannual variability in summer anoxia dynamics in a eutrophic lake over 37 years. *Hydrology and Earth System Sciences*, *25*(2), 1009–1032. https://doi.org/10.5194/hess-25-1009-2021

Lee, N., Grunwald, U., Rosenlieb, E., Mirletz, H., Aznar, A., Spencer, R., & Cox, S. (2020). Hybrid floating solar photovoltaics-hydropower systems: Benefits and global assessment of technical potential. *Renewable Energy*, *162*, 1415–1427. https://doi.org/10.1016/j.renene.2020.08.080

Lenz, J. (2018). *Impact Assessment of Floating Houses on Water Temperature and Dissolved Oxygen in Himpenser Wielen, Leeuwarden (Netherlands)* [Master Thesis]. Freie Universität Berlin.

Liu, Z., Ma, C., Yang, Y., Li, X., Gou, H., & Folkard, A. M. (2024). Water temperature and energy balance of floating photovoltaic construction water area—field study and modelling. *Journal of Environmental Management*, *365*. https://doi.org/10.1016/j.jenvman.2024.121494

Lopes, M. P. C., Neto, S. de A., Branco, D. A. C., Vasconcelos de Freitas, M. A., & da Silva Fidelis, N. (2020). Water-energy nexus: Floating photovoltaic systems promoting water security and energy generation in the semiarid region of Brazil. *Journal of Cleaner Production*, *273*, 122010. https://doi.org/10.1016/j.jclepro.2020.122010

Marcon, L., Bleninger, T., Männich, M., & Hilgert, S. (2019). High-frequency measurements of gas ebullition in a Brazilian subtropical reservoir—identification of relevant triggers and seasonal patterns. *Environmental Monitoring and Assessment*, *191*(6), 357. https://doi.org/10.1007/s10661-019-7498-9

Martin, J. L., & Mccutcheon, S. C. (1999). *Hydrodynamics and transport for water quality modeling*. CRC Press Inc.

Mathijssen, D., Hofs, B., Spierenburg-Sack, E., Vanasperen, R., Vanderwal, B., Vreeburg, J., & Ketelaars, H. (2020). Potential impact of floating solar panels on water quality in reservoirs; pathogens and leaching. *Water Practice and Technology*, *15*(3), 807–811. https://doi.org/10.2166/wpt.2020.062

Morris, G. L., & Fan, J. (1998). *Reservoir Sedimentation Handbook*. McGraw-Hill Book Co.

NASA. (2023). *POWER | Data Access Viewer*. Https://Power.Larc.Nasa.Gov/Data-Access-Viewer/.

Nobre, R. L. G., Vagnon, C., Boulêtreau, S., Colas, F., Azémar, F., Tudesque, L., Parthuisot, N., Millet, P., & Cucherousset, J. (2025). Floating photovoltaics strongly reduce water temperature: A whole-lake experiment. *Journal of Environmental Management*, *375*, 124230. https://doi.org/10.1016/J.JENVMAN.2025.124230

Nobre, R., Rocha, S. M., Healing, S., Ji, Q., Boulêtreau, S., Armstrong, A., & Cucherousset, J. (2024). A global study of freshwater coverage by floating photovoltaics. *Solar Energy*, *267*, 112244. https://doi.org/10.1016/j.solener.2023.112244

Olsson, F., Mackay, E. B., Moore, T., Barker, P., Davies, S., Hall, R., Spears, B., Wilkinson, J., & Jones, I. D. (2022). Annual water residence time effects on thermal structure: A potential lake restoration measure? *Journal of Environmental Management*, *314*(December 2021), 115082. https://doi.org/10.1016/j.jenvman.2022.115082

Padilha Campos Lopes, M., de Andrade Neto, S., Alves Castelo Branco, D., Vasconcelos de Freitas, M. A., & da Silva Fidelis, N. (2020). Water-energy nexus: Floating photovoltaic systems promoting water security and energy generation in the semiarid region of Brazil. *Journal of Cleaner Production*, *273*. https://doi.org/10.1016/j.jclepro.2020.122010

Padilha Campos Lopes, M., Nogueira, T., Santos, A. J. L., Castelo Branco, D., & Pouran, H. (2022). Technical potential of floating photovoltaic systems on artificial water bodies in Brazil. *Renewable Energy*, *181*, 1023–1033. https://doi.org/10.1016/j.renene.2021.09.104

Penman-Monteith. (1948). Natural evaporation from open water, bare soil and grass. *Proceedings of the Royal Society of London. Series A. Mathematical and Physical Sciences*, *193*(1032), 120–145. https://doi.org/10.1098/rspa.1948.0037

Polli, B. A., & Bleninger, T. (2019). Reservoir 1D heat transport model. *Journal of Applied Water Engineering and Research*, *7*(2), 156–171. https://doi.org/10.1080/23249676.2018.1497560

Pouran, H. M., Padilha Campos Lopes, M., Nogueira, T., Alves Castelo Branco, D., & Sheng, Y. (2022). Environmental and technical impacts of floating photovoltaic plants as an emerging clean energy technology. *IScience*, *25*(11). https://doi.org/10.1016/j.isci.2022.105253

Pouran, H., Padilha Campos Lopes, M., Ziar, H., Alves Castelo Branco, D., & Sheng, Y. (2022). Evaluating floating photovoltaics (FPVs) potential in providing clean energy and supporting agricultural growth in Vietnam. *Renewable and Sustainable Energy Reviews*, *169*, 112925. https://doi.org/10.1016/j.rser.2022.112925

Ravichandran, N., Ravichandran, N., & Panneerselvam, B. (2021). Floating photovoltaic system for Indian artificial reservoirs—an effective approach to reduce evaporation and carbon emission. *International Journal of Environmental Science and Technology*, *0123456789*. https://doi.org/10.1007/s13762-021-03686-4

Rocha, S. M. G., Armstrong, A., Thackeray, S. J., Hernandez, R. R., & Folkard, A. M. (2024). Environmental impacts of floating solar panels on freshwater systems and their techno-ecological synergies. In *Environmental Research: Infrastructure and Sustainability* (Vol. 4, Issue 4). Institute of Physics. https://doi.org/10.1088/2634-4505/ad8e81

Roider, H. (2024, July 18). *Fraunhofer quantifies German floating PV potential*. Https://Www.Bayern-Innovativ.de/En/Detail/Fraunhofer-Quantifies-German-Floating-Pv-Potential.

Rosenberry, D. O., Winter, T. C., Buso, D. C., & Likens, G. E. (2007). Comparison of 15 evaporation methods applied to a small mountain lake in the northeastern USA. *Journal of Hydrology*, *340*(3–4), 149–166. https://doi.org/10.1016/j.jhydrol.2007.03.018

Saloranta, T., & Andersen, T. (2004). *MyLake (v.1.1): Technical model documentation and user's guide for version 1.1*. http://hdl.handle.net/11250/212445.

SANEPAR. (2023). *FotoÁgua - Efeitos de sistemas fotovoltaicos flutuantes sobre processos de transferência na interface ar-água e alterações para qualidade de água*.

Schmidt, W. (1928). Über Die Temperatur- Und Stabili-Tätsverhältnisse Von Seen. *Geografiska Annaler*, *10*(1–2), 145–177. https://doi.org/10.1080/20014422.1928.11880475

SEMIL. (2024, January 17). *Governo de SP apresenta maior usina solar flutuante do país na represa Billings*. Https://Semil.Sp.Gov.Br/2024/01/Governo-de-Sp-Apresenta-Maior-Usina-Solar-Flutuante-Do-Pais-Na-Represa-Billings/.

Silvério, N. M., Barros, R. M., Tiago Filho, G. L., Redón-Santafé, M., Santos, I. F. S. dos, & Valério, V. E. de M. (2018). Use of floating PV plants for coordinated operation with hydropower plants: Case study of the hydroelectric plants of the São Francisco River basin. *Energy Conversion and Management*, *171*(January), 339–349. https://doi.org/10.1016/j.enconman.2018.05.095

Smits, J., Boderie, P., & Van Beek, J. (2009). *Modeling of the Nam Theun 2 Reservoir: Water quality and greenhouse gases emissions*.

Sotiri, K., Hilgert, S., Mannich, M., Bleninger, T., & Fuchs, S. (2021). Implementation of comparative detection approaches for the accurate assessment of sediment thickness and sediment volume in the Passaúna Reservoir. *Journal of Environmental Management*, *287*, 112298. https://doi.org/10.1016/J.JENVMAN.2021.112298

Sotiri, K., Kishi, R. T., Hilgert, S., Scheer, M. B., Gabriel, P. G., Benatto, D. A., & Fuchs, S. (2022). Assessment of Phosphorus Input from Urban Areas in the Passaúna River and Reservoir. *Water (Switzerland)*, *14*(5). https://doi.org/10.3390/w14050809

Soulignac, F., Vinçon-Leite, B., Lemaire, B. J., Scarati Martins, J. R., Bonhomme, C., Dubois, P., Mezemate, Y., Tchiguirinskaia, I., Schertzer, D., & Tassin, B. (2017). Performance Assessment of a 3D Hydrodynamic Model Using High Temporal Resolution Measurements in a Shallow Urban Lake. *Environmental Modeling and Assessment*, *22*(4), 309–322. https://doi.org/10.1007/s10666-017-9548-4

Stumm, W., & Morgan, J. J. (1996). *Aquatic Chemistry: Chemicalequilibria and rates in natural waters* (3rd ed.). Wiley.

Taboada, M. E., Cáceres, L., Graber, T. A., Galleguillos, H. R., Cabeza, L. F., & Rojas, R. (2017). Solar water heating system and photovoltaic floating cover to reduce evaporation: Experimental results and modeling. *Renewable Energy*, *105*, 601–615. https://doi.org/10.1016/j.renene.2016.12.094

Trapani, K., & Redón Santafé, M. (2015). A review of floating photovoltaic installations: 2007–2013. *Progress in Photovoltaics: Research and Applications*, *23*(4), 524–532. https://doi.org/10.1002/pip.2466

Valiantzas, J. D. (2006). Simplified versions for the Penman evaporation equation using routine weather data. *Journal of Hydrology*, *331*(3–4), 690–702. https://doi.org/10.1016/j.jhydrol.2006.06.012

Vogel, J. L., & Beauchamp, D. A. (1999). Effects of light, prey size, and turbidity on reaction distances of lake trout (*Salvelinus namaycush*) to salmonid prey. *Canadian Journal of Fisheries and Aquatic Sciences*, *56*(7), 1293–1297. https://doi.org/10.1139/f99-071

Wahl, B., & Peeters, F. (2014). Effect of climatic changes on stratification and deep-water renewal in Lake Constance assessed by sensitivity studies with a 3D hydrodynamic model. *Limnology and Oceanography*, *59*(3), 1035–1052. https://doi.org/10.4319/lo.2014.59.3.1035

Wang, T., Chang, P., Huang, Y., Lin, T., Yang, S., Yeh, S., Tung, C., Kuo, S., Lai, H., & Chen, C. (2022). Effects of floating photovoltaic systems on water quality of aquaculture ponds. *Aquaculture Research*, *53*(4), 1304–1315. https://doi.org/10.1111/are.15665

Ward, G. J. (1994). The RADIANCE lighting simulation and rendering system. *Proceedings of the 21st Annual Conference on Computer Graphics and Interactive Techniques - SIGGRAPH '94*, 459–472. https://doi.org/10.1145/192161.192286

Wei, Y., Khojasteh, D., Windt, C., & Huang, L. (2025). An interdisciplinary literature review of floating solar power plants. *Renewable and Sustainable Energy Reviews*, *209*, 115094. https://doi.org/10.1016/J.RSER.2024.115094

Weinberger, S., & Vetter, M. (2012). Using the hydrodynamic model DYRESM based on results of a regional climate model to estimate water temperature changes at Lake Ammersee. *Ecological Modelling*, *244*, 38–48. https://doi.org/10.1016/j.ecolmodel.2012.06.016

Winslow, M. L., Winslow, L., Read, J., Woolway, R., Brentrup, J., Leach, T., Zwart, J., Albers, S., & Collinge, D. (2022). *Package "rLakeAnalyzer" Title Lake Physics Tools*. https://github.com/GLEON/rLakeAnalyzer/issues

World Bank Group. (2019). *Where Sun Meets Water - FLOATING SOLAR MARKET REPORT*. www.worldbank.org

Yang, P., Chua, L. H. C., Irvine, K. N., Nguyen, M. T., & Low, E. W. (2022a). Impacts of a floating photovoltaic system on temperature and water quality in a shallow tropical reservoir. *Limnology*, *23*(3), 441–454. https://doi.org/10.1007/s10201-022-00698-y

Yang, P., Chua, L. H. C., Irvine, K. N., Nguyen, M. T., & Low, E.-W. (2022b). Impacts of a floating photovoltaic system on temperature and water quality in a shallow tropical reservoir. *Limnology*, *23*(3), 441–454. https://doi.org/10.1007/s10201-022-00698-y

YSG Solar. (2022). *YSG Solar*. Https://Www.Ysgsolar.Com/.

Zouabi-Aloui, B., & Gueddari, M. (2014). Two-dimensional modelling of hydrodynamics and water quality of a stratified dam reservoir in the southern side of the Mediterranean Sea. *Environmental Earth Sciences*, *72*(8), 3037–3051. https://doi.org/10.1007/s12665-014-3210-0

APPENDIX A. A COMPREHENSIVE RESERVOIR SEGMENTATION FOR HYDRODYNAMICS AND WATER QUALITY ASSESSMENT

RBRH

Revista Brasileira de Recursos Hídricos
Brazilian Journal of Water Resources
Versão On-line ISSN 2318-0331
RBRH, Porto Alegre, v. 29, e43, 2024
Scientific/Technical Article

https://doi.org/10.1590/2318-0331.292420240079

A comprehensive reservoir segmentation for hydrodynamics and water quality assessment

Segmentação de reservatórios para hidrodinâmica e avaliação da qualidade da água

Camila Bergmann Goulart[1,2], João Marcos Carvalho[1], Julio Werner Yoshioka Bernardo[1], Bruna Arcie Polli[3], Cristóvão Fernandes[1], Stephan Fuchs[2] & Tobias Bleninger[1]

[1]Universidade Federal do Paraná, Curitiba, PR, Brasil
[2]Karlsruhe Institut für Technologie, Karlsruhe, Baden-Wütternberg, Alemanha
[3]Lactec, Curitiba, PR, Brasil

E-mails: camilabgoulart@gmail.com (CBG), joao.mar.huf.carvalho@gmail.com (JMC), juliowernery@gmail.com (JWYB), brunapolli@gmail.com (BAP), cris.dhs@ufpr.br (CF), stephan.fuchs@kit.edu (SF), bleninger@ufpr.br (TB)

Received: August 06, 2024 - Revised: September 26, 2024 - Accepted: September 30, 2024

ABSTRACT

Reservoirs present different and intrinsic characteristics from the point of view of physical, chemical, and biological nature from other environmental systems. They therefore should be characterized differently for a better representation aiming for proper planning and management strategies. This paper analyzes eleven reservoirs and develops a classification and zonation strategy for those systems. First, temporal variation and statistical analysis are performed, followed by a residence time calculation, to assess the reservoir's dynamics. Next, stratification and spatial variation analysis are proposed to verify their necessity. Three of the reservoirs analyzed behave as lentic systems, with a high residence time. In addition, all three have significant tributaries, indicating the potential necessity of considering spatial variation for their classification, later verified in 3D modeling. Even if every reservoir is unique in its dynamics and characteristics, the classification scheme is suitable for different types of reservoirs, since it works like a decision tree, where input loads and hydrodynamics are considered.

Keywords: Reservoir classification; Residence time; Reservoir dynamics; Zonation.

RESUMO

Os reservatórios apresentam características diferentes e intrínsecas, do ponto de vista da natureza física, química e biológica, em relação a outros sistemas ambientais. Portanto, eles devem ser caracterizados de forma diferente para uma melhor representação, visando a estratégias adequadas de planejamento e gerenciamento. Este artigo analisou onze reservatórios e desenvolveu uma estratégia de classificação e zoneamento para esses sistemas. Primeiro, são realizadas análises estatísticas e de variação temporal, seguidas de um cálculo do tempo de residência, para avaliar a dinâmica do reservatório. Em seguida, são propostas análises de estratificação e variação espacial para verificar a necessidade de zoneamento. Três dos reservatórios analisados se comportam como sistemas lênticos, com alto tempo de residência. Além disso, todos os três têm afluentes significativos, indicando a necessidade potencial de considerar a variação espacial para sua classificação, posteriormente verificada na modelagem 3D. Mesmo que cada reservatório seja único em sua dinâmica e características, o esquema de classificação é adequado para diferentes tipos de reservatórios, pois funciona como uma árvore de decisão, em que as cargas de entrada e a hidrodinâmica são consideradas.

Palavras-chave: Classificação de reservatórios; Tempo de residência; Dinâmica de reservatórios; Zoneamento.

INTRODUCTION

Studies of river system classification usually associate an input (L, annual average, mass per time per segment) to a segment of a river, from point and diffuse sources, calculated through geoprocessing models or monitoring databases (Calmon et al., 2016). This input is associated with the reference flow rate (Q, volume per time) and the concentration C is calculated as C = L/Q (mass per volume). This concentration is compared to the concentration limits for water quality assessments (Pessôa et al., 2015). In the diagnosis phase, values from measurements or modeling in the current system state are used; in the prognosis phase, expected variations in the basin are included, and in the planning phase, adaptation actions are considered (Petriki et al., 2017).

The same principle is used for reservoirs and they are considered as a simple section. However, several studies show that reservoirs follow different processes compared to other environmental systems (Shivers et al., 2018; Hayes et al., 2017; Irz et al., 2006), particularly rivers, as they are accumulation systems with different substance kinetics.

Reservoir zonation is observed not only through concentrations of water quality parameters but also by biological aspects. Santos et al. (2010) found spatial and temporal variations in the Funil reservoir (Paraíba do Sul River, in Rio de Janeiro, Brazil) considering the number of fish species.

In cases where many parameters measured over long periods are available, it is possible to define reservoir compartments with distinct characteristics and thus distinct water quality (Pompêo et al., 2015; Cardoso-Silva et al., 2014). A disadvantage of these classification and compartmentalization methods is the large requirement for measured data, both in space and time. Usually, for classification and regulation studies, not all these data are available. Instead, the classification diagnosis is even used to define monitoring strategies. Thus, mathematical models are used to complement the measurements and obtain enough information to classify and compartmentalize.

Another disadvantage of the methodologies presented is that the modeling is only valid for the reservoir studied, thus requiring a case-by-case analysis. To get around this limitation, there are initiatives to identify universal patterns in reservoirs, using databases with data from lakes and reservoirs around the world (Kirillin & Shatwell, 2016; Messager et al., 2016).

Even when using water quality indexes to classify these reservoirs, they are usually analyzed as a whole, regardless of the area they occupy. The most conventional lake classification is the one based on the trophic state used worldwide (Smaoune et al., 2021; Hoang et al., 2017). Nojavan et al. (2019) proposed an updated lake trophic classification model that is multi-variable, continuous, and classifies lakes in probabilistic terms, but without considering the spatial distributions inside each reservoir. Also, in order to improve the TSI, claiming the need for a range of classification for each reservoir, Chen et al. (2021) presented the Trophic State Footprint Index (TFI) based on the relationship of the response index (Chlorophyll a) and the main cause index (e.g., total phosphorus, total nitrogen).

Different types of classification are found in the literature, depending on the region and the specific interests related to each lake. Gądek et al. (2019) classified Tatra Mountain lakes (border between Slovakia and Poland) regarding the duration of the ice cover. Other classification schemes already proposed are about fish habitat (Petriki et al., 2017; Sutela et al., 2016; Krogman & Miranda, 2015).

Not only fish but also invertebrates are used for lake and reservoir classification, like macroinvertebrates (Pan et al., 2014), benthic invertebrates (Ozoliņš et al., 2021). Tison-Rosebery et al. (2023) presented a diatom-based index developed for French lakes, developed with data from 93 lakes, to monitor lake eutrophication.

These studies are based on measurements of water quality parameters and general reservoir characteristics and suggest spatial and temporal compartmentalization for the characterization of reservoir susceptibility. Suppose those spatial and temporal variations are not considered within the assessment and management phase. In that case, results for the reservoir status and critical regions and periods might be misleading or even wrong. This article investigates the hypothesis that reservoir compartmentalization will improve the identification of critical areas and periods, and therefore the related investments to reduce associated problems. Reservoir compartmentalization, in theory, is nothing new, but often is only done for a few specific water quality monitoring parameters, and not, as proposed here, including hydrodynamic and morphological aspects, as well as catchment characteristics.

Most of the classification schemes mentioned above treat the reservoir as a simple single-response unit. Therefore, there is a lack of defining proper management options for the reservoir as a whole and there is a need to classify/categorize different reservoir regions with specific management aims. This classification is the main objective of this paper. The data used was based on monitoring data and complemented with modeling data.

MATERIAL AND METHODS

Study site

The Paranapanema River is an important axis for generating electricity in Brazil, with a cascade of reservoirs on its main river. Some of these structures generate electricity and help with public, agricultural, and industrial supply. Its basin covers about 106,500 km^2, with 4.7 million inhabitants, concentrating approximately 2.1% of Brazil's Gross Domestic Product - GDP (Agência Nacional de Águas, 2016). Recently, the reservoirs in this river basin have been the subject of a study aimed at classifying their water bodies (Agência Nacional de Águas, 2021).

The Paranapanema River has eleven hydropower plants in operation, which has transformed its original course into a succession of contiguous reservoirs. The plants are as follows: Jurumirim, Piraju, Paranapanema, Chavantes, Ourinhos, Salto Grande, Canoas II, Canoas I, Capivara, Taquaruçu, and Rosana (Figure 1). They are classified into two basic types, according to their characteristics and types of operation, directly influencing the water quality and the distribution of aquatic communities, including fish fauna, as:

a) Accumulation reservoirs: Usually they have greater depth and wide flooded areas and may present quite accentuated water level variations (altimetric quotas). The water in the reservoir

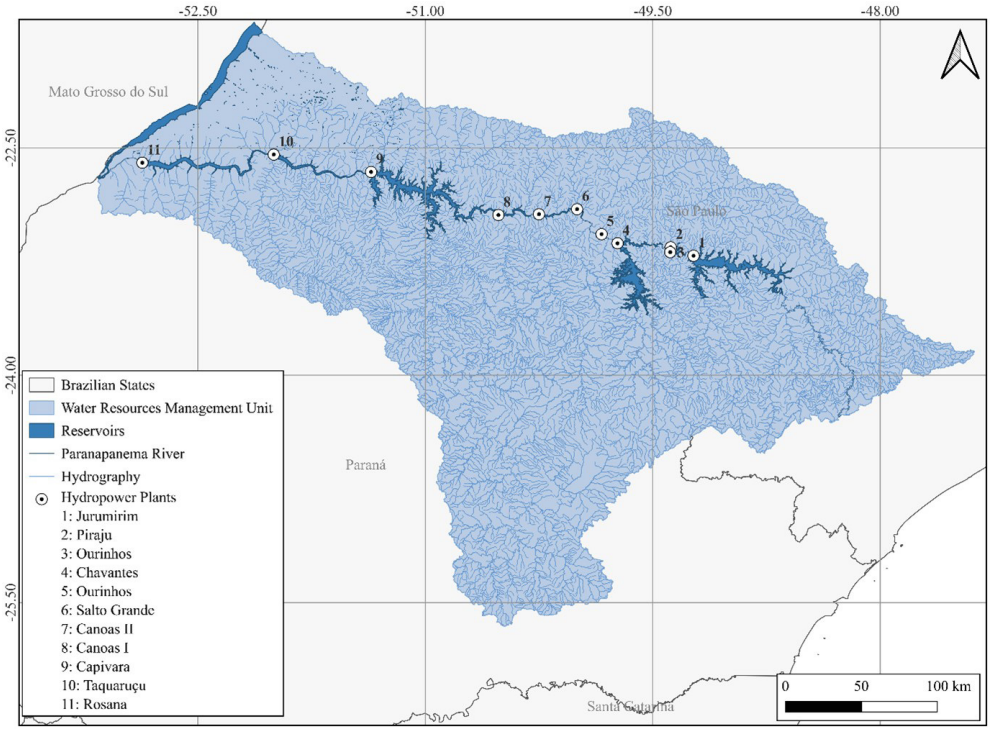

Figure 1. Location and reservoirs of the water resources management unit of Paranapanema River.

takes a long time to reach its complete renewal (possibly several months), in other words, a long residence time;

b) Run-of-river reservoirs: They may have higher to lower flooded areas and moderate depth, but the main characteristic is a low residence time (a few days or a few weeks until complete renewal).

The river system was differentiated from the lentic system following CONAMA Resolution nº 357 of 2005 (Brasil, 2005), which determines the lentic waters for residence times greater than 40 days. Residence time is defined as the average time it takes for the water to traverse the entire water body (1).

$$RT = \frac{Vol}{Q} \quad (1)$$

in which Vol is the reservoir volume (m^3), Q is the mean discharge (m^3/day) and RT is the residence time (days). The Paranapanema reservoirs' results are shown in Table 1 using annual averaged parameters.

The Jurumirim, Chavantes, and Capivara power plants belong to the accumulation category. They are lacustrine water bodies with a wide water surface and a dendritic shape. The others are run-of-river reservoirs. It has to be mentioned here already, that the resulting residence times are related to a full reservoir and mean annual discharge, thus may vary significantly over time.

Classification scheme

The analysis of the reservoirs followed the classification scheme illustrated in Figure 2, which could be applied to different systems. The proposed scheme consists of four main steps: as a first step, the reservoirs should be differentiated using residence time and thus dividing them between riverine environments (residence times smaller than 40 days) and reservoirs (residence times greater than 40 days).

In the second step, the temporal variation of the physical and chemical characteristics of the reservoirs should be analyzed using statistical analyses of the parameters involved (hydrological, geometric, water quality), to differentiate between dynamic and permanent systems, based on the coefficient of variation of the main parameters. For permanent systems, the temporal variations could be neglected, and the classification may be done using representative values (e. g., annual load, annual mean flow). For dynamic systems, a temporal variation analysis of the main parameters is recommended. In this step, it is also possible to identify the most critical parameter for water quality.

For a third step, the mixing regime (holomictic, meromictic, amictic, and no stratification) should be analyzed. Completely mixed reservoirs can be classified using simple strategies and do not need complex models. However, reservoirs that have stratification periods need more attention and the variation in the water column should be better analyzed, possibly including one-dimensional models.

As a fourth step, it should be determined whether the reservoir should be considered as a whole or whether the reservoir should be sectorized for classification and management purposes. This analysis can be done by data analysis or computational modeling to define if the horizontal variations in the water body could or not be neglected. In this case study, it was carried out using 3D modeling which was also compared with geostatistical clustering methods of the parameters involved.

Table 1. Water residence time for reservoirs in Paranapanema River Basin (Paraná and São Paulo states, Brazil).

Reservoir	Max. Normal level (m)	Area (km^2)	Volume (hm^3)	Q[1] (m^3/s)	Theoretical residence time (days)
Jurumirim	568.00	437.1	7011.21	223	364
Piraju	531.50	14.2	127.36	220	7
Chavantes	474.00	363.2	8873.84	347	296
Ourinhos	398.00	1.6	25.83	319	1
Salto Grande	384.67	5.8	53.02	459	1
Canoas II	366.00	19.9	159.00	471	4
Canoas I	351.00	27.0	223.27	489	5
Capivara	334.00	563.6	11746.33	1115	122
Taquaruçu	284.00	84.4	929.69	1175	9
Rosana	258.00	201.9	1996.24	1317	18

[1]Long-term mean annual discharge.

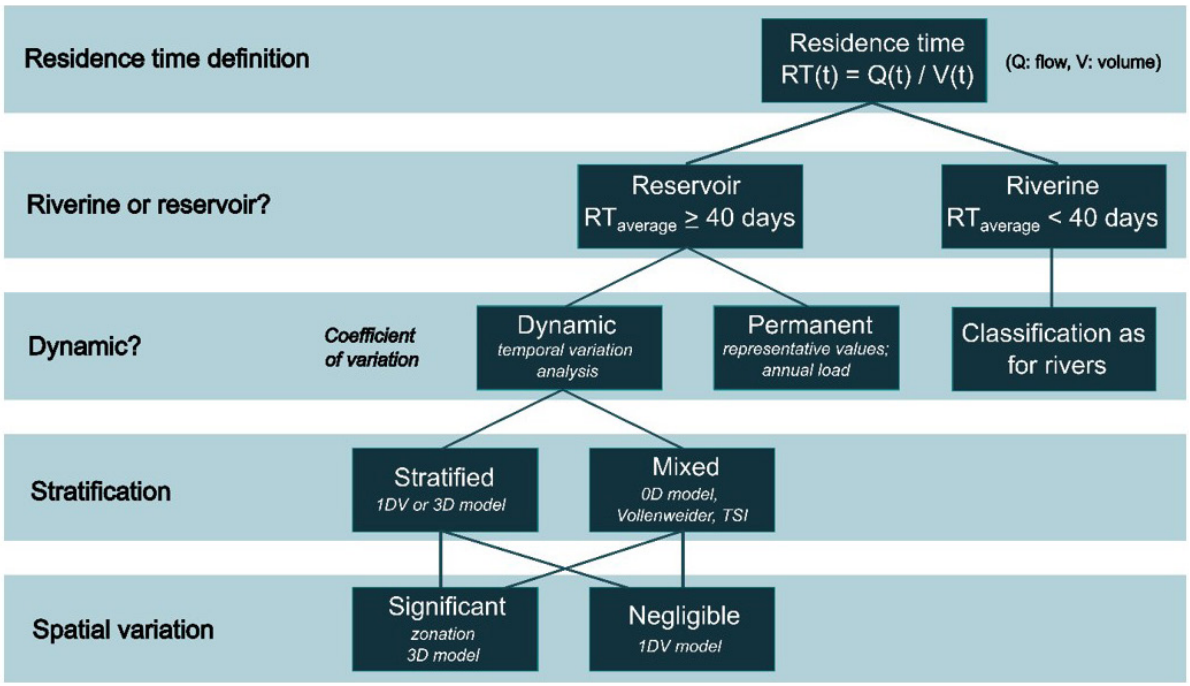

Figure 2. Reservoir classification scheme.

Analysis of reservoir dynamics

Data: temporal variation and statistical analysis

To understand the operation and hydrodynamics of reservoirs, it is essential to analyze the temporal and spatial variations that occur in them, as well as the environment in which they are inserted. Therefore, initially, these variations are analyzed in terms of inflow and outflow, water level, and reservoir volume (historical time series). The data used for this analysis were obtained from different sources, namely: HidroWeb (ANA), Department of Water and Electric Energy (DAEE), and Reservoir Monitoring System (SAR). Later the nutrient concentration was analyzed, based on historical time series from State Environmental Company of Sao Paulo (CETESB), as well as a complementary campaign in 2011 during the GIA project (Grupo Integrado de Aquicultura e Estudos Ambientais, 2013). The main statistical parameters analyzed were mean values, standard deviation (SD), amplitude, and coefficient of variation (CV), from 2005 to 2022 (period of available data in common for the 11 reservoirs). The parameters analyzed were: water flow, water level, reservoir volume, water temperature, dissolved oxygen (DO), biochemical oxygen demand (BOD) total phosphorus (TP), total nitrogen (TN), nitrate (NO_3), Ammonium (NH_4).

Residence time

The variation in water level and volume, as well as the variation in inflows and outflows, are directly correlated with the volume and water balance curve of each reservoir. Higher inflows than outflows increase the reservoir level, and vice versa. To better evaluate the consequence of all possible combinations of variables,

characteristic parameters that combine the effect of volume variation with flow variation can be used. A widely used parameter is the fraction of volume by flow, resulting in a time magnitude, and called residence time. This is because the interpretation of the residence time (RT) is the average time it takes for a particle to cross the entire reservoir, which is the ratio between the volume and the flow of the water body (Bernardo, 2018).

However, this definition of residence time was made for permanent systems (Nauman, 2008), where inlet flow equals outlet flow, which does not necessarily apply to reservoirs with regulatory operations. For this purpose, for the three accumulation reservoirs the residence time series was calculated based on four proposed methods, listed in Equations 2 to 5:

$$RT_{in} = \frac{Vol}{Q_{in}} * \frac{1}{86400} \quad (2)$$

$$RT_{out} = \frac{Vol}{Q_{out}} * \frac{1}{86400} \quad (3)$$

$$RT_{dif} = \frac{Vol}{Q_{out} - Q_{in}} * \frac{1}{86400} \quad (4)$$

$$RT_{me} = \frac{2 * Vol}{Q_{in} + Q_{out}} * \frac{1}{86400} \quad (5)$$

Where:

- RT = residence time (days)
- Q_{in} = inflow discharge (m^3/s)
- Q_{out} = outflow discharge (m^3/s)
- Vol = reservoir total volume (m^3)

RT_{in} (Equation 2) is the conventional residence time, used in the literature (Nauman, 2008), and determines the time that the water needs, on average, to cross the reservoir, considering that the average flow in the reservoir is close to the inflow (often in flood periods). RT_{out} (Equation 3) is the residence time calculated with the outflow (turbines and spillway). This time corresponds best to the average path time of a particle passing the reservoir when it is mainly forced by the outflow (e.g., in a dry period).

The difference-based residence time (Equation 4) not only determines the time it takes for a particle to cross the entire reservoir but also indirectly indicates the rise and fall times of this particle in the water body. When its value is negative, there is a filling of the reservoir, while when positive, there is an emptying, so that the higher the magnitude of the residence time, the faster the particle travels vertically. Equation 5) is the residence time based on the average between Q_{in} and Q_{out}.

Extreme scenarios

Reservoirs can be of great importance in river systems, acting as regulators of water flow. To analyze that, a series of hydrodynamic and water quality modeling scenarios were proposed, with the aim of evaluating reservoirs in relation to their dynamics in the face of different conditions and forcings. These are called hypothetical scenarios, as they represent situations that combine characteristics of reservoirs (empty/full), tributaries (low/high flow), and loads (low/high) that have not necessarily already occurred. A summary of these scenarios is presented in Table 2. The meteorological data was gathered from the National Institute of Meteorology (INMET).

The model system MoRE (Modeling of Regionalized Emissions, Fuchs et al., 2017) was used to determine the input load of the scenarios, considering the point sources (wastewater, industrial discharges) and diffuse sources (land use, erosion) of the Paranapanema basin (Agência Nacional de Águas, 2020a). The modeling approaches of MoRE are grouped into emission pathways that are summed up: atmospheric deposition, erosion, surface runoff, drainage, groundwater, sewer systems, wastewater treatment plant, industrial direct drainage and abandoned mining. Complete information about the model can be found in Fuchs et al., 2017. In this scenarios, total phosphorus (TP), total nitrogen (TN), and biochemical oxygen demand (BOD) were considered.

Stratification analysis

Seasonal stratification is fundamental for all other processes that occur in the reservoir, physical, chemical, or biological (Boehrer & Schultze, 2008). It determines the transport of DO and nutrients in the water column as well as the light environment. Shallow lakes are more frequently mixed, having different behavior than deeper lakes that usually stratify during heating seasons, where a warmer layer is formed above the cooler and nutrient-rich deep layer (Kirillin & Shatwell, 2016). Therefore, the analysis of stratification of water bodies is one of the bases for reservoir classification.

For the Paranapanema case study, the stratification of the accumulation reservoirs was analyzed based on measurement data and simulations with a one-dimensional model, considering water temperature, DO, and TP profiles (Carvalho & Bleninger, 2021). The model used was the General Lake Model (GLM, Hipsey et al., 2019), the simulation was developed from 1980 to 2013, calibrated with measured data from 2011, and validated from 2012 to 2013. This model was chosen for an initial assessment

Table 2. Summary of the extreme scenarios proposed for reservoir simulations.

Scenarios	0 (Base)	1a	1b	2a	2b
Stratification	Yes	No	Yes	No	Yes
Inflow	Representative year	Strong	Strong	Historical Mean	Historical Mean
Water level	Representative year	Mean	Mean	Critical (drought)	Critical (drought)
Meteorological data	Representative year	Characteristic month of the mixed period	Characteristic month of the stratified period	Characteristic month of the mixed period	Characteristic month of the stratified period
Fish farming	Yes	Yes	Yes	Yes	Yes
Water quality	Yes	Yes	Yes	Yes	Yes

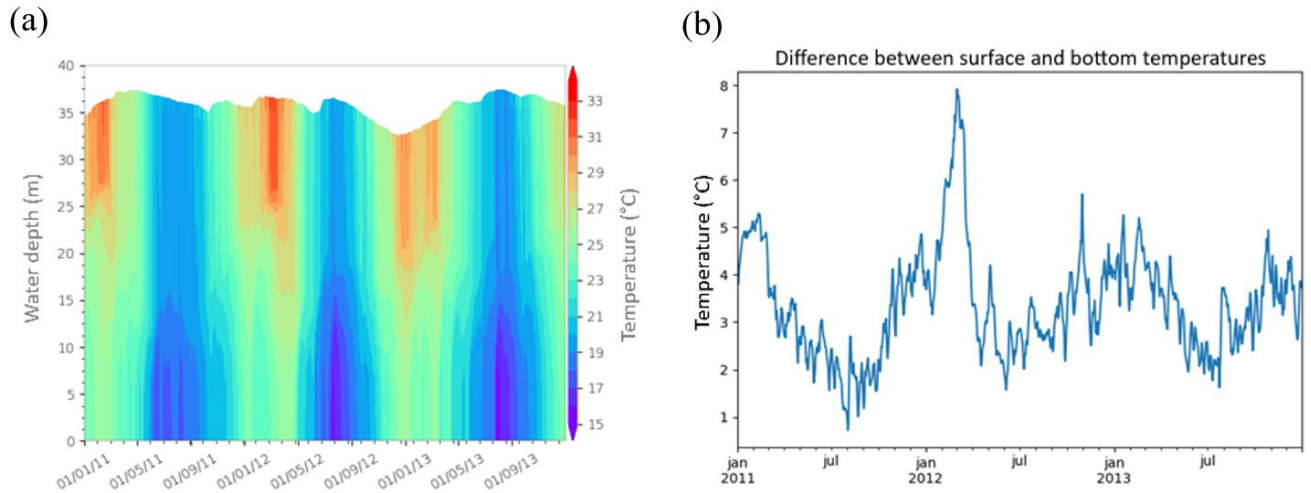

Figure 3. GLM results for the Jurumirim reservoir. (a) Development of the thermal profile and (b) temperature difference between surface and bottom, from 2011 to 2013. (Adapted from Agência Nacional de Águas, 2020b).

of reservoir stratification due to its low computational cost. The boundary conditions were time series of total inflow and water level for output. Meteorological time series were also included in the simulation.

The three lentic reservoirs showed some stratification during the summer, the peak appearing in January 2011 for the Jurumirim and Capivara reservoirs, and January 2012 for the Chavantes reservoir, with a difference between surface and bottom temperature of 7.8°C, 9°C and 14°C, respectively. The results of the periods of calibration and validation of the simulation for the Jurumirim reservoir are shown in Figure 3.

Spatial variation

In addition to temporal variations, reservoirs may have spatial variations in their characteristics. Unlike rivers, three zones are traditionally identified in reservoirs (Ji, 2008): the lotic/riverine zone, with higher speeds and characteristics similar to those of rivers; the lacustrine zone, represented by higher water column heights, lower velocities, and behavior similar to lakes; and the intermediate zone between the two. Therefore, an important question for the classification of these water bodies is: are the spatial variations in the concentration, transport, and mixing of substances significant in the reservoir?

To evaluate spatial variations and the need for reservoir zonation, hydrodynamic and water quality simulations were carried out using the Delft3D model (Deltares, 2014). Delft3D is a three-dimensional model widely used to solve problems related to reservoirs and thermal stratification (Soulignac et al., 2017; Wahl & Peeters, 2014; Smits et al., 2009) and water quality (Smits et al., 2009). The hydrodynamic module (Delft3D-Flow) simulates non-steady flows and transport due to meteorological forcing, including density effects. The water quality module (DELWAQ) allows the simulation of various substances, including nutrients, dissolved oxygen, micropollutants, and algae (Deltares, 2014).

For the Jurumirim reservoir, a model with a curvilinear grid was developed, with an average resolution of 150 x 200 m

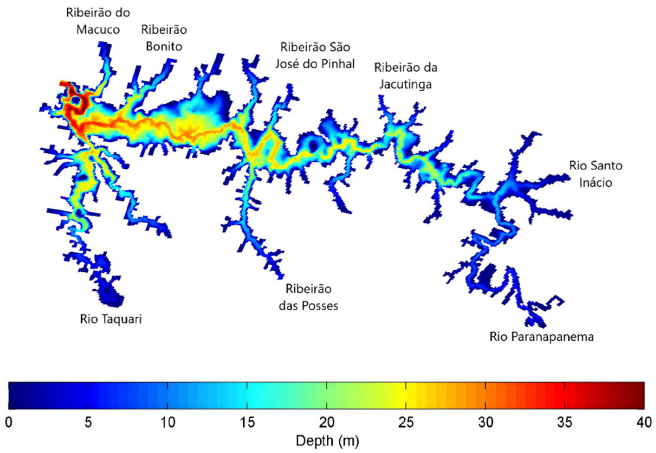

Figure 4. Bathymetry of the Jurumirim reservoir and the considered tributaries.

per cell, with approximately 19067 grid cells in the horizontal area and 10 vertical layers. The bathymetry of the reservoir is shown in Figure 4, together with the different tributaries considered in the model. The model was built with 9 boundary conditions, 8 of which were input conditions of tributary flow (Rio Paranapanema, Rio Santo Inácio, Rio Taquari, Ribeirão das Posses, Ribeirão da Jacutinga, Ribeirão São José do Pinhal, Ribeirão Bonito e Ribeirão do Macuco) and one output condition of level. Meteorological forces (wind, relative humidity, radiation, air temperature, cloud cover) were also considered. The reservoir was considered stratified in its initial condition (GLM results). The simulation was conducted for the representative year.

For zonation purposes, these results were used to test different zonation methods, described below.

a) **Morphological clustering zonation** is based on the hypothesis that distinct water quality regions are highly correlated with reservoir shapes, depths, and tributary locations. The different geometric/morphological parameters are then expected to correspond with different water quality

regions. To test this hypothesis, different geometric and morphological combinations were analyzed and compared with the modeling results.

b) **The basin-based zonation** assumes that distinct water quality regions are highly correlated with the loads and flows of adjacent tributaries, enabling zoning based on these correlations. The reservoir branches near the larger basins and with higher loads are expected to have lower water quality compared to the other regions. To test this hypothesis, data from the basin and all subbasins were analyzed, ranked, and compared with modeling results.

c) **The hydrodynamic zonation** is proposed with the hypothesis that reservoirs have characteristic hydrodynamic regions. In these regions, we expect to observe distinct hydrodynamic conditions that prevail for significant periods. To test this hypothesis, velocity fields (intensity and direction) were analyzed. For these parameters, only simulation results were used since there are no measurements for the region.

d) **The water quality zonation** is based on the hypothesis that reservoirs have regions with different concentrations' patterns of water quality parameters. In these regions, we expect to observe distinct concentrations that prevail for significant periods. To test this hypothesis, concentration fields of the most critical parameter were analyzed using simulation results.

RESULTS AND DISCUSSION

Reservoir's dynamics

The historical series of discharge evaluated, even if short, have shown great variability, both inflow and outflow (Table 3, Table 4). This makes it interesting to consider at least high, medium, and low flows, to better understand the dynamics between hydrodynamics and water quality. At the decision level of 5%, all inflow time series seem to fit the normal statistical distribution (Figure 5).

The water level and volume time series are strongly linearly correlated, and their shape is always very similar. Both series seem to fit the normal statistical distribution, in addition to having low variability (Table 5 and Table 6). None of the reservoirs had a water level lower than the minimum necessary for its operation or the operation of the superficial spillway of the dams. The water level of Jurumirim, Chavantes, and Capivara reservoirs presents little variation, with a coefficient of variation below 1%. However, the standard deviation for these three reservoirs is greater than 1 m, while the others stay around 0.1 m. Unlike the water level, the volumes of the reservoirs have considerable variations. As shown by Pedrazzi et al. (2013), these temporal variations can also be reflected in zones inside the reservoir. Depending on its geometry, periods with higher or lower volumes can reveal different zones in terms of water quality. Given the importance of both parameters

Table 3. Basic statistics of the inflow time series, from 2005 to 2022, of the Paranapanema reservoirs.

Reservoir	Mean (m^3/s)	SD (m^3/s)	Minimum (m^3/s)	Maximum (m^3/s)	Median (m^3/s)	Amplitude (m^3/s)	CV (%)
Jurumirim	223.3	166.3	18.9	2060.6	172.0	2041.8	74%
Piraju	223.2	128.8	53.0	1226.0	193.0	1173.0	58%
Chavantes	345.4	225.1	76.9	4712.0	296.6	4635.1	65%
Ourinhos	335.3	223.6	76.5	2066.8	311.0	1990.2	67%
Salto Grande	460.7	272.9	114.7	3204.1	421.4	3089.4	59%
Canoas II	461.6	268.2	134.9	3061.6	418.0	2926.7	58%
Canoas I	497.5	286.9	139.0	3381.6	455.6	3242.6	58%
Capivara	1196.6	805.2	260.4	10960.1	998.5	10699.8	67%
Taquaruçu	1232.0	782.3	299.0	13438.0	1118.9	13139.0	63%
Rosana	1379.1	822.4	373.0	13897.0	1252.0	13524.0	60%

Table 4. Basic statistics of the outflow time series, from 2005 to 2022, of the Paranapanema reservoirs.

Reservoir	Mean (m^3/s)	SD (m^3/s)	Minimum (m^3/s)	Maximum (m^3/s)	Median (m^3/s)	Amplitude (m^3/s)	CV (%)
Jurumirim	225.4	131.3	59.0	1195.0	190.0	1136.0	58%
Piraju	223.2	128.9	53.0	1226.0	193.0	1173.0	58%
Chavantes	346.8	217.2	93.0	1993.0	329.0	1900.0	63%
Ourinhos	326.6	227.1	0.0	2069.0	304.9	2069.0	70%
Salto Grande	460.7	272.6	130.0	3176.0	421.0	3046.0	59%
Canoas II	460.6	267.5	134.0	3067.0	418.0	2933.0	58%
Canoas I	497.6	288.6	136.0	3415.0	452.0	3279.0	58%
Capivara	1201.7	761.9	282.0	13501.0	1102.0	13219.0	63%
Taquaruçu	1232.0	790.4	354.0	13647.0	1124.0	13293.0	64%
Rosana	1379.3	838.9	403.0	13482.0	1251.0	13079.0	61%

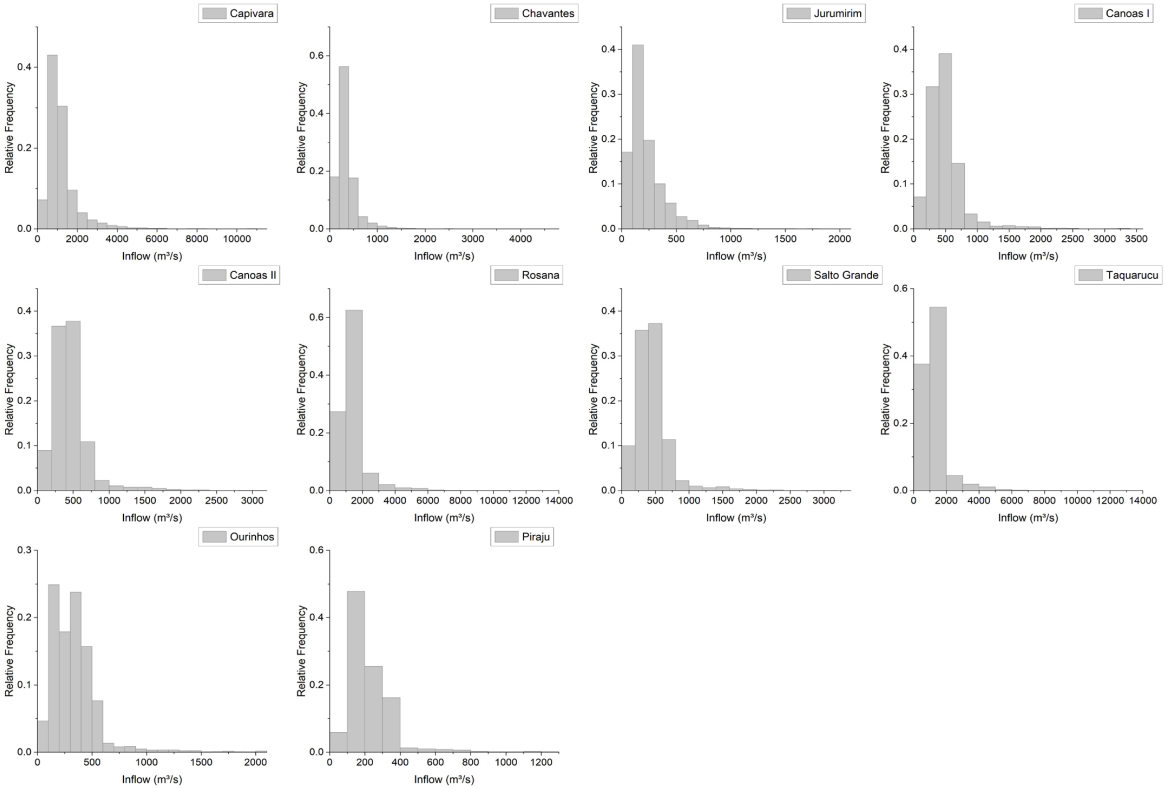

Figure 5. Histograms of the inflow time series, from 2005 to 2022, of the Paranapanema reservoirs.

Table 5. Basic statistics of the water level time series, from 2005 to 2022, of the Paranapanema reservoirs.

Reservoir	Mean (m)	SD (m)	Minimum (m)	Maximum (m)	Median (m)	Amplitude (m)	CV (%)
Jurumirim	564.9	1.8	560.9	567.8	565.5	6.9	0.3%
Piraju	531.5	0.1	531.3	532.1	531.5	0.8	0.0%
Chavantes	470.6	1.9	466.2	473.8	471.1	7.6	0.4%
Ourinhos	398.0	0.1	396.6	398.4	398.0	1.8	0.0%
Salto Grande	384.2	0.4	382.0	385.3	384.3	3.3	0.1%
Canoas II	365.9	0.1	365.6	366.3	366.0	0.7	0.0%
Canoas I	350.9	0.1	350.0	351.3	351.0	1.3	0.0%
Capivara	330.3	3.1	321.5	334.2	331.0	12.6	0.9%
Taquaruçu	283.6	0.1	282.7	284.2	283.6	1.4	0.0%
Rosana	257.7	0.1	256.6	258.1	257.7	1.5	0.1%

Table 6. Basic statistics of the volume time series, from 2005 to 2022, of the Paranapanema reservoirs.

Reservoir	Mean (m^3)	SD (m^3)	Minimum (m^3)	Maximum (m^3)	Median (m^3)	Amplitude (m^3)	CV (%)
Jurumirim	5690.8	720.8	4177.8	6926.0	5922.6	2748.2	13.0%
Piraju	125.6	1.1	122.6	133.9	125.5	11.3	1.0%
Chavantes	7597.3	685.1	6087.8	8794.8	7744.1	2706.9	9.0%
Ourinhos	24.5	0.3	19.3	25.8	24.4	6.5	1.0%
Salto Grande	47.7	4.1	24.7	62.1	48.5	37.3	9.0%
Canoas II	157.6	1.5	150.1	165.1	157.8	15.0	1.0%
Canoas I	220.6	3.9	195.5	230.9	221.0	35.4	2.0%
Capivara	9712.7	1635.7	5651.2	11851.0	9973.9	6199.8	17.0%
Taquaruçu	894.0	11.6	823.9	942.0	892.7	118.1	1.0%
Rosana	1940.3	28.4	1701.7	2026.1	1940.8	324.4	1.0%

within the models scenarios, it is interesting to create scenarios with reservoirs in at least three states: "full, normal, and empty", to evaluate its influence on water quality.

Regarding concentration variations, Table 7, Table 8, and Table 9 present the contribution of TP, TN, and BOD loads, respectively, considering the Paranapanema River, Taquari River, other tributaries, and aquaculture inputs. According to Table 7, the Taquari River contributes 25% of the phosphorus load in the Jurumirim reservoir, while aquaculture contributes 8%. In the case of nitrogen, according to Table 8, the largest contribution comes from the Paranapanema River (40%) and from the Taquari River, 25%. The average annual load (kg/km^2/year) is lower than the estimated for agricultural watersheds (Li et al., 2015). In the case of BOD, the largest loads are from the Taquari River (47.2%) while the other affluents contribute 20.1% of the total load to the reservoir (Table 9).

In this case study, for all reservoirs, the phosphorus concentration was the critical parameter, originating from the basin loads and aquaculture. It was observed that Jurumirim, Chavantes, and Capivara reservoirs act as attenuators of inflows and forcings and that temporal variations do not need to be analyzed in detail for classification purposes.

The time series of the residence time were calculated for all reservoirs, from 2005 to 2022. Even though all the reservoirs showed large variations in residence time (Figure 6, Table 10), the only ones with an average of more than 40 days were Jurumirim, Chavantes and Capivara.

Run-of-river reservoirs have riverine characteristics and can be classified by the same approach as rivers since the hydrodynamics and water quality processes are different than lacustrine systems. Nine of the eleven Paranapanema reservoirs belong to this category, as shown in the previous analysis. Thus, the three accumulation reservoirs (Jurumirim, Chavantes, and Capivara) were analyzed in greater detail. Since the results for the three reservoirs were very similar, only the graphs for Jurumirim are shown. However, the statistics for the three reservoirs are presented.

Figure 7 presents the residence times for the Jurumirim reservoir from 2011 to 2022. Table 11 presents its basic statistics for RT_{in}, RT_{out}, and RT_{med}. The negative values in the RT_{dif} indicate that, for that time interval, the reservoir is filling.

Residence times present a great variability (CV) and amplitude of values, more pronounced in the Jurumirim reservoir, given its first position in the Paranapanema River cascade, which limits its operation capacity compared to the others. The residence time variability is between 40 to 65% around the mean (Table 11), which is considered significant and justifies the dynamic analysis of water quality in the accumulation reservoirs under these conditions. As shown by Rueda et al. (2006), this temporal variations occur

Table 7. The proportion of the TP load contributing to the Jurumirim reservoir in the Paranapanema River, Taquari River, other tributaries, and aquaculture.

Source	Mean inflow (m^3/s)	Area (km^2)	TP load (kg/day)	TP load (kg//km^2/year)	% of total load
Paranapanema river	125.45	10074.82	654.13	23.7	40%
Taquari river	56.48	4536.00	414.86	33.4	25%
Other tributaries	41.37	3322.49	440.55	48.4	27%
Aquaculture	–	-	122.94	-	8%
Total	–	17933.31	1632.48	-	100%

Table 8. The proportion of TN load that contributes to the Jurumirim reservoir in the Paranapanema River, Taquari River, other tributaries and aquaculture.

Source	Mean inflow (m^3/s)	Area (km^2)	TN load (kg/day)	TN load (kg//km^2/year)	% of total load
Paranapanema river	125.45	10074.82	8481.5	307.3	53%
Taquari river	56.48	4536.00	4275.03	344.0	27%
Other tributaries	41.37	3322.49	3012.39	330.9	19%
Aquaculture	–	-	292.87	-	2%
Total	–	17933.31	16061.79	-	100%

Table 9. The proportion of the BOD load contributing to the Jurumirim reservoir in the Paranapanema River, Taquari River, other tributaries, and aquaculture.

Source	Mean inflow (m^3/s)	Area (km^2)	DBO load (kg/day)	DBO load (kg/km^2/year)	% of total load
Paranapanema river	125.45	10074.82	19786.85	716.9	51%
Taquari river	56.48	4536.00	9573.4	770.3	25%
Other tributaries	41.37	3322.49	9293.5	1021.0	24%
Aquaculture	–	-	-	-	-
Total	–	17933.31	38653.75	-	100%

at seasonal and shorter scales, and the transport and mixing processes that occur inside the reservoir are closely related to it.

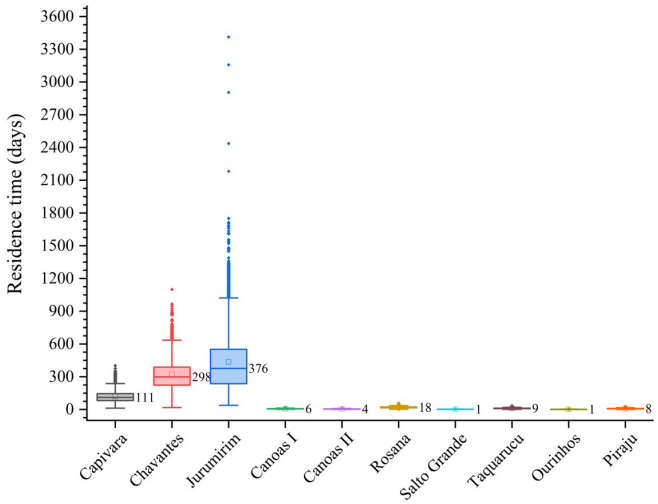

Figure 6. Boxplots of the residence time of the Paranapanema reservoirs (black numbers on the right side of the graphs are the median values).

After the time series analysis, 2012 was considered a representative year for the concentration and zonation analysis. Inflow variations (tributaries) are greater than reservoir variations, indicating that it is not very sensitive to temporal variations in inflow concentrations and acts as a buffer (Table 12). Furthermore, the differences between the base scenario and hypothetical scenarios were small. The base scenario is representative of the state of the reservoir.

Reservoir zonation

After analyzing the reservoir dynamics, it is important to evaluate the spatial variations and the necessity of a zonation for classification and management purposes. Four different types of zonation were analyzed, and at the end a proposal of the reservoir zonation guideline is presented, based on the results.

Hydrodynamic zonation analysis

The velocity fields for the Jurumirim reservoir in a mixed (a) and stratified (b) situation are shown in Figure 8. Results show regions with distinct velocities; however, the regions change at

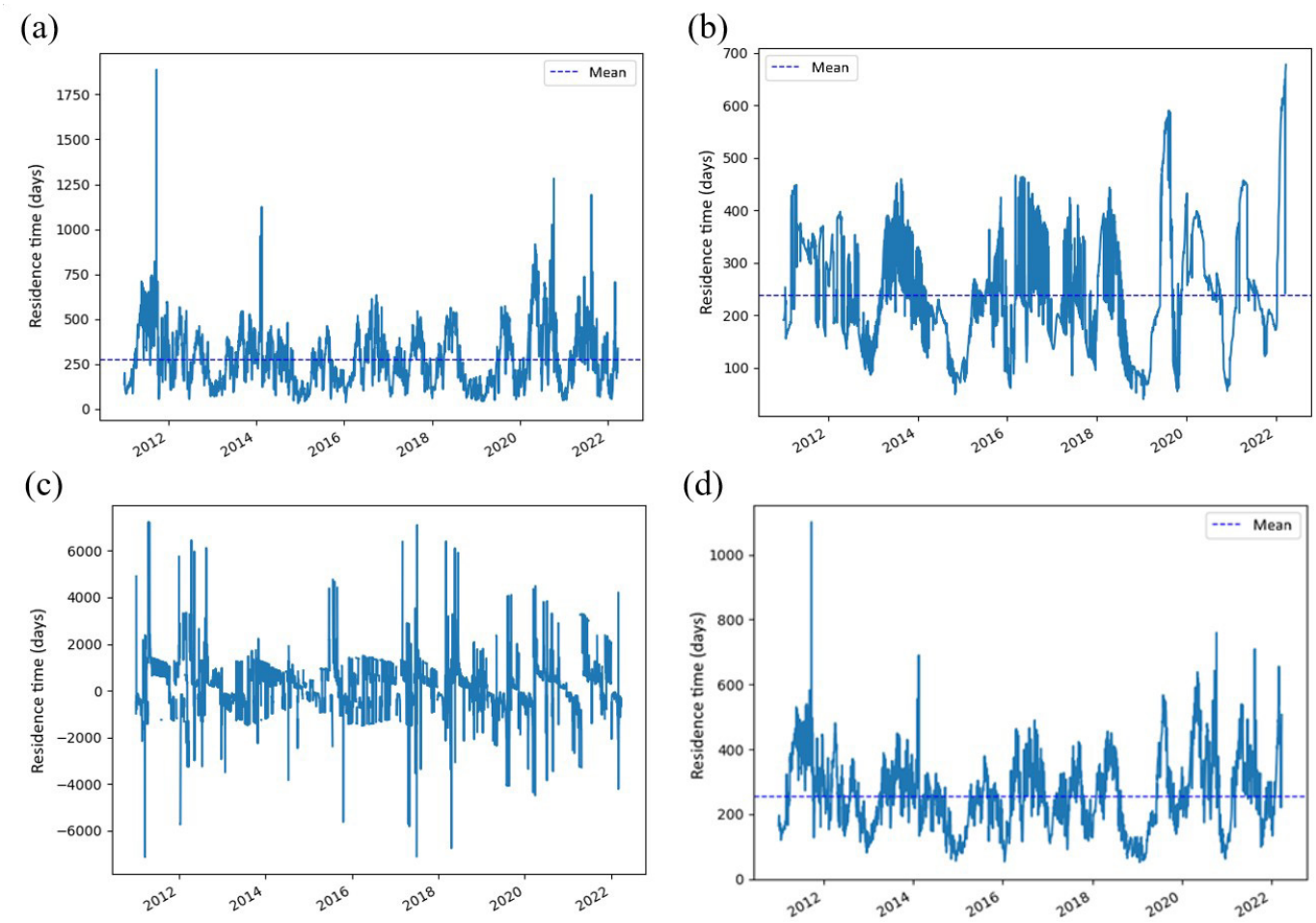

Figure 7. Time series of residence times at the Jurumirim reservoir. (a) TR_{in}, (b) TR_{out}, (c) TR_{dif}, and (d) TR_{me}.

Table 10. Basic statistics of the residence time, from 2005 to 2022, of the Paranapanema reservoirs.

Reservoir	Mean (days)	SD (days)	Minimum (days)	Maximum (days)	Median (days)	Amplitude (days)	CV (%)
Jurumirim	435	273	38	3413	376	3375	63%
Piraju	8	4	1	27	8	26	51%
Chavantes	323	147	18	1099	298	1081	45%
Ourinhos	1	1	0	4	1	4	61%
Salto Grande	2	1	0	5	1	4	53%
Canoas II	5	2	1	14	4	13	49%
Canoas I	6	3	1	18	6	18	50%
Capivara	119	54	12	402	111	391	45%
Taquaruçu	11	6	1	35	9	34	52%
Rosana	20	9	2	60	18	58	44%

Table 11. Basic statistics of the dynamic residence time series of the three lentic reservoirs, from 2005 to 2021.

	TRin (days)			TRout (days)			TRme (days)		
	Jur	Cha	Cap	Jur	Cha	Cap	Jur	Cha	Cap
Mean	435	8	323	360	343	117	363	321	113
SD	273	4	147	160	188	55	158	154	47
Min	38	1	18	66	50	10	53	33	11
Max	3413	27	1099	1000	894	385	1071	886	354
Median	376	8	298	337	277	102	333	278	105
CV	63%	51%	45%	45%	55%	47%	43%	48%	41%

Jur: Jurumirim; Cha: Chavantes; Cap: Capivara.

Table 12. Coefficients of variation and amplitude of water temperature, dissolved oxygen, total phosphorus, nitrate, and ammonium concentrations observed in the reservoirs and their intakes, for the year 2012.

		Jurumirim		Chavantes		Capivara	
		Amplitude	CV	Amplitude	CV	Amplitude	CV
Water temperature (°C)	Inflow	12.90	14%	13.40	15%	14.20	14%
	Reservoir	10.00	13%	3.80	6%	11.50	15%
Dissolved oxygen (mg/L)	Inflow	5.50	16%	4.70	13%	4.30	12%
	Reservoir	1.80	6%	0.60	3%	1.60	6%
Total phosphorus (mg/L)	Inflow	0.27	62%	0.55	77%	0.06	38%
	Reservoir	0.04	5%	0.03	5%	0.01	8%
Nitrate (mg/L)	Inflow	0.53	33%	0.79	42%	0.40	22%
	Reservoir	0.06	5%	0.11	27%	0.07	10%
Ammonium (mg/L)	Inflow	0.79	104%	2.16	173%	0.47	65%
	Reservoir	0.02	103%	0.04	88%	0.06	49%

Source: Adapted from Agência Nacional de Águas (2020b).

each time, and even on average do not show clear distinct regions. As shown by Oliveira et al. (2020), identifying the reservoir hydrodynamics can help to identify limnological zones within the reservoir, which have influence in the water quality. Reservoir hydrodynamics is dominated by wind and radiation, and the effect of tributaries is secondary, and only local velocities in reservoirs are low (cm/s or less). Velocities in most parts of the reservoir vary with meteorological forces that do not have a sufficient spatial pattern. Hydrodynamics in these reservoirs do not follow a unique spatial pattern, and thus the use of this parameter for zonation is not recommended. Areas with higher velocities in the two largest tributaries (Paranapanema and Taquari) stand out, however, only in the region near the inlet.

Basin-based zonation analysis

Figure 9 shows the result of the basin analysis for Jurumirim Reservoir, while Table 7 shows the ranking of the loads from the tributaries. The basins with the highest loads are correlated with regions of water quality concentrations. Thus, it is possible to zone the reservoir just by analyzing the loads entering the reservoir. As shown by Deeds et al. (2020), that applied a hydrogeomorphic-based lake classification in Maine (USA), the water quality of lakes and reservoirs is highly influenced by anthropogenic watershed activities and local-scale characteristics of lake basins. Zone boundaries can be defined using the boundaries of adjacent basins. The disadvantage is that this type of analysis does not result in

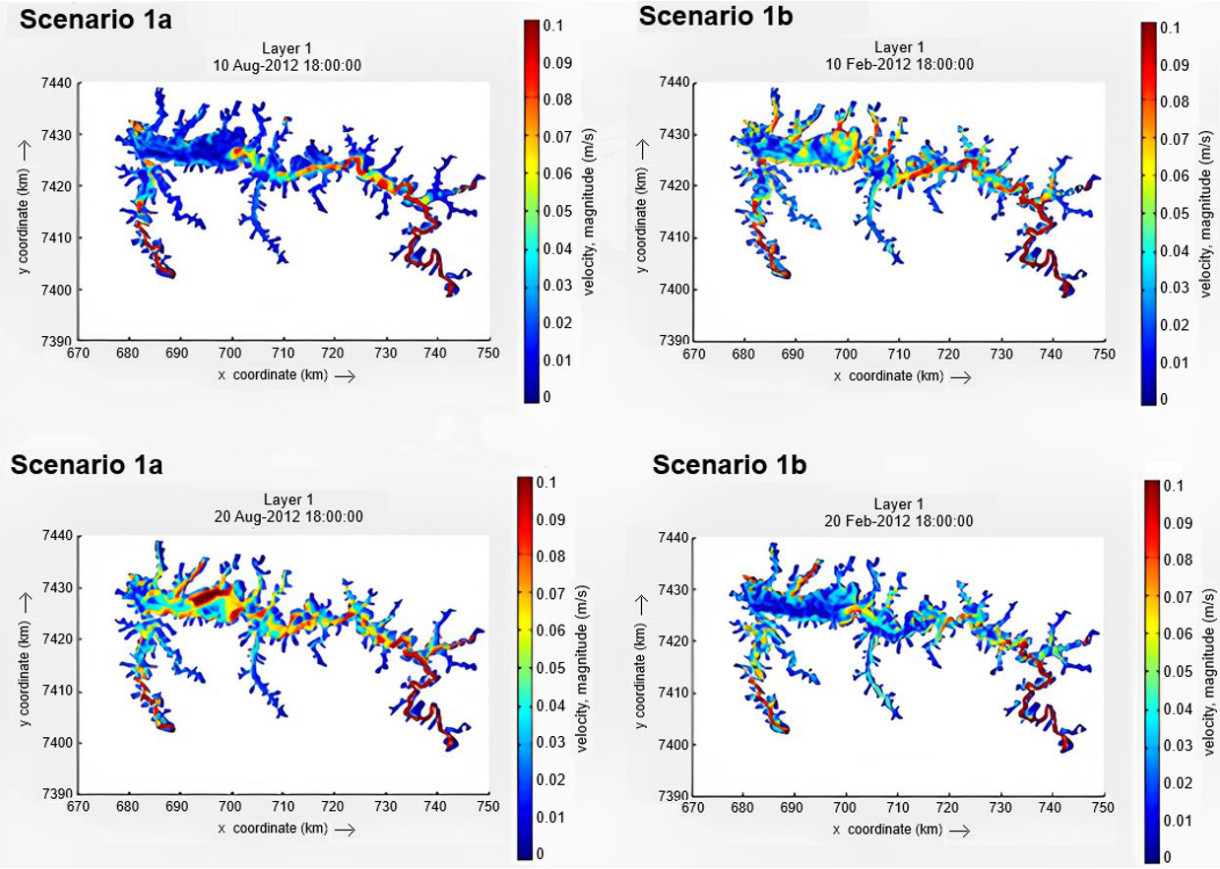

Figure 8. Surface velocity maps for Jurumirim Reservoir and four scenarios of a strong flow pulse entering the (a) mixed and (b) stratified situation for two different dates (Agência Nacional de Águas, 2020b).

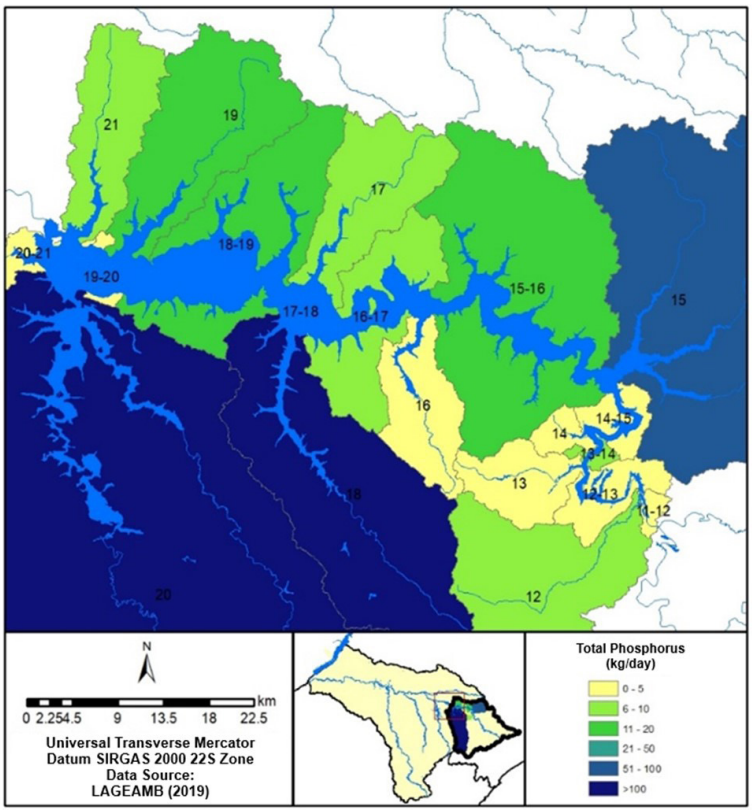

Figure 9. Estimation of Total Phosphorus load in the tributary basins of the Jurumirim Reservoir (Agência Nacional de Águas, 2019).

water quality concentrations. However, these can be estimated with simplified calculations (e.g. Vollenweider-type classifications).

The ranking of the main inputs allows the identification of the main sources. Gunkel et al. (2018) observed changes in Chlorophyll-a concentrations in the longitudinal profile of Itaparica Reservoir, in the semi-arid region of Brazil, indicating multiple contamination sources.

In this study case, the three rivers with the highest loads (Paranapanema, 40%, Taquari, 25%, and Ribeirão das Posses, 18%) represent 83% of the total phosphorus load entering the reservoir. In this case, to improve the water quality of the reservoir, more efficient measures should be recommended for these three rivers. Aquaculture contributes only 8% and was also shown in water quality modeling to have little relevance for water quality in this reservoir.

Water quality zonation analysis

The results of the water quality simulations indicated TP as a critical parameter. The spatial analyses showed four distinct main regions based on TP concentrations (Figure 10). However, these patterns are also observed in TN concentration, as shown in the boxplots (Figure 11). OD and DBO concentrations were very similar over the time in all sectors.

Contrary to hydrodynamic analyses, these regions are stable over time, indicating their potential for use as a zoning method. It should be noted that the two regions identified with high concentrations (in the figure, > 0.07 mg.L^{-1}) in the modeling are associated with tributaries in which there is a greater load compared to the others (Sectors 2 and 3). This suggests that tributaries are the main sources of potential water quality problems.

The stratified and mixed periods have differences; however, they highlight the same spatial zones. The areas with the highest concentrations do not change significantly between the strong pulse and the low-level moments, showing that the critical regions are independent of reservoir conditions and depend mainly on loads. Different from Pedrazzi et al. (2013), who showed temporal and spatial variations of measured concentrations at the Itupararanga Reservoir, in Brazil, already processed to map the trophic state index. In their case, the reservoir had different zones of trophic state index that change according to the period (dry or wet).

Geometric/morphological compartmentalization analysis

Inspired by the results of the water quality zonation and basin-based, the zonation based on the basic parameters of both

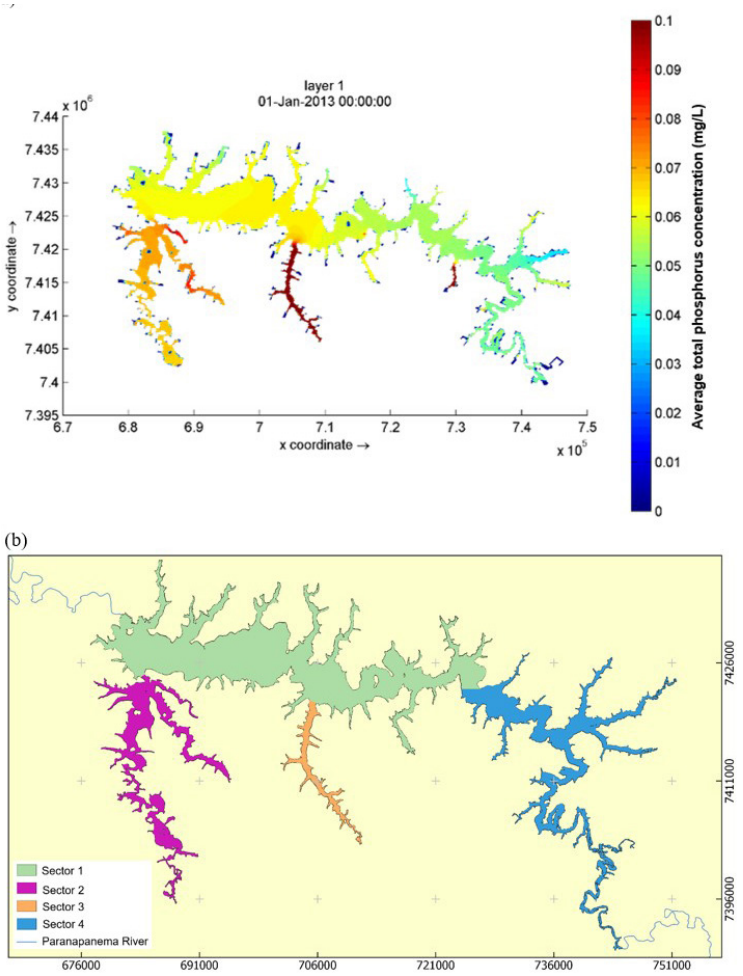

Figure 10. Water quality zonation results from Delft3D simulations. (a) the average concentration of total phosphorus in 2012, (b) resultant zoning.

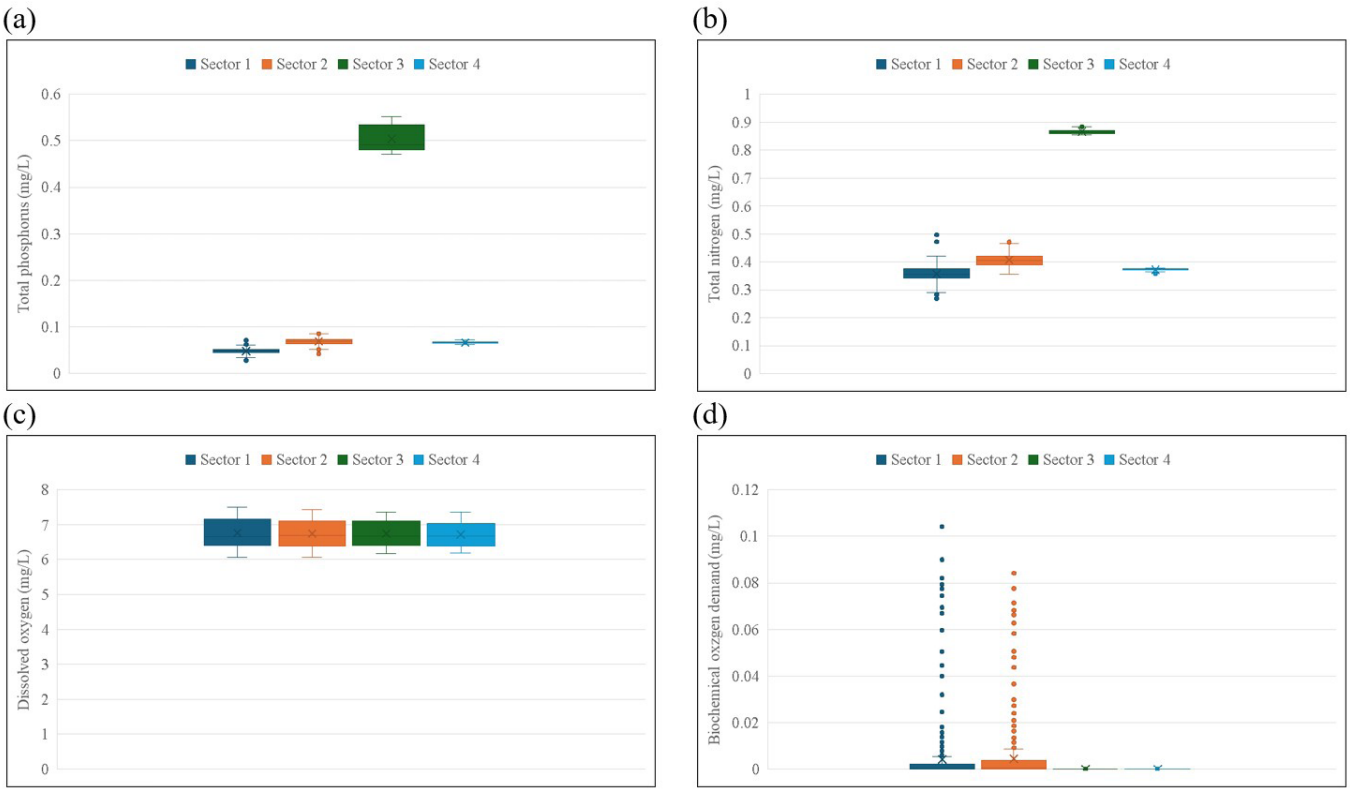

Figure 11. Water quality zonation results from Delft3D simulations – Boxplots of (a) TP, (b) TN, (c) DO, and (d) BOD concentrations in the sectors defined for the Jurumirim reservoir.

parties was elaborated. These are the reservoir bank coordinates and depths. Figure 12 shows the results of the k-means method, which correlates these parameters to obtain "clusters", then specific zones, with the more combined influence of these parameters. The separation into 3 sectors already results in a high score (last graph in Figure 12), and the obtained clusters have similarities with the results from modeling. However, the method does not provide concentration information and would have to be supplemented with load information for each sector (e.g. Vollenweider-type classifications).

Zonation proposition

The regions identified by the water quality parameters by both methods showed regions associated with tributaries with higher loads. This suggests that the tributaries are the main sources of potential water quality problems. This also led to the hypothesis of basing zoning on basin characteristics alone, analyzed as follows. From the results presented, the following zonation strategy is proposed.

1. Ranking of associated loads

In the ranking, the percentage of load for each source (tributary, fish farming) is calculated, and the largest sources (for example, all above 10%) are selected for zoning. Table 13 shows the example of the Jurumirim reservoir, resulting in 3 main zones (Paranapanema, Taquari, Ribeirão das Posses).

2. Hydrodynamic ranking

Knowing that large loads could be assimilated by reservoir arms that have large volumes and large flows, the hydrodynamic effect should also be evaluated specifically in the regions adjacent to the sectors identified in Step 1.

To do this, the volume of each sector will be calculated and estimates made for:

- Residence time in the sector/arm: $Volume_{sector} / Q_{in,sector}$
- Average velocity in the sector: $Q_{in,sector} / (Volume_{sector} x \; Length_{secto})$
- Characteristic numbers for water quality

It should be noted that these data are generally easy to obtain and process. The sectors with the lowest speed and/or longest residence time with the highest loads will be considered the most critical sectors.

3. Water Quality Classification

Zonation and ranking in steps 1 and 2 allow critical sectors of the reservoir to be identified but do not provide information on concentrations or classes for regulation purposes. Therefore, in this third step, the average concentrations in each sector should be calculated as $C_{sector} = \frac{Load_{in,sector}}{Q_{sector}}$. In addition, simplified conventional methods of Vollenweider type may be tested to obtain the trophic state of the system.

4. Refinement and validation

If necessary, to test, refine, or validate the zoning obtained with the water quality classification, there is a recommendation

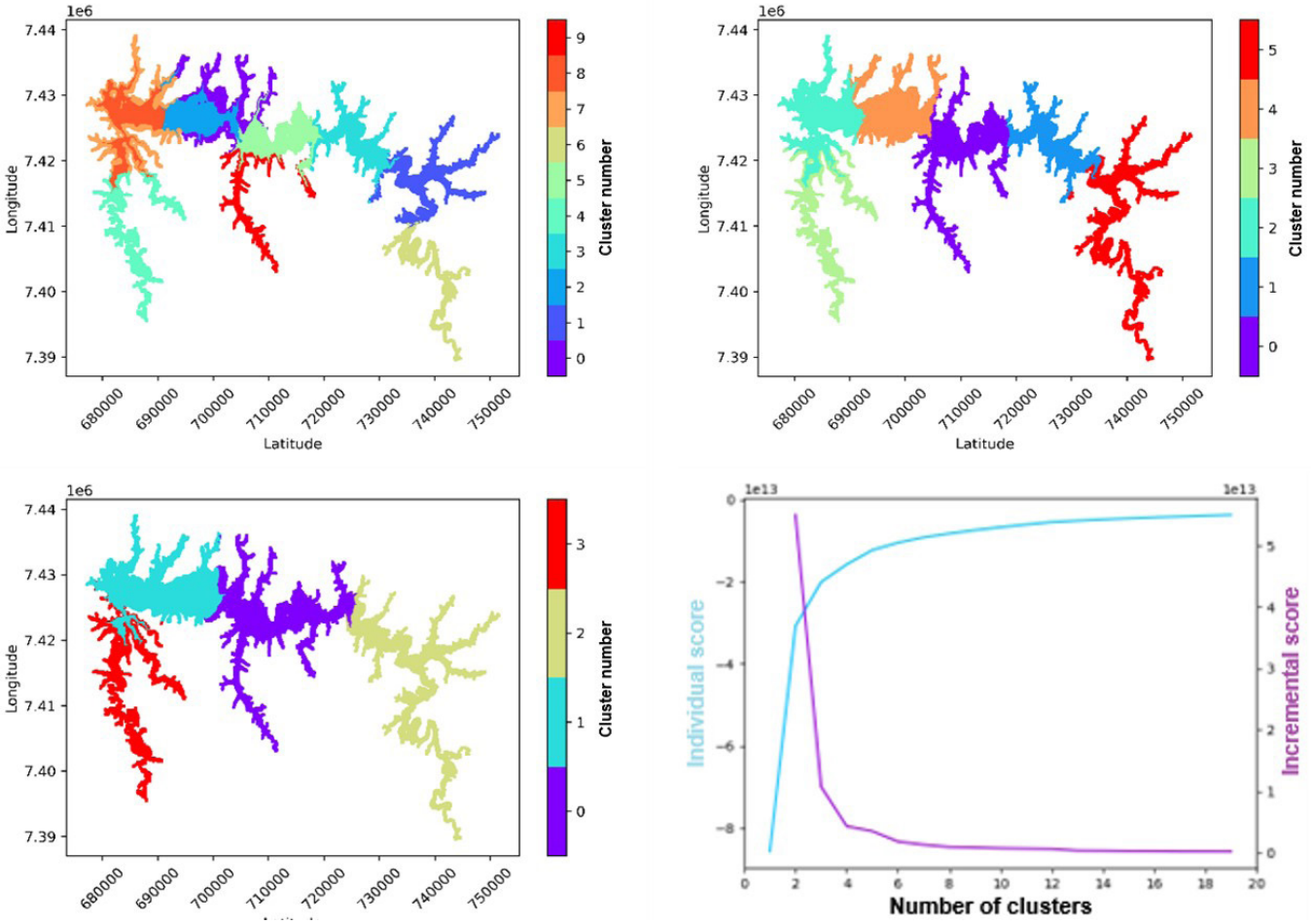

Figure 12. Results of the creation using the k-means method and the edge coordinates and depth. The different clusters illustrated depend on the number of clusters to be created (defined by the user) (Agência Nacional de Águas, 2020b).

Table 13. Basic parameters of adjacent sub-basins and absolute and relative contributions.

River	Área (km²)	Inflow (m³/s)	Load (kg/day)			Load (%)		
		Rainy	BOD	TN	TP	BOD	TN	TP
Paranapanema	10074	161.86	19787	8482	654	51%	53%	40%
Taquari	4536	62.01	9573	4275	415	25%	27%	25%
Santo Inácio	1411	19.42	2308	1015	66	6%	6%	4%
Rib. da Jacutinga	543	1.75	812	345	21	2%	2%	1%
Rib. Bonito	495	3.42	1134	380	29	3%	2%	2%
Rib. das Posses	405	3.33	3666	867	293	9%	5%	18%
Sao José dos Pinhais	304	1.60	913	261	20	2%	2%	1%
Rib. Macuco	163	1.32	460	144	11	1%	1%	1%
Aquaculture	-	-	-	293	123	0%	2%	8%
Total	17931		38653	16062	1632			

to do: (i) Comparison with Remote Sensing; (ii) Clustering with Statistical Parameters; (iii) 3D modeling

CONCLUSIONS

Reservoirs present different characteristics from distinct environmental systems (i.e rivers, coastal waters) and therefore should be characterized differently concerning regulation aspects. Many reservoirs with large, flooded areas may also be divided into various regions with similar behavior, but that stand out from the others.

The case study highligths that, even for different types of reservoirs, the application of the comprehensive classification scheme presented it is possible for a better understanding of the

true hydrodynamic nature of the reservoir . Of all the eleven water bodies considered at the beginning, eight could be classified as run-of-river reservoir, and thus follow the river characterization for water quality. The three remaining, defined as lentic systems at the first step, were analyzed and classified as dynamic systems with significant spatial variability, requiring a zonation for better management.

Even though it is possible to identify zones with different hydrodynamic characteristics in the reservoir, they vary over time. Therefore, these variables are not suitable for zoning the reservoir in this case study. The zoning based on basin data is a good starting point, as it indicates the main load contributions in the sub-basins that influence the reservoir. The zoning based on water quality substances (in this case, the TP) showed distinct zones that remained the same over time. They also coincide with the incident load zones. The zoning based purely on geomorphological data showed the same pattern concerning water quality, indicating its great influence on the processes occurring inside the reservoir. Following the classification scheme, it was possible to verify the critical water quality parameter and assess the main regions of interest, which could facilitate management decisions.

However, it should be noted that the definition of the zones does not take into account, for example, (i) socio-economic aspects, (ii) hydrodynamic changes caused by the structures, (iii) the effect of internal loads, and (iv) seasonality. For internal structures (e.g., aquaculture, fish farming, floating photovoltaic systems), this classification scheme might not be enough. In this case study, the fish farming was small compared to the watershed load, and therefore had no significant effect on the water quality of the reservoir. Although this scheme could be an application to assist in a first decision on where to locate such structures, more elaborate studies should be conducted to assess the local effects and their impacts on the reservoir.

ACKNOWLEDGEMENTS

This study was financed in part by the Coordenação de Aperfeiçoamento de Pessoal de Nível Superior – Brasil (CAPES) – Finance Code 001. To the multidisciplinary team that formed part of the project for the Elaboration of a Study for the Implementation and Application of Hydrodynamic and Quality Models of Surface Waters in the Federal Domain as support for Decision Making in a Framework Proposal carried out by UFPR and the National Water Agency (ANA). Tobias Bleninger acknowledges the productivity stipend from the National Council for Scientific and Technological Development – CNPq, grant no. 313491/2023-2, call no. 09/2023. Cristovão Fernandes acknowledges the productivity stipend from the National Council for Scientific and Technological Development – CNPq, grant no. 311888/2023-9, call no. 09/2023.

REFERENCES

Agência Nacional de Águas – ANA. (2016). *Plano Integrado de Recursos Hídricos da Unidade de Gestão de Recursos Hídricos Paranapanema (PIRH)*. Brasília, DF: ANA.

Agência Nacional de Águas – ANA. (2019). *RT-SP2-01: modelagem de qualidade da água na UGRH Paranapanema*. Brasília, DF: ANA.

Agência Nacional de Águas – ANA. (2020a). *RT-SP2-02: cenarização dos usos pretensos dos recursos hídricos superficiais, da potencialidade, disponibilidade e demanda da água na UGRH PARANAPANEMA*. Brasília, DF: ANA.

Agência Nacional de Águas – ANA. (2020b). *RT-SP2-02: modelagem hidrodinâmica e de qualidade da água para as cenarizações nos horizontes de planejamento do prognóstico na UGRH Paranapanema*. Brasília, DF: ANA.

Agência Nacional de Águas – ANA. (2021). *RT-SP2-03: proposta de metas relativas às alternativas de enquadramento da calha dos rios de domínio da união e dos reservatórios na UGRH Paranapanema*. Brasília, DF: ANA.

Bernardo, J. W. Y. (2018). *Linking water quality to residence time and dimensionless numbers in a stratified, dendritic reservoir during intense inflow events* (Doctoral thesis). Universidade Federal do Paraná, Curitiba.

Boehrer, B., & Schultze, M. (2008). Stratification of lakes. *Reviews of Geophysics*, *46*(2), 2006RG000210. http://doi.org/10.1029/2006RG000210.

Brasil. Conselho Nacional de Meio Ambiente – CONAMA. (2005). Resolução CONAMA nº 357/2005. Dispõe sobre a classificação dos corpos de água e diretrizes ambientais para o seu enquadramento, bem como estabelece as condições e padrões de lançamento de efluentes, e dá outras providências. *Diário Oficial [da] República Federativa do Brasil*, Brasília. Retrieved in 2024, August 6, from https://www.icmbio.gov.br/cepsul/images/stories/legislacao/Resolucao/2005/res_conama_357_2005_classificacao_corpos_agua_rtfcda_altrd_res_393_2007_397_2008_410_2009_430_2011.pdf

Calmon, A. P. S., Souza, J. C., Reis, J. A. T., & Mendonça, A. S. F. (2016). Uso combinado de curvas de permanência de qualidade e modelagem da autodepuração como ferramenta para suporte ao processo de enquadramento de cursos d'água superficiais. *Revista Brasileira de Recursos Hídricos*, *21*(1), 118-133. http://doi.org/10.21168/rbrh.v21n1.p118-133.

Cardoso-Silva, S., Nishimura, P. Y., Padial, P. R., Mariani, C. F., Luiz, M., & Pompêo, M. (2014). Compartimentalização e qualidade da água: o caso da Represa Billings. *Bioikos*, *28*(1), 31-43.

Carvalho, J. M., & Bleninger, T. (2021). State-transition matrices as an analysis and forecasting tool applied to water quality in reservoirs. *Revista Brasileira de Recursos Hídricos*, *26*, e30. http://doi.org/10.1590/2318-0331.262120210072.

Chen, Q., Zhao, J., Gao, Q., Liu, H. X., & Han, X. M. (2021). Trophic state footprint index model and its application to Dianchi Lake, China. *Ecological Indicators*, *132*, 108317. http://doi.org/10.1016/j.ecolind.2021.108317.

Deeds, J., Amirbahman, A., Norton, S. A., & Bacon, L. C. (2020). A hydrogeomorphic and condition classification for Maine, USA,

lakes. *Lake and Reservoir Management*, *36*(2), 122-138. http://doi.org/10.1080/10402381.2020.1728597.

Deltares. (2014). *Delft3D 3D-FLOW user manual*. Retrieved in 2024, August 6, from https://content.oss.deltares.nl/delft3d4/Delft3D-FLOW_User_Manual.pdf

Fuchs, S., Kaiser, M., Kiemle, L., Kittlaus, S., Rothvoß, S., Toshovski, S., Wagner, A., Wander, R., Weber, T., & Ziegler, S. (2017). Modeling of Regionalized Emissions (MoRE) into water bodies: an open-source river basin management system. *Water*, *9*(4), 239. http://doi.org/10.3390/w9040239.

Gądek, B., Szumny, M., & Szypuła, B. (2019). Classification of the Tatra mountain lakes in terms of the duration of their ice cover (Poland and Slovakia). *Journal of Limnology*, *79*(1), 70-81. http://doi.org/10.4081/jlimnol.2019.1920.

Grupo Integrado de Aquicultura e Estudos Ambientais – GIA. (2013). *Estudos para a definição dos parques aquícolas nos reservatórios do paranapanema. Volume 2: parâmetros abióticos e modelagem*. Brasília, DF: Ministério da Pesca e Aquicultura.

Gunkel, G., Selge, F., Keitel, J., Lima, D., Calado, S., Sobral, M., Rodriguez, M., Matta, E., Hinkelmann, R., Casper, P., & Hupfer, M. (2018). Water management and aquatic ecosystem services of a tropical reservoir Itaparica, São Francisco, Brazil). *Regional Environmental Change*, *18*(7), 1913-1925. http://doi.org/10.1007/s10113-018-1324-8.

Hayes, N. M., Deemer, B. R., Corman, J. R., Razavi, N. R., & Strock, K. E. (2017). Key differences between lakes and reservoirs modify climate signals: a case for a new conceptual model. *Limnology and Oceanography Letters*, *2*(2), 47-62. http://doi.org/10.1002/lol2.10036.

Hipsey, M. R., Bruce, L. C., Boon, C., Busch, B., Carey, C. C., Hamilton, D. P., Hanson, P. C., Read, J. S., Sousa, E., Weber, M., & Winslow, L. A. (2019). A General Lake Model (GLM 3.0) for linking with high-frequency sensor data from the Global Lake Ecological Observatory Network (GLEON). *Geoscientific Model Development*, *12*(1), 473-523. http://doi.org/10.5194/gmd-12-473-2019.

Hoang, T. T., Van, A. D., & Nguyen, H. T. T. (2017). Driving variables for eutrophication in lakes of Hanoi by data-driven technique. *Water and Environment Journal : the Journal / the Chartered Institution of Water and Environmental Management*, *31*(2), 176-183. http://doi.org/10.1111/wej.12231.

Irz, P., Odion, M., Argillier, C., & Pont, D. (2006). Comparison between the fish communities of lakes, reservoirs and rivers: can natural systems help define the ecological potential of reservoirs? *Aquatic Sciences*, *68*(1), 109-116. http://doi.org/10.1007/s00027-005-0812-3.

Ji, Z. G. (2008). *Hydrodynamics and water quality modeling rivers, lakes, and estuaries*. Hoboken: John Wiley & Sons.

Kirillin, G., & Shatwell, T. (2016). Generalized scaling of seasonal thermal stratification in lakes. *Earth-Science Reviews*, *161*, 179-190. http://doi.org/10.1016/j.earscirev.2016.08.008.

Krogman, R. M., & Miranda, L. E. (2015). A classification system for large reservoirs of the contiguous United States. *Environmental Monitoring and Assessment*, *187*(4), 174. http://doi.org/10.1007/s10661-014-4244-1.

Li, Y., Jiao, J., Wang, Y., Yang, W., Meng, C., Li, B., Li, Y., & Wu, J. (2015). Characteristics of nitrogen loading and its influencing factors in several typical agricultural watersheds of subtropical China. *Environmental Science and Pollution Research International*, *22*(3), 1831-1840. http://doi.org/10.1007/s11356-014-3446-y.

Messager, M. L., Lehner, B., Grill, G., Nedeva, I., & Schmitt, O. (2016). Estimating the volume and age of water stored in global lakes using a geo-statistical approach. *Nature Communications*, *7*(1), 13603. http://doi.org/10.1038/ncomms13603.

Nauman, E. B. (2008). Residence time theory. *Industrial & Engineering Chemistry Research*, *47*(10), 3752-3766. http://doi.org/10.1021/ie071635a.

Nojavan, A. F., Kreakie, B. J., Hollister, J. W., & Qian, S. S. (2019). Rethinking the lake trophic state index. *PeerJ*, *7*(11), e7936. http://doi.org/10.7717/peerj.7936.

Oliveira, T. F., Brandão, I. L. S., Mannaerts, C. M., Hauser-Davis, R. A., Oliveira, A. A. F., Saraiva, A. C. F., Oliveira, M. A., & Ishihara, J. H. (2020). Using hydrodynamic and water quality variables to assess eutrophication in a tropical hydroelectric reservoir. *Journal of Environmental Management*, *256*, 109932. http://doi.org/10.1016/j.jenvman.2019.109932.

Ozoliņš, D., Skuja, A., Jēkabsone, J., Kokorite, I., Avotins, A., & Poikane, S. (2021). How to assess the ecological status of highly humic lakes? Development of a new method based on benthic invertebrates. *Water*, *13*(2), 223. http://doi.org/10.3390/w13020223.

Pan, B., Wang, H., & Wang, H. (2014). A floodplain-scale lake classification based on characteristics of macroinvertebrate assemblages and corresponding environmental properties. *Limnologica*, *49*, 10-17. http://doi.org/10.1016/j.limno.2014.07.003.

Pedrazzi, F. J. M., Conceição, F. T., Sardinha, D. de S., Moschini-Carlos, V., & Pompêo, M. (2013). Spatial and temporal quality of water in the Itupararanga Reservoir, Alto Sorocaba Basin (SP), Brazil. *Journal of Water Resource and Protection*, *5*(1), 64-71. http://doi.org/10.4236/jwarp.2013.51008.

Pessôa, Z. B., Fontes, A. S., & Medeiros, Y. D. P. (2015). Enquadramento de corpos d'água para fins de consumo humano em regiões semiáridas: avaliação conforme Resolução CONAMA 357/2005 e Portaria MS 2914/2011. *Revista Brasileira de Recursos Hídricos*, *3*(2), 495-506. http://doi.org/10.17565/gesta.v3i2.15103.

Petriki, O., Lazaridou, M., & Bobori, D. C. (2017). A fish-based index for the assessment of the ecological quality of temperate lakes. *Ecological Indicators*, *78*, 556-565. http://doi.org/10.1016/j.ecolind.2017.03.029.

Pompêo, M. L. M., Kawamura, P., Moschini-Carlos, V., Silva, S. C., Lobo, F. de L., & Meirinho, P. A., Bitencourt, M. D., & Meirelles, S. T. (2015). Heterogeneidade espacial horizontal da qualidade da água no reservatório Rio Grande, complexo billings, São Paulo, Brasil. In *Ecologia de Reservatórios e Interfaces* (pp. 82-95). São Paulo: Instituto de Biociências, Universidade de São Paulo. Retrieved in 2024, August 6, from https://www.researchgate.net/publication/273754918

Rueda, F., Moreno-Ostos, E., & Armengol, J. (2006). The residence time of river water in reservoirs. *Ecological Modelling*, *191*(2), 260-274. http://doi.org/10.1016/j.ecolmodel.2005.04.030.

Santos, A. B. I., Terra, B. F., & Araújo, F. G. (2010). Influence of the river flow on the structure of fish assemblage along the longitudinal gradient from river to reservoir. *Zoologia*, *27*(5), 732-740. http://doi.org/10.1590/S1984-46702010000500010.

Shivers, S. D., Golladay, S. W., Waters, M. N., Wilde, S. B., & Covich, A. P. (2018). Rivers to reservoirs: hydrological drivers control reservoir function by affecting the abundance of submerged and floating macrophytes. *Hydrobiologia*, *815*(1), 21-35. http://doi.org/10.1007/s10750-018-3532-0.

Smaoune, G., Bouchelouche, D., Taleb, A., & Arab, A. (2021). Evaluation of the trophic status in three reservoirs in Algeria (north west) using physicochemical analysis and rotifers structure. *Environmental Science and Pollution Research International*, *28*(34), 46627-46642. http://doi.org/10.1007/s11356-020-11233-w.

Smits, J., Boderie, P., & Van Beek, J. (2009). *Modeling of the Nam Theun 2 Reservoir: water quality and greenhouse gases emissions*. The Netherlands: Deltares.

Soulignac, F., Vinçon-Leite, B., Lemaire, B. J., Scarati Martins, J. R., Bonhomme, C., Dubois, P., Mezemate, Y., Tchiguirinskaia, I., Schertzer, D., & Tassin, B. (2017). Performance assessment of a 3D hydrodynamic model using high temporal resolution measurements in a shallow urban lake. *Environmental Modeling and Assessment*, *22*(4), 309-322. http://doi.org/10.1007/s10666-017-9548-4.

Sutela, T., Vehanen, T., & Rask, M. (2016). A littoral fish index that responds to eutrophication in boreal lakes. *Fisheries Research*, *173*, 88-92. http://doi.org/10.1016/j.fishres.2015.06.006.

Tison-Rosebery, J., Boutry, S., Bertrin, V., Leboucher, T., & Morin, S. (2023). A new diatom-based multimetric index to assess lake ecological status. *Environmental Monitoring and Assessment*, *195*(10), 1202. http://doi.org/10.1007/s10661-023-11855-w.

Wahl, B., & Peeters, F. (2014). Effect of climatic changes on stratification and deep-water renewal in Lake Constance assessed by sensitivity studies with a 3D hydrodynamic model. *Limnology and Oceanography*, *59*(3), 1035-1052. http://doi.org/10.4319/lo.2014.59.3.1035.

Authors contributions

Camila Bergmann Goulart: Development of the entire study, hydrodynamic and water quality modeling with Delft3D.

João Marcos Carvalho: 1D modeling, stratification analysis, and zoning based on clustering. He assisted in writing.

Julio Werner Yoshioka Bernardo: Worked on water quality modeling and load allocation methodology.

Bruna Arcie Polli: Hydrodynamic modeling.

Cristóvão Fernandes: Worked on coordinating the project, and defining the study guidelines. He assisted in writing.

Stephan Fuchs: Load modeling (MoRE), zonation analysis.

Tobias Bleninger: Worked on coordinating the project, and defining the study guidelines. He assisted in writing.

Editor-in-Chief: Adilson Pinheiro

Associated Editor: Iran Eduardo Lima Neto

APPENDIX B. HYDROLOGICA AND ECOLOGICAL EFFECTS OF FLOATING PHOTOVOLTAIC SYSTEMS: A MODEL COMPARISON CONSIDERING MUSSEL, PERIPHYTON AND MACRPPHYTE GROWTH

Knowl. Manag. Aquat. Ecosyst. 2025, 426, 11
© K. Ilgen *et al.*, Published by EDP Sciences 2025
https://doi.org/10.1051/kmae/2025008

www.kmae-journal.org

Knowledge & Management of Aquatic Ecosystems

Journal fully supported by Office français de la biodiversité

RESEARCH PAPER OPEN ACCESS

Hydrological and ecological effects of floating photovoltaic systems: a model comparison considering mussel, periphyton, and macrophyte growth

Konstantin Ilgen[1,2,*], Camila Bergmann Goulart[3,4], Stephan Hilgert[5], Dirk Schindler[6], Klaus van de Weyer[7], Rafael de Carvalho Bueno[8], Tobias Bleninger[3], Raffaello Lastrico[1,2], Leonhard Gfüllner[1], Alexander Graef[1], Stephan Fuchs[4] and Jens Lange[2]

[1] Fraunhofer Institute for Solar Energy Systems ISE, Freiburg, Baden-Württemberg, Germany
[2] Hydrology, Faculty of Environment and Natural Resources, University of Freiburg, Freiburg, Baden-Württemberg, Germany
[3] Post-Graduate Programme on Water Resources and Environmental Engineering, Federal University of Paraná, Curitiba, Paraná, Brazil
[4] Water Quality Management, Institute for Water and Environment, Karlsruhe Institute of Technology, Karlsruhe, Baden-Württemberg, Germany
[5] limknow GmbH & Co. KG, Karlsruhe, Germany
[6] Environmental Meteorology, Faculty of Environment and Natural Resources, University of Freiburg, Freiburg, Baden-Württemberg, Germany
[7] Lanaplan GbR, Nettetal, Germany
[8] Post-Graduate Programme on Environmental Engineering, Federal University of Paraná, Curitiba, Paraná, Brazil

Received: 14 October 2024 / Accepted: 10 April 2025

Abstract – Floating photovoltaic (FPV) systems are increasingly deployed on gravel pit lakes to generate renewable energy and mitigate land-use conflicts. However, their environmental impacts on hydrological and ecological processes remain insufficiently studied. This study investigates the effects of a 1.5-MWp FPV system covering 8% of a 19-ha gravel pit lake in Germany. The General Lake Model (GLM-AED2) and Delft3D-FLOW were used to simulate FPV-induced changes. Meteorological data—including irradiance, air temperature, wind speed, and relative humidity—were recorded above and below the PV modules. Water quality data—including water temperature, dissolved oxygen, pH, dissolved organic carbon, and chlorophyll-*a*—were collected beneath the FPV and in open water. Mussel colonisation of the FPV substructure was assessed, and its filtration impact on water quality analysed. Macrophyte distribution was assessed beneath the FPV system and along the shorelines. Results showed a modelled 88% solar irradiance and 57% wind speed reduction beneath the FPV system. Water quality impacts were minimal and primarily influenced by mussels colonising the substructure. Macrophytes occurred in littoral zones up to 5.25 m deep up to 5.25 m deep, but habitat-typical species were scarce due to gravel extraction and herbivorous fish. These findings highlight complex interactions between FPV, mussel filtration, macrophytes, and human activities, suggesting that other anthropogenic factors may outweigh FPV impacts. Model simulations indicated that FPV coverage above 45% could destabilise thermal stratification and alter primary production. This study underscores the need for empirical monitoring and modelling to optimise FPV deployment and inform regulatory frameworks for sustainable development.

Keywords: Floating solar / environmental impact / hydrodynamic modelling / quagga mussel / macrophyte abundance

1 Introduction

Floating photovoltaic (FPV) is an innovative technology that generates renewable electricity and reduces greenhouse gas emissions. Unlike ground-mounted and rooftop photovoltaic (PV) systems, FPV extends solar deployment across inland and offshore waters, reducing land-use conflicts. As such, FPV offers an additional opportunity to address global challenges such as climate change, increasing energy demand, and land scarcity (World Bank Group *et al.*, 2019a; Xia *et al.*, 2023; Nobre *et al.*, 2024). Furthermore, synergies can be expected from coupling with other forms of energy generation, such as hydropower or wind (Lee *et al.*, 2020; Kakoulaki *et al.*, 2023; Ogunjo *et al.*, 2023). The expansion of FPV has been dynamic

*Corresponding author: konstantin.ilgen@ise.fraunhofer.de

in recent years, with significant growth in Asia and Europe, where many projects are either operational or in the planning stage (World Bank Group *et al.*, 2019b). Although most FPV installations in Europe are constructed on artificial waterbodies such as gravel pit lakes and reservoirs, their environmental impacts remain insufficiently studied (Nobre *et al.*, 2024). In Germany, current legislation limits FPV coverage to 15% of the water surface and mandates a minimum distance of 40m from the shore (Bundesamt für Justiz, 2023). However, these limits do not have an empirical basis, underscoring the need for further research on ecological consequences. A comprehensive review of FPV's potential environmental impacts on aquatic ecosystems identified key influencing factors such as system design, site-specific conditions, and meta-ecosystem dynamics (Nobre *et al.*, 2023).

Previous studies have investigated FPV impacts on lake processes using various hydrodynamic models. Ji *et al.* (2022) employed the CE-QUAL-W2 model to simulate FPV effects on the Xiangjiaba Reservoir in China. They reported water temperature reductions and changes in thermal stratification, with effects extending beyond the FPV-covered area, influencing approximately 20% of the reservoir's total length. A maximum reduction in surface water temperature below FPV of up to 3.3 °C was simulated, and the reservoir was predicted to benefit from reduced evaporation of up to 35 million m^3. Exley *et al.* (2021) studied the effects of an FPV system on Windermere, England, using the MyLake model and suggested that a larger FPV coverage was positively correlated with a stronger reduction in water temperature. Their study found that FPV reduced water temperature by up to 8.0 °C and significantly affected stratification stability. Similarly, Ilgen *et al.* (2023) observed a 2.8 °C cooling effect in a German gravel pit lake with a 750 kWp FPV system due to a 73% reduction in solar irradiance. On-site measurements were used to calibrate the General Lake Model (GLM), with simulations indicating that FPV coverages below 15% had minimal influence on stratification, whereas notable changes occurred above 50%. These studies revealed two opposing FPV effects on lake stratification: reduced irradiance lowers energy input and weakens stratification, whereas reduced wind shear limits vertical mixing and stabilises stratification. This interplay highlights the complexity of physical processes in FPV-covered lakes. Empirical validation of these mechanisms is essential to enhance hydrodynamic model accuracy. Moreover, previous research suggests that FPV may mitigate certain climate change effects on lake ecosystems.

Other modelling studies examined FPV influences on chemical and biological lake processes. Yang *et al.* (2022) coupled the Estuary, Lake, and Coastal Ocean Model (ELCOM) with the Computational Aquatic Ecosystem Dynamics Model (CAEDYM) to simulate FPV impacts on a shallow tropical reservoir in Singapore. Their results indicated increased thermal stability at 30% FPV coverage, alongside reductions in chlorophyll-*a*, total organic carbon, and dissolved oxygen by 30%, 15%, and 50%, respectively, while total nitrogen and phosphorus concentrations increased. Haas *et al.* (2020) applied the ELCOM-CAEDYM model to a hydropower reservoir in Chile, finding that FPV occupancies between 40% and 60% could help to prevent algal blooms while maintaining hydropower efficiency. Exley *et al.* (2022) used the MyLake model to assess phytoplankton dynamics in a reservoir in England, demonstrating that a 10% FPV coverage reduced chlorophyll-*a* concentrations by 17% to 48%, depending on seasonal variability. Karpouzoglou *et al.* (2020) simulated FPV impacts on primary production in a brackish water system in the Netherlands using the General Ocean Turbulence Model (GOTM) coupled with the European Regional Seas Ecosystem Model (ERSEM-BFM). They found that FPV occupancies below 20% had negligible effects, but above this threshold, net primary production declined significantly. Château *et al.* (2019) used the Simulation Modelling System for Aquatic Bodies (SIMSAB) to predict FPV effects on fishponds in Taiwan. While FPV slightly reduced fish production due to lower dissolved oxygen, it provided substantial energy gains, suggesting an overall benefit of FPV integration into aquaculture systems.

The introduction of FPV structures into water bodies creates new colonisation opportunities for sessile organisms, including native species and invasive mussels such as the quagga *(Dreissena rostriformis bugensis)* and zebra mussels (*Dreissena polymorpha*). The quagga mussel, originally from Eastern Europe, was first observed in Western Europe in 2006 and has since s rapidly spread through major rivers such as the Rhine and Danube at an average rate of 120 km per year (Orlova *et al.*, 2004; Son, 2007; Matthews *et al.*, 2014). By filtering water, mussels remove plankton, nutrients, and suspended matter, potentially altering aquatic ecosystems (Rowe *et al.*, 2017). Their colonisation of technical infrastructure can cause economic damage to waterworks and fisheries (Connelly *et al.*, 2007). Quagga mussels form a mutually beneficial relationship with Nuttall's waterweed (*Elodea nuttallii*), as filtration improves light penetration, enhancing plant growth, while dense macrophyte stands provide habitat for mussels (Wegner *et al.*, 2019). This accelerates their spread and intensifies competition with native species, posing a significant threat to freshwater ecosystems. Under a colonised FPV system, two opposing processes occur: the reduction of solar irradiance, due to shading, is confined to the FPV area, while filtering mussels increase water clarity beneath the installation which may extend across the entire lake, including shoreline habitats, and thus influence the depth of the euphotic zone. As both mussel filtration and FPV-induced changes in light availability affect underwater vegetation dynamics, their combined impact on macrophyte growth and competition remains largely unexplored. While modelling may provide valuable insights into FPV effects, empirical validation is essential to improve predictive accuracy. Field data are required to refine model outputs and assess broader ecological implications, including shifts in trophic interactions.

This study aims to (1) empirically assess the dominant factors influencing water quality in FPV lakes by comparing FPV-induced changes with external drivers such as inflows and excavation activities, (2) evaluate the capability of two hydrodynamic models (Delft3D-FLOW and GLM–AED2) to simulate FPV-induced changes by validating model outputs with *in situ* data and predicting long-term effects under higher FPV coverage scenarios (15%, 30%, 45%, and 90%), (3) investigate the relationship between empirically estimated mussel filtration due to colonisation on FPV structures and modelled macrophyte growth responses resulting from increased water clarity, and (4) assess the suitability of current FPV regulations by integrating empirical field data and

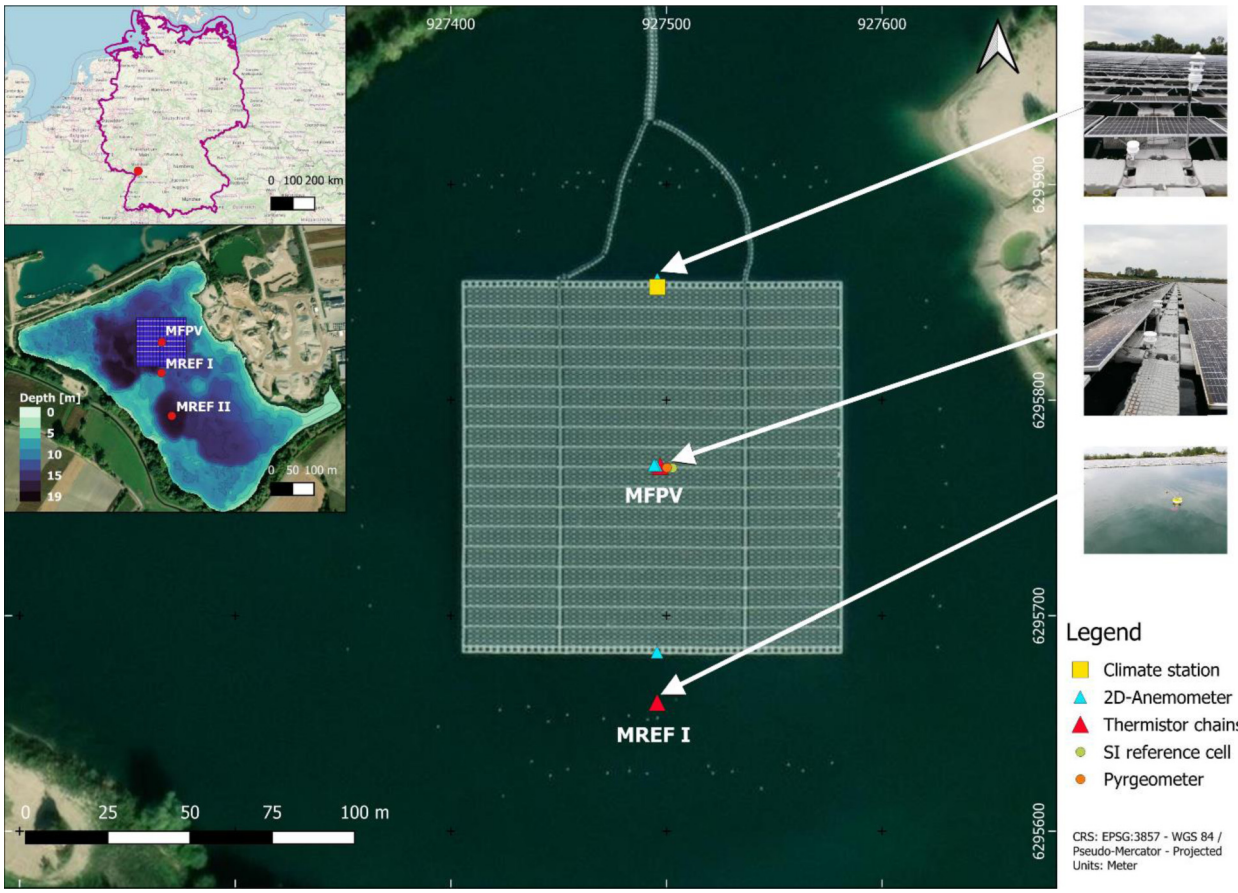

Fig. 1. The monitored floating photovoltaics (FPV) system. The two insets show the location of the studied gravel pit lake in Germany and the measurement points (MFPV, MREFI, MREFII) in the lake. The yellow square indicates the position of the meteorological measuring system.

hydrodynamic modelling to propose ecologically informed regulatory measures. These findings will contribute to a science-based framework for sustainable FPV deployment in aquatic ecosystems.

2 Materials and methods

2.1 Study site

The gravel pit lake near Leimersheim (Lake Leimersheim; latitude 49.123, longitude 8.332) is located in southwest Germany in the Upper Rhine Valley. The mean lake depth is 9.3 m, maximum depth is 19 m, the total lake area is 19 ha, and its water volume is 1.7×10^6 m^3. The lake has no river in- or outflows, and its water level is almost constant, balanced by groundwater inflow. Lake Leimersheim is one of more than 700 gravel pit lakes in the Upper Rhine Valley. Given its depth and hydrological characteristics, Lake Leimersheim is expected to exhibit seasonal thermal stratification, with a thermocline forming at intermediate depths during the summer months. The absence of natural surface inflows or outflows suggests that vertical mixing primarily depends on atmospheric forcing, with full overturn occurring during the colder months. Lake Leimersheim may be characterised as oligotrophic, with low nutrient concentrations and high oxygen availability. Anthropogenic influences, particularly from gravel processing activities, locally affect water clarity and chemical parameters.

The studied FPV system is located in the northern part of the lake (Fig. 1). The first part of the system, with a capacity of 750 kWp, was commissioned in autumn 2020, and the second part, with an additional 750 kWp, in autumn 2021. Both parts have a length and width of 115 m each and consist of 3,744 PV panels arranged over 8% of the lake's total surface area. The total annual electric yield is 1.7 GWh, which is either transferred directly to the adjacent gravel plant or fed into the public grid. The gravel plant can cover 20–30% of its electricity consumption with the electricity from the FPV system. During the study period from 1 January 2023 to 31 July 2024, no excavation took place. The gravel works occasionally resulted in the discharge of sediment-rich process water into the lake.

2.2 Measurement methods

2.2.1 Meteorological data collection

A climate station (WS510-UMB, Lufft) was located at the northern edge of the FPV system to measure global horizontal irradiance (W m^{-2}), wind speed (m s^{-1}), and direction (°), relative humidity (%), atmospheric pressure (hPa), and air temperature (°C) (Fig. 1). Long-wave radiation measurements

Fig. 2. Photograph of the mussel population of a fully submerged floater, taken from the below by the remotely operated underwater vehicle.

were carried out in the centre of the FPV system using a pyrgeometer (SGR3, Kipp & Zonen).

In addition, 2D ultrasonic anemometers (WS200-UMB, Lufft) measured wind speed near the surface. Anemometers at the southern and northern edges of the system were placed at the height of the upper edge of the solar panels, while two anemometers in the centre of the system were installed at different heights. One was mounted 40 cm above the water surface, the other 20 cm above the water surface, with the top edge of the solar panel positioned between the two sensors at 30 cm above the water. The accuracy of the wind direction measurement was ±3°, for wind speed it was ±3% in the range 0–35 m s^{-1}.

By comparing the wind speed at different heights, it was possible to quantify the reduction in wind speed caused by the FPV system. Solar irradiance reduction by FPV was calculated using the Radiance ray-tracing model (Ward, 1994). All sensors were connected using a daisy-chain distributed Modbus architecture, ensuring synchronised and continuous data collection.

2.2.2 Hydrodynamic and temperature monitoring

Water temperature profiles were monitored using thermistor chains (accuracy: ±0.1 °C) to assess thermal stratification and temperature variations beneath the FPV system and in open water. A 10m thermistor chain was deployed beneath the FPV system at its centre (MFPV, Measurement Point Floating PV) to measure water temperature at 50 cm intervals along the vertical profile. An identical chain was installed at a second measurement point located in the open water south of the system (MREF I, Measurement Point Reference I), serving as a reference for comparison (Fig. 1). To obtain a detailed representation of the lake bathymetry, echo sounders were used to record depth profiles, which were then used to generate a depth raster and a hypsographic curve.

2.2.3 Water quality measurements

Water quality was measured using an EXO2 multiparameter probe (YSI Inc. / Xylem Inc.) at MFPV, MREF I and MREF II (Fig. 1). Measurements at MREF I and MREF II were averaged (MREF) and used for comparison with data collected beneath the FPV system at MFPV. During 17 measurement campaigns carried out from 9 May 2023 to 9 July 2024, profile measurements of water temperature, dissolved oxygen, oxygen saturation, specific conductivity, pH, redox potential, nitrate, turbidity, phycocyanin, chlorophyll-*a*, and dissolved organic carbon were conducted at 1m depth intervals down to the lake bottom. Measurements concentrated on the vegetation period and on transition periods of lake mixing regimes. In winter, measurements were taken at larger time intervals during isothermal conditions caused by lake turnover. There was no period with ice coverage.

To further investigate the influence of mussel respiration on oxygen concentrations, two water temperature and dissolved oxygen loggers (miniDOT, PME) were placed at MFPV and MREF I. Both loggers were deployed at a depth of 1 m, recording measurements every 15 minutes with an accuracy of ±0.3 mg l^{-1}. The first measurements were recorded on 5 September 2023, the last on January 9, 2024.

2.2.4 Periphyton and mussel sampling

Mussel colonisation on FPV floaters was also assessed. One floater beneath the FPV panels was removed, and all periphyton was scraped off using hard plastic spatulas. To allow for an estimation of the full population of the FPV system, a remotely operated underwater vehicle (Deep Trekker, DTG3) took pictures of other floaters from below, to ensure that the mussel coverage was comparable between floaters (Fig. 2).

The obtained mussels and periphyton material were sealed and transported to the laboratory, where they were stored in the fridge at −18 °C until further investigation. In the next step, all mussels were counted and the species determined. Each individual was grouped into size classes between <5 mm, 5–10 mm, 11–15 mm, 16–20 mm, and 21–25 mm. Considering the size class distribution of the mussels, 100 mussels of each species were selected, and the shell was

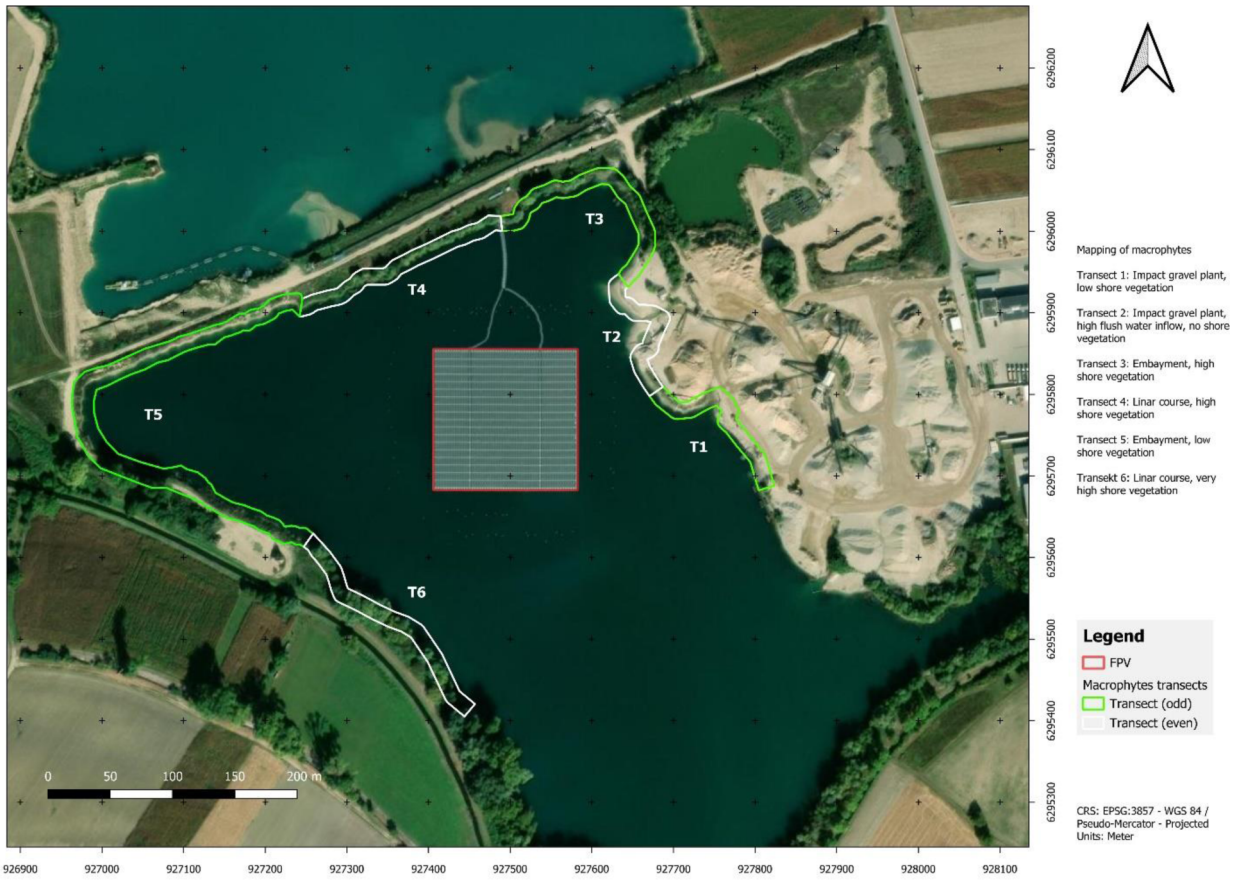

Fig. 3. Boundaries of the macrophyte transects (T1–T6) along the gravel pit lake shoreline. The floating photovoltaic (FPV) system is highlighted with a red rectangle. Coordinates are given in metres.

separated from the body. Fresh and dry weight was measured before and after drying at 105 °C. The dry material was then ground and analysed for phosphorus content.

To evaluate the overall mussel filtration performance, an effective clearance rate of 41.95 ml ind^{-1} h^{-1} was derived from literature values (Yu and Culver, 2001), with a range between 15.3 mL ind^{-1} h^{-1} and 68.6 mL ind^{-1} h^{-1}. Diggins (2001) reported 309 mL ind^{-1} h^{-1} for quagga mussels and 226 mL ind^{-1} h^{-1} for zebra mussels. Consequently, the derived estimate represents a conservative assumption for a mixed mussel population. This estimate enabled a comparison of the total filtered water volume relative to the overall lake volume.

2.2.5 Macrophyte sampling

To assess the suitability of current FPV regulations and to propose ecologically informed regulatory measures, macrophyte sampling was conducted. In Germany, the construction of FPV installations is regulated by the Water Resources Act (WHG), a national legal framework for water protection and management. This law mandates a 40 m distance from the shoreline for FPV systems, to protect littoral zones, where macrophyte communities are typically found.

The size of the littoral zone can vary significantly within a lake and may also depend on the lake type. While the WHG serves as a national German law, the European Water Framework Directive (WFD) provides an overarching framework for ecological water quality. The WFD establishes standardised ecological quality criteria and specific assessment methods for aquatic ecosystems, including macrophytes, to ensure a harmonised evaluation across Europe. Accordingly, the macrophyte investigation in this study was carried out in July 2024, following the WFD assessment guidelines for macrophytes in lakes (van de Weyer and Stelzer, 2021). For this purpose, the shoreline area around the FPV system was divided into six transects (Fig. 3).

The transects were of similar length but differed in shoreline characteristics. Transects 1 (T1) and 2 (T2) were located near the gravel plant, with T2 receiving water from the gravel washing process. T3 extended along a bay and had dense riparian vegetation, while T4 was linear, with a south-eastern exposure. T3 and T4 were separated by the FPV system's floating power cable. T5 had recently been excavated, resulting in sparse vegetation. T6 was linear, similar to T4, and exposed to the north-east. It had the densest riparian vegetation, including overhanging trees. Macrophyte sampling was conducted at depths of 0.0–1.0 m, 1.1–2.0 m, 2.1–4.0 m, and >4.0 m by a team of two divers and a protocol writer.

In addition to transect sampling, a cross-sectional control dive beneath the FPV system identified potential macrophyte communities. A field protocol recorded shoreline conditions and species abundance classified on a scale from 1 (very rare)

to 5 (abundant). The lower macrophyte limit (LML) was determined and compared with multibeam echosounder data. The LML describes the maximum depth at which submerged macrophytes can grow under specific light conditions, serving as an ecological indicator of water transparency and habitat suitability.

A Helix 7 SI GPS G4 sonar (Humminbird, USA) was used to map macrophyte distribution. The lake was evaluated based on WFD metrics, including structure, number of habitat-typical species, and LML. Lake type classification considered stratification, calcium content, altitude, and catchment size. Ecological status was assessed based on habitat-typical vegetation cover (%), species richness, and LML. This was evaluated using WFD reference tables (van de Weyer and Stelzer, 2021), providing an overall rating of the lake's ecological condition.

2.3 Statistical analysis

For measurements obtained with the EXO2 multiparameter probe, mean values were calculated at corresponding depths for MFPV and MREF, and deviations at MFPV were assessed relative to MREF. *t*-tests were conducted for all parameters, and the observed deviations were compared with measurement uncertainties provided by the manufacturer. To represent FPV in hydrodynamic models, mean values with standard deviations and statistical significance were calculated for reductions in wind and solar irradiance, as well as for light extinction. For the mussel distribution, a χ^2 test was applied to assess the statistical significance of the differences in species composition across size classes.

2.4 Hydrodynamic and ecological modelling

2.4.1 Model Configuration

The General Lake Model (GLM–AED2, V3.0.0) was used to model FPV-induced changes and predict long-term effects under high FPV coverage. GLM uses a Lagrangian grid and energy balance approach for surface mixing (Hipsey *et al.*, 2019), while AED2 simulates aquatic ecodynamics, including nutrient cycling and geochemistry (Hipsey, 2022).

For comparison, Delft3D-FLOW was used as an alternative model for unsteady, 3D flows simulations, incorporating meteorological forcing, and density variations (Deltares, 2024). Both models used the same meteorological input — initially from NASA's POWER project (1 January 2023 – 12 August 2023; NASA, 2023) and thereafter from a climate station on the FPV system. Variables included shortwave and longwave radiation, air temperature, wind speed/direction (direction only for Delft3D-FLOW), relative humidity, rain, and snow. As no precipitation data were collected on-site, values were taken from a nearby German Meteorological Service station (ID: 05906). Reductions in solar irradiance and wind, simulated via a ray-tracing model, along with wind measurements, were integrated into both models.

For lake bathymetry, Delft3D-FLOW utilised a depth raster from echo sounder data, while GLM-AED2 applied a hypsographic curve. Given the same initial conditions (water temperature and water level), both models were calibrated using depth profile measurements from reference points (MREF I, MREF II), with GLM-AED2 employing the CMA-ES method (Varelas *et al.*, 2018). Calibration and validation periods were split by a ratio of 2:1, and the total modelling period was from 1 January 2023 to 30 June 2024. Model performance was evaluated using Root Mean Square Error (RMSE), Nash–Sutcliffe model efficiency coefficient (NSE) and Kling–Gupta efficiency (KGE).

2.4.2 FPV coverage scenarios

Simulations were conducted for FPV coverage scenarios of 8% —correspond to the existing FPV system—as well as 15%, 30%, 45%, and 90%. In Germany, the legal maximum FPV coverage is 15%, while 90% represents the technical limit of FPV installations (Wirth *et al.*, 2021). Globally, FPV installations typically cover between 10% and 45% of a water surface, with higher coverage being less common due to environmental and technical constraints (Xia *et al.*, 2023; Nobre *et al.*, 2024). The selected coverage scenarios therefore reflect both current regulatory limits and potential future expansion.

Model simulations were evaluated by comparing key hydrodynamic metrics, including lake surface water temperature, Schmidt stability, and thermocline depth. Schmidt stability represents the energy required to mix the entire water column to a uniform temperature (Schmidt, 1928; Idso, 1973). If Schmidt stability is positive, stratification and thermocline formation can be assumed. Thermocline depth was calculated as the depth at which the maximum density gradient occurs, provided water temperature exceeded 4.0 °C and density difference between surface and bottom layers was greater than 0.1 kg m^{-3} (Ladwig et al., 2021).

Both Schmidt stability and thermocline depth were computed using the rLakeAnalyzer package (Winslow *et al.*, 2018). Additionally, the trophic state index (TSI; Carlson, 1977) was simulated using GLM-AED2 to assess potential shifts in lake productivity under different FPV scenarios:

$$TSI(Chl) = 10\left(6 - \frac{2.04 - 0.68\,ln(Chl)}{\ln 2}\right) \quad (1)$$

where Chl is the chlorophyll-*a* concentration (μg l^{-1}) at the water surface. TSI values range from 0 to 100, with each major interval (10, 20, 30, *etc.*) representing a doubling in algal biomass.

2.4.3 Macrophyte distribution and FPV coverage optimisation

By comparing current LML with theoretical LML under the Trophic Reference State (TRS), GLM-AED2 provided a spatial assessment of macrophyte expansion potential and its implications for FPV siting. TRS represents the ecological baseline of the lake in an undisturbed state, where macrophytes could extend deeper due to improved water quality and reduced anthropogenic pressure. Macrophyte growth was considered light-limited, with a threshold set at 1% of surface irradiance (Schwoerbel and Brendelberger, 2013; Liu *et al.*, 2016). The model also accounted for mussel filtration effects on water clarity, as colonies attached to the FPV substructure

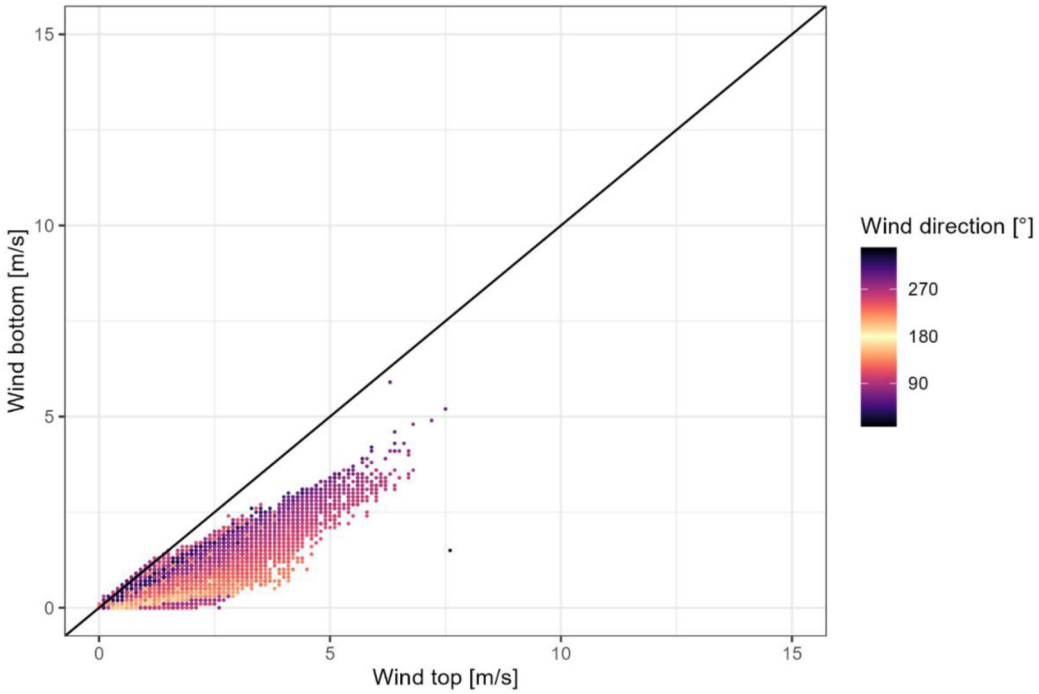

Fig. 4. Comparison of wind speed measured above (*Wind top*) and below (*Wind bottom*) the PV modules, depending on the wind direction.

improve light penetration, potentially expanding macrophyte habitats and influencing FPV placement constraints. First, the macrophyte-free zone under TRS conditions was determined. Then, FPV coverage scenarios were simulated for 8%, 15%, 30%, 45% and extended to cover the entire macrophyte-free zone. To assess the maximum FPV coverage in a restored ecosystem, the model simulated scenarios with and without mussel filtration, quantifying LML shifts and the corresponding reduction in the macrophyte-free zone. Mussel filtration effects were incorporated into the GLM-AED2 simulation by adjusting the light extinction coefficient (k_w), which can be calculated using measurements of light intensity or turbidity at different depths:

$$k_w = \frac{1}{z}\ln\left(\frac{I_0}{I_z}\right) \tag{2}$$

where I_0 is the light intensity at reference depth directly below the water surface, and I_z is the light intensity at distance z below reference depth (Schwoerbel and Brendelberger, 2013). Assuming proportionality of light intensity and turbidity, k_w was determined by:

$$k_w = \left(\frac{ln}{z}\right) \times \left(\frac{Turb}{z}\right) \tag{3}$$

where *ln* is the natural logarithm and Turb is turbidity in Nephelometric Turbidity Units (NTU). This analysis is particularly relevant for FPV deployment beyond the excavation phase, as it highlights the importance of integrating ecological restoration objectives into site selection and long-term lake management.

3 Results

3.1 Meteorological forcing and FPV-induced wind and irradiance reduction

Continuous wind measurements conducted at the FPV system revealed a substantial wind reduction of 57% (±22.6%) beneath the FPV system ($p < 2.2 \times 10^{-16}$). This reduction increased with rising wind speeds, indicating a stronger reduction at higher wind velocities. Southern winds, which directly impinged upon the southward-oriented foundations of the array, resulted in a more substantial wind reduction compared to northern winds (Fig. 4).

Radiance simulations indicated an 88% (±10.3%) reduction in solar irradiance reaching the water body beneath the system ($p < 2.2 \times 10^{-16}$). While some areas—particularly along cable routes and at the array's edges—experienced minimal or no shading, a high degree of shading was observed under the modules and the substructure. This reduction in light availability was accompanied by a 36% (±31.1%) decrease in k_w, as derived from turbidity measurements ($p = 0.0062$). These measured reductions, along with wind reduction, were used to represent the FPV system in the models through coverage-based adjustments of model parameters (Tab. 1).

3.2 Water quality effects under FPV coverage

There was no significant difference in water temperature between MFPV and MREF ($p = 0.856$; Fig. 5). In contrast, a significant decrease in both dissolved oxygen concentrations (ΔDO, $p = 0.011$) and oxygen saturation (ΔDO Sat, $p = 0.01$) was observed beneath the FPV system. Nitrate concentrations

Table 1. Parameters adjusted to represent FPV in GLM-AED2 and Delft3D-FLOW.

Parameter	Without FPV	With FPV	Deviation (%)
Scaling factor for shortwave radiation (*sw_factor*)	1.0	0.12	88
Scaling factor for wind speed (*wind_factor*)	1.0	0.43	57
Light extinction coefficient (k_w)	0.383	0.244	36

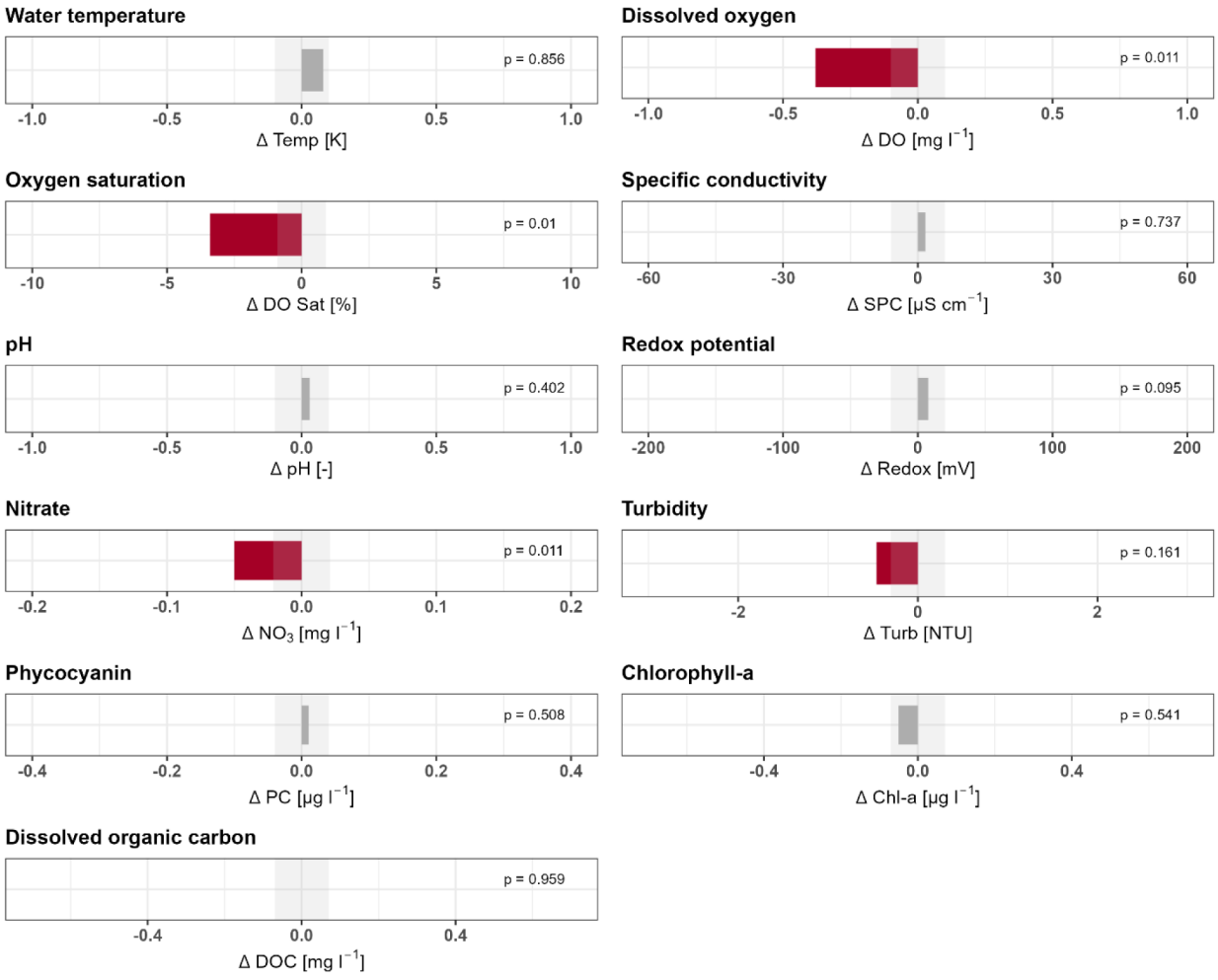

Fig. 5. Deviations of measured parameters between MFPV and MREF. MREF is defined as the mean of MREFI and MREFII. The grey shaded area represents measurement uncertainty; if a deviation falls within this range, the corresponding bar is coloured dark grey. Red bars indicate deviations that exceed the measurement uncertainty. Statistical significance is determined using *p*-values, which are displayed in the upper right corner of each plot, with $p < 0.05$ indicating statistical significance.

also exhibited a significant reduction (ΔNO_3, $p = 0.011$). Turbidity showed a decreasing trend ($p = 0.161$), with deviations exceeding the measurement uncertainty, indicating a measurable effect of the FPV system on water clarity. Other parameters—including specific conductivity ($p = 0.737$), pH ($p = 0.402$), redox potential ($p = 0.095$), phycocyanin ($p = 0.508$), chlorophyll-*a* ($p = 0.541$), and dissolved organic carbon ($p = 0.959$)—showed no significant differences between MFPV and MREF, with deviations falling within the range of measurement uncertainty. The relatively low concentrations of chlorophyll-*a* (1.08 µg l^{-1} at MREF) and nitrate (0.21 mg l^{-1} at MREF), along with the calcareous sediment signature inferred from the specific conductivity (594 µS cm^{-1}) and pH (8.14) values, are characteristic of an oligotrophic trophic state, which aligns with the expected water quality of the gravel pit lake.

3.3 Mussel colonisation and filtration impact

3.3.1 Mussel colonisation and population density

Mussel density on the hard substrate with permanent water coverage was so high that periphyton assessment was impossible. The coverage was completely dominated by the mussels. On half a floater, 1,771 individuals were counted,

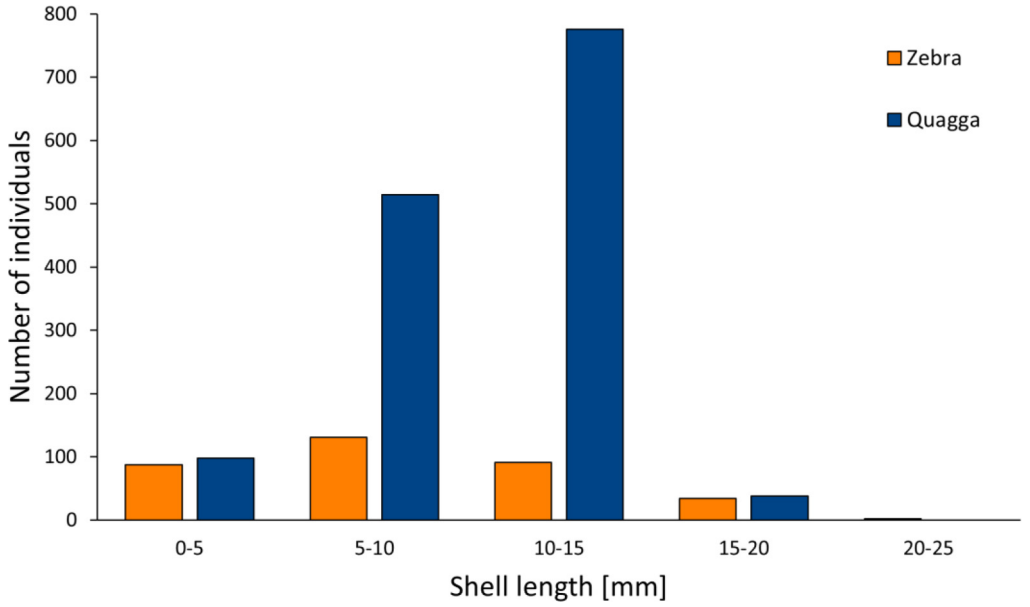

Fig. 6. Distribution of shell length values of zebra (*Dreissena polymorpha*) and quagga mussel (*Dreissena rostriformis bugensis*) on one half of a floater.

with quagga mussels (80.5%; 1,426) outnumbering zebra mussels (19.5%; 345). Shell length analysis showed significant quagga dominance (p-value = 2.01×10^{-37}), particularly in the 5–10 and 15–20 mm size classes (Fig. 6).

The sampled floater contained approximately 3,500 mussels. Since it was only 50% submerged, fully submerged floaters carrying PV panels were estimated to host around 7,000 mussels each. Considering that approximately 10% of the floaters (walkways) have reduced weight and reduced a specific water-contact-surface, the total mussel population across 3,952 floaters was estimated at 26.3 million.

3.3.2 Effects of mussel filtration on water quality

Oxygen concentrations varied significantly between sites, with a daily amplitude of up to 7 mg l^{-1} at MREF I, which remained below 0.8 mg l^{-1} at MFPV. Beneath low or moderate global horizontal irradiance, dissolved oxygen was reduced under FPV (Fig. 7, zoom window 1). During periods of warm and stable weather, dissolved oxygen fluctuations in the open water were significantly higher than below the FPV (Fig. 7, zoom window 2).

To estimate the phosphorus removal potential of the mussel population on the FPV system, various parameters were measured and calculated, including dry weight, phosphorus content, and filtration capacity. A dry weight of 0.589 g and 0.554 g was measured for 100 individuals of quagga and zebra mussels respectively. The average phosphorus content was 10.38 mg g^{-1}, binding 414 mg of phosphorus per floater. Shells contained 0.16 mg g^{-1} phosphorus, with a dry weight of 6.3 g (quagga) and 8.3 g (zebra) per 100 shells, binding 81.8 mg phosphorus per floater. Across all floaters, mussel bodies stored 1.64 kg of phosphorus, and shells 0.32 kg. The calculated effective clearance rate for mussel population attached to the FPV system was 26,460 m^3 d^{-1}, filtering 1.5% of the total lake volume or 3.1% of the epilimnion per day.

3.4 Macrophyte distribution and ecological lake condition

A total of 15 macrophyte species were identified during the diving surveys in T1–T6 (Fig. 8).

Species diversity was highest in T3 and T4, with up to ten species identified (Fig. 9). Fewer species were observed in other transects, including T2 and T6. Macrophyte abundance peaked at 1–2 m depth but was lower at 0–1 m. At depths exceeding 4 m, abundance declined, with *Ceratophyllum demersum* and *Potamogeton lucens* dominating, while *Myriophyllum spicatum* prevailed in shallower areas. *Chara virgata* (coverage ratio = 0.5%) was the only habitat-typical species, according to the WFD assessment for this lake type. Others, *e.g., Nitella spp.*, *Nitellopsis obtusa* and *Tolypella spp.*, were missing.

Based on stratification patterns, water quality (SPC and pH), geographical location, and the absence of natural surface inflows, the lake was categorised as a stratified, calcium-rich lowland lake with a small catchment (type 13) and an oligotrophic TRS. Mean LML of 5.25 m (±0.52 m), along with the cover ratio and habitat-typical species count, classified the lake's ecological condition as insufficient (Tab. 2).

Macrophytes were only observed in nearshore areas, with no growth detected beneath the FPV system. This corresponds with current LML of 5.25 m, suggesting that bathymetric constraints, rather than direct FPV shading, limited macrophyte growth below the system.

3.5 Hydrodynamic modelling performance and FPV impact analysis

3.5.1 Model calibration and validation

Both GLM-AED2 and Delft3D-FLOW demonstrated high performance during the calibration period, based on averaged measurements from MREFI and MREFII, achieving RMSE

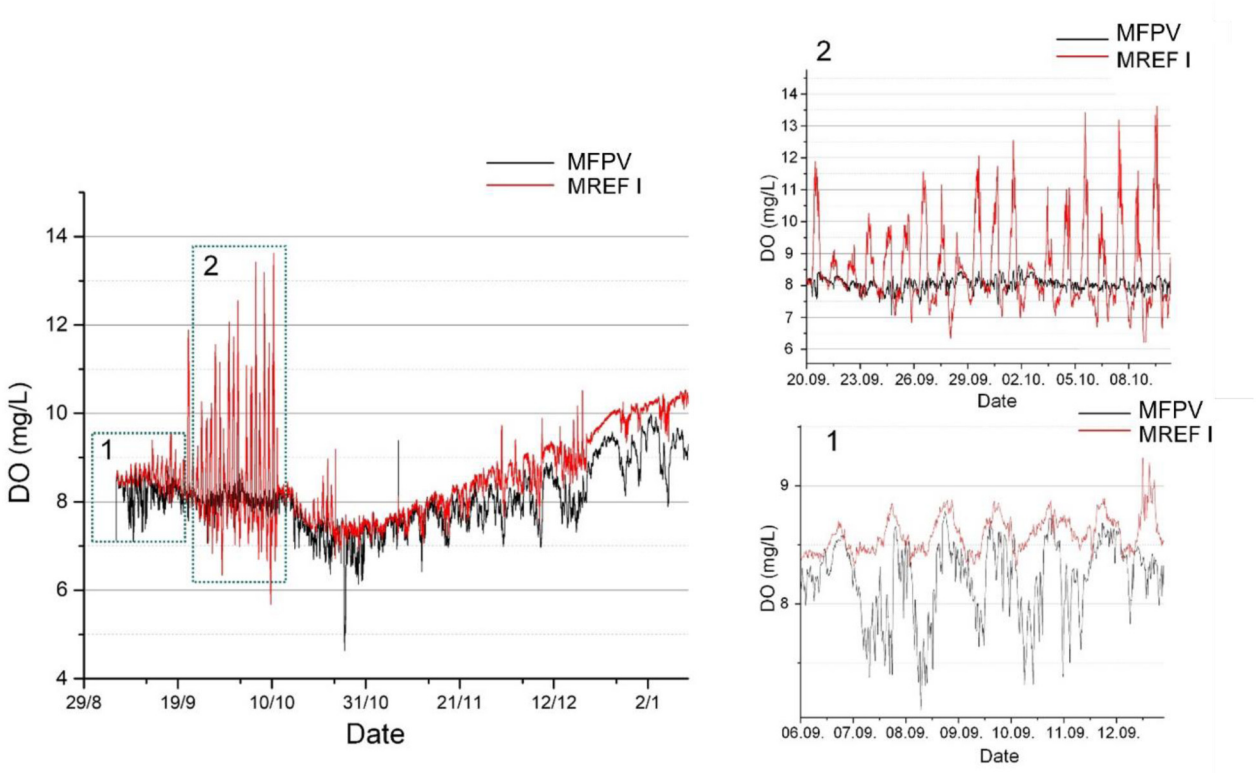

Fig. 7. Dissolved oxygen concentrations at 1 metre depth below the FPV and in open water (MREF I) from 5 September 2023 to 9 January 2024, as measured by the miniDOT loggers.

values below 1 °C and NSE values exceeding 0.9 for water temperature profiles (Tab. 3).

Using the same metrics, modelling results were evaluated for the entire simulation period, both at the reference and below FPV, assuming the current FPV coverage of 8%. Both models achieved NSE values above 0.6 and RMSE between 1 °C and 2 °C, indicating a satisfactory representation of the system (Tab. 4).

3.5.2 FPV coverage effects on stratification, mixing, and trophic state

Simulated water temperature profiles at various depths were compared with field data for both models (Fig. 10). While both models captured overall water temperature trends, they differed in detail. GLM-AED2 predicted smaller fluctuations in surface water temperatures, whereas Delft3D-FLOW overestimated surface temperatures, especially during summer 2023. Both models performed better for epilimnetic than hypolimnetic temperatures. GLM-AED2 predicted higher bottom temperatures at the onset of stratification, while Delft3D-FLOW tended to underestimate them. The formation of inverse stratification in winter was more pronounced in the Delft3D-FLOW simulation.

Both models accurately reproduced thermal stratification during summer (Fig. 11). At an FPV coverage of 45%, stratification became more unstable in both models, suggesting an upward shift in the thermocline.

With increasing FPV coverage, both models showed a general decline in lake surface water temperature (Fig. 12). For low FPV occupancies (≤15%), temperature reductions remained moderate, with differences of approximately 1 °C compared to the baseline scenario. For 90% FPV coverage, GLM-AED2 simulated a 3.6 °C temperature reduction, whereas Delft3D-FLOW predicted a reduction of 7.2 °C.

Schmidt stability, an indicator of stratification strength, decreased at high FPV coverage in both models. In Delft3D-FLOW, Schmidt stability initially increased at 15% and 30% FPV coverage, before sharply declining from 45% and onwards, indicating a mid-range peak in stratification intensity. In contrast, GLM-AED2 exhibited a steady decline already up to 45%, followed by a more pronounced drop.

Despite these differences, both models converged to similar stability levels for 90% FPV coverage, suggesting that extensive FPV deployment results in comparable reductions in stratification. This weakening was also evident in reduced thermocline depths. While Delft3D-FLOW consistently simulated a shallower thermocline than GLM-AED2, both models showed notable decreases in thermocline depth beyond 30% FPV coverage. The TSI, simulated only by GLM-AED2, declined with increasing FPV coverage, suggesting potential reductions in lake productivity. This trend aligned with observed reductions in lake surface water temperature and increased shading, both of which constrain primary production. Compared to the baseline, TSI decreased by approximately 20% at 30% FPV coverage and by 60% at 90% coverage.

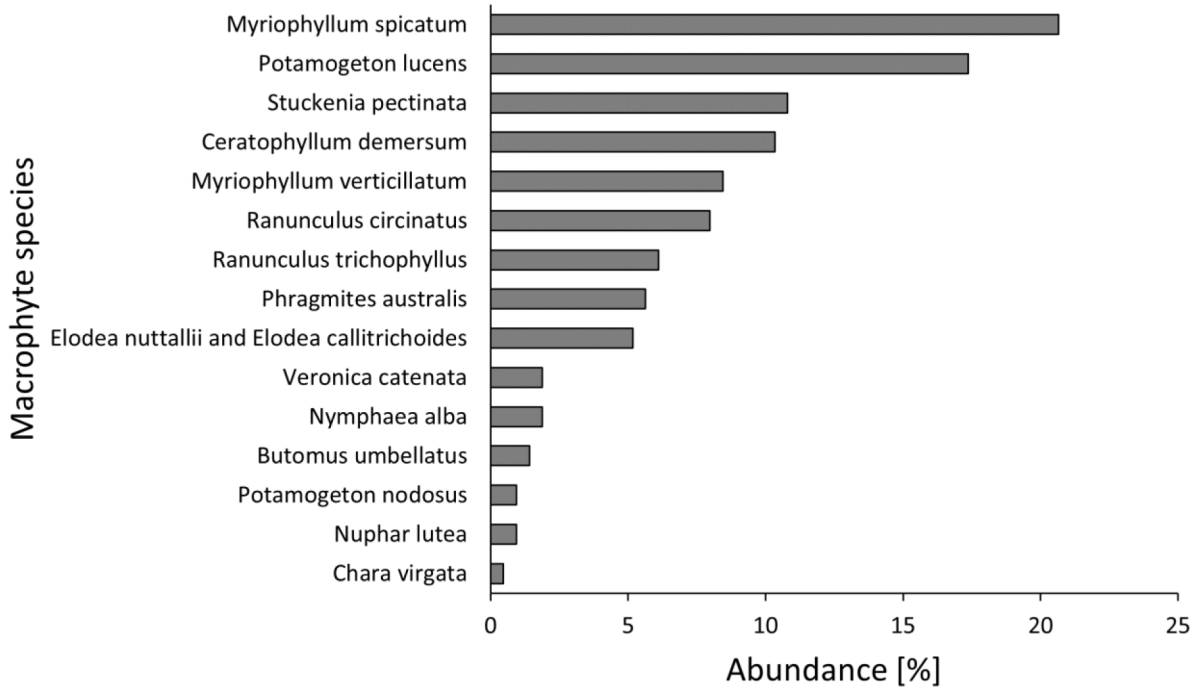

Fig. 8. Abundance of the macrophyte species found within the six macrophyte transects along the shore of the gravel pit lake (T1–T6).

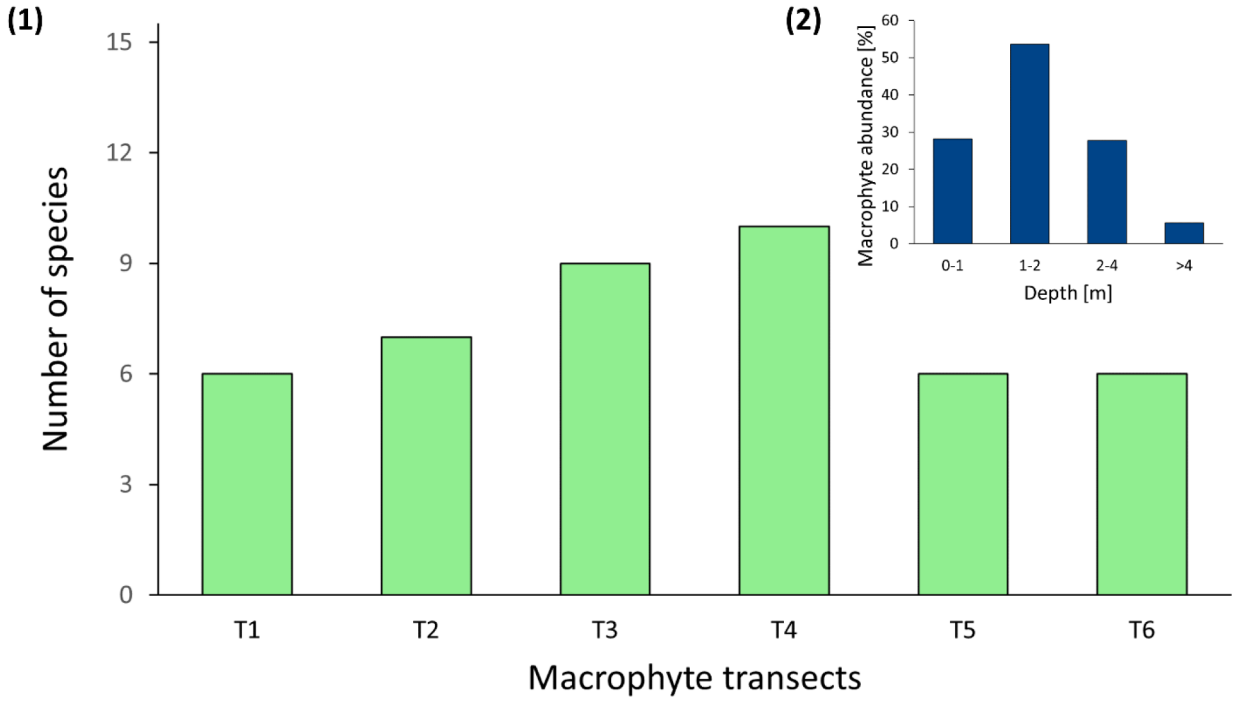

Fig. 9. (1) Number of species found in six macrophyte transects (T1–T6, Fig 3); (2) distribution of macrophyte abundance in relation to water depth.

3.5.3 Modelling mussel filtration effects on lower macrophyte limit

To assess the impact of mussel filtration on macrophyte expansion, GLM-AED2 simulations were used to estimate shifts in the lower macrophyte limit (LML) under varying FPV coverage scenarios (Fig. 13). The current LML-based macrophyte distribution was expanded by the WFD-defined theoretical LML for good (oligotrophic) lake conditions. The latter LML formed a potential contact zone northeast of the FPV system. The maximum observed shoreline distance to the current LML was 35 m. In contrast, the shoreline distance to theoretical LML

Table 2. Quality levels (very good, good, moderate, insufficient, bad) for ecological evaluation according to the European Water Framework Directive (WFD). The quality levels determined by the study were as follows: cover ratio of habitat-typical vegetation – bad, habitat-typical species – bad, mean lower macrophyte limit – moderate.

TRS	Very good	Good	Moderate	Insufficient	Bad
Cover ratio of habitat-typical vegetation	>75%	50–75%	10–50%	5–10%	< 5%
Habitat-typical species	>9	6–9	4–5	2–3	1–0
Mean lower macrophyte limit	>10 m	>6.5–10.0 m	>5.0–6.5 m	2.5–5.0 m	<2.5 m

Table 3. Calibration and validation results for GLM-AED2 and Delft3D-FLOW water temperature simulations. Model performance is given by Root Mean Square Error (RMSE), Nash-Sutcliffe model efficiency coefficient (NSE) and Kling-Gupta efficiency (KGE).

Model	Calibration period			Validation period		
	RMSE [°C]	NSE [–]	KGE [–]	RMSE [°C]	NSE [–]	KGE [–]
GLM-AED2	0.77	0.92	0.83	2.41	0.61	0.79
Delft3D	0.71	0.95	0.59	2.91	0.58	0.5

Table 4. Total period results for GLM-AED2 and Delft3D simulations for the reference and FPV (actual coverage, 8%).

Model	Reference			FPV		
	RMSE [°C]	NSE [–]	KGE [–]	RMSE [°C]	NSE [–]	KGE [–]
GLM-AED2	1.94	0.72	0.84	1.5	0.95	0.87
Delft3D	1.78	0.77	0.52	2.63	0.69	0.47

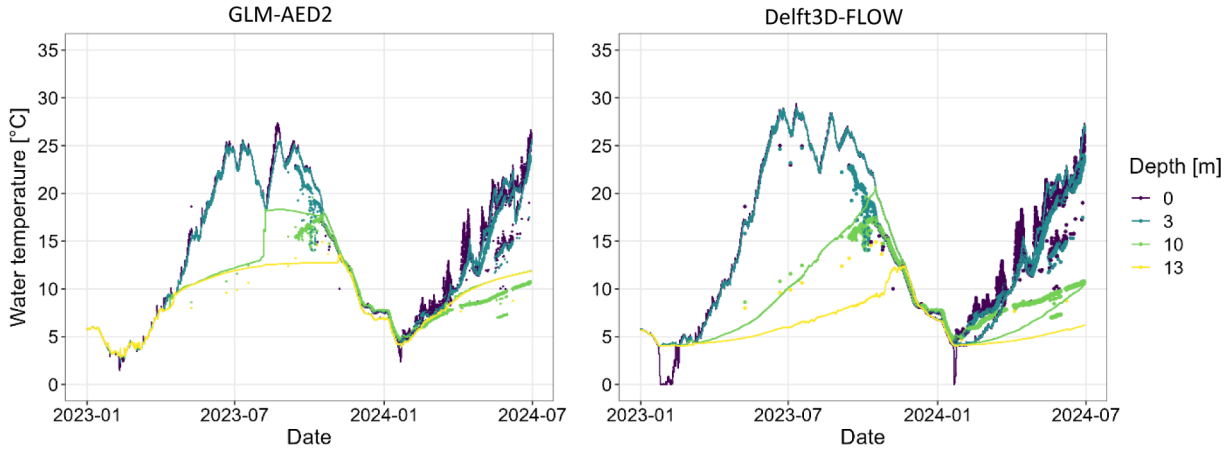

Fig. 10. Comparison of modelled water temperature at different depths for both models (lines), in relation to measured values (dots), below the FPV system with 8% lake coverage.

reached up to 200 m, indicating a heterogeneous distribution based on lake morphology. The GLM-AED2 was calibrated to this theoretical LML, defining the macrophyte-free zone as 58% of the total lake area. Including mussel filtration into the model simulations resulted in LML shifts of 0.32, 0.61, 1.21, 1.99 and 3.07 m for 8%, 15%, 30%, 45%, and 58% FPV coverage, respectively. With increasing water clarity, macrophyte expansion reduced the macrophyte-free zone from 58% down to 46%.

4 Discussion

4.1 Measured effects of FPV on water quality

The overall impact of the installed FPV system on water quality was limited, with considerable reductions observed only in dissolved oxygen, nitrate concentrations, and turbidity. A statistically significant decrease in dissolved oxygen (ΔDO, $p = 0.011$) and oxygen saturation (ΔDO Sat, $p = 0.01$) was recorded beneath the FPV system, along with a reduction in nitrate concentrations (ΔNO_3, $p = 0.011$). De Lima *et al.* (2021) reported oxygen reductions of 1.1–1.7 mg l^{-1} beneath an FPV system covering 30% of a lake in the Netherlands, while Château *et al.* (2019) reported a reduction of 0.86 to 0.89 mg l^{-1} beneath a 40% FPV coverage system in Taiwan.

In comparison, our study—focusing on a system covering 8% of the lake—observed a smaller average reduction of 0.38 mg l^{-1}, suggesting a negative correlation between oxygen concentration and FPV coverage. Additionally, both Château *et al.* (2019) and Li *et al.* (2023) found significant reductions in nitrate concentrations beneath FPV systems,

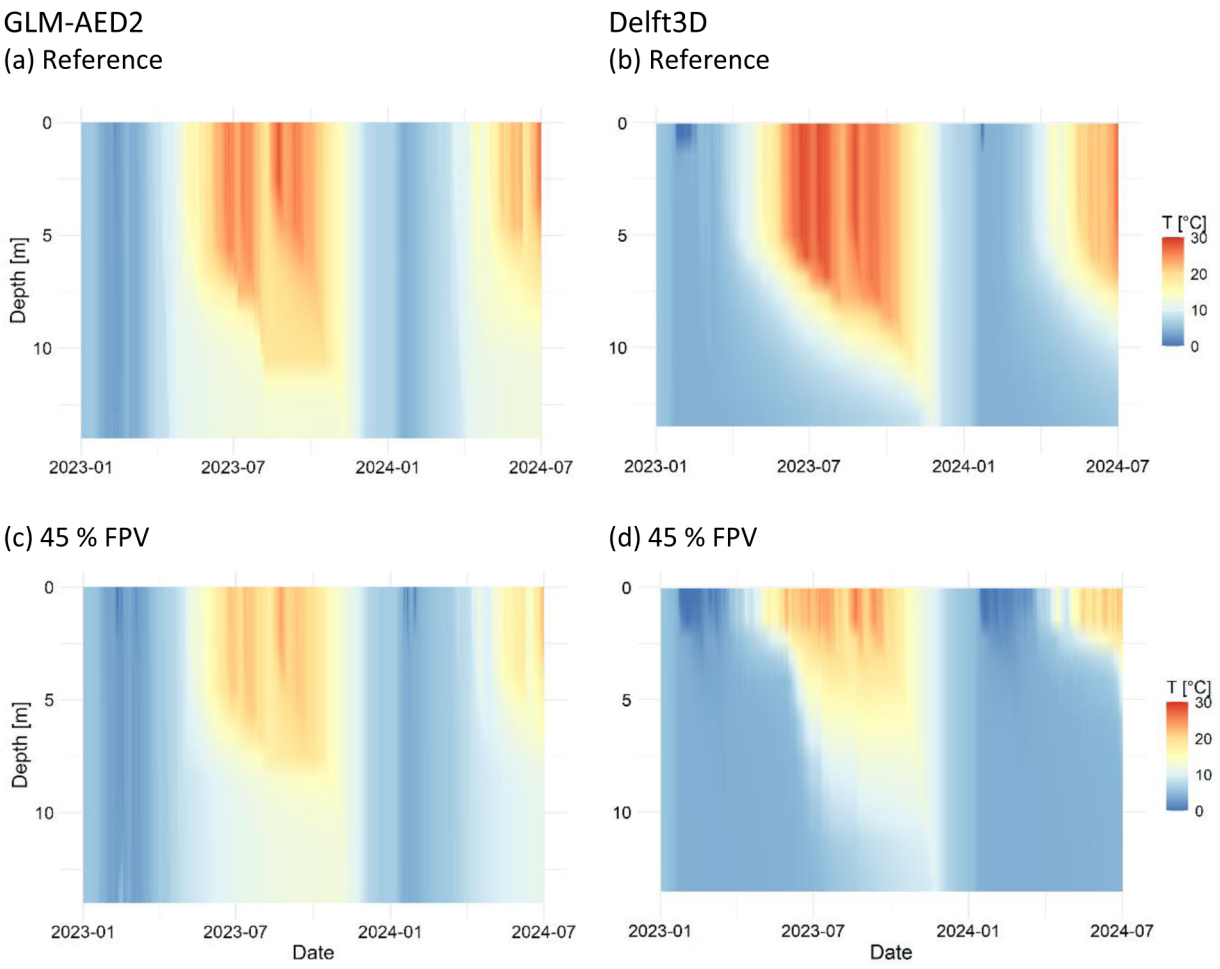

Fig. 11. (a, b) GLM-AED2 and Delft3D-FLOW water temperature profiles at MFPV during the simulation period (January 2023 to July 2024) for the reference scenario; (c, d) water temperature profiles at MFPV with 45% FPV coverage for each model.

which is consistent with our results. Other water quality parameters in our study—including water temperature, pH, specific conductivity, and chlorophyll-*a*—showed no significant differences between MFPV and MREF, indicating that the FPV system's impact on overall water quality was minimal.

4.2 FPV substructure as a new mussel habitat

FPV substructures provide habitat for sessile organisms, particularly mussels, which filter nutrients and suspended solids – potentially reinforcing the shift towards oligotrophic conditions. These mussels filter particles from 1.5 to >40 µm (Lei *et al.*, 1996; Roditi *et al.*, 1996). On our FPV system, nearly 2 kg of phosphorus was bound in mussel biomass, reducing its availability to phytoplankton and macrophytes, which could alter species composition. Drops in oxygen at MFPV compared to MREFI during low solar irradiance (Fig. 7) may indicate higher respiration rates and increased biological activity from periphyton and mussels. In contrast, pronounced diurnal oxygen fluctuations under high solar irradiance at MREFI suggest enhanced primary production at MREF I, while limited variation at MFPV suggested lower net oxygen production. Reduced photosynthesis under FPV can be expected, since shading limits autotrophic metabolism —potentially affecting oxygen dynamics, nutrient cycling, and ecosystem functioning. Mussels typically inhabit benthic zones, but colonising FPV substructures places them in the epilimnion—a warmer, oxygen-rich layer—potentially affecting growth, reproduction, and feeding. This might promote the spread of invasive species but also affect FPV buoyancy. In lakes with a high presence of invasive mussel species, the additional colonisation on the FPV system may be mitigated through designs that minimise float–water contact.

Further manage mussel colonisation, strategies might include encouraging native species – particularly those at risk –or establishing edible mussel farms (Haag and Williams, 2014; Dalderup *et al.*, 2020; Benjamins *et al.*, 2024). Active mussel harvesting could further counteract eutrophication by removing excess nutrients (Soto and Mena, 1999; Gren *et al.*, 2009; Petersen *et al.*, 2014). By reducing nutrient availability, mussel filtration on FPV structures may reinforce FPV-induced effects and contribute to a long-term shift towards oligotrophic conditions, mitigating eutrophication in nutrient-rich lakes. Further research is needed here to fully understand ecological effects of colonised FPV systems.

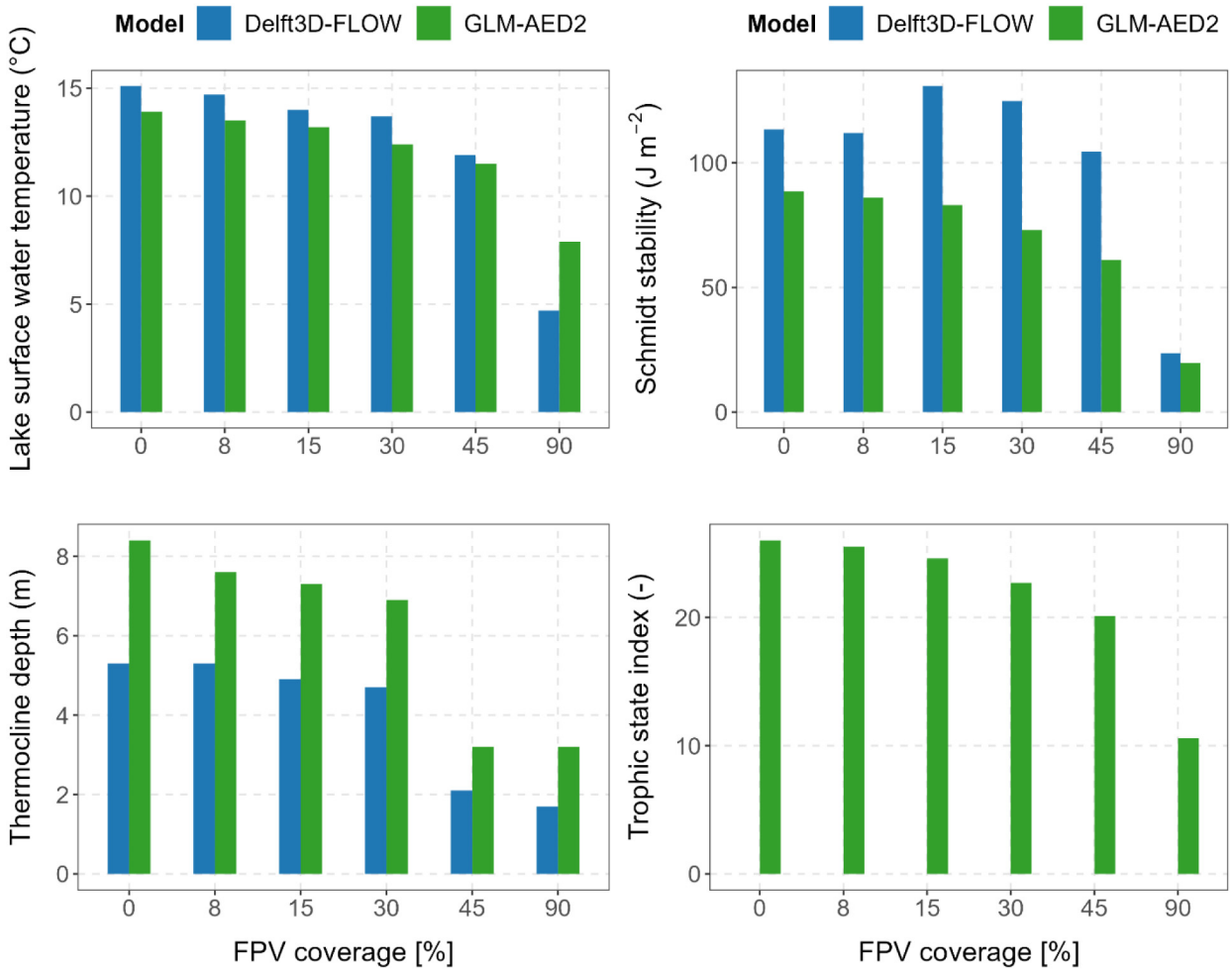

Fig. 12. Simulated impact of FPV coverage on mean lake surface water temperature, Schmidt stability, thermocline depth, and Trophic State Index (TSI) as calculated by GLM-AED2 (green) and Delft3D-FLOW (blue).

4.3 Macrophyte dynamics and limiting factors in FPV-integrated lakes

The highest species diversity was observed in T3 and T4, with up to ten species identified (Fig. 9), likely due to their south-facing location and relatively undisturbed shoreline. Sunlight exposure and reduced anthropogenic disturbance evidently promoted a broader range of species. In contrast, fewer species were found in transects T2 and T6, likely influenced by process water input (T2) or shading from riparian vegetation (T6). Everywhere, macrophyte abundance peaked at 1–2 m water depth and was lower at 0–1 m, possibly due to light oversaturation (Schwoerbel and Brendelberger, 2013) or sediment deposition on unstable slopes, which both may hinder growth. Below 2 metres, macrophyte abundance declined sharply. The distribution was limited to the littoral zone, with an average depth of 5.25 m (±0.52 m). No macrophyte growth was observed beneath the FPV system. The low abundance of habitat-typical species indicates an ecologically compromised lake condition, which is typical for anthropogenic gravel pit lakes. In these lakes, several factors (*e.g.,* steep shorelines, shoreline erosion, increased sedimentation from process water) likely constrain macrophyte expansion, independent of FPV (Mollema and Antonelli, 2016). Furthermore, high cyprinid densities may contribute to sediment resuspension and herbivory, suppressing macrophyte growth (Hansson *et al.*, 1987; Zambrano and Hinojosa, 1999; Yuan, 2021). In all lakes, the trophic state plays a major role for macrophytes. Oligotrophic systems generally support a more extensive LML, while eutrophication reduces light penetration and restricts submerged vegetation. In Lake Leimersheim, the installed FPV system affected local light conditions, but the primary constraints on macrophyte distribution were driven by other factors such as lake morphology, sediment loading, and fish community composition. These existing conditions supposedly overrode potential FPV-related effects, highlighting the need for a comprehensive assessment of site-specific ecological constraints before attributing changes in macrophyte dynamics to FPV.

4.4 Hydrodynamic modelling and FPV impact analysis

4.4.1 Model performance and applicability

Both GLM-AED2 and Delft3D-FLOW effectively simulated the hydrodynamics of our gravel pit lake. On the one hand, Delft3D-FLOW provided detailed local FPV impact

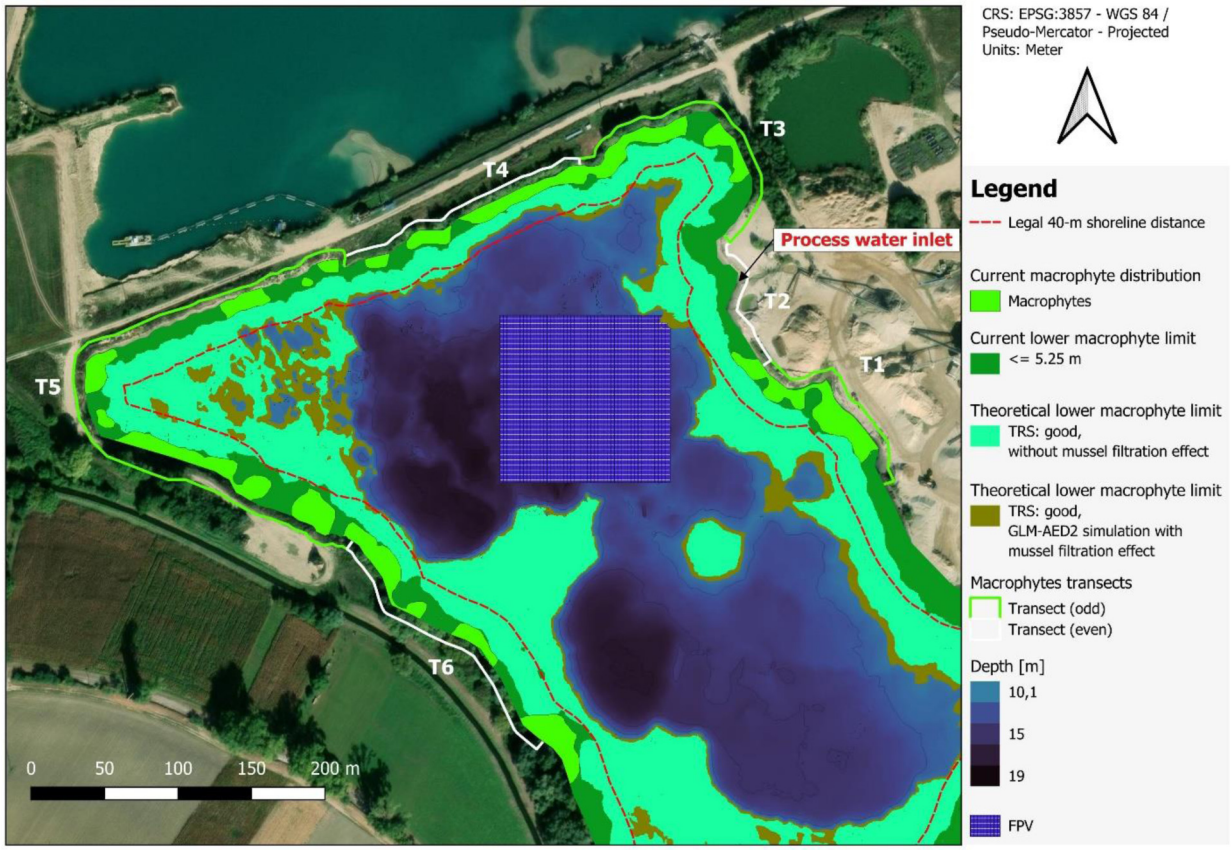

Fig. 13. Current macrophyte distribution (light green areas) and lower macrophyte limit (dark green areas). The potential macrophyte distribution (turquoise area) corresponds to the theoretical lower macrophyte limit under good ecological conditions (Trophic Reference State) as defined by the European Water Framework Directive. Mussel filtration by colonies attached to the 58 % FPV system—covering the macrophyte-free zone as simulated by GLM-AED2—resulted in an expanded macrophyte distribution (brown area). The legal 40 m shoreline distance is marked with a red dashed line.

predictions but required significantly more computational time, limiting scenario-based ecological analyses. Its simulated flow velocity remained uncertain and would require validation, such as with upward-looking Acoustic Doppler Current Profiler measurements (Parsapour-Moghaddam and Rennie, 2017; Goulart *et al.*, 2023). Nevertheless, Delft3D-FLOW appears to be a good choice for heterogeneous lakes or small FPV systems in large water bodies. On the other hand, GLM-AED2, while assuming horizontal homogeneity, proved effective for advanced FPV impact assessments, offering high computational efficiency (Ishikawa *et al.*, 2022; Amorim et al., 2023). GLM-AED2 can approximate species distribution using a quasi-2D approach, making it useful for multi-lake assessments, climate change simulations, and FPV design evaluation. The choice between models depends on the required level of detail: Delft3D-FLOW is preferable for local assessments in complex lakes, while GLM-AED2 is more efficient for large-scale FPV scenarios. Combining the two models may provide synergistic benefits, leveraging their respective strengths. Optimising hydrodynamic models for FPV is still in its early stages but will depend on detailed monitoring data sets.

4.4.2 Thermal and ecological impacts of FPV coverage scenarios

empirical and modelling studies consistently show that FPV installations reduce lake surface water temperature, though the extent varies with lake characteristics, FPV coverage, and methodology. Nobre *et al.* (2025) measured a 1.2 °C annual mean reduction, peaking at 3.0 °C on the warmest days in French gravel pit lakes, while Ilgen *et al.* (2023) recorded a 2.8 °C cooling in a German gravel pit lake during summer. Modelling studies predicted a broader range. Exley *et al.* (2021) simulated 8.0 °C cooling in Windermere, UK, and Ji *et al.* (2022) estimating a 3.3 °C reduction in the Xiangjiaba Reservoir, China. The present results fell within this range, as GLM-AED2 predicted a 3.6 °C reduction and Delft3D-FLOW a stronger 7.2 °C reduction at 90% FPV coverage. FPV-induced cooling also affects lake stratification, weakening Schmidt stability and altering mixing regimes. Ilgen *et al.* (2023) found little impact below 15% FPV, with significant shifts beyond 50% coverage, a threshold also supported by the present study. Both simulation models indicated a decline in Schmidt stability for high FPV

occupancies, which was accompanied by a thermocline shift to shallower depths. The TSI in GLM-AED2 declined with increasing FPV coverage, though considerable changes only occurred beyond 45% FPV. Yang *et al.* (2022) reported reduced chlorophyll-*a* and primary production in a tropical reservoir at 30% FPV coverage, while Karpouzoglou *et al.* (2020) found significant declines already above 20%. These numbers suggest that FPV effects on lake ecology depend on the individual lake but may counteract global warming-induced stratification intensification (Woolway *et al.*, 2020), which enhances nutrient retention in the epilimnion and primary production (O'Beirne *et al.*, 2017).

4.4.3 Implications of mussel filtration for macrophyte dynamics in FPV-integrated lake restoration

Given a 25–30-year service life, FPV systems may outlast anthropogenic influences like gravel extraction, highlighting the need to integrate lake renaturation into FPV planning. We used GLM-AED2 to simulate macrophyte distribution, applying a quasi-2D approach calibrated to the WFD trophic reference state. We also incorporated mussel filtration effects at the FPV structure, showing its potential to influence lake-wide ecological dynamics. Mussels primarily colonise FPV substructures, but their filtration extends across the entire lake, improving water clarity and promoting macrophyte expansion, counteracting eutrophication.

Ray *et al.* (2024) demonstrated that improper FPV placement, particularly over macrophyte-dominated areas, can also result in negative effects, such as reduced oxygen levels and increased greenhouse gas emissions, likely due to the decomposition of macrophytes. This highlights the importance of optimised FPV siting and calls for adequate simulation of potential impacts before new systems are installed.

4.5 Regulatory considerations for FPV placement

In Germany, FPV installations are subject to a regulatory limit of 15% lake surface coverage and a minimum shoreline distance of 40 metres. For the FPV system at Lake Leimersheim, the observed distance to LML was approximately 35 metres, while the theoretical LML, derived from the trophic reference state, extended up to 200 metres. This discrepancy suggests that fixed-distance regulations may not consistently reflect the depth-dependent distribution of macrophytes, particularly in artificial lakes with steep bathymetry and heterogeneous morphometry. In addition, active sediment input and anthropogenic shoreline modification can influence aquatic vegetation independently of FPV siting. These factors may also vary over time, depending on the lake's stage of ecological succession.

Model simulations using Delft3D-FLOW and GLM–AED2 indicated that substantial alterations in lake stratification and water quality only occurred at FPV coverages above 45%. This modelled response differs markedly from the regulatory threshold, suggesting that fixed limits may not uniformly correspond to ecological effects across different lake types. The interpretation of such thresholds thus appears to depend on local morphometric and ecological characteristics, as well as on the specific FPV design and coverage.

5 Conclusions

This study assessed an FPV system covering 8% of a gravel pit lake in southwest Germany and found no major ecological impacts. External stressors, such as sediment-rich inflows and herbivorous fish, exerted a stronger influence on water quality and macrophyte growth than the FPV installation itself. Colonisation of the FPV substructure by invasive mussels improved water clarity and promoted macrophyte growth, indicating possible synergies with lake restoration. However, ecological risks remain and require site-specific evaluation. Hydrodynamic model simulations (Delft3D-FLOW and GLM-AED2) showed substantial changes in lake dynamics only above 45% FPV coverage. These findings suggest that the current regulatory framework in Germany – limiting FPV installations to 15% surface coverage and a 40-metre shoreline buffer – though precautionary, may be overly conservative for artificial lakes subject to strong external pressures. This study calls for more flexible, site-specific regulations that account for lake depth, morphometry, and trophic state. Classification-based thresholds should reflect lake type, usage, and ecological status. Expert assessments combining empirical field data and modelling may offer ecologically sound alternatives to fixed criteria. Such flexibility would enable context-sensitive FPV integration. Further empirical and modelling studies are needed to support this approach.

Acknowledgements

The authors kindly thank Erdgas Südwest GmbH, which offered the FPV system for research purposes. In addition, our thanks go to the Pfadt GmbH Kieswerk-Baustoffe, which provided unrestricted and safe access to the study site. We also thank Annie Schlöffel for her support in the field and laboratory during the sampling and monitoring of the biofilm and mussels. Finally, the authors acknowledge the support of the technical team at Fraunhofer ISE during the installation and maintenance of the monitoring system.

Funding

K.I. was supported by a scholarship from the German Federal Foundation for the Environment (DBU, no. 08020211210/002). The researchers of Fraunhofer ISE acknowledge the support from the FPV4Resilience project, funded by the Sustainability Center Freiburg (LZN). This study was financed in part by the Coordenação de Aperfeiçoamento de Pessoal de Nível Superior – Brasil (CAPES) – Finance Code 001. C.G. was supported by a sandwich doctorate scholarship by the Coordination for the Improvement of Higher Education Personnel (CAPES) during her time in Germany – CAPES-PrInt, call no. 01/2022 CAPES-PRINT-UFPR – Sandwich Doctorate. T. B. acknowledges the productivity stipend from the National Council for Scientific and Technological Development – CNPq, grant no. 313491/2023-2, call no. 09/2023.

Competing interest

The authors have no relevant financial or non-financial interests to disclose.

References

Amorim LF, Duarte BPDS, Martins JRS. 2023. Comparison between methods to predict climate change impacts on tropical shallow lakes. *J Water Clim Change* 14: 4299–4313.

Benjamins S, Williamson B, Billing S-L, Yuan Z, Collu M, Fox C, Hobbs L, Masden EA, Cottier-Cook EJ, Wilson B. 2024. Potential environmental impacts of floating solar photovoltaic systems. *Renew Sustain Energy Rev* 199: 114463.

Bundesamt für Justiz. 2023. §36 WHG – Einzelnorm. Available from: https://www.gesetze-im-internet.de/whg_2009/__36.html (last consult: 2024/10/10).Carlson RE. 1977. A trophic state index for lakes. *Limnol Oceanogr* 22: 361–369.

Château P-A, Wunderlich RF, Wang T-W, Lai H-T, Chen C-C, Chang F-J. 2019. Mathematical modeling suggests high potential for the deployment of floating photovoltaic on fish ponds. *Science of The Total Environment* 687: 654–666.

Connelly NA, O'Neill CR, Knuth BA, Brown TL. 2007. Economic impacts of zebra mussels on drinking water treatment and electric power generation facilities. *Environmental Management* 40: 105–112.

Dalderup T, Van Leijsen M, Meppelink M, Van den Oord T, Richardson T, Verdonk M, Van Zeil V. 2020. Aquaculture activities in energy storage lake: advice for cultivating shellfish and seaweed in combination with a floating solar park. *Aquaculture in Delta21 Energy Storage Lake Final Report*. Available from: https://www.delta21.nl/wp-content/uploads/2020/06/AQUACULTUUR-rapport.pdf

de Lima RLP, Paxinou K, C. Boogaard F, Akkerman O, Lin FY. 2021. In-situ water quality observations under a large-scale floating solar farm using sensors and underwater drones. *Sustainability* 13: 6421.

Deltares. 2024. Delft3D-FLOW: transport phenomena, including sediments – User manual hydro-morphodynamics.

Diggins T.P. 2001. A seasonal comparison of suspended sediment filtration by quagga (*Dreissena bugensis*) and zebra (*D. polymorpha*) mussels. *J Great Lakes Res* 27: 457–466.

Exley, G., Armstrong, A., Page, T., Jones, I.D. 2021. Floating photovoltaics could mitigate climate change impacts on water body temperature and stratification. *Solar Energy* 219:, 24–33.

Exley G, Page T, Thackeray SJ, Folkard AM, Couture R-M, Hernandez RR, Cagle AE, Salk KR, Clous L, Whittaker P, Chipps M, Armstrong, A. 2022. Floating solar panels on reservoirs impact phytoplankton populations: A modelling experiment. *Journal of Environmental Management* 324, 116410.

Goulart, C.B., Bleninger, T., de Oliveira Fagundes, H., Fan, F.M. 2023. Modeling uncertainties of reservoir flushing simulations. *International Journal of Sediment Research* 38, 698–710.

Gren, I.-M., Lindahl, O., Lindqvist, M. 2009. Values of mussel farming for combating eutrophication: An application to the Baltic Sea. *Ecological Engineering* 35, 935–945.

Haag, W.R., Williams, J.D., 2014. Biodiversity on the brink: an assessment of conservation strategies for North American freshwater mussels. *Hydrobiologia* 735, 45–60.

Haas, J., Khalighi, J., De La Fuente, A., Gerbersdorf, S.U., Nowak, W., Chen, P.-J. 2020. Floating photovoltaic plants: Ecological impacts versus hydropower operation flexibility. *Energy Conversion* and Management 206: 112414.

Hansson L.-A., Johansson L., Persson L. 1987. Effects of fish grazing on nutrient release and succession of primary producers. *Limnol Oceanogr* 32: 723–729.

Hipsey M.R. 2022. Modelling aquatic eco-dynamics: Overview of the AED modular simulation platform. Available from: https://doi.org/10.5281/ZENODO6516222

Hipsey M.R., Bruce L.C., Boon C., Busch B., Carey C.C., Hamilton D.P., Hanson P.C., Read J.S., de Sousa E., Weber M., Winslow L.A. 2019. A general lake model (GLM 3.0) for linking with high-frequency sensor data from the Global Lake Ecological Observatory Network (GLEON). *Geosci. Model Dev.* 12: 473–523.

Idso S.B. 1973. On the concept of lake stability. *Limnol. Oceanogr.* 18: 681–683.

Ilgen, K., Schindler, D., Wieland, S., Lange, J., 2023. The impact of floating photovoltaic power plants on lake water temperature and stratification. *Sci Rep* 13:, 7932.

Ishikawa M., Gonzalez W., Golyjeswski O., Sales G., Rigotti J.A., Bleninger T., Mannich M., Lorke A. 2022. Effects of dimensionality on the performance of hydrodynamic models for stratified lakes and reservoirs. *Geosci. Model Dev.* 15: 2197–2220.

Ji Q., Li K., Wang Y., Feng J., Li R., Liang R. 2022. Effect of floating photovoltaic system on water temperature of deep reservoir and assessment of its potential benefits: a case on Xiangjiaba Reservoir with hydropower station. *Renewable Energy* 195: 946–956.

Kakoulaki G., Gonzalez Sanchez R.Gracia Amillo A. Szabo S. De Felice M. Farinosi F. De Felicek L. Bisselin B. Seliger R. Kougias I. Jaeger-Waldau A. 2023. Benefits of pairing floating solar photovoltaics with hydropower reservoirs in Europe. *Renewable and Sustainable Energy Reviews* 171: 112989.

Karpouzoglou T., Vlaswinkel B., van der Molen J. 2020. Effects of large-scale floating (solar photovoltaic) platforms on hydrodynamics and primary production in a coastal sea from a water column model. *Ocean Science* 16: 195–208.

Ladwig R, Hanson PC, Dugan HA, Carey CC, Zhang Y, Shu L, Duffy CJ, Cobourn KM. 2021. Lake thermal structure drives interannual variability in summer anoxia dynamics in a eutrophic lake over 37 years. *Hydrol Earth Syst Sci* 25: 1009–1032.

Lee N, Grunwald U, Rosenlieb E, Mirletz H, Aznar A, Spencer R, Cox S. 2020. Hybrid floating solar photovoltaics-hydropower systems: Benefits and global assessment of technical potential. *Renewable Energy* 162: 1415–1427.

Lei J, Payne BS, Wang SY. 1996. Filtration dynamics of the zebra mussel, Dreissena polymorpha. *Can. J. Fish. Aquat. Sci.* 53: 29–37.

Li W, Wang Y, Wang G, Liang Y, Li C, Svenning JC. 2023. How do rotifer communities respond to floating photovoltaic systems in the subsidence wetlands created by underground coal mining in China? *J. Environ. Manag.* 339: 117816.

Liu X, Zhang Y, Shi K, Lin J, Zhou Y, Qin B. 2016. Determining critical light and hydrologic conditions for macrophyte presence in a large shallow lake: The ratio of euphotic depth to water depth. *Ecol. Indic.* 71: 317–326.

Matthews J, Van der Velde G, Bij de Vaate A, Collas FPL, Koopman KR, Leuven RSEW. 2014. Rapid range expansion of the invasive quagga mussel in relation to zebra mussel presence in The Netherlands and Western Europe. *Biol. Invasions* 16: 23–42.

Mollema, Pauline N., and Marco Antonellini. 2016. Water and (bio) chemical cycling in gravel pit lakes: A review and outlook. *Earth-Science Reviews* 159: 247–270

NASA. 2023. POWER | Data Access Viewer [WWW Document]. Available from: https://power.larc.nasa.gov/data-access-viewer/ (accessed 3 August 2023).

Nobre R, Boulêtreau S, Colas F, Azemar F, Tudesque L, Parthuisot N, Favriou P, Cucherousset J. 2023. Potential ecological impacts of floating photovoltaics on lake biodiversity and ecosystem functioning. *Renewable and Sustainable Energy Reviews* 188: 113852.

Nobre R, Rocha SM, Healing S, Ji Q, Boulêtreau S, Armstrong A, Cucherousset J. 2024. A global study of freshwater coverage by floating photovoltaics. *Solar Energy* 267: 112244.

Nobre RLG, Vagnon C, Boulêtreau S, Colas F, Azémar F, Tudesque L, Parthuisot N, Millet P, Cucherousset J. 2025. Floating photovoltaics strongly reduce water temperature: A whole-lake experiment. *Journal of Environmental Management* 375: 124230.

O'Beirne MD, Werne JP, Hecky RE, Johnson TC, Katsev S, Reavie ED, 2017. Anthropogenic climate change has altered primary productivity in Lake Superior. *Nature communications* 8: 15713.

Ogunjo S, Olusola A, Olusegun C. 2023. Potential of using floating solar photovoltaic and wind farms for sustainable energy generation in an existing hydropower station in Nigeria. *Clean Techn Environ Policy* 25: 1921–1934.

Orlova MI, Muirhead JR, Antonov PI, Shcherbina GK, Starobogatov YI, Biochino GI, Therriault TW, MacIsaac HJ. 2004. Range expansion of quagga mussels *Dreissena rostriformis bugensis* in the Volga River and Caspian Sea basin. *Aquatic Ecology* 38: 561–573.

Parsapour-Moghaddam P, Rennie Cd. 2017. Hydrostatic versus nonhydrostatic hydrodynamic modelling of secondary flow in a tortuously meandering river: Application of Delft3D. *River Research and Applications* 33: 1400–1410.

Petersen JK, Hasler B, Timmermann K, Nielsen P, Tørring DB, Larsen MM, Holmer M. 2014. Mussels as a tool for mitigation of nutrients in the marine environment. *Marine Pollution Bulletin* 82: 137–143.

Ray NE, Holgerson MA, Grodsky SM. 2024. Immediate effect of floating solar energy deployment on greenhouse gas dynamics in ponds. *Environmental Science & Technology* 58: 22104–22113.

Roditi HA, Caraco NF, Cole JJ, Strayer DL. 1996. Filtration of Hudson River water by the zebra mussel (Dreissena polymorpha). *Estuaries* 19: 824.

Rowe MD, Anderson EJ, Vanderploeg HA, Pothoven SA, Elgin AK, Wang J, Yousef F. 2017. Influence of invasive quagga mussels, phosphorus loads, and climate on spatial and temporal patterns of productivity in Lake Michigan: A biophysical modeling study. *Limnology and Oceanography* 62: 2629–2649.

Schmidt W. 1928. Über die Temperatur und Stabilitätsverhältnisse von Seen. *Geografiska Annaler* 10: 145–177.

Schwoerbel J, Brendelberger H. 2013. *Einführung in die Limnologie*, 10th ed.Berlin Heidelberg: Springer Spektrum.

Son M. 2007. Native range of the zebra mussel and quagga mussel and new data on their invasions within the Ponto-Caspian Region. *AI* 2:, 174–184.

Soto D, Mena G. 1999. Filter feeding by the freshwater mussel, *Diplodon chilensis*, as a biocontrol of salmon farming eutrophication. *Aquaculture* 171: 65–81.

van de Weyer K, Stelzer D. 2021. Handlungsanweisung zur WRRL-Bewertung von Makrophyten in Seen nach dem NRW-Verfahren. Available from: https://www.laenderfinanzierungsprogramm.de/static/LFP/Dateien/LAWA/AO/O_2.20_Handlungsanweisung%20NRW%20Verfahren%20Makrophyten%20Seen%20WRRL%20Stand%20Oktober%202021.pdf.

Varelas K, Auger A, Brockhoff D, Hansen N, ElHara OA, Semet Y, Kassab R, Barbaresco F. 2018. A comparative study of large-scale variants of CMA-ES, in: *Parallel Problem Solving from Nature-PPSN XV: 15th International Conference, Coimbra, Portugal*, September 8-12, 2018, Proceedings, Part I 15. Springer, pp. 3–15. Available from: https://doi.org/10.1007/978-3-319-99253-2_1.

Ward, G.J. 1994. The RADIANCE lighting simulation and rendering system. In: *Proceedings of the 21st Annual Conference on Computer Graphics and Interactive Techniques – SIGGRAPH '94. Presented at the 21st annual conference*, ACM Press, Not Known, pp. 459–472.

Wegner, B., Kronsbein, A.L., Gillefalk, M., van de Weyer, K., Köhler, J., Funke, E., Monaghan, M.T., Hilt, S. 2019. Mutual facilitation among invading Nuttall's waterweed and quagga mussels. *Front. Plant Sci*. 10. Available from: https://doi.org/10.3389/fpls.2019.00789.

Winslow, L., Albers, S., DougCollinge, Read, J.S., Leach, T., Zwart, J., Snortheim. 2018. Gleon/Rlakeanalyzer: Rlakeanalyzer 1.11.4. Available from: https://doi.org/10.5281/ZENODO.1198428.

Wirth, H., Eggers, J.-B., Trommsdorf, M., Neuhaus, H., Heinrich, M., Wieland, S., Schill, C. 2021. Potenziale der Integrierten Photovoltaik in Deutschland. Fraunhofer ISE, Freiburg. Available from: https://www.ise.fraunhofer.de/de/geschaeftsfelder/solarkraftwerke-und-integrierte-photovoltaik/integrierte-photovoltaik.html.

Woolway RI, Kraemer BM, Lenters JD, Merchant CJ, O'Reilly CM, Sharma S. 2020. Global lake responses to climate change. *Nature Reviews Earth & Environment* 1: 388–403.

World Bank Group, ESMAP, SERIS. 2019a. Where Sun Meets Water: Floating Solar Handbook for Practitioners. WorldBank, Washington DC. Available from: http://documents.worldbank.org/curated/en/418961572293438109/Where-Sun-Meets-Water-Floating-Solar-Handbook-for-Practitioners

World Bank Group, Energy Sector Management Assistance Program, Solar Energy Research Institute of Singapore. 2019b. Where sun meets water – floating solar market report. © World Bank, Washington, DC. Available from: http://documents.worldbank.org/curated/en/579941540407455831/Floating-Solar-Market-Report-Executive-Summary

Xia Z, Li Y, Guo S, Chen R, Zhang W, Zhang P, Du P. 2023. Mapping global water-surface photovoltaics with satellite images. *Renewable and Sustainable Energy Reviews* 187: 113760.

Yang P, Chua LHC, Irvine KN, Nguyen MT, Low EW. 2022. Impacts of a floating photovoltaic system on temperature and water quality in a shallow tropical reservoir. *Limnology* 23: 441–454.

Yu N, Culver DA. 2001. Estimating the effective clearance rate and refiltration by zebra mussels, Dreissena polymorpha, in a stratified reservoir. *Freshwater Biology* 41: 481–492.

Yuan LL. 2021. Continental-scale effects of phytoplankton and non-phytoplankton turbidity on macrophyte occurrence in shallow lakes. *Aquatic sciences* 83: 14.

Zambrano L, Hinojosa D. 1999. Direct and indirect effects of carp (*Cyprinus carpio* L.) on macrophyte and benthic communities in experimental shallow ponds in central Mexico. *Hydrobiologia* 408: 131–138.

Cite this article as: Ilgen K, Goulart CB, Hilgert S, Schindler D, van de Weyer K, de Carvalho Bueno R, Bleninger T, Lastrico R, Gfüllner L, Graef A, Fuchs S, Lange J. 2025. Hydrological and ecological effects of floating photovoltaic systems: a model comparison considering mussel, periphyton, and macrophyte growth. *Knowl. Manag. Aquat. Ecosyst.*, 426, 11. https://doi.org/10.1051/kmae/2025008

APPENDIX C. MODEL SETUP

Gravel pit lake

Table 7-1. Model setup parameters for the gravel pit lake – hydrodynamic model.

Setup	Parameter	Value
Initial conditions	Water level (m)	0
	Temperature (°C)	5.7
Physical parameters	Manning coefficient (Chow, 1959)	0.05
	Wind drag coefficients	
	Vertical eddy diffusivity (m^2/s)	0.001
	Turbulence model	k- ε
	Secchi depth (m)	4.5
	Dalton number	0.0001
	Stanton number	0.0013
Additional parameters	Zmodel	#Y#
	Zbot	-19
	Ztop	0.3
	Precipitation and evaporation	*file.eva
	Spatial and time varying meteorological conditions	a file for each parameter (*.amu, *.amv, *.amp, *.amr, *.amt, *.amc, *.ams)

Table 7-2. Model setup parameters for the gravel pit lake – water quality model.

Setup	Parameter	Value
Initial conditions	Conservative tracer (g/m^3)	0
	Decayable tracer (g/m^3)	0
	Dissolved oxygen (g/m^3)	8
Physical parameters	Decay rate tracer (1/d)	0.01
	Ambient water temperature	Flow output for WAQ: *.tem
	Wind speed	Space and time varying file created with python: *.bin
	Reaeration formula	9
	Reaeration transfer coefficient (m/d)	1
Numerical option	Integration method	22-Local flux-corrected transport (Boris-Book)
Discharges	Tracer	0.0001 m^3/s flow rate 10000 g/m^3 concentration 8 g/m^3 DO

Passaúna reservoir

Table 7-3. Model setup parameters for the Passauna reservoir – hydrodynamic model.

Setup	Parameter	Value
Initial conditions	Water level (m)	-0.51
	Temperature (°C)	16.9
Physical parameters	Manning coefficient (Chow, 1959)	0.035
	Wind drag coefficients	
	Vertical eddy diffusivity (m²/s)	0.001
	Turbulence model	k-ε
	Secchi depth (m)	2
	Dalton number	0.00405
	Stanton number	0.00405
Additional parameters	Zmodel	#Y#
	Zbot	-17.2
	Ztop	0.3
	Precipitation and evaporation	specific file *.eva
	Spatial and time varying meteorological conditions	a file for each parameter (*.amu, *.amv, *.amp, *.amr, *.amt, *.amc, *.ams)

Table 7-4. Model setup parameters for the gPassaúna reservoir– water quality model.

Setup	Parameter	Value
Initial conditions	Conservative tracer (g/m³)	0
	Decayable tracer (g/m³)	0
	Dissolved oxygen (g/m³)	8
Physical parameters	Decay rate tracer (1/d)	0.01
	Ambient water temperature	Flow output for WAQ: *.tem
	Wind speed	Space and time varying file created with python: *.bin
	Reaeration formula	13
	Reaeration transfer coefficient (m/d)	1
Numerical option	Integration method	22-Local flux-corrected transport (Boris-Book)
Discharges	River inflow	8 g/m³ DO
	Tracer	0.0001 m³/s flow rate 10000 g/m³ concentration 8 g/m³ DO

APPENDIX D. COMPLEMENTARY RESULTS

Gravel Pit Lake

- Timeseries results

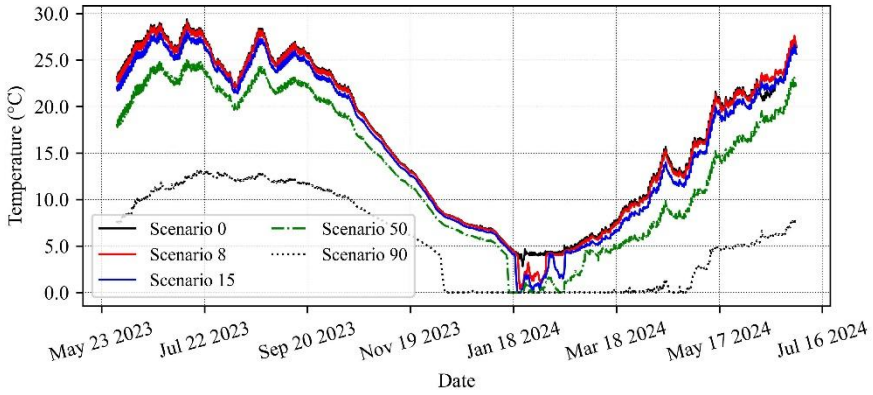

Figure 7-1. Surface temperature timeseries results for the simulated scenarios of the gravel pit lake, at MFPV point.

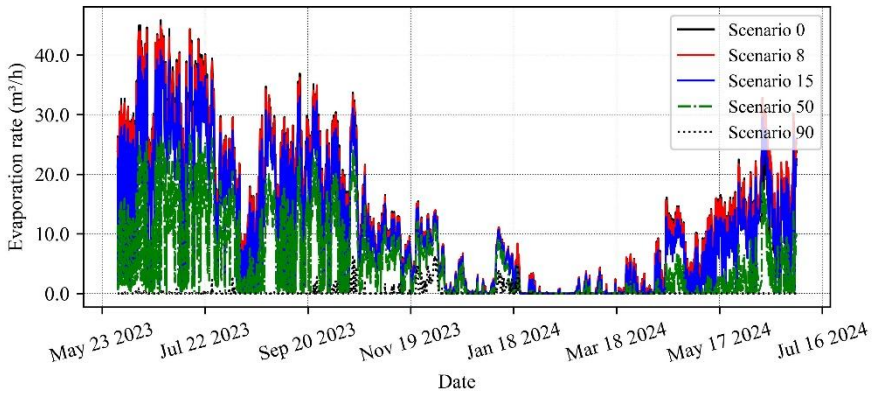

Figure 7-2. Evaporation rate timeseries results for the simulated scenarios of the gravel pit lake, at MFPV point.

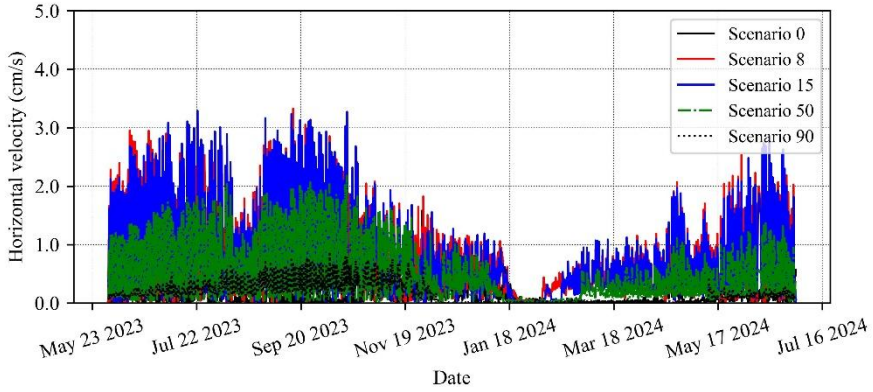

Figure 7-3. Horizontal velocity timeseries results for the simulated scenarios of the gravel pit lake, at MFPV point.

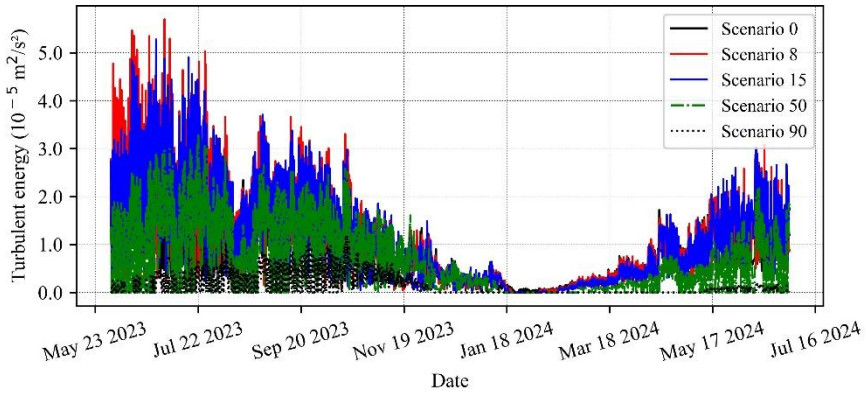

Figure 7-4. Turbulent energy timeseries results for the simulated scenarios of the gravel pit lake, at MFPV point.

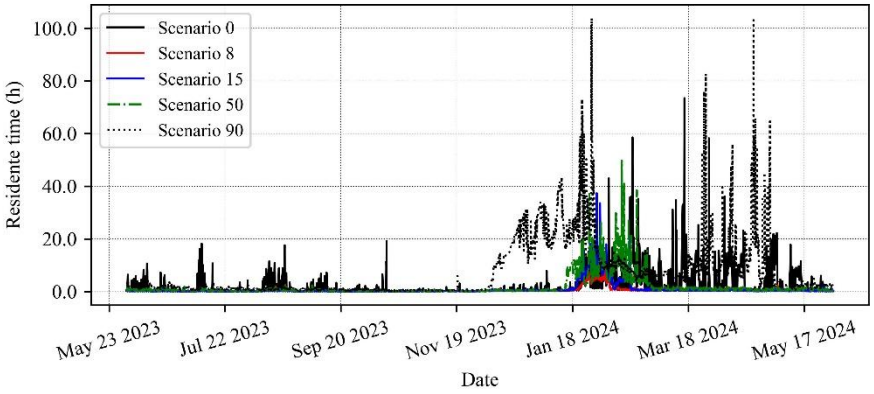

Figure 7-5. Residence time timeseries results for the simulated scenarios of the gravel pit lake, at MFPV point.

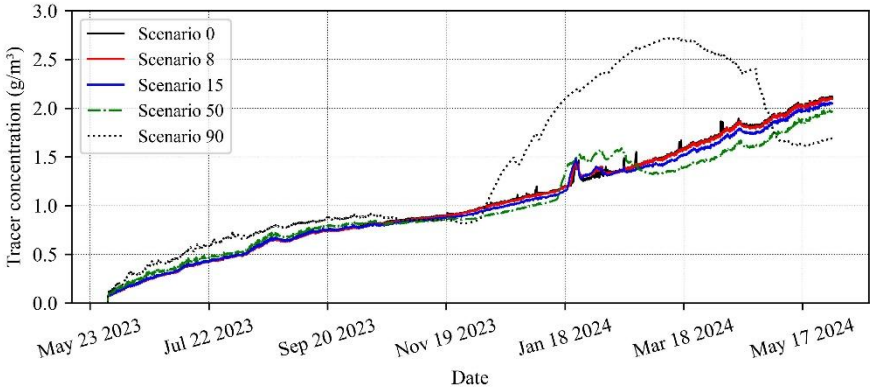

Figure 7-6. Tracer concentration timeseries results for the simulated scenarios of the gravel pit lake, at MFPV point.

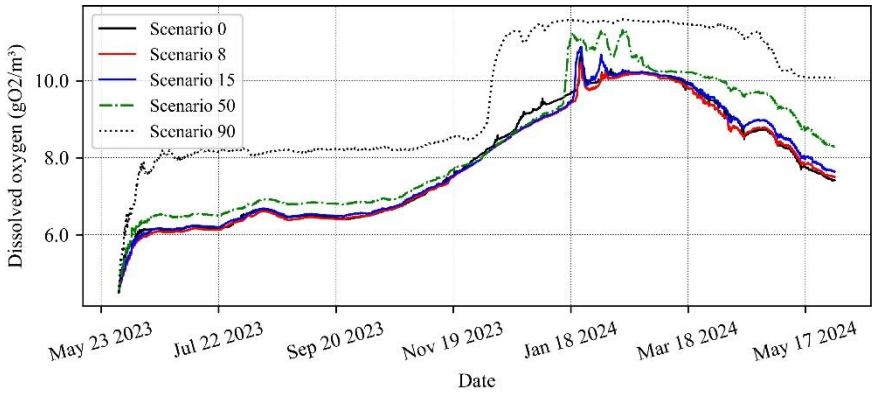

Figure 7-7. Dissolved oxygen concentration timeseries results for the simulated scenarios of the gravel pit lake, at MFPV point.

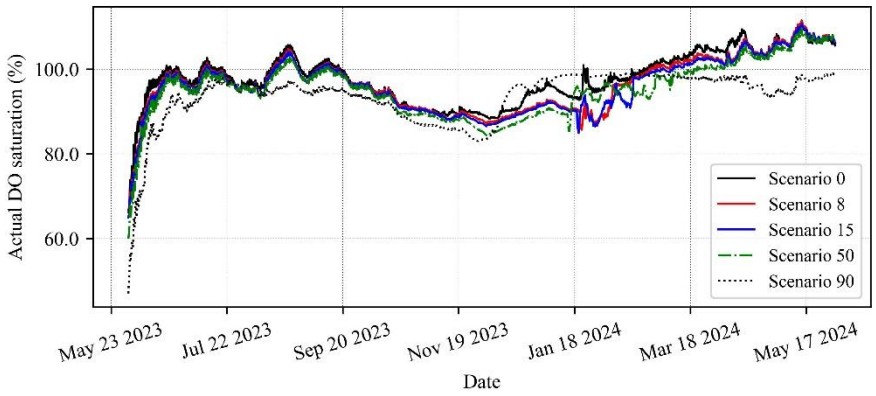

Figure 7-8. Actual DO saturation timeseries results for the simulated scenarios of the gravel pit lake, at MFPV point.

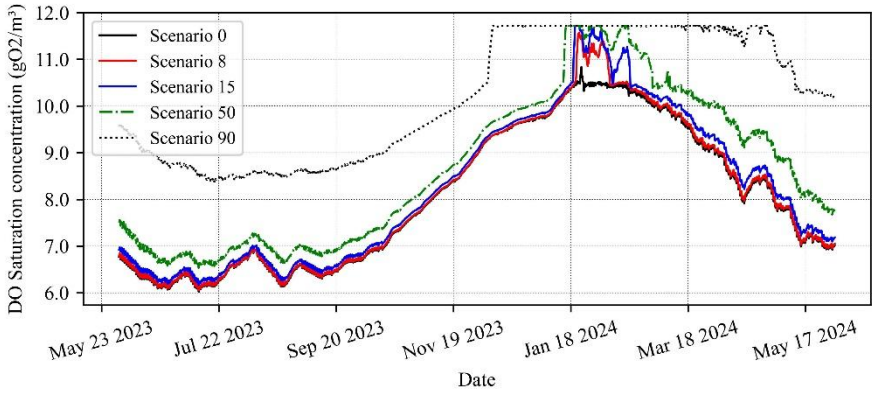

Figure 7-9. DO saturation concentration timeseries results for the simulated scenarios of the gravel pit lake, at MFPV point.

Passaúna Reservoir

- Timeseries results

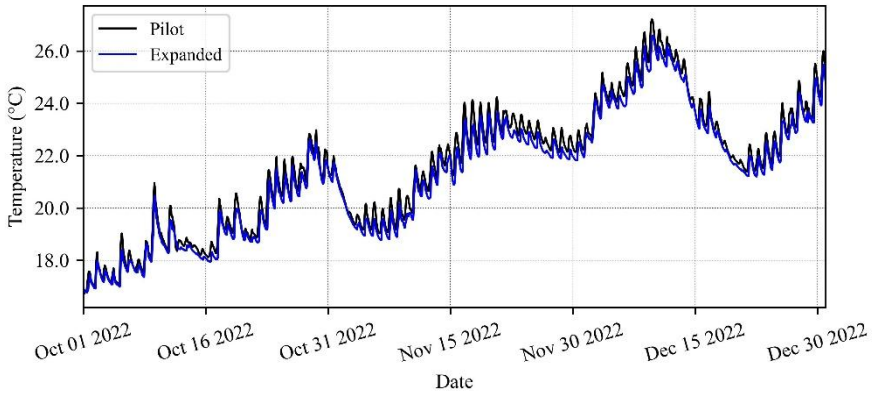

Figure 7-10. Surface temperature timeseries results for the two simulated scenarios of Passaúna reservoir, at Cell Cover point.

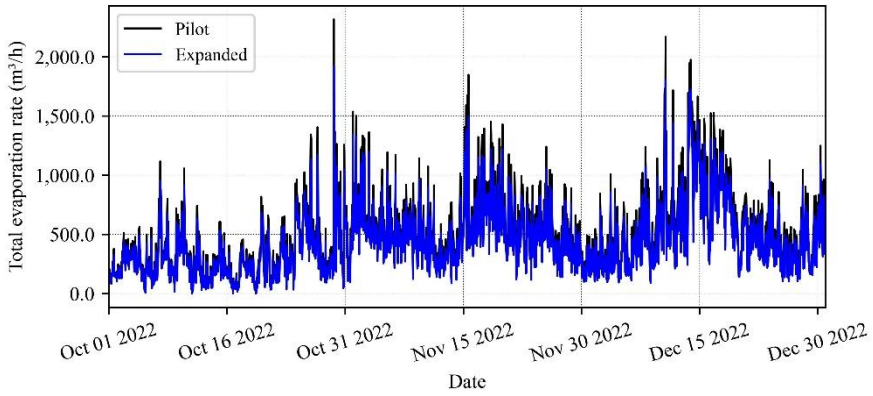

Figure 7-11. Evaporation rate timeseries results for the two simulated scenarios of Passaúna reservoir, at Cell Cover point.

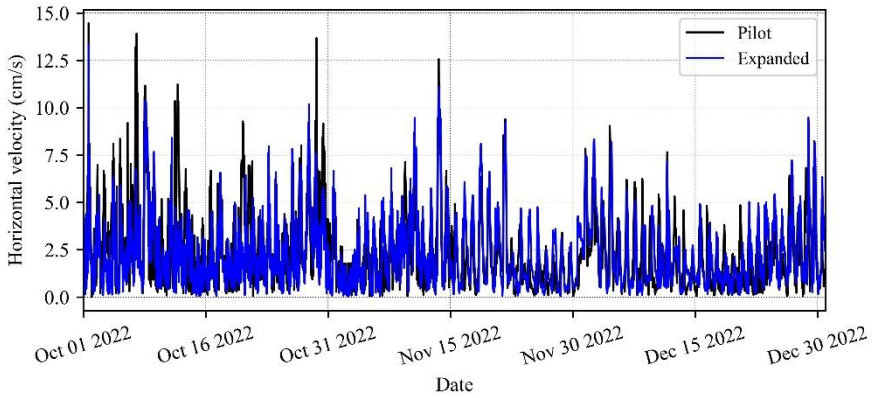

Figure 7-12. Horizontal velocity timeseries results for the two simulated scenarios of Passaúna reservoir, at Cell Cover point.

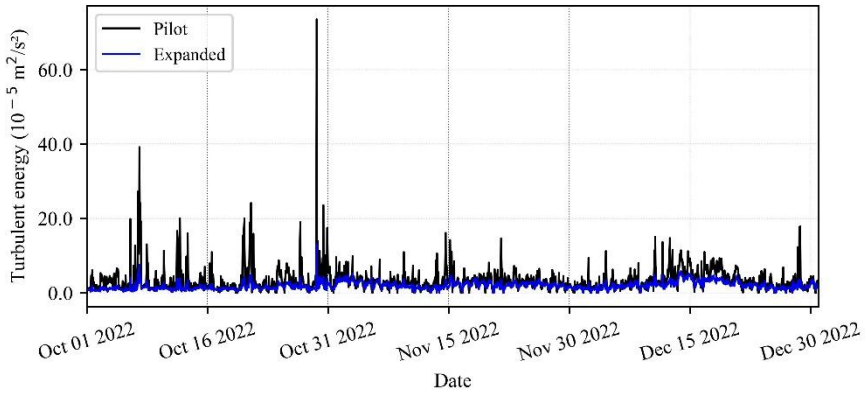

Figure 7-13. Turbulent energy timeseries results for the two simulated scenarios of Passaúna reservoir, at Cell Cover point.

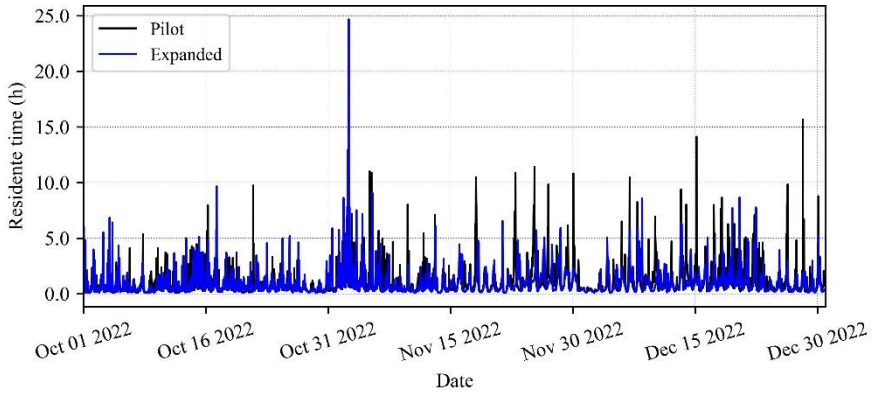

Figure 7-14. Residence time timeseries results for the two simulated scenarios of Passaúna reservoir, at Cell Cover point.

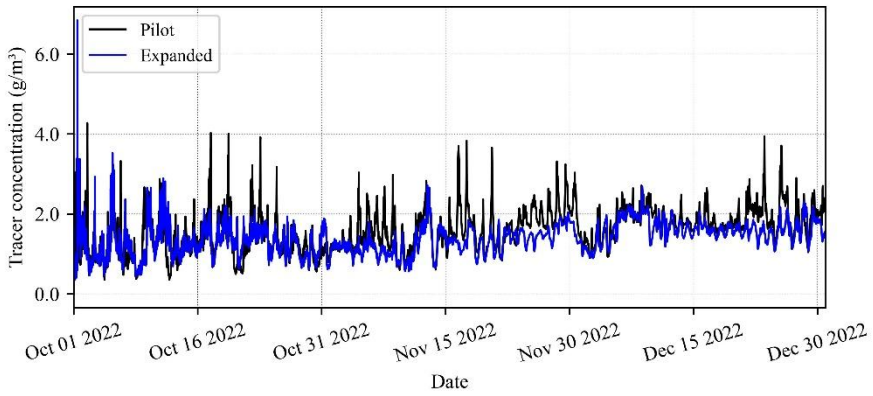

Figure 7-15. Tracer concentration timeseries results for the two simulated scenarios of Passaúna reservoir, at Cell Cover point.

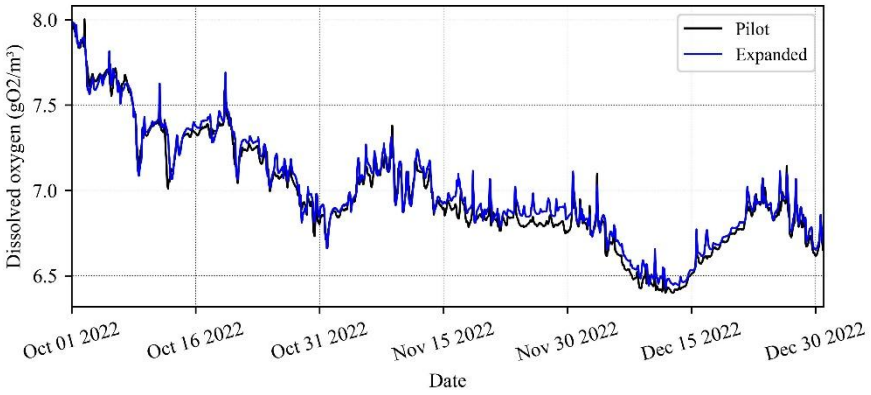

Figure 7-16. Dissolved oxygen timeseries results for the two simulated scenarios of Passaúna reservoir, at Cell Cover point.

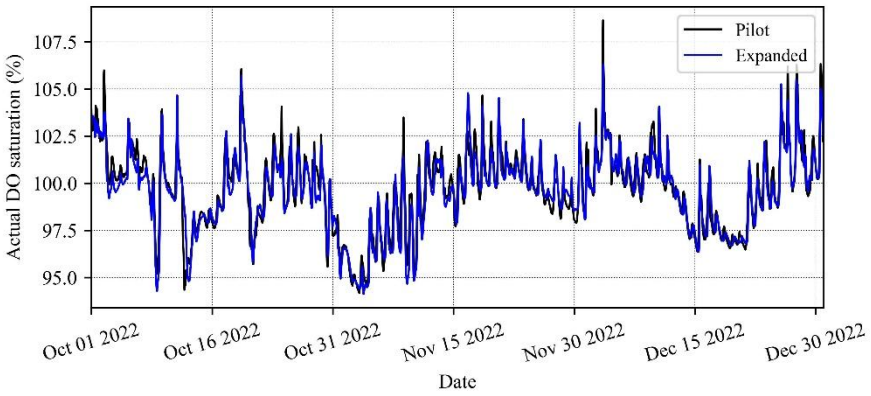

Figure 7-17. Actual DO saturation timeseries results for the two simulated scenarios of Passaúna reservoir, at Cell Cover point.

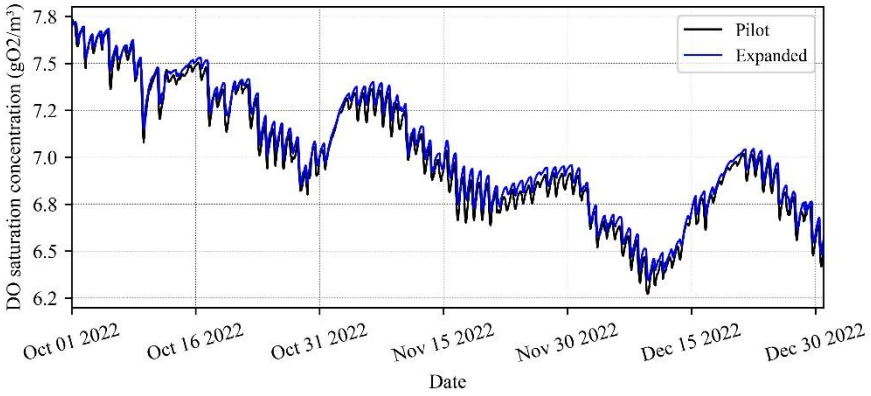

Figure 7-18. DO saturation concentration timeseries results for the two simulated scenarios of Passaúna reservoir, at Cell Cover point.